THE LUMINOSITY DISTRIBUTIONS OF EDGE-ON SPIRAL AND LENTICULAR GALAXIES

MARTIN ANTHONY SHAW

DOCTOR OF PHILOSOPHY

UNIVERSITY OF EDINBURGH

1987

EX BIBL. UNIV. EDINBURGH

This thesis has been composed by me and consists entirely of my own work, except where specifically indicated in the text

Martin A. Shaw

October 1987

Acknowledgements

This thesis would not have been possible without the support and advice of my principal supervisor Gerry Gilmore. In addition, however, I would wish to thank Peter Brand and Althea Wilkinson for critical reading of various sections of this thesis, and to Malcolm Longair for constant encouragement during the final months leading to submission. Photolabs, and in particular Eric Robertson, are thanked for their continued attempts to keep pace with my photographic requests, whilst the COSMOS team undertook several mapping programmes as a supplement to the material presented here. I also gratefully acknowledge financial support provided by the SERC (including funding for two trips to the AAT) and by the University of Edinburgh under a Carmichael bequest fund. However, most of all I am indebted to my parents for their constant support and backing. This thesis is dedicated to the loving memory of a dear father.

- CONTENTS -

IV RESULTING OBSERVATIONS OF THE PROGRAMME GALAXIES

V PHOTOMETRIC PROPERTIES OF THE PROGRAMME GALAXIES

VI THE NATURE OF "BOX" AND "PEANUT" SHAPED GALACTIC BULGES

Abstract

This thesis presents the results of a study into the nature of the luminosity distributions of edge-on spiral and lenticular galaxies. To this end, a procedure for self-consistent deconvolution of the observed luminosity profiles into their component parts has been constructed, and the results of its application to observational data for 15 galaxies of widely varying bulge-to-disc ratios, supplemented by two additional candidates from the literature, described. Evidence is presented of the extent to which the galaxies studied here depart from a "normal" morphology, and the implications for the applicability of traditional population deconvolution techniques addressed. In particular, the existence and possible nature of intermediate components are analysed and the results obtained are used to place constraints on current schemes for galaxy formation. In the light of those galaxies studied here which show clear evidence of "box" and "peanut" shaped bulge isophotes, the results of a systematic, all-sky search of such systems are also presented and their implications for current formation histories outlined.

- Chapter I -

General Introduction

I.1 Background

Ever since external galaxies were first identified as "island universes", there has been a continued desire to study these objects with a view to elucidating their forms and also of placing such results within the larger context of galaxy morphology as a whole. The use of such information to act as a testbed for theories of galaxy formation is a rather more recent development in this regard.

The true nature of external galaxies only really became apparent in the years leading to 1950 with the realisation that such systems are comprised of stars just as in our own Galaxy. Concomitant with this came the concept, initially prompted by Baade on the basis of the growing amount of observational data becoming available at the time, that some of the apparent differences between spiral discs and bulges/elliptical galaxies could be ascribed to differing stellar populations - the discs containing (young) blue stars and the bulges/ellipticals solely (old) red stars. [Sandage (1986) gives a more detailed account of the background to such a concept.] An inevitable consequence of the steady accumulation of information since that time has been to provide a considerably more rigorous test of this concept, with the result that certain modifications of this scheme may now be required.

The changing emphasis in studies of galactic structure is perhaps most graphically illustrated in the context of devising a global classification scheme. Despite the seeming continued success of schemes (whose original formulations are at least 50 years old) to accommodate the greatly increased sample of galaxies for which morphological information is now available, it is becoming increasingly clear that structural deviations from the "norm" are relatively common. Indeed, some of the features (lenses and rings are two that immediately come to mind) now appear sufficiently frequent as to require a specific inclusion within the main framework of the classification scheme itself. As a result, the concept of what constitutes a "peculiar" galaxy is having to become increasingly more restrictive than was the case when the schemes were originally devised. Disc warps and "box"/"peanut" bulge shapes - previously thought of as interesting but infrequent oddities - are also being isolated in increasingly larger numbers (see chapter VI), as are other systems showing morphological features generally ascribed as resulting from mergers/interactions.

Nevertheless, insofar as a general scheme of galaxy formation is applicable to the entire class of spirals/lenticulars and to ellipticals, it is of considerable importance to compare the global photometric properties of all morphological types. Any systematic deviations from a "typical" morphology may perhaps then be understood in terms of local variants on the evolutionary scheme adopted (were such a model sufficiently flexible) or as subsequent evolutionary processes arising after completion of the original epoch of galaxy formation.

Within this broad framework, one particular question which arises concerns the similarity or otherwise of elliptical galaxies and the bulge populations of spirals and lenticulars. The notion of evolutionary links between these two forms would, for example, be particularly attractive were one to find that they show similar luminosity distributions. A casual inspection of sky survey plate material, however, appears to indicate considerable dissimilarity in their morphologies - for those spiral galaxies in which the luminosity distribution exterior to the disc can be reliably defined show very flat shapes (section V.5) wheras ellipticals are, in the main, known to be considerably rounder (typical axial ratios $\gtrsim$ 0.6 for the 168 systems studied by Sandage et al 1970). However, considerable caution has to be attached to these results as they refer to the axis ratio at a specific surface brightness level (generally $\sim$ 25 B mag. arcsec^{-2}, henceforth μ). Furthermore, the work of Strom & Strom (1978 and references therein) indicates that changes in isophotal axis ratios with surface brightness are, for ellipticals at least, a distinct possibility.

Indeed, several lines of evidence now exist to suggest a degree of similarity between the formation histories of bulges and ellipticals. For example, equivalent relations are found between luminosity and central velocity dispersion (the Faber-Jackson relation) for all morphological types (Whitmore et al (1979), Whitmore & Kirshner (1981), Kormendy & Illingworth (1983), Kormendy (1985)). Although it is now well established (Kormendy & Illingworth 1982) that spiral bulges on the whole show a larger degree of rotational support than do luminous ellipticals, Davies et al (1983) noted that spiral bulges and ellipticals of like luminosity show similar dynamical properties. Furthermore, Dressler (1987) finds a striking similarity between the correlations of

galaxian isophotal diameter and central velocity dispersion for all morphological types in clusters. These conclusions are, by necessity of there being few inherently bright spiral bulges, somewhat uncertain due to limited sample sizes, and it is true that a more detailed comparison does highlight certain differences between these varying morphologies. There is also some concern that the dynamical arguments are based on spectroscopic observations of the spiral bulges which may be significantly contaminated by light from the disc component, even for those edge-on candidates studied by Kormendy & Illingworth (1982) - see chapter VII. Nevertheless, the conclusions implied are sufficiently important as to warrant continued study from both the dynamical and photometric viewpoints.

Equally important is the possible existence and nature of any "intermediate" populations in addition to those components originally conceived by Baade. Interest in such a field has been prompted by the isolation of "thick discs" in lenticular galaxies by Tsikoudi (1977, 1979) and Burstein (1979b), allied to the more recent identification of a potentially similar component in our own Galaxy (Gilmore & Reid 1983). The situation is somewhat less certain for external spirals, although claims for similar structure have been made by van der Kruit & Searle (1981a, 1981b). At the very least, the isolation of such an additional component is of great significance in the light of the stringent constraints one would thence be able to place on galaxy formation schemes. Were both the structural and dynamical properties of the "intermediate" components truely intermediary between the extremes of the bulge and disc populations, for example, then formation models such as that of Eggen et al (1962) [invoking the rapid formation of a bulge followed by a dissipational collapse phase

prior to significant star formation within a disc] must clearly be "tuned" in such a way as to ensure that the collapse is not so rapid that too few "thick disc" stars can form. Alternatively, if, as has recently been proposed, a subsequent perturbation (such as from an infalling satellite galaxy) is sufficient to thicken a pre-existing disc in just such a way as to mimic the existence of an additional component, then this is another important proposition to test as it has a bearing on our understanding of the subsequent evolution of a system with its environment. A related point concerns the extent to which such intermediate components may be influenced by, and co-exist with, the other stellar populations within the galaxies concerned.

It is these two fundamental questions which provide the major stimulus for the current work. This thesis therefore addresses these points in some detail primarily by attempting to deconvolve the constituent components within galaxian luminosity distributions in a more systematic way than has been undertaken thus far. These results should allow extraction of more reliable structural parameters for the bulge components themselves which then act as a basis for future comparison to elliptical galaxies of like luminosity. In addition, the evidence for, and nature of, possible intermediate components is addressed by determining the extent to which the luminosity distributions perpendicular to the disc plane of a galaxy are adequately described by the contributions from a photometrically "simple" combination of a disc and, for example, an $r^{1/4}$ law component alone, or whether they are sufficiently complex that the inclusion of a third component within the non-thin disc light distribution is required to describe their forms.

Previous studies of external galaxies have tended to concentrate on systems of moderate inclination to the line-of-sight. However, an inspection of such galaxies clearly reveals a luminosity distribution dominated by the young (spiral arm) disc population [the photographs of M31, M81 and NGC 253 in the Hubble Atlas (Sandage 1961) serve to illustrate the problems concerned]. For this reason, the present study has been geared towards an investigation of galaxies as close to an edge-on aspect as possible, following the same motivation as the studies of Tsikoudi (1977) and van der Kruit (1979 and subsequent papers).

However, considerable caution is still required in analysing the light distribution in such systems because of the severe optical depths found within the disc components. As no well-determined scheme yet exists to describe (and hence allow for) obscuration effects along the line-of-sight in such cases, no corrections have been applied in the present data set other than to discard regions of the surface brightness distributions which a visual inspection indicated were so affected.

I.2 Sample definition

The source from which the objects comprising this thesis were selected is principally the Second Reference Catalogue of de Vaucouleurs, de Vaucouleurs & Corwin (1976, henceforth RC2) as it is largely complete and reliable for relatively nearby systems and is also easily accessible to computerised search procedures.

The present database was defined using the SCAR package on STARLINK using the revised Hubble classification number (T) assigned to each object in that catalogue. A preliminary search of the RC2 for spiral and lenticular galaxies yielded a total of 3679 objects, with the sample being further limited to only those systems possessing major axis dimensions at the $\mu_B \sim 25\ \mu$ isophotal level (or $\log_{10} D_{25}$) in excess of 1.55 [D_{25} is measured in units of 0.1 arcmins such that this limitation in size corresponds to $\sim$ 4.9 arcmins or 4.3 mm at the plate scale of the SERC/ESO and Palomar Observatory/National Geographical Society (hereafter POSS) survey material]. Subsequent removal of all objects satisfying the above criteria but defined as irregular or peculiar in the RC2 resulted in a total of 505 spirals and lenticulars.

The next step was to define how many of these objects are of sufficiently edge-on aspect for consideration in the present study. This was of some importance in the light of the increasingly dominant disc contribution noted previously for those systems at inclinations some way from edge-on. By necessity this definition was very subjective - I relied on a visual inspection of each object on the available POSS or SERC/ESO survey plate or film material to suffice. One could equally use the more "traditional" method of adopting the axis ratios quoted in the RC2 ($\log_{10} R_{25}$) to derive an inclination angle. Such a procedure was, however, not adopted here as it was deemed too unreliable owing to the fact that log R_{25} only gives information as to the whole galaxy shape at the 25 μ isophotal level, such that inclination angles derived on this basis can be strongly influenced by an unusually dominant bulge or disc.

This final selection procedure yielded a total of 108 RC2 galaxies. I was, however, able to supplement this database by using lists of northern and southern edge-on candidates kindly supplied by Harold Corwin (private communication, 1981). An additional 9 galaxies were isolated from the latter using the same selection criteria outlined above, giving a total of 117 objects in the final "master list". Such a sample forms the basis from which objects from both the CCD observations described in chapter II and the sky survey analyses of chapter VI were selected.

I.3 Rationale behind current observations

The CCD observations presented here are of a subset of this "master list" and were defined under the following precepts :

1. Ease of accessibility from the AAT (resulting in a typical declination limit of $\lesssim +15^{o}$ to avoid excessive atmospheric extinction),
2. Coverage of a considerable range of bulge:disc ratio (as defined from visual inspection of the objects from the plate material) thus enabling one to investigate stellar populations in galaxies showing widely varying degrees of dominance from the non-thin disc,
3. The limits imposed by the amount of telescope time made available for the project.

The latter point, however, proved to be somewhat of a restriction and as a result the current sample also contains a number of galaxies which do not satisfy one or more of the selection criteria detailed above (principally the major axis dimension or inclusion within the RC2). Table 1.1 lists the objects concerned and highlights salient

Galaxy (1)	type (2)	log D_{25} (3)	I (°) (4)	m_B (5)	$-M_B$ (6)	D (Mpc) (7)	A_H (kpc) (8)	visual B:D ratio (9)	PA (degs) (10)	references to previous work (11)
NGC 2295	Sab	1.22*	84					intermediate	50	
NGC 2310	S0	1.70	79	12.16	17.73	9.5	8.5	intermediate (B/P, W)	47	11,14,15
NGC 3115	S0	1.92	(72)	9.89	18.52	4.8	7.7	galaxy standard	46	2,3,7,10,11,15
NGC 3379	E0	1.65	(32)	10.33	19.19	8.0		galaxy standard	51	1,4,5,6,9,11,12,13,15,16,17
NGC 3573	S0	1.64	83	13.62				bulge dominated	6	11
NGC 4289	Scd	1.59	86	15.00				intermediate	3	
NGC 4469	SB(s)0/a	1.59	72	11.29	18.86	10.7	16.7	intermediate (P)	89	11
NGC 5078	SA(s)a	1.51	82	12.50				bulge dominated	148	15
NGC 5170	SA(s)c	1.91	85	10.49	20.15	13.4	41.1	disc dominated	128	11,14
IC 2531	Sc	1.74	90	12.93	18.77	21.9	62.7	disc dominated (P, W ?)	76	11
IC 4351	SA(s)b	1.74	85	10.86	21.12	24.9	69.3	intermediate	17	11,14,15
A0902-68	Sb	1.47*	87			41.2	33.6	intermediate (P)	58	8
A0919-33	Sbc	1.36*	85					disc dominated	72	
A0931-32	Scd	1.67	90	12.84	17.00	3.2	20.9	disc dominated	91	11,14
A1611-00	Scd	1.56*	88	13.57				disc dominated	90	11,15
UGC 7170	Sc	1.53*	90	13.78	18.10	23.9	30.6	disc dominated (W)	14	

TABLE 1.1

NOTES TO TABLE 1.1 :

col. 3 : calculated measures of log D_{25} marked by a *

col. 6 : absolute magnitudes from the sources detailed in the text, all corrected for an assumed H_o of 100 km s^{-1} Mpc^{-1}.

col. 7 : All distances assume an H_o of 100 km s^{-1} Mpc^{-1} - sources quoted in the text. That of NGC 3379 is taken from de Vaucouleurs & Capaccioli (1979).

col. 8 : The absolute diameters of NGC 2310, NGC 3115 and A0902-68 are based on an object size as gleaned from the SERC J plates and are uncertain by ~ ± 10 kpc.

cols. (4) & (10) : Inclination angles and position angles are as derived in the present work aside from those of NGC 3115 and NGC 3379. The latter measures are, however, very uncertain.

col. (9) : B or P denotes the existence of a "box" or "peanut" bulge, W denotes the presence of a disc warp.

col. (11) - sources of data :

1 : Burkhead & Kalinowski (1974)
2 : Strom et al (1976)
3 : Strom et al (1977)
4 : Okamura (1977)
5 : Burstein (1979)
6 : de Vaucouleurs & Capaccioli (1979)
7 : Tsikoudi (1979)
8 : West et al (1981)
9 : Whitmore & Kirshner (1982)
10 : Hamabe & Okamura (1982)
11 : Longo & de Vaucouleurs (1983)
12 : Nieto (1983)
13 : Kent (1984)
14 : Lauberts & Sadler (1984)
15 : Longo & de Vaucouleurs (1985)
16 : Michard (1985)
17 : Davis et al (1985)

parameters for each one.

Data for an additional 7 candidates were obtained from scans of SERC J plate material made by the COSMOS automated plate measuring machine of the Royal Observatory Edinburgh. However, subsequent analysis showed this material to suffer from a far too limited dynamic range to be useful in the current programme despite the choice of solely A grade plates for this purpose. The observational material of this thesis thus comprises the CCD data alone.

The outline of the thesis is as follows. Chapter II describes the methods of data aquisition and reduction whilst chapter III presents a new iterative fitting technique aimed at describing the full 2-D light distribution in these galaxies. Also described is the application of such a technique to "model galaxies", and to literature data for two large, edge-on spirals. The results of adopting such a technique for the present dataset are described in chapter IV, and the general conclusions concerning the departure of the luminosity distributions from a "simple" form, the existence and form of any intermediate components, the existence of colour gradients and the nature of any possible radial disc cutoffs are discussed in chapter V. With a view to elucidating in some detail those bulges showing pronounced "box" and "peanut" shapes, chapter VI describes the results of the first ever systematic, all-sky survey of such morphologies and discusses the possible implications of these results for the formation mechanisms currently proposed in such galaxies. A general summary, together with suggestions for future work, is given in chapter VII. Three appendices are also included: appendix A contains the tabulated results discussed in chapter IV, whilst appendix B describes the

techniques of digital unsharp masking and the results of applying such techniques to the present sample galaxies. Appendix C presents a selection of photographs of the galaxies studied in chapter IV.

- Chapter II -

Data acquisition and preliminary reduction

II.1 Current observations

The CCD observations presented in this thesis were acquired over two separate runs using the RGO CCD system on the Anglo-Australian Telescope (AAT) during 23-25 April 1985 and 15-17 February 1986 (henceforth runs 1 and 2 respectively). Details of the system used are given elsewhere (see, for example, the AAO observers manual (1981) and Jorden et al (1982)) but the salient points, together with an outline of the performance characteristics particular to these observations, are outlined in table 2.1.

The first run was almost totally unsuccessful owing to adverse weather conditions. Additional problems were encountered during run 2 from repeated readout crashes and resulted in some loss of data, although such difficulties were overcome during the second half of the first nights observing. Excellent observing conditions occured throughout the whole of run 2, with estimated seeing of between 1 and 1.5 arcsecs common to much of each night.

The greatly reduced CCD quantum efficiency shortward of ~ 4000 A and longward of ~ 7000 to 8000 A, coupled with an increasing sky brightness beyond ~ 7000 A, considerably minimises the useful range of colour indices available to determine the existence of colour gradients in galaxies. Further, several previous studies (e.g. Simkin

(a) General parameters :

readout noise	70 e^-/pixel
plate scale	16.4 arcsec/mm at prime focus
pixel size	30 micron (~0.48 arcsec) square
CCD format	350 x 512 pixels (last 30 pixels in X-axis constitute the bias strip)
useful detector area	2.6 x 4.2 arcmin
conversion factor	1 ADU = 16 e^- = 16 photons
estimated QE	80 % over both B and R bands

(b) Results from the present study :

maximum steps in bias frame	1 to 3 % peak-to-peak
underlying bias gradient	$\lesssim$ 0.01 ADU/ pixel
dark current contribution	0.01 ADU/ sec of integration/ pixel
scale of flat-field structure	3 % (peak-to-peak) in R 1 % (") in B
scale of fringing in region of strong concentration	4 % of sky (peak-to-peak) maximum 2 % " average
fringing in region of average concentration	3 % of sky (peak-to-peak) maximum 1.5 % " average
pixel-to-pixel sensitivity variations in 100 secs frame	1.5 % peak-to-peak in B (0.9 % after co-adding) 1.6 % peak-to-peak in R (0.6 % after co-adding)
estimated accuracy of sky determination	$\lesssim$ 0.5 %
linearity of CCD over both runs	0.1 % or better

(c) Noise estimates :

typical photon shot noise on sky	0.09 ADU/sec in B 0.16 ADU/sec in R
S/N on sky in galaxy frames	0.10 /sec in R 0.06 /sec in B

Table 2.1 : Summary of performance characteristics of the CCD system during both runs.

(1975), Sandage & Visvanathan (1978) and Schweizer (1976)) have found (B-V) and (V-R) colours to be largely ineffective in the search for colour gradients, although gradients are commonly found to be stronger in (B-R) (Thompson et al, 1982). In the light of these findings it was decided that, to achieve complete coverage across a number of galaxies, "first pass" observations would be limited to the B and R bands alone. Imaging in V and U would have been attempted had time been available, but this did not accrue. As a result, I was able to map a total of 9 galaxies in both B and R, with a further 6 being covered solely in the R band (the presence of the moon during the first part of each night in run 2 tending to limit the time available for imaging in B). Seven of the galaxies observed were sufficiently large that complete areal coverage required several exposures taken at selected positions across the image (2 to 3 being the norm but 4 being required in the case of NGC 5078). To facilitate ease of merging these respective frames in the subsequent reduction process, it was decided to adopt a typical overlap between positions ~ 30 to 50 pixels, or ~ 15 to ~ 25 arcsec in either RA or dec. as appropriate. The observations also included shorter exposure frames of the galaxies NGC 3115 (S0) and NGC 3379 (E0) to act as galaxy standards and hence allow comparison of the results obtained to those of previous observers.

In view of the desire to observe detailed structure in the non-thin disc light of the sample objects, I attempted to undertake photometry to the faintest light levels possible within the allowed constraints. As a result, 2x1000 second frames of each galaxy at each position in each colour were routinely obtained, aside from the "standard" galaxies which were observed with shorter exposures (<

500 secs in all cases). Although I was not strictly interested in detailed properties of the nuclear regions of the galaxies observed, it was clearly desirable not to saturate the central regions to an excessive degree as any "bleeding" of charge across the CCD would contaminate the fainter outer parts of the objects concerned. Careful checks indicated that no serious effects resulted from such saturation. Since most of the sample objects are so edge-on, dust obscuration within the disc plane serves to mask the brightest central regions.

Between each pair of 1000 secs exposures, the telescope was consistently offset by ~ 5 arcsec or so in random RA and/or dec. shifts to allow a more reliable discrimination to be made between "true" light variations across each frame and those effects resulting from structure in the flat-field and from fringing. The flat-field calibration frames were taken on the sky during twilight and dawn (additional dome flats were taken before the start of the first nights observing in run 2), whilst bias frames were taken throughout each night. The effects of the contribution from dark current were investigated by taking two long exposures during the second day of run 2, with fringe frames for the R band obtained over the second night of run 1 alone. Details of these observations are given in section II.2 below.

In addition, a total of 38 frames were obtained of standard stars in the two regions E3 and E5 outlined by Graham (1982) to allow absolute calibration of the galaxy photometry. Stars *o* and *v* were observed in region E3 whilst two sets (namely stars *m*, *k*, *o* and *c*, *Y*) were imaged from region E5. The general procedure adopted was to

take pairs of frames for each set of standards in each colour and attempt to intersperse these between galaxy frames as much as possible. The length of the exposure times required in such frames was dictated by the requirement of achieving a reasonable signal (~ several thousand ADU's) for the "typical" standard, and as a result they vary greatly from one set of observations to the next (over the range 10 to 150 secs for individual frames). Once again, respective sets of such frames were offset by arbitrary RA and dec. shifts, and great care was taken to ensure that no such position was adopted whereby the standards of interest were affected by defects on the chip.

The present observations thus comprise 68x1000 secs exposures alone, with a total ~ 200 frames (or ~ 80 000 secs). Observations taken during run 2 account for ~ 87 % of the total. Table 2.2 presents a log of the observations undertaken.

II.2 Characteristics of the CCD performance

II.2.1 Read-out noise and bias subtraction

The application of a bias (or global DC voltage) offset to the CCD allows one to define an absolute level with which to reference the signal from an individual pixel. This bias value also carries an associated shot-noise which, combined with other internal noise sources within the device, is commonly referred to as the read-out noise. Being an intrinsic property of the chip used, the value of this noise sets an absolute lower limit (or "noise floor") to the performance of the CCD system - at least in the low signal regime.

Galaxy	passband	asec Z (mag.)	$A_{B,R}$ (mag.)	adopted (B-V)	adopted (V-R)	exposure time (secs)	counts in sky (ADU's/pixel)	FWHM seeing (arcsecs)	secZ	weighted μ_o^{corr} (mag arcsecs^{-2})	$\sigma_{\mu o}$ (mag arcsec^{-2})	Night observed
NGC 2295	(R)	0.13	0.48		0.90*	2000	5264 (±4)	1.25	1.007	28.86	0.01 (mean = 28.85)	3
NGC 2310	(B)	0.34	0.44	0.97[B]		2000	978 (±3)	1.33	1.238	29.35	0.02 (mean = 29.38)	1
	(R)	0.13	0.22		0.86[A]	2000	3708 (±5)	1.77	1.016	29.16	0.01 (mean = 29.17)	1
NGC 3115	(B)	0.30	0.12	1.00[A]		220	132 (±2) :	1.80 :	1.124	27.34	0.01 (mean = 27.36)	2
	(R)	0.17	0.06		0.92[A]	1500	4307 (±45) :	1.38	1.328*	28.97	0.01 (mean = 28.97)	2,3
NGC 3573	(B)	0.28	0.32	1.04[B]		2000	965 (±2)	1.39	1.031	29.57	0.03 (mean = 29.52)	3
	(R)	0.14	0.18		0.54[B]	2x2000	2737 (±3)	1.56	1.079	29.16	0.01 (mean = 29.15)	3
NGC 4289	(R)	0.24	0.02		0.90*	2x1000	1673 (±3)	1.71	1.839	28.55	0.004 (mean = 28.55)	2
NGC 4469	(B)	0.36	0.00	0.98[B,C]		3000	1609 (±2)	2.54	1.351	30.24	0.03 (mean = 30.19)	3
	(R)	0.18	0.00		0.90*	2000 + 1000	2926 (±2)	2.08	1.374	29.31	0.01 (mean = 29.30)	3
NGC 5078	(R)	0.14	0.12		0.90*	3x2000 + 1000	1245 (±2)	1.85	1.112	28.50	0.01 (mean = 28.49)	1,2,3
NGC 5170	(B)	0.29	0.24	1.03[B]		3x2000	1075 (±2)	1.37	1.079	29.64	0.01 (mean = 29.65)	2
	(R)	0.13	0.12		0.57[B]	2x2000	2861 (±4)	1.48	1.035*	29.27	0.005 (mean = 29.28)	1,2
IC 2531	(B)	0.32	0.24	0.91[B]		3x1000	599 (±1)	2.46	1.182	27.91	—	run 1
	(R)	0.15	0.12		0.62[C]	3x1000 + 2x2000	1572 (±4)	1.59	1.134*	28.51	0.004 (mean = 28.51)	run1, run2 (2)
IC 4351	(R)	0.13	0.09		0.64[B]	300	614 (±2)	1.81	1.033	27.07	0.05 (-)	run 1
A0902-68	(B)	0.34	0.44	1.00*		2000	1012 (±6)	1.72	1.251	29.35	0.02 (mean = 29.38)	1
	(R)	0.16	0.22		0.90*	2000	3092 (±5)	1.76	1.266	29.14	0.01 (mean = 29.15)	1
A0919-33	(B)	0.28	1.04	1.00*		2000	955 (±2)	1.29	1.051	28.84	0.01 (mean = 28.85)	2
	(R)	0.17	0.52		0.90*	2000	4981 (±14)	1.66	1.271	28.84	0.004 (mean = 28.84)	2
A0931-32	(R)	0.13	0.34		0.42[B]	2000	4277 (±4)	1.64	1.026	29.01	0.01 (mean = 29.00)	3
A1611-00	(R)	0.16	0.09		1.0(:)[C]	2000	4695 (±5)	1.91	1.232	28.16	—	run 1
UGC 7170	(B)	0.45	0.12	1.00*		2000	1119 (±1)	1.69	1.635	29.57	0.02 (mean = 29.60)	1
	(R)	0.20	0.06		0.90*	2000	3532 (±2)	1.99	1.568	29.28	0.01 (mean = 29.29)	1

TABLE 2.2

NOTES TO TABLE 2.2 :

all uncertain measures marked with a (:)

col. 5 : A - effective aperture colour taken from RC2
B - adopted arithmetic mean of all measures in Longo & de Vaucouleurs (1983, 1985)
C - taken from Griersmith (1980)
* - assumed value of 1.00 as no reference measures available

col. 6 : A - taken from Sandage & Visvanathan (1978) assuming

$$(V-R) = 1.11(V-r) + 0.29$$

B - taken from Lauberts & Sadler (1984)
C - given by Smyth (private communication, 1987)
* - assumed value of 0.90 as no reference measures available

col. 10 : * - secZ averaged over separate nights and/or runs

col. 12 : Standard error on an arithmetic mean of μ_o (mean in brackets)

col. 13 : Assumed to be from run 2 unless otherwise stated

Janesick et al (1984) have outlined the independent sources contributing to read-out noise, potentially the most significant being that introduced by the operation of the output amplifier. However, working at operating temperatures of typically ~ 150 K (LN_2 cooled) reduces the *1/f* component of the amplifier noise almost to the absolute limiting performance of this device over a wide range of frequencies (see, for example, figure 36 of Janesick et al (1984)).

Additional noise sources arise during the process of transferring charge between the potential wells (called the charge transfer noise), and from resetting the bias level after the readout of each individual pixel (the reset noise). The former is relatively unimportant when due account is taken of the very high charge transfer efficiencies now routinely obtained with CCD's (Janesick et al (1984) and Mackay (1986) quote ~0.99998 per transfer), whilst the latter is reduced by adopting the technique of "correlated double sampling", the principles of which are outlined in Wright (1982), Janesick et al (1984), and Mackay (1986).

Hence, the first step in the reduction procedure is the removal of the bias level imposed on each frame. The level itself, and its associated noise, are both determined by taking frames of zero length exposure time and with the shutter closed - these being the bias frames. Although it is widely considered that there is no considerable drift in the bias over a nights observing, checks were facilitated by ensuring that a number of bias frames were taken throughout the night. This typically amounted to 3 at the beginning, during and/or at the end of each session - a total of 6 frames being acquired during the first run, and 26 during the second. No evidence was

found for any zero point shifts from night-to-night although there was one of ~ 20 ADU's between the separate runs. Thus, the creation of a final "master" frame relevant for all the CCD data obtained was precluded. Structure was evident on all frames, as figure 2.1 shows. The structure is already well documented although its origin remains unclear - Jedrzjewski (1985) gives a more detailed description of its form. In brief, a number of parallel slices taken across each bias frame show 3 bands of varying intensity parallel to the long axis of the CCD. Maximum (peak-to-peak) steps in intensity amount to between ~ 1 and 3 % of the local rms "background". However, tests carried out on the bias frames obtained during the first night of run 1 clearly indicate that, aside from these zonal features, the underlying bias level is extremely flat - with a gradient of typically less than 0.01 counts/pixel.

Even so, the adoption of a single bias level is inappropiate in this situation (the spatial variations are still clearly seen after subtraction of such a mean value). Hence, a global mean bias frame was constructed for each run in turn (the mean for run 1 derived from all 6 taken throughout the night, with 18 of the 26 used from run 2). That from the first run (weighted by the standard deviations on the mean of each frame in the co-add process) has an average count of 136.0 (±0.6, standard error) ADU's and that for the second of 114.1 (±0.2) ADU's.

Each mean bias frame then had any cosmic-ray events removed using an interpolation routine across the pixels affected (done at this stage to prevent the creation of "negative" events in the bias subtracted frames thus produced). Such events are characterised as

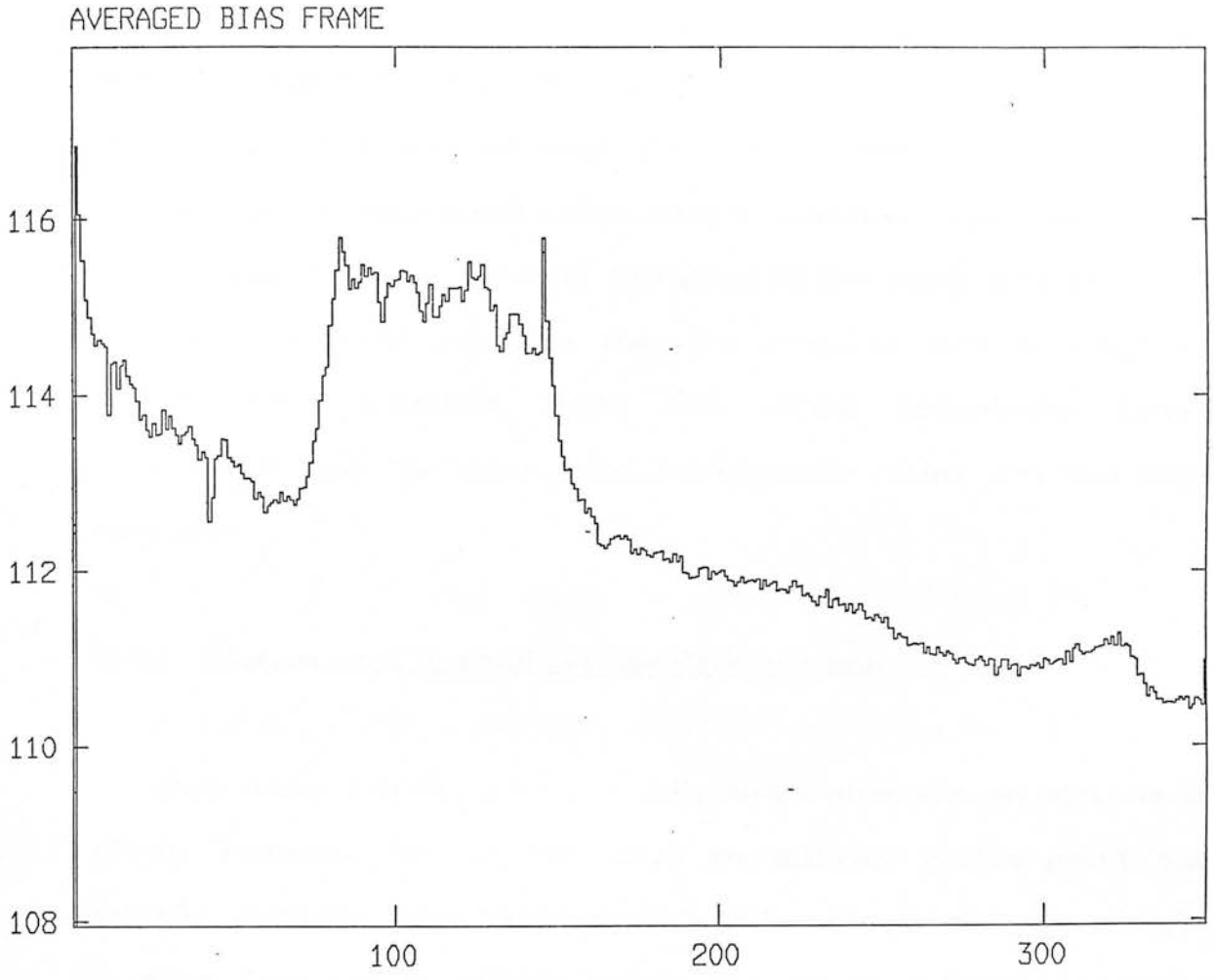

Figure 2.1 : A slice taken across the averaged bias frame used for run 2 - formed by binning together all slices taken across each individual row. The vertical axis is counts in ADU's and the X axis refers to the slice length along the ccd. in pixels.

being confined to a small number of "hot" pixels (usually one) and are thus easily identifiable. All subsequent galaxy and standard star images had the bias subtracted using the appropiate mean frame. Possible variations in level between that of the mean frame and of the image frame were checked using the average value in the bias strip of the latter as determined either from 6 individual point measures or by construction of an intensity histogram of the whole bias strip and adopting the modal value as the bias level. If such a difference existed, the calibration frame was scaled accordingly before subtraction, with the bias strip subsequently being removed from each one.

II.2.2 Sources (and removal) of the dark current

Dark current is the term generally ascribed to the registration of photon reception by the CCD when no incident photon event has actually occurred. Such sources of "additional" photons are thought to arise from thermal effects within the silicon substrate, and the generated signal thus produced will clearly possess its own associated shot-noise. In the sense that the combination of dark current and corresponding noise partially arises as a result of defects within the semi-conductor, i.e. being a feature intrinsic to the device used, it could be seen as another contributing factor to the global read-out noise for that device (Janesick et al, 1984). However, it is treated separately here as it is a function of exposure time and as such requires the adoption of a slightly different reduction technique from that used for the bias removal outlined previously.

An additional contributor to the dark current arises from so-called "luminescence" within the CCD. Such a general term serves to describe the noise resulting from photons created within the silicon due to the action of simply clocking the output gates (called "clocking luminescence"); from the creation of photons as a result of too high a bias being applied to the output amplifier (the "diffusion luminescence") and from the effects of defective pixels which happen to saturate much quicker than expected ("blemish luminescence"). A more detailed discussion of these features and their origins is given in Janesick et al (1984).

Clearly, as the dark current arises from thermal origins, it is drastically reduced by operating the CCD at low temperatures. [The actual dependance is $\propto \exp(-\text{constant}/T)$.] However, as in many other areas of CCD design, such a benefit has to be traded against detrimental effects to other aspects of the device - in this case a lower temperature reduces the absorption coefficient of silicon and thereby reduces the responsivity of the device (particularly at longer wavelengths (Wright, 1982)). In addition, the ability of the device to transfer charge from one potential well to another when clocking out (the charge transfer efficiency or CTE) is also found to be considerably reduced at lower operating temperatures.

The optimised intermediate value used for the current device (~150 K) is quoted in the AAO observers manual (1981) as generating ~ 0.1 e^-/pixel/second of integration (or ~ 0.007 ADU/pixel/second assuming a transformation of 1 ADU = 15 e^-). Although the quoted value seems very small, it must be remembered that this is a global mean estimate - there are regions of the frame considerably more

affected by the effects of dark current than others - and that the present observations relied on the acquisition of images over relatively long exposure times.

Therefore this effect has to be allowed for. The normal procedure (and the one adopted here) is to integrate "on the chip", without opening the shutter, for as long as reasonably possible and then read out the CCD in the normal way. Two such "dark frames" were taken (one of 3000 secs and one of 5000 secs, both during run 2). They were bias subtracted and then co-added. The interpolation routine was again used to remove all cosmic-ray events and also the single bad column (number 142) from the final image before the latter was normalised to a mean frame of 1 sec duration. Removal of the former is a process of some importance in a paired frame of such long exposure time.

Again, structure was evident, particularly around the edges of the frame and in the lower left-hand corner - the latter almost certainly resulting from the effects of "diffusion luminescence". However, analysis indicated that the expected contribution from the dark current in a single 1000 sec. exposure image frame was no more than ~ 10 ADU (or less than 8 % of the bias level), in very good agreement with the expected value quoted previously.

The dark current was subtracted from each image frame as, being extended objects, most galaxies are of sufficient dimensions to be affected (albeit very slightly) by these edge effects. No correction was, however, made to those of the standard stars. The typical exposure times of the latter were much less and the objects of

interest were centred on the CCD where the effects of such dark current corrections are minimal.

II.2.3 Flat-fielding

In the sense that the CCD can be viewed as an array of individual detectors (pixels), any differences in the operating characteristics of each pixel will lead to global response non-uniformities across the device. The procedure adopted in an attempt to remove this effect is called flat-fielding. The differences from pixel-to-pixel most commonly arise from imperfections introduced during the manufacturing process such as variations in pixel size across the array (Mackay, 1986), although quantum efficiency changes (i.e. differences in the ratio of output electrons to input photons) between pixels are also a contributing factor. At relatively low charge levels an additional feature becomes important in this context, namely "deferred charge". This effect, describing non-uniformities between columns of pixels over the CCD, manifests itself as a threshold charge level below which any input charge to a particular pixel (or set thereof) either fails to be detected or is registered in a completely non-linear fashion. Baum et al (1981) present a detailed description of how one might attempt to model this effect in astronomical observations. In essence it is yet another manifestation of the CTE mentioned previously and as such its effect, like that of the CTE, is most often countered by adding additional charge to the device (the so-called "fat zero") before reading out. However, this technique can be questioned in that the associated shot-noise on such an input charge only serves to increase the read-out noise already present. No such "fat zero" was applied to any frames obtained in the present

study, and as a result longer exposures were required when taking flat-fields on the sky to ensure that there was enough charge generated to overcome the threshold level of the particular pixels or pixel columns most affected.

The mapping of pixel-to-pixel non-uniformities is made more difficult because the effects are strongly wavelength dependant - the absorption coefficient of silicon itself being a strong function of the wavelength of the incoming photons. Since the longer wavelength photons penetrate more deeply into the substrate, they are more likely to be affected by such non-uniformities than are shorter wavelength photons. Although this is clearly not an important factor in narrow-band imaging, it is certainly so for the wide-band filters used throughout the present observations.

To remove any residual flat-field curvature across the object frames in question, both dome and twilight sky flat-fields were obtained. It is critical to ensure that such frames are taken through the same imaging optics as the object frames since vignetting and distortions within the telescope are additional contributors to such curvature together with the pixel non-uniformities detailed above. Two separate dome flats were derived in each colour using an illuminated white screen which, being out-of-focus, produces (hopefully) uniform illumination across the CCD. For run 2, sky flats were routinely obtained at the start and end of each nights observing (with typically 3 in each band at any one time), whilst those of run 1 were taken throughout the night. They were taken in regions of the sky known to be devoid of any moderately bright stars and galaxies using a list of field centres made available by the AAO, thus making it

unnecessary to interpolate the pixel response at any position across the CCD.

Each flat-field frame was both bias and dark current subtracted (the latter being achieved by using a mean frame described previously and suitably scaled to match the exposure time of the flat-field). Extensive analysis of the structure of the flat-fields in each colour showed no variation from one set to the next (i.e. from the start to the end of the night or from night-to-night) so they were all scaled by their respective exposure times and then co-added to produce "master" B and R flat-fields for that particular run. It is, however, notable that considerable changes in the uniformity of the flat-field were evident between runs, and hence a "master" frame applicable to observations for both runs could not be constructed. Any defects such as cosmic-rays etc. were removed at this stage and the average pixel value determined. Each "master" was then normalised by this average count (the bad column being removed previously to, once again, ensure such a normalised frame more closely centres on a mean of 1.0).

The resulting flat-fields show considerable structure, both in the sense of curvature at the edges of the frame (not unlike that seen in the dark frames) together with the effects of out-of-focus dust particles across the field, a fact that is clearly evident in figure 2.2 which shows mean row slices (averaged down each column of the chip) across both B and R sky flat-fields. As anticipated, these effects were more prominent in the R band than in B (the maximum peak-to-peak intensity variations are ~ 3 % of the local "background" level in the former, but only ~ 1 % in the latter). Note, however, that despite

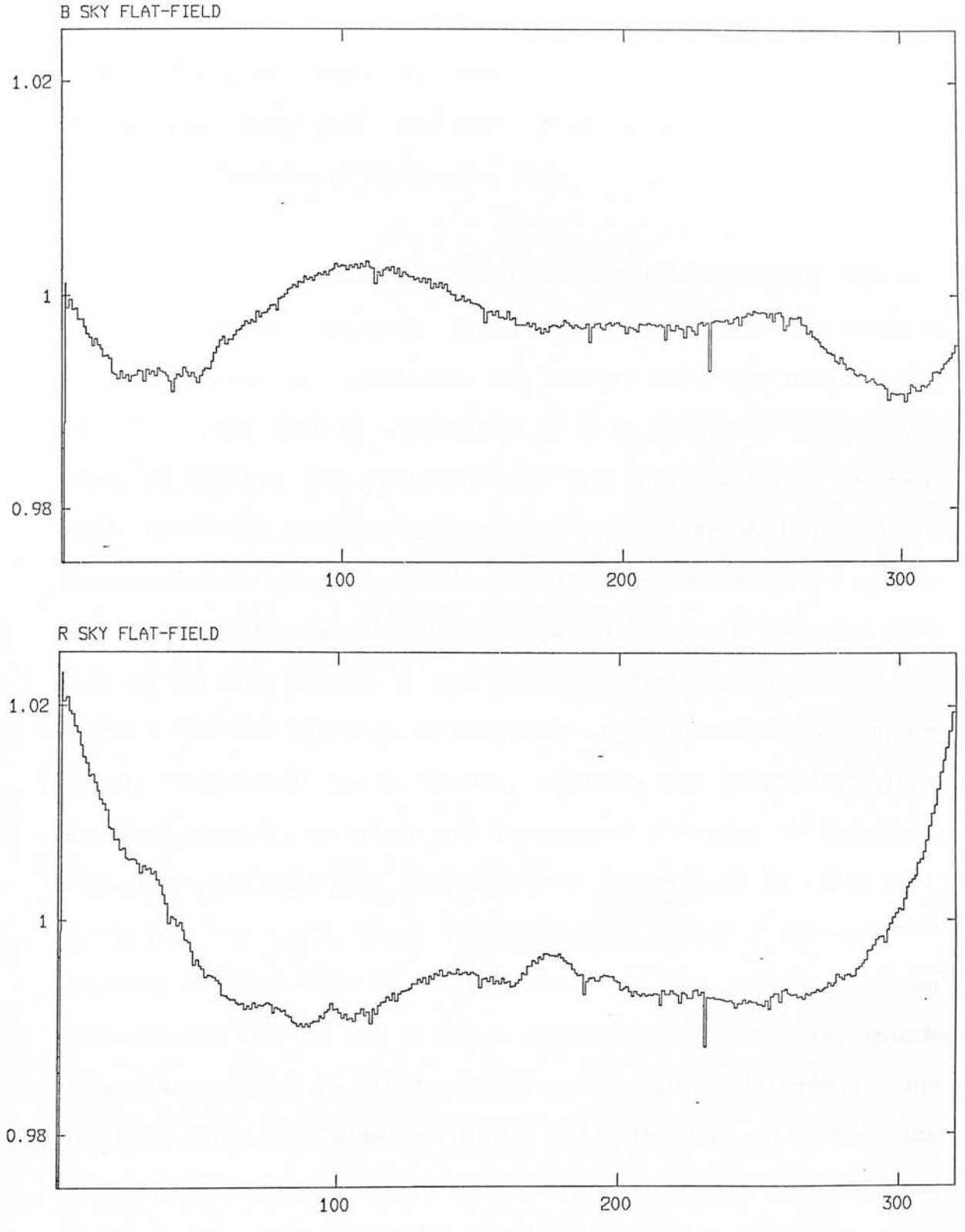

Figure 2.2 : Slices taken across the final averaged sky flat-field calibration frames (after normalisation) for run 2 in both B and R bands. These averaged slices were formed as in figure 2.1, and again the vertical axes refer to counts in ADU's and the horizontal axes to the slice length across the col. in pixels.

similar structure appearing in the average flat-field and dark frames, flat-fielding of the image frames in general would not remove structure resulting from the effects of dark current as the former are generally very short exposures while the strength of the dark current is a function of integration time.

Subsequent experimentation indicated that considerable residual structure remained in those images flat-fielded using the average dome flats, structure which was not evident when the relevant sky flats were used. This is particularly so in B, figure 2.3 showing the result of dividing the normalised sky and dome flat-fields in each band. The effect probably arises as a result of spectral differences between frames taken on the sky and those on the dome, or equally from the fact that the illumination from the screen is different from that of the sky because of non-uniform reflection from the diffuse surface. The sky spectrum is comprised of an underlying continuum (almost exclusively so at shorter wavelengths) originating from scattered sunlight, on which are superposed a number of prominent atmospheric emission lines (particularly in the red), all of which vary throughout the night. These features almost certainly preclude the matching of dome flats to the sky spectrum. This will be the case even allowing for the use of filters to match the shorter wavelength range as proposed by Wright (1982) in his improved procedure for obtaining such flat-fields. An added difficulty also arises from the fact that, for extended objects such as those observed here, one has to allow for colour variations across each frame depending upon whether the sky or the galaxy light was more dominant (the latter being considerably redder than the former). As a result, the dome flats were subsequently discarded and only those taken on the sky

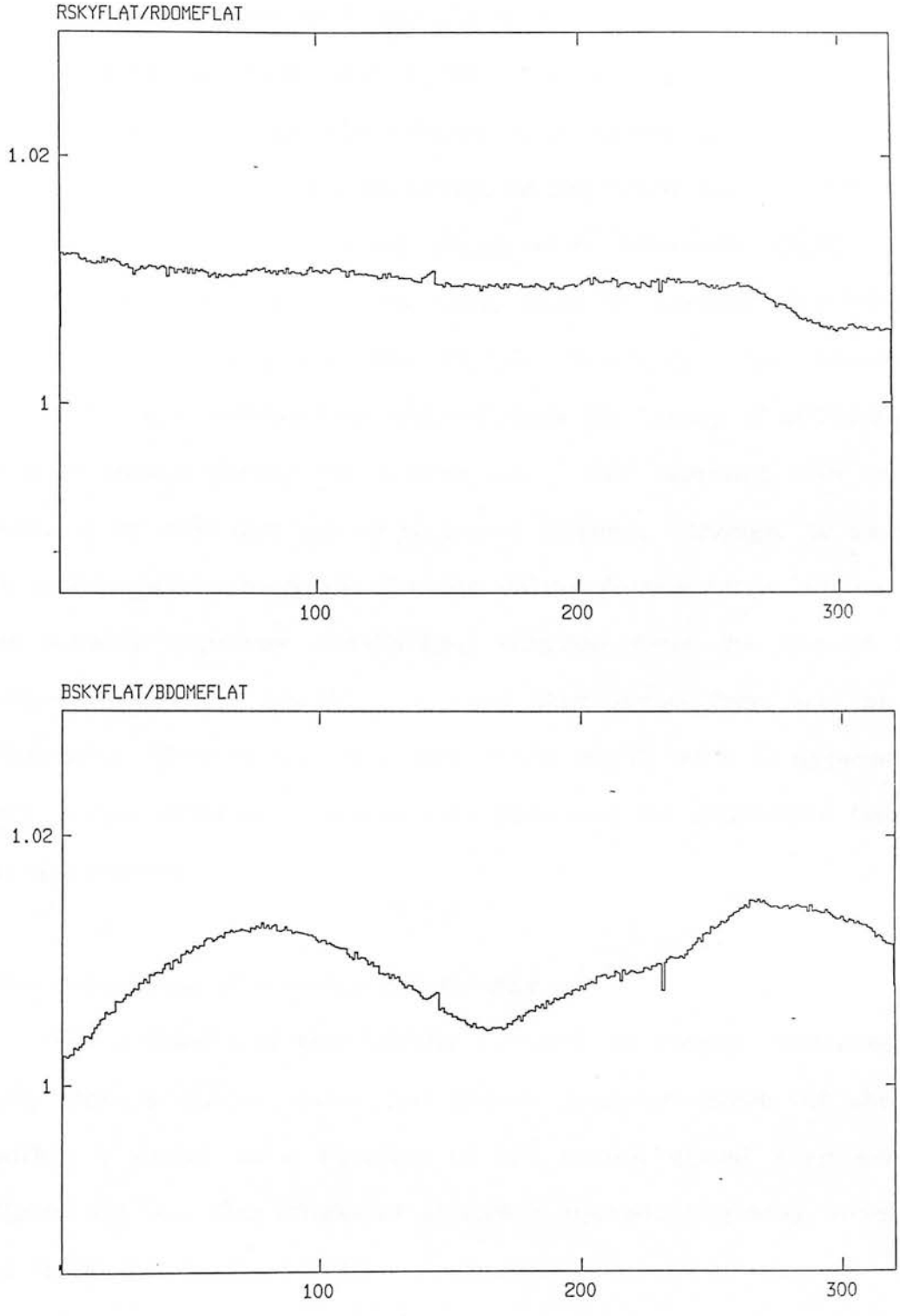

Figure 2.3 : Averaged slices (formed as in figures 2.1 and 2.2) but now across the respective B and R band sky flat-field frames after division by the corresponding dome flats. The axes are as previously.

used in further analysis.

It is noted here that sky flat-fields obtained at the very start and end of the night also suffer from spectral mismatch with the image frames subsequently obtained (the former are considerably too blue). However, the great advantage of flat-fields taken at this time is that one can obtain a good signal over relatively short exposure times, which is clearly not the case if median flat-fields are accumulated throughout the nights observing. The considerable pressure on observing time did not allow the luxury of obtaining such median frames during the second run - this mismatch still exists in most of my data and has to be borne in mind, although its magnitude is anticipated to be small. For the galaxy frames taken during run 1 no notably improved flat-fielding resulted from the use of frames taken during the nights observing than arose from use of those flat-fields taken at the very end of the night, so it is apparent that any colour differences between my data and the respective flat-fields is quite small.

The importance of accurate flat-fielding :

The necessity of flat-fielding correctly is clearly evidenced when one plots a curve, called the photon transfer curve, of the noise within a device as a function of the output signal - as shown in figure 2.4 (see also Blouke et al (1981); Djorgovski (1984); Janesick et al (1984) and Mackay (1986)).

This curve illustrates the particular regimes of signal over which the expected noise contributors are expected to dominate. As previously described, the read-out noise defines the limiting

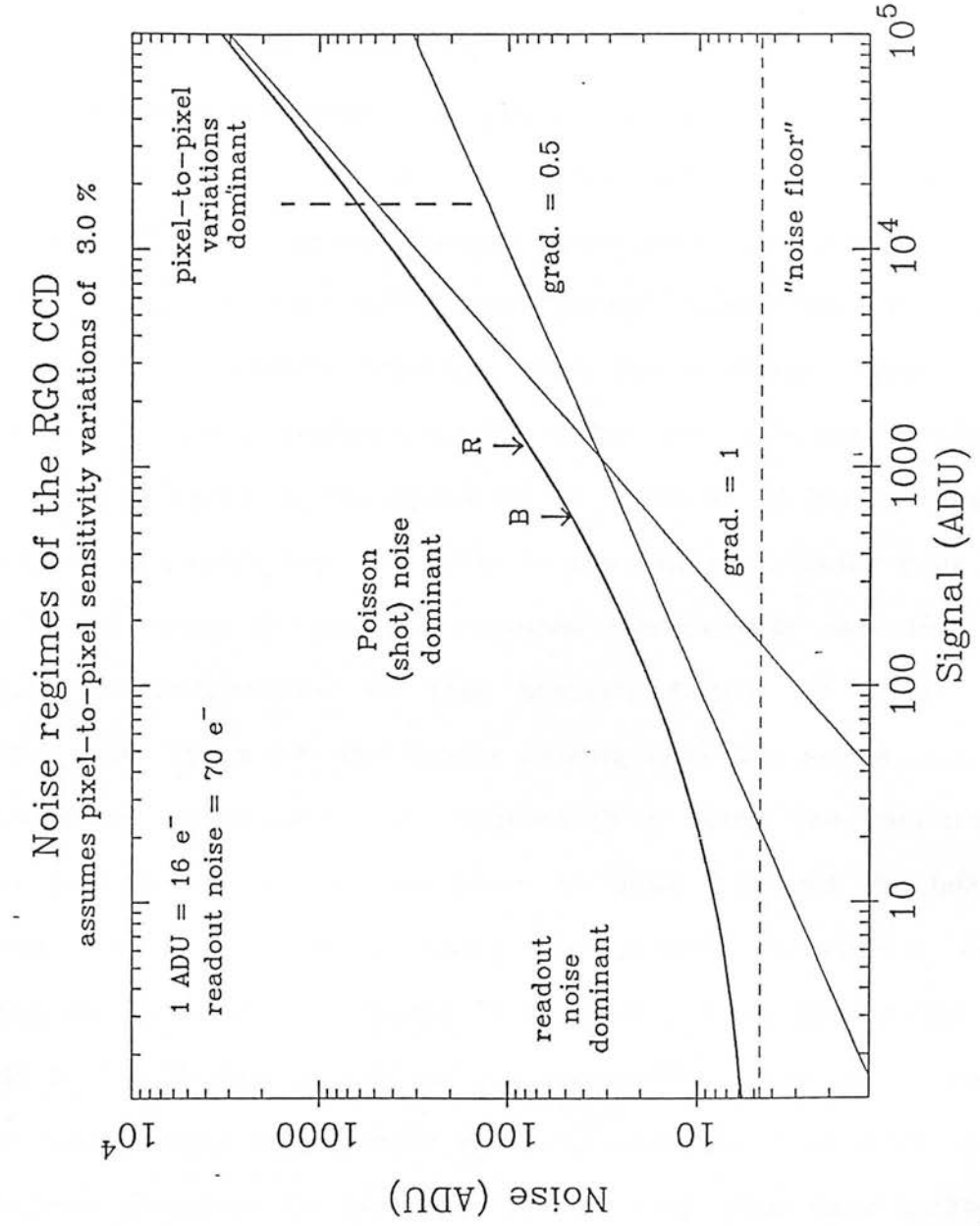

Figure 2.4 : Photon Transfer curve for the RGO CCD based on the assumption of variations across the chip ~ 3.0 % of the adopted sky level (i.e. before flat-fielding and de-fringing). The regions over which each contributor to the overall noise of the system (thick solid line) is most prominant are broadly indicated. The "noise floor" is set by the read-out noise of the chip; the shot-noise gives rise to a line of slope 1/2; and the sensitivity changes to one varying linearly with signal. The vertical dashed line at a count of 16 383 ADU represents the saturation level of the A/D converter (and thus sets the dynamic range of the device at ~ 3700). The arrows (marked B and R) refer to the minimum counts obtained on the sky in the galaxy frames taken in the B and R bands respectively (full-well capacity being taken as a rough upper limit in all cases). For comparison, the standard star frames have counts upwards of ~ 95 ADU (B) and ~ 150 ADU (R), but are well short of saturation.

performance of the device at low light levels (70 e^- in the case of the CCD used here), whilst at intermediate signal levels the shot-noise becomes dominant - this factor having a gradient of ½ because the noise is here simply proportional to the square root of the signal (or number of incident photons). At the highest signal levels, however (and before saturation effects become important), the pixel-to-pixel sensitivity variations (also called the "scene" noise) are dominant. Since the shot-noise results from the Poissonian statistics inherent in any detector employing photon counting techniques, it is the idealised absolute limiting factor to the operation of CCD's at all higher signal values. Thus, to ensure that the latter is the sole contributor over as large a signal range as possible requires considerable reduction in the pixel non-uniformities. In this context, figure 2.4 is to be contrasted with figure 2.5, the former arising from the assumption of no flat-fielding corrections being applied (3 % being the variations typically seen in the R band as given in table 2.1) and the latter after appropriate flat-fielding using the present techniques and indicating improvement of a factor of 3. Clearly even the ability to flat-field to ~ 1 % greatly reduces the contribution from the "scene" noise at intermediate count rates routinely obtained here such that one is almost always in the ideal position of being "shot-noise limited" - certainly up to signal values ~ 10^4 ADU. This is certainly not the case in figure 2.4 in which the turnover point occurs at roughly an order-of-magnitude lower signal level.

II.2.4 De-fringing

In an attempt to improve blue response and enhance quantum efficiency in the present CCD, it is illuminated from the back (i.e.

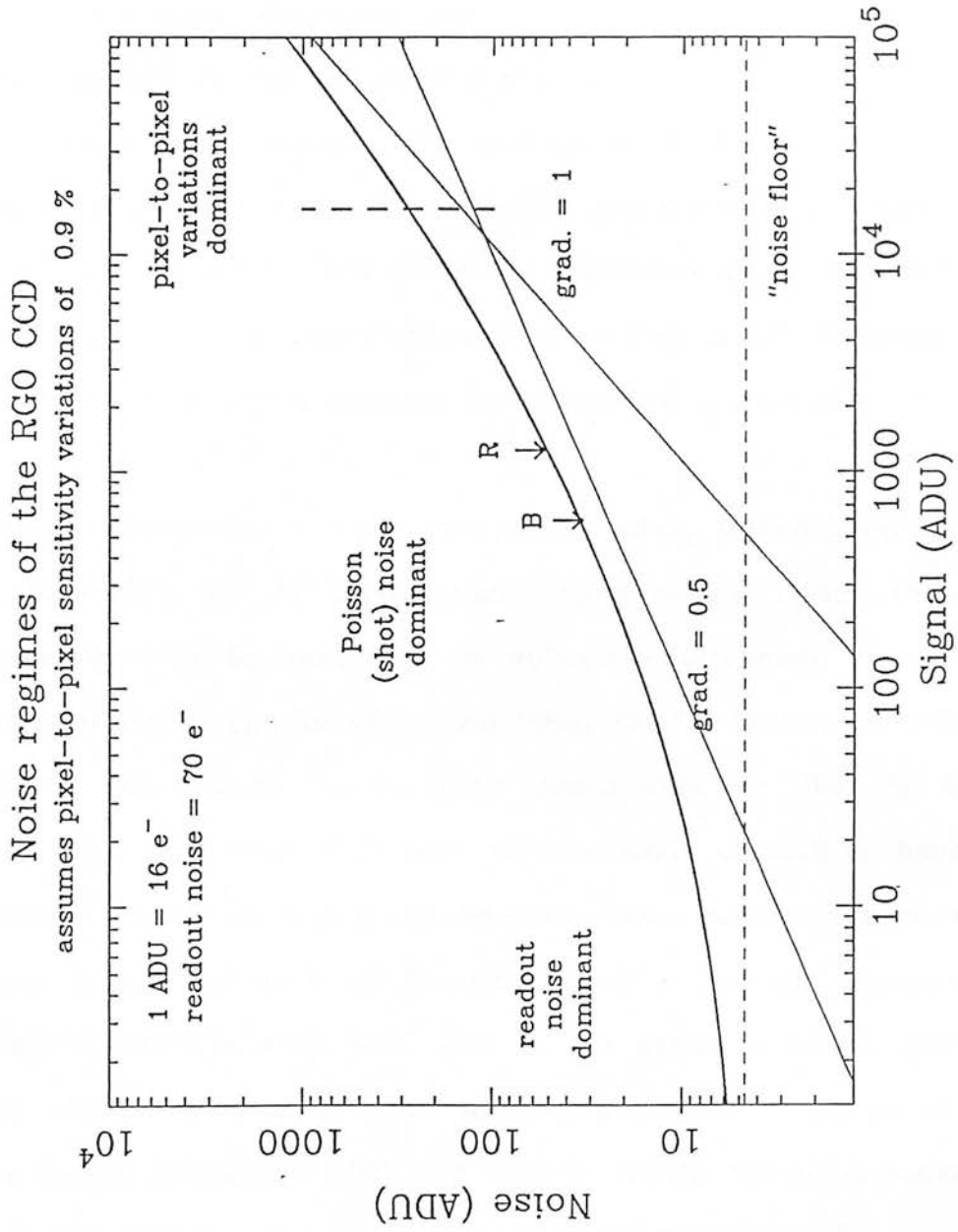

Figure 2.5 : As figure 2.4 but assuming the procedures of flat-fielding and de-fringing reduce the pixel-to-pixel non-uniformities to a level ~ 0.9 %

through the surface beneath the electrodes) since such a procedure is designed to prevent absorption of these short wavelength photons within the electrode structure itself. However, to ensure that the incoming photons do not travel too far into the silicon (a process which would greatly degrade the resolution of the device at that wavelength and would make determination and removal of cosmic-ray events almost impossible), the substrate layer has to be considerably thinned. This technique is an alternative to that of UV flooding (see Janesick et al (1984) for a detailed description of the latter).

Because silicon has a high refractive index, internal reflections within the device will be commonplace. As a result, if the thinning process gives rise to variations in substrate thickness across the chip, as it almost certainly will, then "thin film" interference fringes will result over those wavelengths comparable to the Si layer thickness (i.e. in V and at longer wavelengths) if such a band is contaminated by strong night sky emission lines. Fortunately no such prominent lines occur in B so fringing is not a problem. However, a considerable effect is seen in R due to the presence of OI emission lines at λ5577, λ6300 and λ6364 A, together with a series of OH emission bands between ~ 6000 and 7000 A, within the most sensitive region of the CCD (i.e. a peak in the convolution between the quantum efficiency and the filter response). My experience indicated that the problem of fringing is at least as significant as that of flat-field variations, and is indeed more so over certain regions of the chip. Figure 2.6 illustrates the relevant fringe pattern in R for the device used here, as derived from a co-add of two individual R band fringe frames (each of 500 secs exposure) obtained during the first night of run 1. The field chosen for this purpose was, in 1950 coordinates, α =

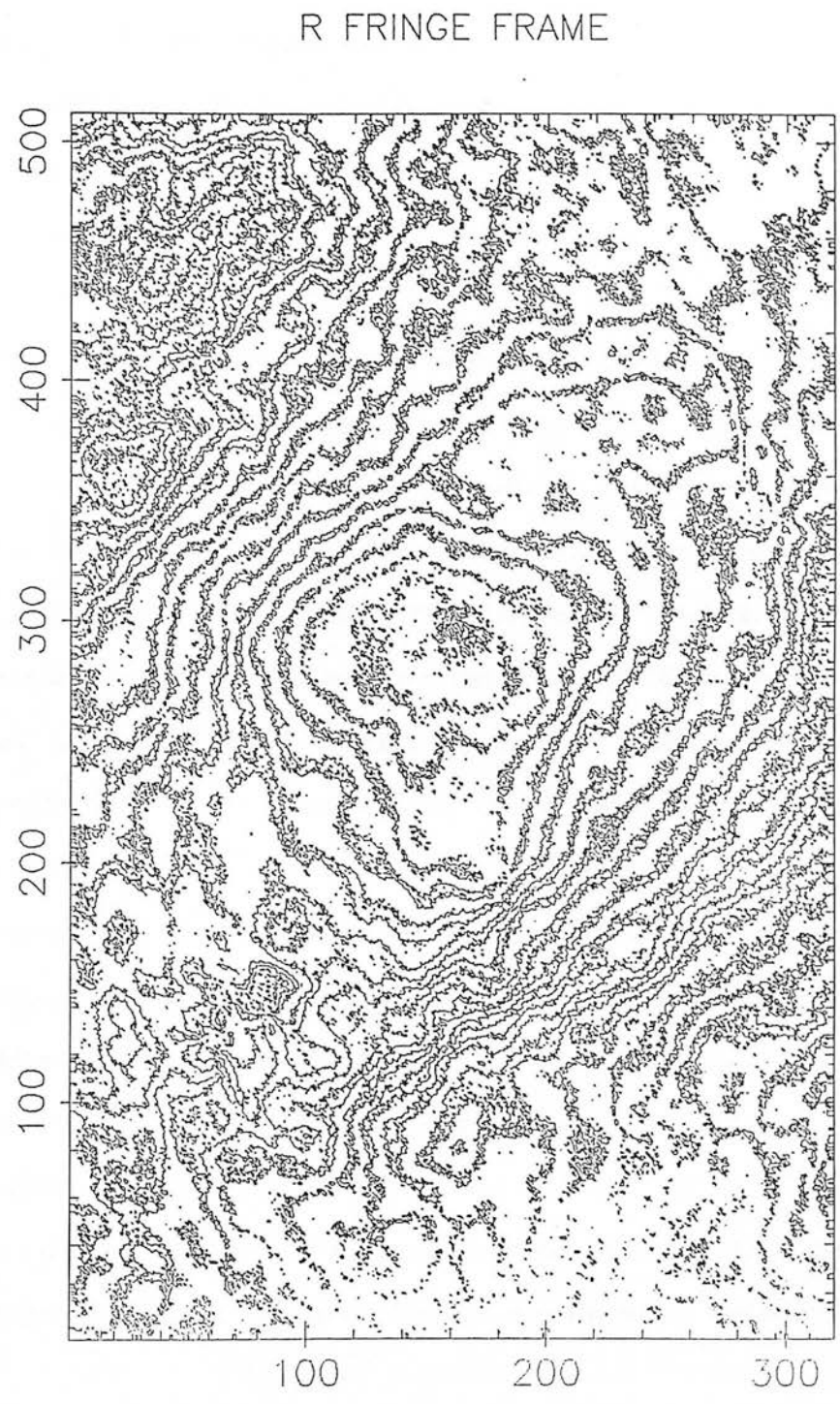

Figure 2.6 : A contour plot of the adopted mean R band fringe frame for both runs after removal of the bias level, flat-fielding and de-glitching. The 5 contour levels are linear in intensity, and are set at +12 %, -4 % of the mean value for the whole frame. The labelled (X,Y) axes are in units of pixels.

$11^h\ 07^m\ 06^s$, $\delta = -77^o\ 05'\ 54''$ as it was known to be sufficiently free from stars and galaxies that subsequent removal of such images was unnecessary. These frames were debiased, flat-fielded and any cosmic-rays/CCD defects were removed as described previously. They were then co-added and the mean frame normalised by the average count in that frame.

Analysis indicates that, in a region of high concentration, the maximum (peak-to-peak) amplitude of a particular fringe is ~ 4 % of the mean sky level for that frame (with a typical measure ~ 2 %), whilst for regions of "average" concentration the respective values are ~ 3 % (maximum amplitude) with a mean of ~ 1.5 %. These values are in accord with the preliminary estimate for this device made by Jorden et al (1982). As a result, to ensure reliable results in the galaxy photometry such an effect had to be taken into account.

A comparison of the structure of this normalised fringe frame to the average made available by the AAO (one built up from a number of individual frames taken over a considerable time span) indicated no differences in pattern between the two. Use of my fringe frame for observations in the R band throughout the second run is therefore expected to be valid. This was proved to be the case after considerable testing of the use of such a calibration frame.

The fringes are an additive signal in intensity, and the procedure used for their removal from each R frame either took the form of a global subtraction of the normalised fringe frame from that of the image, or via the standard routine FRINGE which uses a pre-defined region of the image frame - one free from stars but

containing an intense area of fringing - to determine the multiplicative factor required to scale the fringes between the two frames, the suitably scaled calibration frame then being subtracted from that of the image. This scaling factor is proportional to the ratio of the exposure times between the respective frames, and also differences in the sky emission line intensity, thus in the present case it has a value very close to 1.0 (the two independant methods therefore yielding equivalent results).

The continual offsetting of image frames between exposures as described above considerably improved the reliability of the fringe removal process to the point where detailed visual inspection showed no residual fringes across almost all the R frames taken (see table 2.1).

II.3 Reduction procedures

II.3.1 Colour co-adding

After having suitably cleaned the individual frames, one was then in a position to combine each set for a particular object that were initially offset by the ~ 5 arcsec (RA, dec.) shifts noted previously. In the case of the galaxy frames this typically meant the addition of 2x1000 secs exposures for each position in each colour on the object concerned, with up to 4 individual frames being co-added for the standards.

The general procedure for co-adding of a pair of frames was firstly to define which image was to be used as the reference (usually

the deepest of the two was chosen for this purpose). Then approximately 6 fiducial stars common to both images, and distributed roughly evenly across the field, were chosen from the reference frame. A Gaussian fitting routine was then applied to each star to translate approximate (x,y) positions into centroid estimates typically accurate to ~ 1/10 pixel. This was achieved by an iterative process which fitted a 2D Gaussian profile (along the X,Y axis slices) to each star. However, as it was of some importance to minimise any discrepancies which may arise from differences between such a model luminosity profile and the true shape (more accurately approximated by a Lorentzian), each fiducial star was specifically chosen to be bright but not saturated. A least-squares linear transformation was then run to map the second frame to the reference on the basis of these accurate positions, giving a typical rms alignment error between the frames of ~ 0.03 (± 0.01) pixels. The "resampled" image was then co-added to the original to produce the final pair.

Such a procedure has the effect of reducing the random statistical fluctuations across the CCD frame by a factor ~ 2. For example, a single slice across a frame of standard stars obtained on the first night of run 2 reveals typical scatter (peak-to-peak) about an adopted sky value ~ 1.5 % for a single B frame of 100 secs exposure, but of ~ 0.9 % in the co-added 200 secs frame. The equivalent analysis in the case of the R frame shows scatter ~ 1.6 % before and ~ 0.6 % after co-adding.

II.3.2 Extinction corrections

(i) Atmospheric :

Corrections due to airmass effects have been applied to all available data used in this study. The simple form

$$A = C \sec Z \quad \text{mags.} \qquad (1)$$

where, C = constant, and

Z = zenith distance (degrees)

has been used. No significant differences were found when adopting alternative forms, such as those of Young (1974) or Golay (1974), which impose higher order terms on this equation.

Measures of the constant C to be applied to the B band was derived from the value quoted in the UKSTU handbook (1983) for the Siding Spring site. That appropriate to the R band was kindly provided by M. Bessell (private communication, 1986). These values are in agreement with the (suitably scaled) measures over the same wavelength ranges as given in the ESO users manual (1981), and are 0.27 mag. (C_B) and 0.13 mag. (C_R).

An indication of how reliable are the finally derived estimates of airmass corrections from equation (1) comes from a comparison of the values from a number of CCD frames taken of a set of standards in a particular colour. In no cases were the differences found to be more than 0.01 magnitudes and in most cases they were identical to $\lesssim$ 1/100 of a magnitude. This is what one might expect since less than 25 % of all the CCD object frames were taken with zenith distances in excess of 40° (and all had $Z \lesssim 50°$). This is, however, rather a measure of

internal consistency than of absolute accuracy since the adopted airmass constants are unlikely to be accurate to much better than ~ ±0.03 magnitude.

(ii) Galactic :

A variety of means exist for deriving the extinction variations in extra-galactic objects as a result of obscuration along the line-of-sight from within our own Galaxy.

The HI maps of Burstein & Heiles (1982) clearly indicate the distribution of such obscuring material to be highly irregular at all galactic latitudes - sufficiently so that numerical relations of any form, however complex, are at best likely to be simplifications of the effects of reddening. This was confirmed by comparing the estimates for those (8) galaxies observed here and listed in Burstein & Heiles (1984, and thus based on their HI maps) to those values calculated on the basis of the equations given in the RC2. [The coefficients given for the latter are in error, the correct figures being given in appendix C of de Vaucouleurs & Buta (1983).] The results of such a comparison indicate that the RC2 extinction values are always larger. It is not anticipated, however, that any improvement over the estimates derived from the RC2 would result from the use of any alternative extinction relation (such as those of Sandage (1973) or Heiles (1976)).

As a result of these shortcomings in the use of functional relations, I have adopted a combination of the HI maps of Burstein & Heiles (1982) and the list of Burstein & Heiles (1984) to derive the galactic absorption coefficients presented in column 4 of table 2.2.

Such estimates are anticipated to have associated errors of ~ ± 0.06 mag. or ~ 10 % of the calculated extinction (whichever is the larger) based on the expectations of Burstein & Heiles (1982).

II.3.3 Removal of contaminating bright stars

An unfortunate feature of a small number of the sample objects observed was that they suffered from the superposition of bright stars within the field of the CCD. Because such stars have a pronounced effect on the resulting surface brightness profiles generated at that particular position on the galaxy, their effect has to be accounted for.

One possible method is simply to ignore the particular region of the galaxy most affected by such stars. However, this procedure was deemed unsuitable in the present study : it is often difficult to define exactly the extent to which the galaxian isophotes are actually affected (particularly resulting from the faint stellar haloes arising from the internal reflections within the telescope itself) so that removal of a particular region may not completely allow for isophote distortion due to the star. Equally, removing a full quadrant of the galaxy isophotes from further analysis (and thus erring on the side of caution) is often very wasteful in terms of discarded data which is completely unaffected by the star (thereby reducing the available S/N when the individual profiles are co-added).

Two alternative procedures were tested here. In the first, a comparable frame was created for each object frame in question but containing a single bright star centred on the position of that star to

be removed. The amplitude of the two stellar profiles were matched by a simple scaling factor and the two frames then subtracted. However, this procedure has a number of undesirable features. It cannot, for example, easily be used to remove contaminating stars which are saturated (as the stellar profiles have to be matched in their wings rather than by using their peak intensities). Equally serious is the added noise one introduces by subtraction of the two images. In view of the care with which such noise was reduced using the methods outlined previously this was deemed to be a particularly unwelcome aspect of the procedure. A further problem results from the considerable effort involved in removing a single star from each contaminated image frame.

The second scheme was similar to that used by Carter (1977) in that a region around the interfering star was defined, and a low order polynomial fit to the area in an annulus surrounding the region of interest was used to "extrapolate" across the star. This has the considerable advantage that, through the interactive nature of the procedure, the effects of the faint haloes to stellar images can be accounted for. In addition, the polynomial routine should, in principle at least, be able to allow for variations in "background" over the region of the frame specified even if the star is found on an area having a strongly varying underlying sky level. The subtraction process is also achieved relatively quickly. It can, or course, be criticised in that it introduces "artificial" data to the resultant surface brightness profiles. However, in all the situations noted here for which a bright star removal algorithm of some form was required, the percentage of galaxy affected was sufficiently small that such a problem was not thought to be of great concern. For these reasons, it

was decided that the iterative removal routine be adopted in all cases. It is notable that such a method would also have to be adopted even if one were to use a scheme which clips data at standard deviations larger than a certain pre-specified level above the locally defined mean, since the latter procedure would also be unable to allow for the effects of the fainter stellar haloes noted previously.

The star removal method was monitored at each step by the use of both contour and 3D plots in addition to slices taken across affected areas. Figure 2.7 illustrates their use in the study of a small region of the R band frame of the galaxy A0902-68 during the removal process. An interactive scheme making use of the TV monitor was also adopted throughout to test the quality of the process.

Finally, any contamination resulting from "bleeding" of charge along columns from saturated stars was corrected for by invoking the same interpolation routine which was previously used.

II.3.4 Mosaicing of the frames

The first adopted method for subsequently "mosaicing" those frames taken at selected positions across the objects of interest was simply an extension of that used to co-add the offset frames as described in section II.3.1 above. A region of sky common to both frames to be paired was selected and a simple scaling factor evaluated to bring the overall intensity distribution from one region into agreement with that of the other. Such a region was chosen to include at least part of the galaxy concerned thus sampling a large

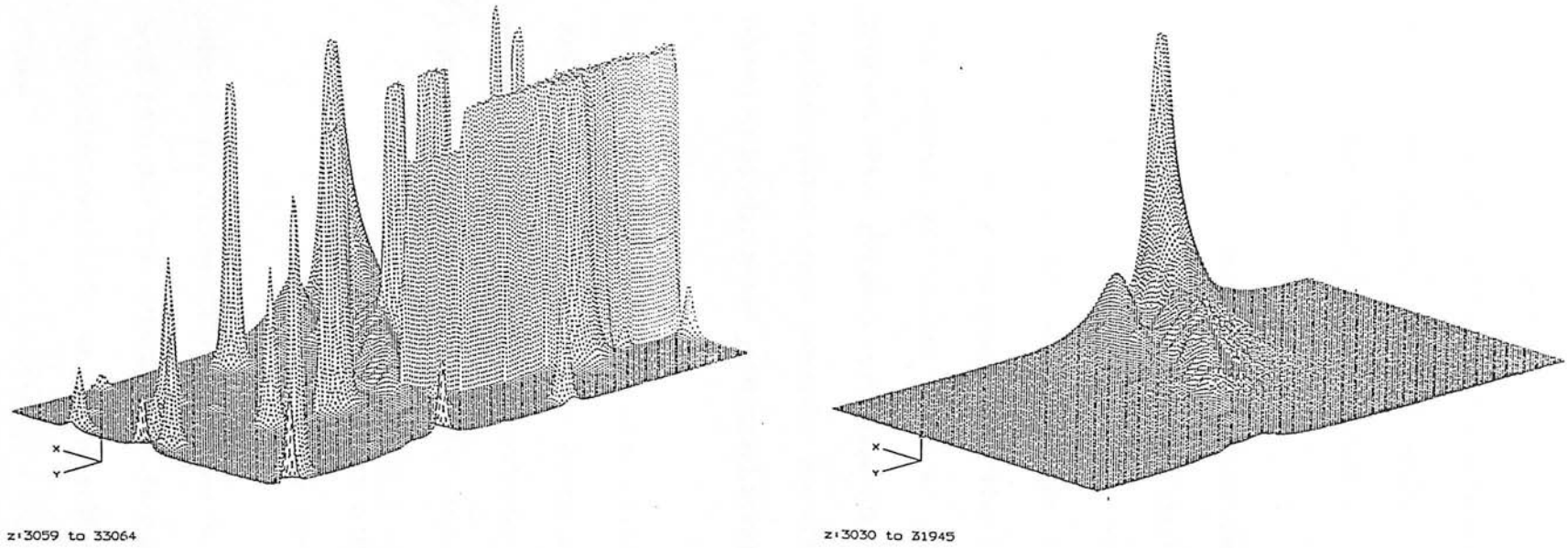

Figure 2.7 : A series of 3-D plots for a subregion of the R band frame of the galaxy A0902-68 before and after application of the bright star removal process. The interpolation routine described in the text was used.

dynamic range when determining this factor. The scaling was then applied to the whole frame concerned. Offsets between frames were defined as above, and the frames were then merged together to form the "mosaic" across each object.

However, such a procedure failed to match up the respective (brighter) isophotes in the frames - giving rise to a step in the levels at the boundary of the overlap region (although the outer contours close to the sky were well matched in most cases). This probably arose because both the atmospheric transparency and also the overall sky value changed between the aquisition of the two frames. The present process, in defining the scaling factor as a multiplicative term, corrects for the former but does not allow for changes in the night sky brightness.

As a result, an alternative algorithm was adopted. The methodology behind this is based on the fact that the observed and actual intensities of a particular object can be related via the respective sky values and the atmospheric transmission thus

$$I1 = A1 \times I0 + B1$$

$$I2 = A2 \times I0 + B2$$

where (I1, I2) are the measured intensities ; (B1, B2) the sky values and (A1, A2) the atmospheric transparencies in the two frames. I0 is the actual intensity in the specified pixel from the object concerned. Thus,

$$I2 = (A2/A1)(I1 - B1) + B2$$

A plot of the intensities in a certain region of each frame common to them both (setting B1 = 0 for convenience) gives the ratio of the

transmission values from one measure to the next, with the intercept giving the sky value in the second frame. Thus scaling frame 1 by both gradient and intercept should allow a direct comparison between the respective images, and thereby improve the reliability of the "mosaic" process. It is assumed in the above, of course, that the sky value is independant of any transparency variations between frames. However, this is expected to be the case, almost all objects having been observed at the same airmass.

As a test of the validity of such a procedure, 3 differing regions were taken for each pair of frames to be averaged. The generated best-fit gradients and intercepts were found to be in very good agreement between each region, weighted means being taken for the adopted gradient and arithmetic means for the intercepts (the errors in the latter are too poorly defined for one to adopt weighted means in such cases). The best-fits are visual rather than least-squares estimates since the latter would be heavily biased by any spurious points. Trimming away these points would, however, tend to introduce a pre-defined quality to the fits. The relations are always sufficiently tight that such a procedure does not introduce much of an error.

Typically the central frame was used as reference, and the suitably scaled additional frames were then "mosaiced" to this. The results of such a process proved very satisfactory in all except two cases. A problem arose in the case of NGC 3115 from the fact that the frames of this galaxy standard were of varying exposure times. They were, therefore, all scaled to the exposure time of the deepest frame (500 secs) before the above procedure was adopted. The results after adopting such scalings were excellent. Observations of IC 2531,

however, suffered from the fact that individual sets of frames for the different positions were taken during separate runs. As a result, my assumption of the sky brightness value being independent of atmospheric effects is no longer valid.

Allowing for this added complication gives, using the same notation as above,

$$I2 = (A2/A1)I1 + A2(B2 - B1)$$

Thus, the translation coefficients between the respective frames in this object are defined exactly as previously. There was, however, an added difficulty which resulted from the fact that the dewar had been slightly changed in orientation between the two runs, thereby giving rise to a slight rotational offset between the outer two frames and the central one. The effect was calculated and taken out of the data using an identical least-squares transformation algorithm to that adopted in the co-adding described in section II.3.1 above. Again, after close inspection, the "mosaicing" process was found to give excellent results.

II.3.5 Frame rotations

To facilitate ease of extraction of the surface brightness profiles in a particular galaxy, it was decided to rotate the frames such that each object was horizontal. This was facilitated using a specifically designed algorithm (ROTATE) which makes use of bi-linear interpolation to ensure an accurate mapping of data pixel-by-pixel during the rotation. Such mapping is achieved without creating gaps in the output array (due to the effects of real-to-integer truncation during the transformation) or through any loss of resolution which

would result if truncation forced data in two individual pixels within the original array to be binned into a single pixel in the final rotated frame.

The position angles used (given in table 1.1) were derived from inspection of contour plots of each "mosaiced" galaxy frame. These values were checked against those existing in the literature, such as from the ESO (Lauberts 1982) or UGC (Nilson 1973) catalogues, with an estimated discrepancy $\lesssim 2^{o}$ in all cases.

II.3.6 Sky flattening

Particularly evident in the (R band) composite frame of NGC 4289 were additional variations in the sky background across the frame over and above those already removed in the flat-fielding process (detailed in II.2.3 previously). The source of such variations are likely to be either heavy contamination by light from a nearby star located ~ 2.5 arcmins to the E or from the residual flat-field structure which the standard techniques were unable to correct for owing to the strongly varying background across these frames. Figure 2.8 (a) shows this original composite frame before flattening. The greyscale display levels are set at ±30 ADU (or ~ ±2 %) of the local sky background across the frame. No other object frames suffered from such an effect.

The method by which this residual signal was removed made use of standard techniques. This involved the removal of all stars, galaxies and defects from the frame concerned, followed by the definition of an exclusion zone around the object of interest outside

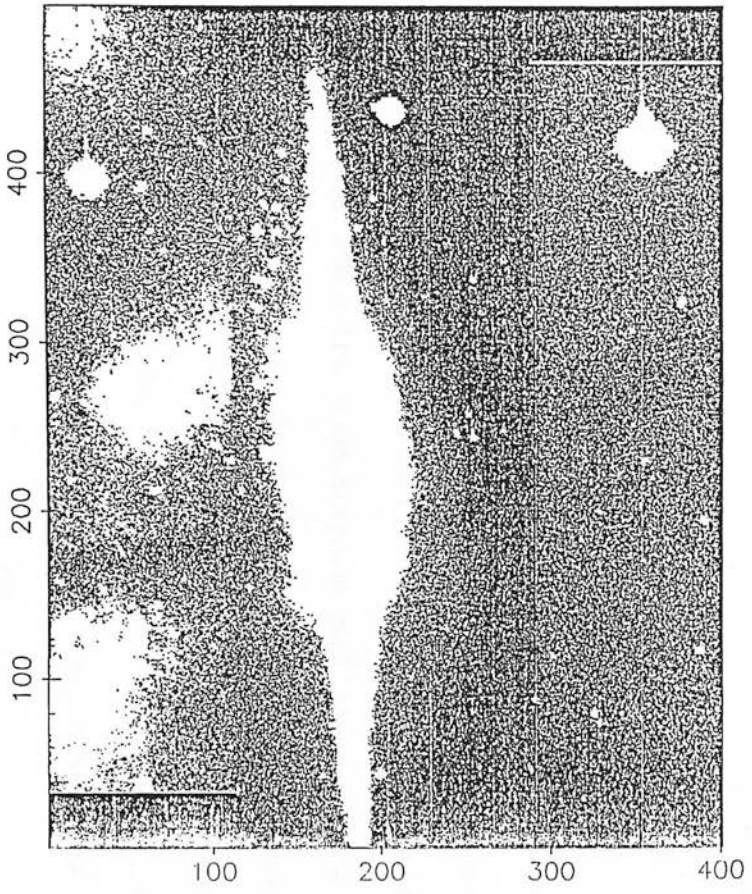

(a)

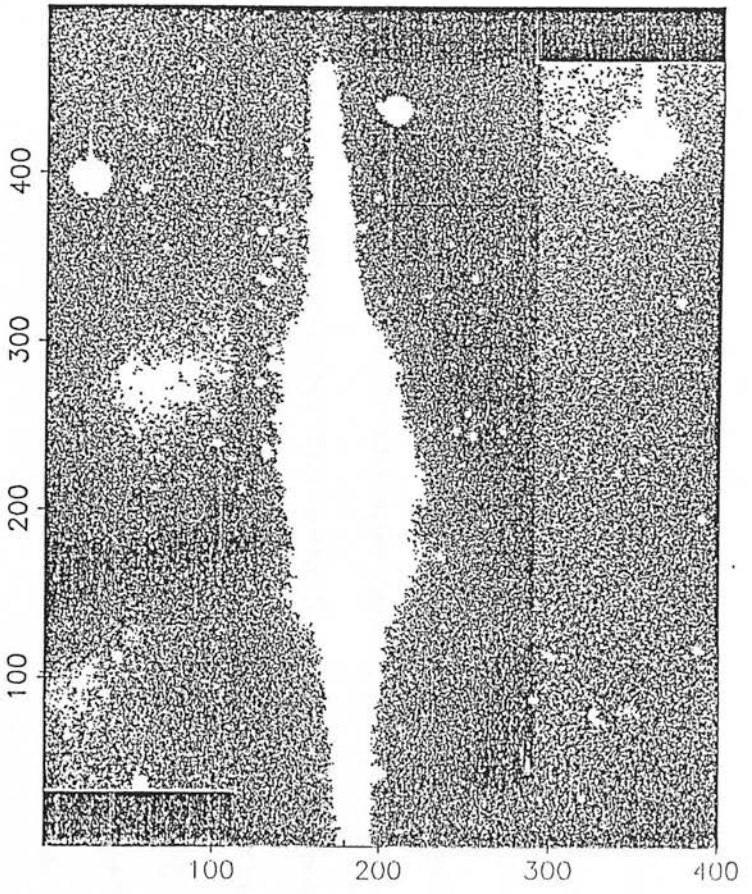

(b)

figure 2.8

which any sky estimate was considered to be free from contamination by light from the galaxy. A low order 2D polynomial was then fitted (by least-squares) over the region of the frame thus defined and was used to extrapolate "beneath" the galaxy itself. Since it is very important to ensure the reliability of such an extrapolation, great care was taken to examine the fit thus produced and thereby ensure that any fitted background smoothly varied over the region dominated by the galaxy. For this reason, the smallest order polynomial necessary to fit such variations was adopted. A third order was found to be optimal, as lower-order fits were found to leave considerable residual structure, whilst no improvement resulted from the use of a higher order than this. Figure 2.8 (b) shows the same R band frame as previously but after the application of such a procedure (note that the edge effects notable in this figure are due to the mosaicing process outlined above and are approximately ±1 % variations in the local sky background value).

II.3.7 Determination of sky

Sky determination using CCD's is one of the most difficult aspects to define, due in the main to the small areal coverage at prime focus. Previous studies have most often made use of sky frames taken both before and after the object frame and have thence assumed a simple extrapolation between the two. This is a very unreliable procedure, relying as it does so strongly on exposure time. For example, Jedrzjewski (1985) estimates an error in the sky determination ~ 5 % using such a procedure, for typical exposure times of only 60 to 100 secs. In view of the fact that the sky may change on the order of minutes, coupled with the correspondingly larger exposure times in

the present study, it was felt that a considerably larger error would result were such a procedure adopted in the present analysis.

An alternative is to use the edges or corners of a particular frame and take the lowest mean value as the most reasonable sky estimate. This method is an improvement on the previous one in the cases where the objects of moderate size are imaged, but it is clearly inapplicable where galaxies covering the whole field are being observed. For this reason I was very careful, when the observations were being acquired, to orientate the CCD in such a way as to maximise the sky content of each frame. With the sample objects being so edge-on this merely limits one to those positions for which the long axis of the CCD is as parallel as possible to the minor axis of the galaxy concerned. This enabled one to be confident that considerable areas of sky are obtained on every frame used.

Procedures to define the actual value for the sky abound. I have investigated two possible methods here. The first made use of a large number of slices taken across the frames of interest, chosen to traverse regions of each frame thought to be dominated by sky. A visual inspection of the graphical output was used to define regions in which contamination of the expected sky value was minimal and the mean of the counts from such areas of each slice were then used to define the sky along that portion of the frame. Investigation of the results of such a procedure on frames of IC 2531 indicates that one can expect accuracies in sky determination along any one slice of typically ~ 0.4 % in B and ~ 0.5 % in R, with slice-to-slice variations of roughly the same magnitude in each case. The only limitations of such a method result from one's need to define regions free from

galaxy and star contamination in the resulting cuts (at best a considerable uncertainty), and from the typical number of slices one would require to derive a reliable measure of the sky over the whole frame.

A second procedure follows the precepts adopted in the reduction of data generated using the COSMOS measuring machine. In such a method, a histogram of the intensities over a specified region of the frame of interest were generated. Because each one of the image frames are likely to be so spatially dominated by sky I took such a region to be the entire frame itself. An estimation of the modal value of the peak in such a (Poissonian) distribution, either visually or using least-squares fitting techniques, should yield a very accurate estimate of the sky level in that particular frame. Preliminary testing of this method was also carried out on the frames of IC 2531. By defining a series of regions across both B and R frames, it was found possible to estimate the sky value to an accuracy ~ 0.1 % in each subregion, although subsequent results implied that between subregions, a more realistic uncertainty was ~ 0.4 %. The similarity in my ability to define the sky level over the use of the previous method, coupled with the fact that the previous method has to be modified to avoid "non" sky regions (in the histogram method the dominant contribution is from sky such that this limitation does not apply) influenced the decision to adopt the latter as a means of determining the sky in the "mosaiced" frames. The values thus derived are given in column 8 of table 2.2 together with their associated uncertainties.

It is interesting to note that at 0.4 %, the estimated accuracy of the sky level determination on a particular frame is a factor of 2 smaller than the pixel-to-pixel sensitivity variations expected across any one portion of the frames (as defined above) after cleaning via the processes in section II.2 above. Such an accuracy translates to ~ 6 magnitudes faintward of sky.

As an aside, I have investigated if there is any significant difference between adoption of a single measure for the sky over results from the use of polynomial background fitting. In fact, no such improvements are found. Up to 4th order poynomials were tested, but a sky accurate to 0.1 % over the region of the particular frame investigated was found each time. It is thus considered justifiable to assume the sky to be flat over all the image frames obtained. Additionally, by correlating derived sky values in such a procedure with exposure time for the frames taken at relatively closely spaced time intervals, I conclude that the CCD is linear to ~ 0.1 %.

II.3.8 Binning factors and profile extraction

Some consideration also has to be given to the effects of convolving the present observations with the seeing profile. It was decided that, since final binning factors adopted to increase S/N were likely to be considerably in excess of the dimensions of the seeing disc, the only allowance for the latter would be to evaluate its magnitude on each "mosaiced" galaxy frame and subsequently compress the frame by that factor prior to later binning.

The seeing disc was evaluated by fitting a Gaussian profile across a number of pre-defined stars distributed randomly over the object frame of interest. The iterative fitting procedure thence defined a FWHM seeing measure (in pixels) for each star separately, and also for a "mean" star (estimated as the average for each of the individual stars after allowance for the effects of image ellipticity on the individual measures). The results of such a process are given in column 9 of table 2.2. All additional images of faint galaxies or stars not removed previously were subsequently taken out of the object frames, and each frame was then compressed by the mean FWHM seeing measure for that particular frame.

Contour plots of these frames were then inspected to define the positions of the surface brightness profiles to be extracted. The perpendicular cuts were separated in the radial direction ($\mathbb{R}$) by a sufficient amount as to provide sufficient "resolution" across the bulge components (when present) - typically 3 profiles being thus obtained across this component plus the minor axis profile itself. The slices were thence extracted from the data, and were folded into mean profiles at that particular $\mathbb{R}$ or Z about all axes since all systems appear axially symmetric.

II.3.9 Analyses of the standard star frames

Average frames for the standard stars observed on a certain night were obtained by cleaning the individual frames of imperfections, removing the device characteristics from each frame, and then co-adding the relevant frames as outlined above. Aperture photometry was then performed on these standards by defining a

circular region around the star concerned, whilst adjacent areas free from contamination of stars, galaxies and any remaining defects were used to define the local sky for that star.

Adoption of an arbitrary zeropoint allowed the derivation of initial magnitudes for each standard in the frame, this zeropoint being subsequently adjusted to bring the calculated and literature values into closer agreement. An iterative process was applied, taking repeated "sky + star" measures for each standard on the frame until the most suitable zeropoint was found which reduced the discrepancies in these magnitude estimates for each star to a minimum. This was adopted as the particular zeropoint for that combination of exposure time and atmospheric extinction.

In the present procedure, I facilitated a check on the repeatability of the magnitudes thus derived by taking ~ 6 to 8 pairs of sky and star measures for each standard. The results of this process indicated a high degree of internal consistency between the calculated magnitudes (of ~ ±0.002 magnitude based on the average standard error derived from all 32 frames of standards obtained during night 2 of run 2). The average value thus defined was taken as the magnitude of the standard in that particular case.

Differences between calculated and literature magnitudes were, on the whole, very small and almost always smaller than the errors quoted by Graham (1982) from which the standards used here were derived. Defining any difference in terms of the parameter

$$|R| = \left| \frac{\text{calculated magnitude - literature magnitude}}{\text{quoted error on literature magnitude}} \right|$$

I find typical estimates for the first night of run 2 of |R| = 0.3 (± 0.05), for night 2 of 0.35 (± 0.04) and for night 3 of 0.60 (± 0.10). This is illustrated in figure 2.9 which shows the magnitude discrepancy (in the sense calculated mag. - literature mag.) for all the standards used in each night (of run 2) as a function of the magnitude of the star concerned. The stars are labelled above each plot. The above estimates for |R| do not include the measures obtained from the *c* and *Y* standards in region E5 for the B band over nights 1 and 2, and for both B and R over the third night, which were found to have considerably larger discrepancies than the rest. The effect on |R| of their inclusion is indicated in the figure - they increase this parameter by a factor ~ 5 in each case. This result is perhaps suprising in view of the fact that these standards were the brightest observed, although subsequent detailed investigation revealed that zeropoints defined using such frames were essentially identical to those for the "good" frames. For this reason, these "errant" frames have been retained in defining the zeropoint for that part of the night.

The "corrected" zeropoint finally adopted for the object frame concerned was defined as follows :

$$\mu_o^{corr} = \mu_o + 2.5\log_{10}(t/T) - (\alpha\sec Z|_{obj} - \alpha\sec Z|_{st}) - A_{B,R} + \underset{(1)}{2.5\log_{10}A'} - \underset{(2)}{CT}$$

where μ_o = zeropoint defined from aperture photometry of the standard star frame,

t = exposure time of the object frame,

T = " " standard star frame,

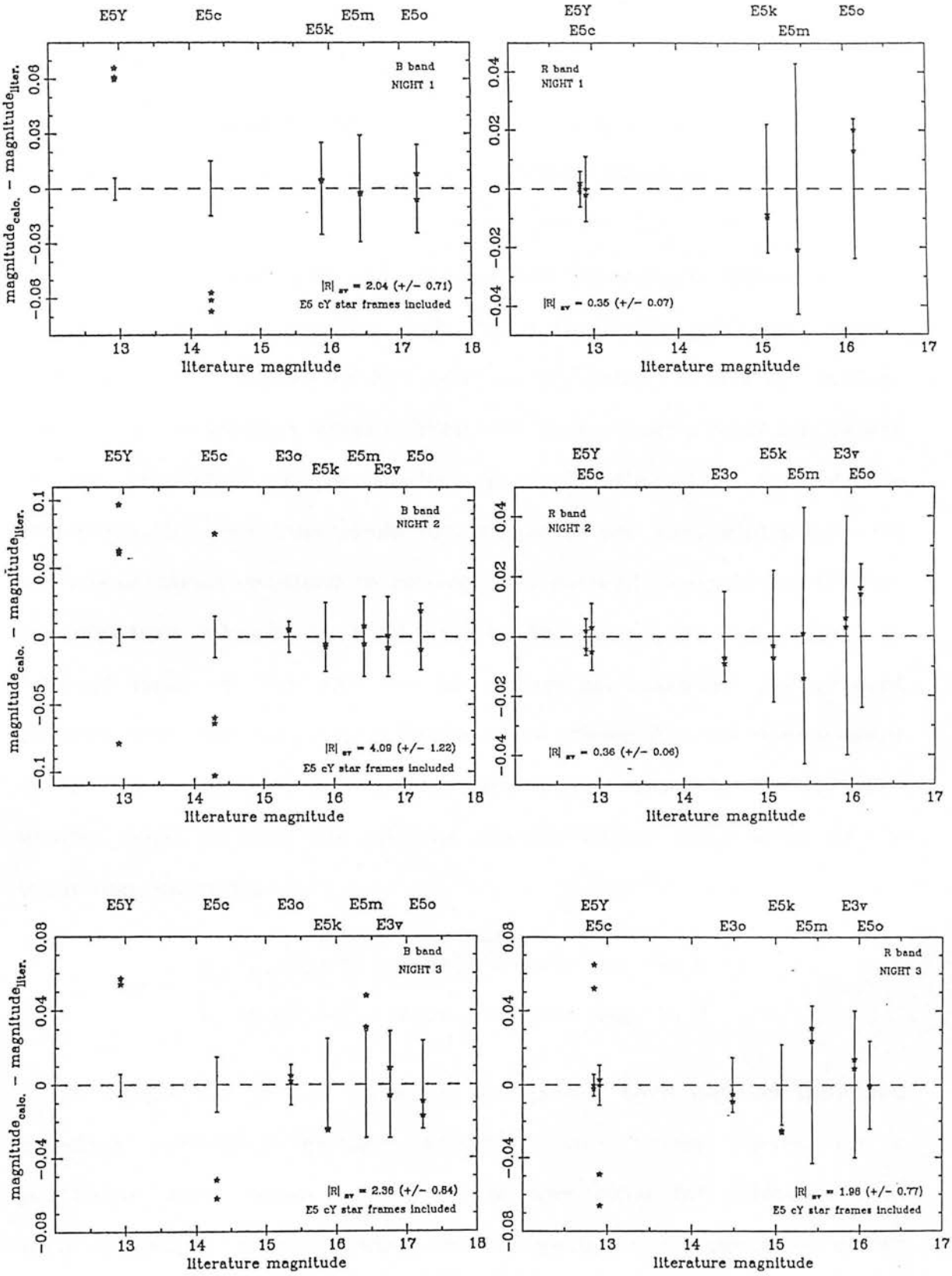
E5Y
E5c
E5k
E5m
E5o
B band
NIGHT 1
R band
NIGHT 1
|R| sv = 2.04 (+/- 0.71)
E5 cY star frames included
|R| sv = 0.35 (+/- 0.07)
E3o
E3v
B band
NIGHT 2
R band
NIGHT 2
|R| sv = 4.09 (+/- 1.22)
|R| sv = 0.36 (+/- 0.06)
B band
NIGHT 3
R band
NIGHT 3
|R| sv = 2.36 (+/- 0.84)
|R| sv = 1.96 (+/- 0.77)
magnitude calc. - magnitude liter.
literature magnitude

figure 2.9

$\propto secZ|_{obj}$ = airmass correction of the object frame,

$\propto secZ|_{st}$ = " standard star frame,

$A_{B,R}$ = galactic extinction correction (in B or R) for the object frame. This factor is derived assuming $A_B = 4E(B-V)$ and $A_R = 2E(B-V)$ (Sandage, 1973).

Although it was realised that allowance for galactic extinction here is not usual, and despite such measures being relatively poorly defined, it was adopted in the light of the desire to assign absolute colour indices to each galaxy. Term (1) in the above equation refers to the correction to be applied in converting the size of the resolution elements from pixels to arcsecs on the sky, whilst term (2) are colour terms required to convert the derived zeropoint to that on the standard Johnson U, B, V system. The latter are taken from an internal memo of the AAO for the filter set used in the present observations, and comprise a factor which allows for the displacement of the band centre in the present filters from those in the standard system, together with one allowing for the colour dependance of the extinction correction :

$$CT = \begin{cases} -0.15(B-V) - 0.01(B-V)secZ & \text{mag. in B} \\ +0.07(V-R) - 0.05(V-R)secZ & \text{mag. in R} \end{cases}$$

A comparison of the corrected zeropoints thus defined indicated excellent agreement between standard star frames taken on a particular night (when due allowance was made for differences in their respective exposure times and extinction corrections) to better than $\sim \pm 0.05$ $\mu_{B,R}$. For this reason, a mean μ_o^{corr} (scaled to a particular exposure time and airmass correction) could be defined in each colour for each night. Surface brightness measures in the object

frames were then defined by

$$\mu|_{B,R} = \mu_o^{corr}|_{B,R} - 2.5\log_{10}(I - I_{sky}) \quad \text{mag. arcsec}^{-2} .$$

I_{sky} being the sky brightness (in ADU's) per pixel. The corrected zeropoints appropriate to each galaxy are given in column 11 of table 2.2. For those (3) galaxies observed during run 1, for which no standard star frames were available, an alternative to the above procedure had to be adopted. Aperture photometry of IC 4351 was used to derive a zeropoint (corrected as described above) based on the V magnitudes of Longo & de Vaucouleurs (1983, 1985) and an assumed (V-R) of 0.68 (Lauberts & Sadler, 1984). Unfortunately, the literature photometry for IC 2531 and A1611-00 (Longo & de Vaucouleurs, 1983 1985) was conducted over much larger apertures than was possible here. Therefore, I derived an aperture-magnitude relation from the present CCD data in each case (open circles in figure 2.10) and fitted a 2nd order polynomial. These curves were then scaled to the literature measures, and the zeropoints derived accordingly. In the case of A1611-00, for which several literature measures exist, the agreement is seen to be particularly good (filled stars in figure 2.10) to ~ ±0.01 mag., and is ~ ± 0.07 mag. for IC 2531.

II.4 Comparisons to previous work

(a) Surface brightness profiles :

Both NGC 3115 and NGC 3379 were specifically chosen to act as galaxy standards on the basis of the large number of derived surface brightness profiles (both major and minor and, in the case of NGC 3379, EW cuts) and aperture photometry investigations presented in the literature.

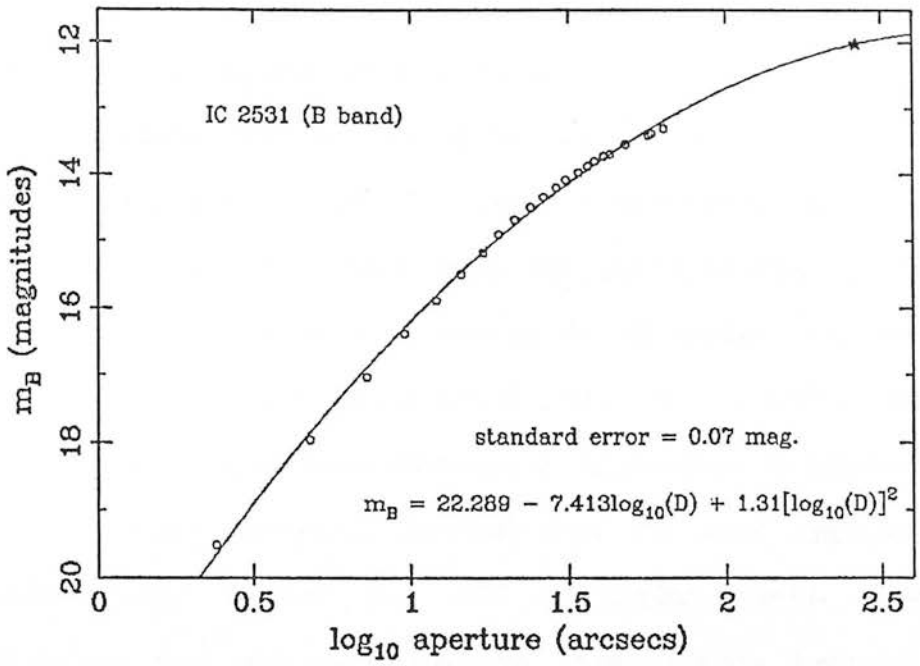
IC 2531 (B band)
standard error = 0.07 mag.
$m_B = 22.289 - 7.413\log_{10}(D) + 1.31[\log_{10}(D)]^2$
m_B (magnitudes)
$\log_{10}$ aperture (arcsecs)
12
14
16
18
20
0
0.5
1
1.5
2
2.5

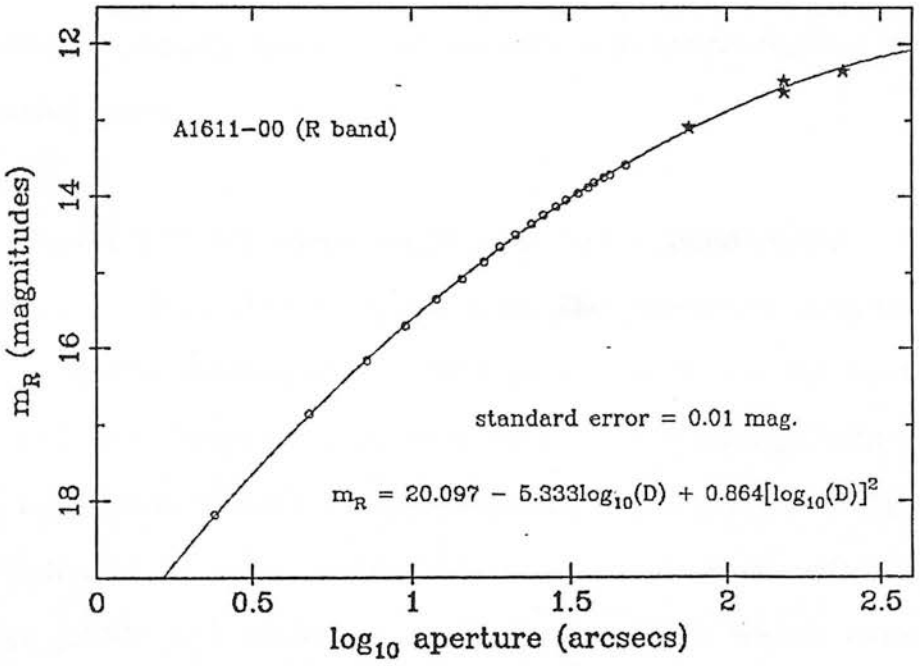
A1611-00 (R band)
standard error = 0.01 mag.
$m_R = 20.097 - 5.333\log_{10}(D) + 0.864[\log_{10}(D)]^2$
m_R (magnitudes)
$\log_{10}$ aperture (arcsecs)
12
14
16
18
0
0.5
1
1.5
2
2.5

figure 2.10

The profiles were derived after having rotated the galaxy frames such that the objects were edge-on in aspect using the technique described above. The centre of the object was located both visually and also semi-automatically (by using a technique which weights each pixel in a prescribed box area by the intensity at that point), although the former was preferred in all cases. The relevant cuts were thus produced to the maximal extent of the CCD in all directions (~ 100 arcsecs) and were converted to surface brightness measures using the mean zeropoint derived from the most appropriate set of standard star frames for that particular night. However, sky subtraction was not performed on these frames because the large spatial extent of both galaxies over the CCD precluded any reliable determination of the sky brightness. Although this will have a significant effect on the comparison over the fainter regions of the profiles, it should have a minimal effect in those regions dominated by galaxian light.

Figure 2.11 (a) compares the derived B band major and minor axis profiles of NGC 3379 to those from the literature sources used. The sharp decline faintward of ~ 20.5 μ_B is due to my not having removed the sky, but brighter than this level (where galaxy light is dominant) the agreement is seen to be reasonably good - figure 2.11 (b). This is particularly so when comparing the present work with that of Davis et al (1985) and Whitmore & Kirshner (1982), where mean magnitude differences of -0.02 μ in both cases are found brightward of 20.5 μ. The increasing discrepancies evident at the brighter magnitudes for all other comparisons are likely to result from a combination of mismatch in the major and minor axes actually adopted (definition of

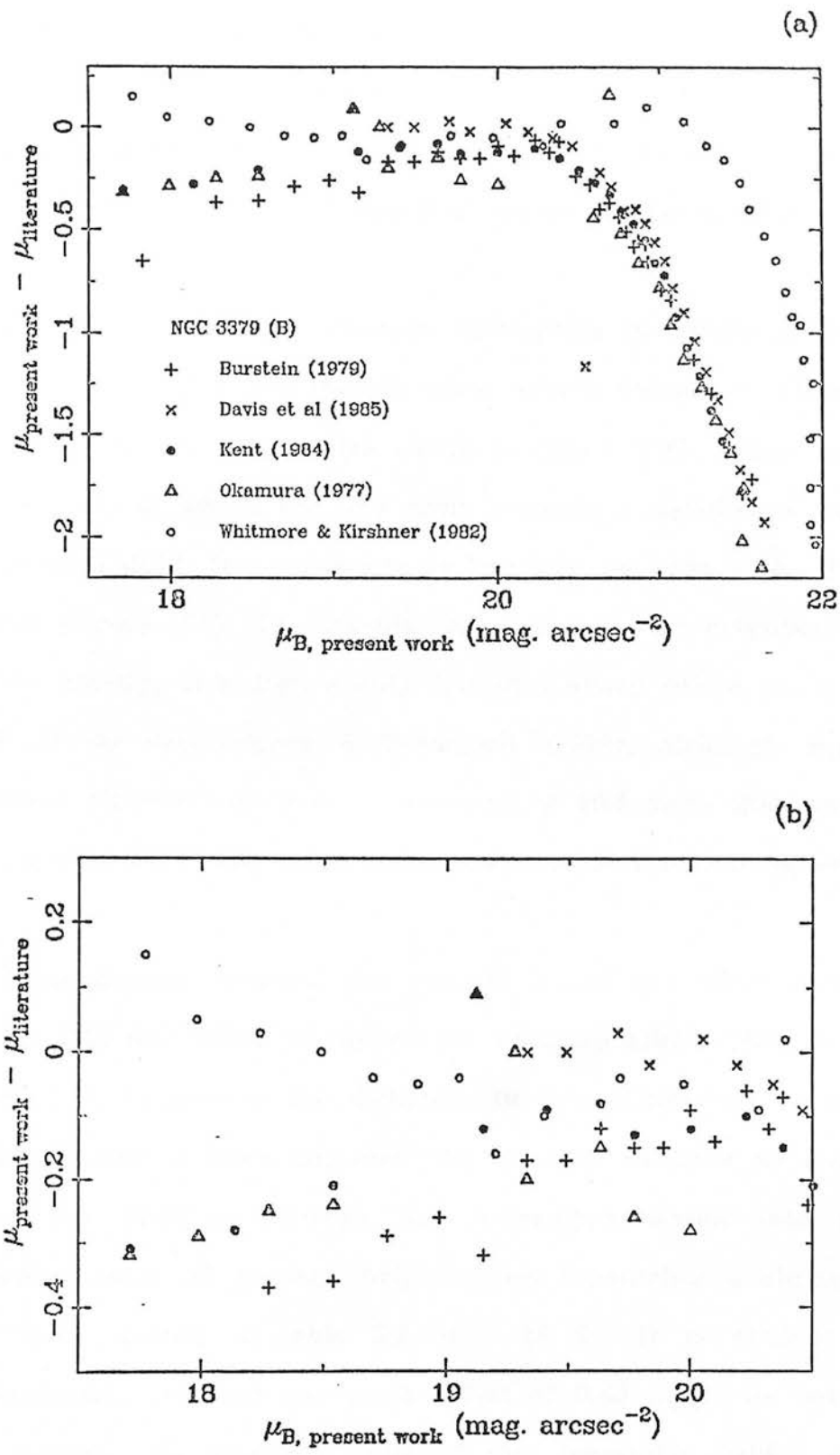
(a)
NGC 3379 (B)
Burstein (1979)
Davis et al (1985)
Kent (1984)
Okamura (1977)
Whitmore & Kirshner (1982)
$\mu_{present\ work} - \mu_{literature}$
$\mu_{B,\ present\ work}$ (mag. arcsec^{-2})
(b)
$\mu_{present\ work} - \mu_{literature}$
$\mu_{B,\ present\ work}$ (mag. arcsec^{-2})

figure 2.11

the position angle of an E0 being inherently uncertain by $\gtrsim \pm 5^{o}$), coupled with the fact that Okamura (1977) and Kent (1984) quote an equivalent surface brightness profile. Burstein (1979c) uses a profile defined 10 arcsecs from the major axis itself. An equivalent figure is shown for the R band in figure 2.12, where similar conclusions apply.

In the light of the inherent difficulties in matching both major and minor axes for this galaxy, more weight should be attached to a comparison of the EW profiles shown in figure 2.13. Again, brightward of the point at which the sky first becomes a significant contributor to the total light, the agreement is found to be good with all previous studies (figure 2.13 (b) expands the region in (a) brighter than 20.5 μ). For clarity, this figure only includes every other point from the work of de Vaucouleurs & Capaccioli (1979), although figure 2.14 compares all available data brightward of 20.5 from this source with the present work. The mean difference here is found to be -0.06 μ.

A comparison between the present major and minor axis profiles of NGC 3115 and those presented by Tsikoudi (1977, 1979) is given in figure 2.15. Because of the difficulty in determining sky in my frames of this galaxy, I have adjusted the present estimate as required to bring the profiles between the respective works into the best agreement over all surface brightnesses (requiring a change in the sky value quoted in table 2.2 of $\sim$ 14 %). It is evident that an approximately constant zeropoint offset of 0.43 μ_B exists between the two studies. The position angle of this lenticular (which possess a strong inner disc component) is sufficiently well-defined to discount profile "mismatch" as being the likely source of such a discrepancy. Unfortunately it is difficult to place this disparity in context as

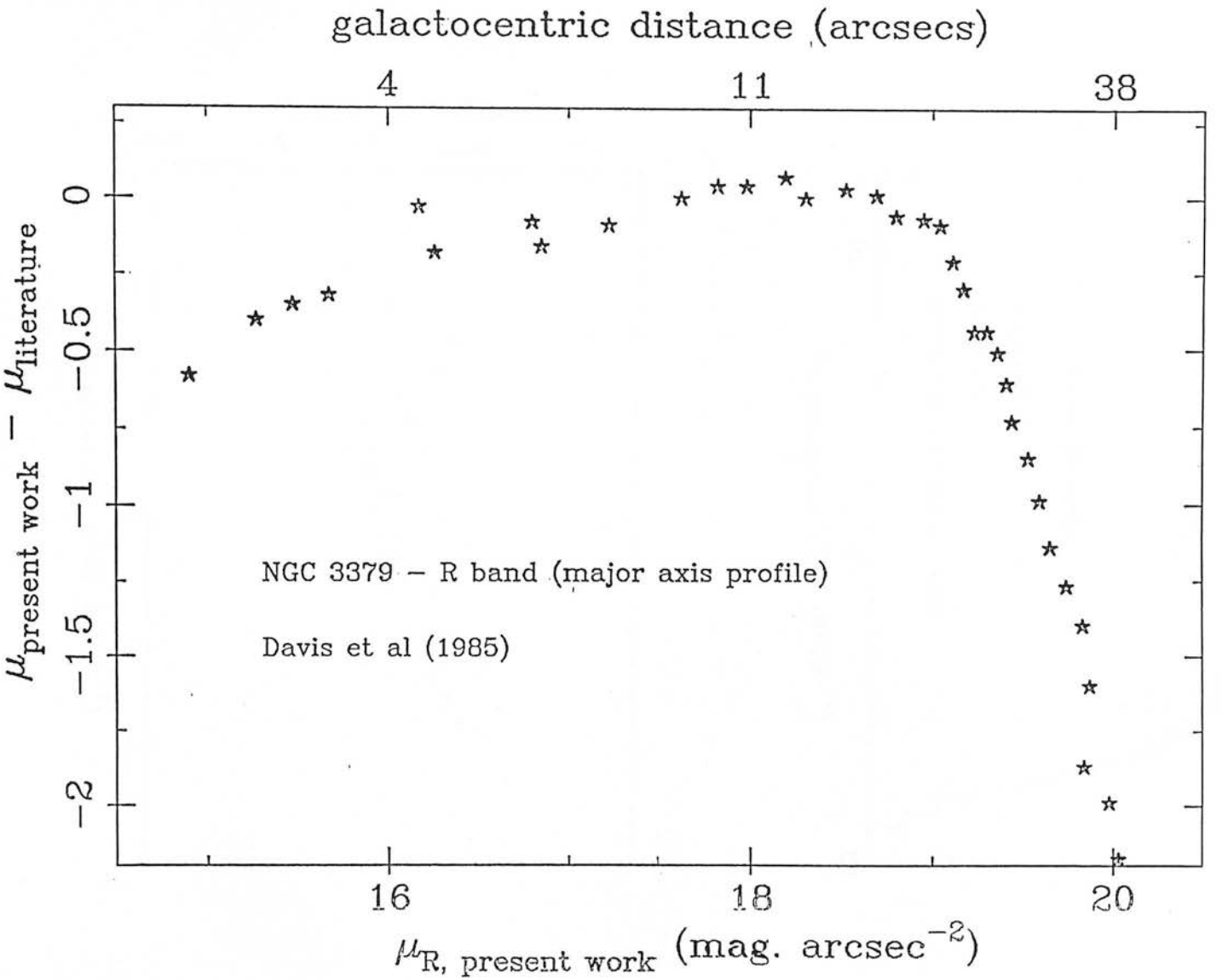
galactocentric distance (arcsecs)
4
11
38
0
−0.5
−1
−1.5
−2
$\mu_{\text{present work}} - \mu_{\text{literature}}$
NGC 3379 – R band (major axis profile)
Davis et al (1985)
16
18
20
$\mu_{\text{R, present work}}$ (mag. arcsec^{-2})

figure 2.12

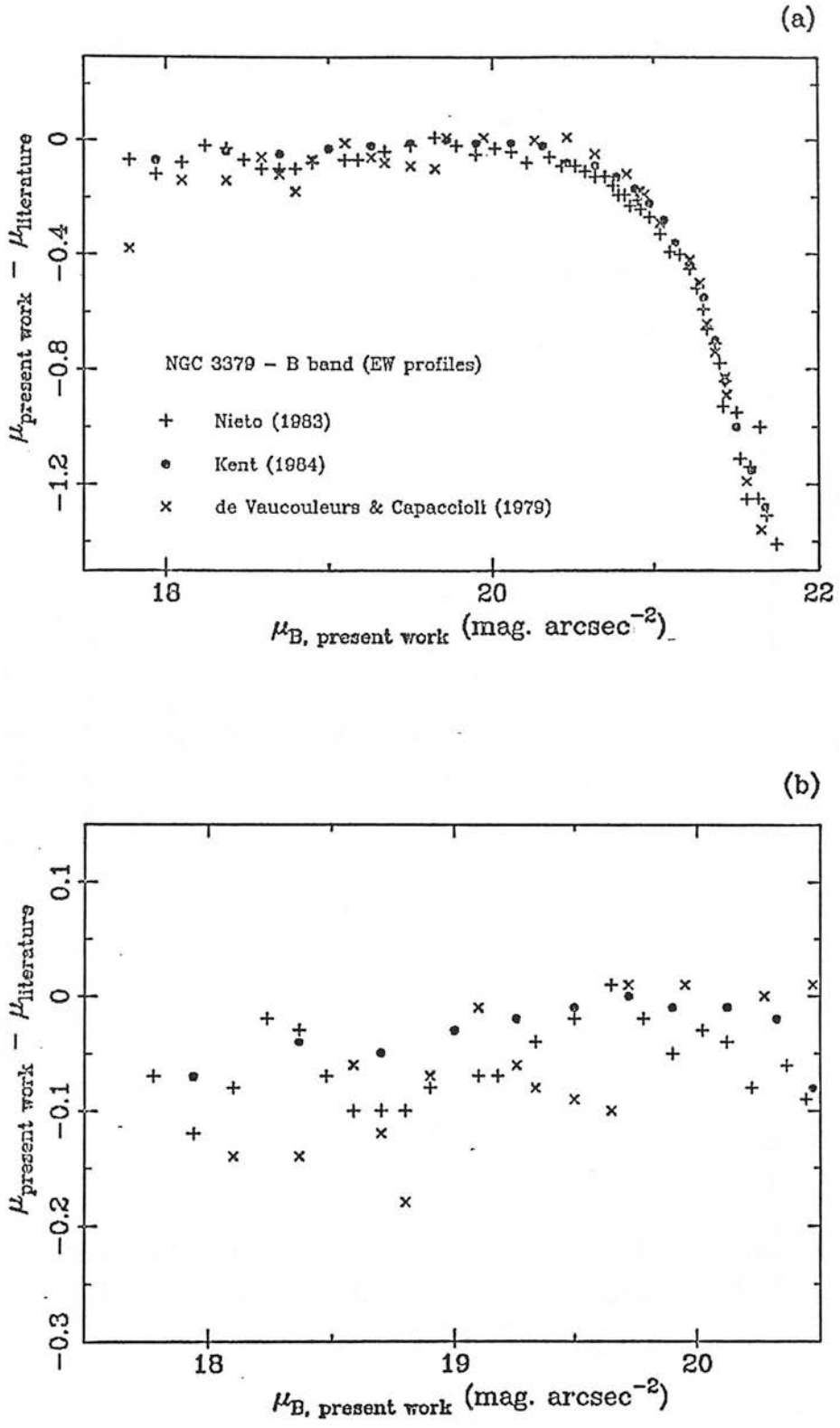
(a)
NGC 3379 – B band (EW profiles)
Nieto (1983)
Kent (1984)
de Vaucouleurs & Capaccioli (1979)
$\mu_{present\ work} - \mu_{literature}$
$\mu_{B,\ present\ work}$ (mag. arcsec^{-2})
(b)
$\mu_{present\ work} - \mu_{literature}$
$\mu_{B,\ present\ work}$ (mag. arcsec^{-2})

figure 2.13

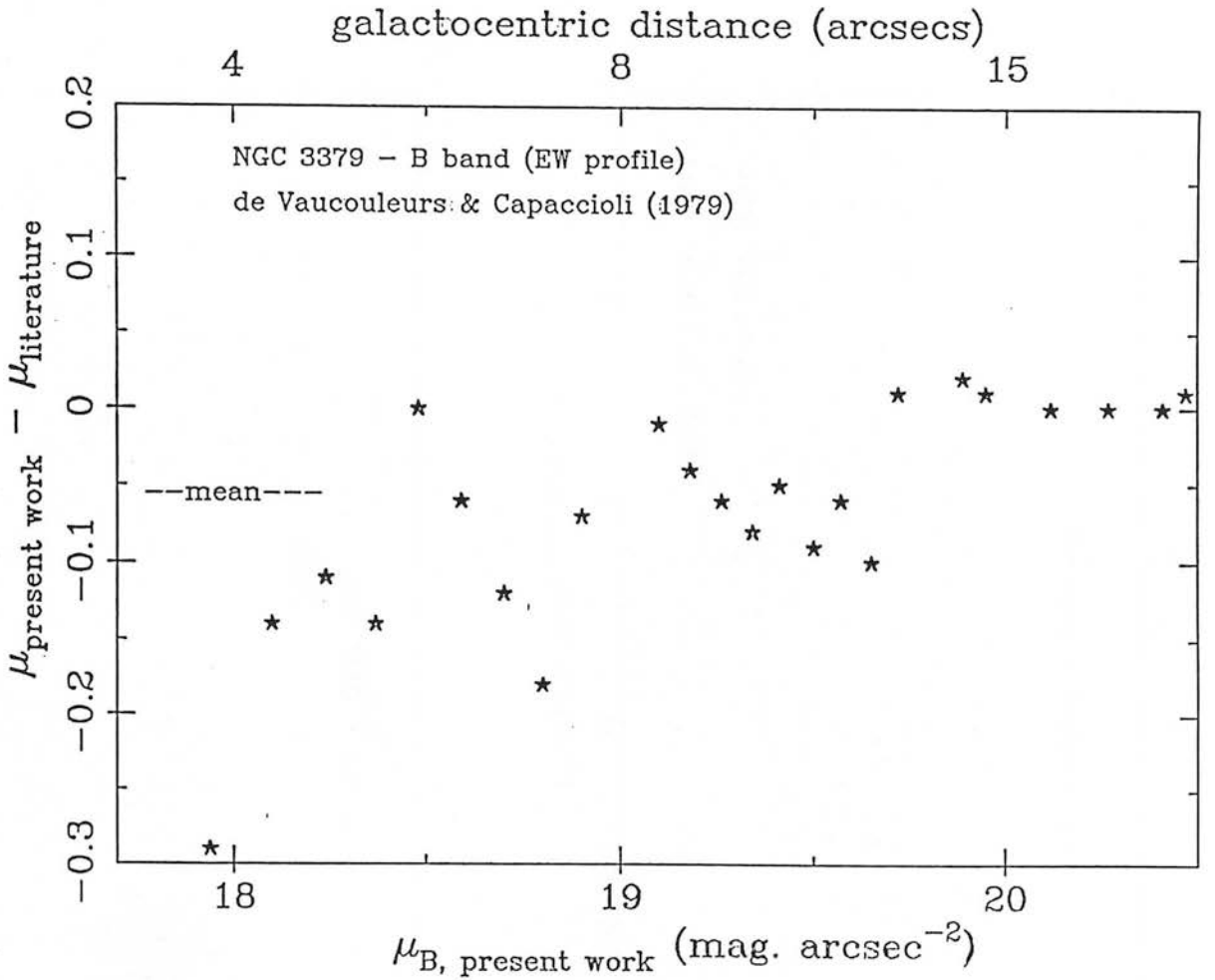
galactocentric distance (arcsecs)
4
8
15
NGC 3379 – B band (EW profile)
de Vaucouleurs & Capaccioli (1979)
--mean---
0.2
0.1
0
−0.1
−0.2
−0.3
$\mu_{present\ work} - \mu_{literature}$
18
19
20
$\mu_{B,\ present\ work}$ (mag. arcsec^{-2})

figure 2.14

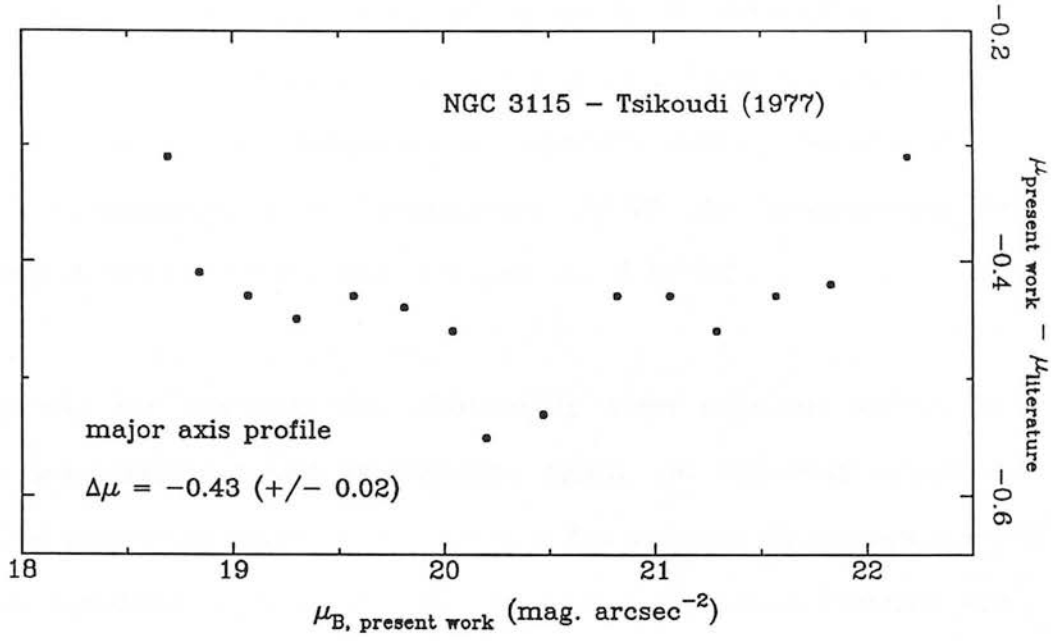
NGC 3115 – Tsikoudi (1977)
major axis profile
Δμ = −0.43 (+/− 0.02)
18
19
20
21
22
−0.2
−0.4
−0.6
μB, present work (mag. arcsec−2)
μpresent work − μliterature

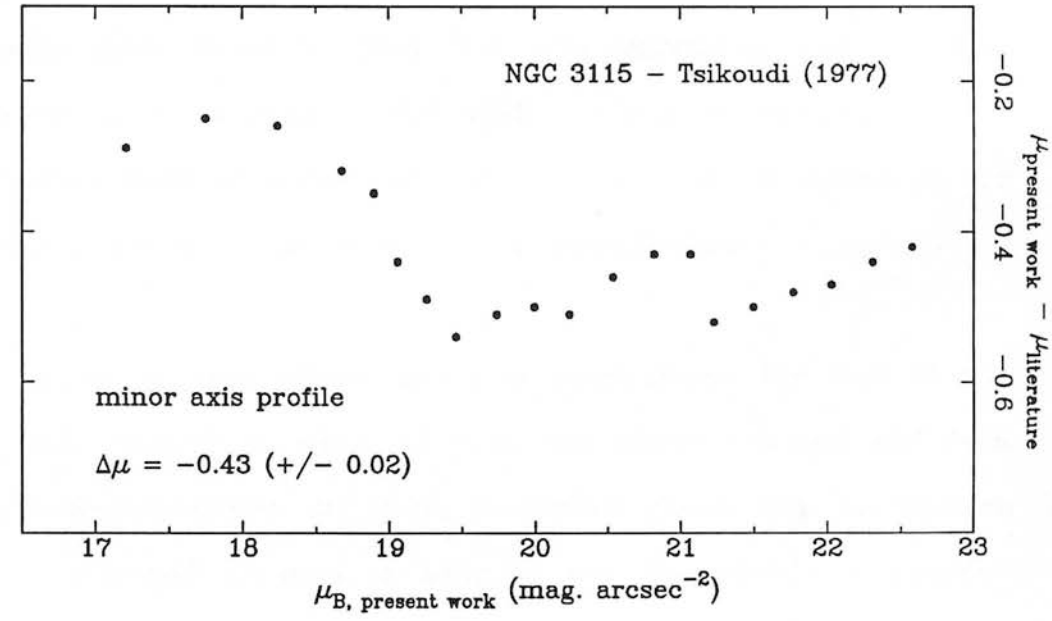
NGC 3115 – Tsikoudi (1977)
minor axis profile
Δμ = −0.43 (+/− 0.02)
17
18
19
20
21
22
23
−0.2
−0.4
−0.6
μB, present work (mag. arcsec−2)
μpresent work − μliterature

figure 2.15

Tsikoudi does not compare her data to previous studies other than to note that her total integrated B magnitude is within 0.1 mag. of the figure quoted in the RC2.

(b) Aperture photometry :

Several sources of aperture photometry exist for both NGC 3115 and NGC 3379, although the work of Longo & de Vaucouleurs (1983, 1985) proved to be most useful in this regard. These measures were supplemented using data presented by Sandage (1973), Persson et al (1979), de Vaucouleurs & de Vaucouleurs (1972), de Vaucouleurs, de Vaucouleurs & Corwin (1978) and Burstein et al (1987).

Zeropoints for the aperture photometry were obtained using the standard star frames noted previously. Again, no sky was removed, and in this particular case no corrections for galactic extinction were made. The resulting agreement with the above literature sources are found to be excellent in the case of NGC 3115, and very good for NGC 3379 as figure 2.16 shows. A marginal decrease in the magnitude difference is again found for NGC 3115 with increasing aperture size, but no such effect is seen in NGC 3379 - primarily because too few such measures exist at sufficiently large galactocentric distances for sky contamination to become a significant contributor.

Also shown in this figure are the comparisons for two of the program CCD galaxies as obtained from the above sources and from Lauberts & Sadler (1984). In these particular cases, sky subtraction has been performed as such a measure can be reliably determined (although again no galactic extinction corrections have been applied). The agreement is again found to be excellent, testifying to the

EX BIBL. UNIV. EDINBURGH

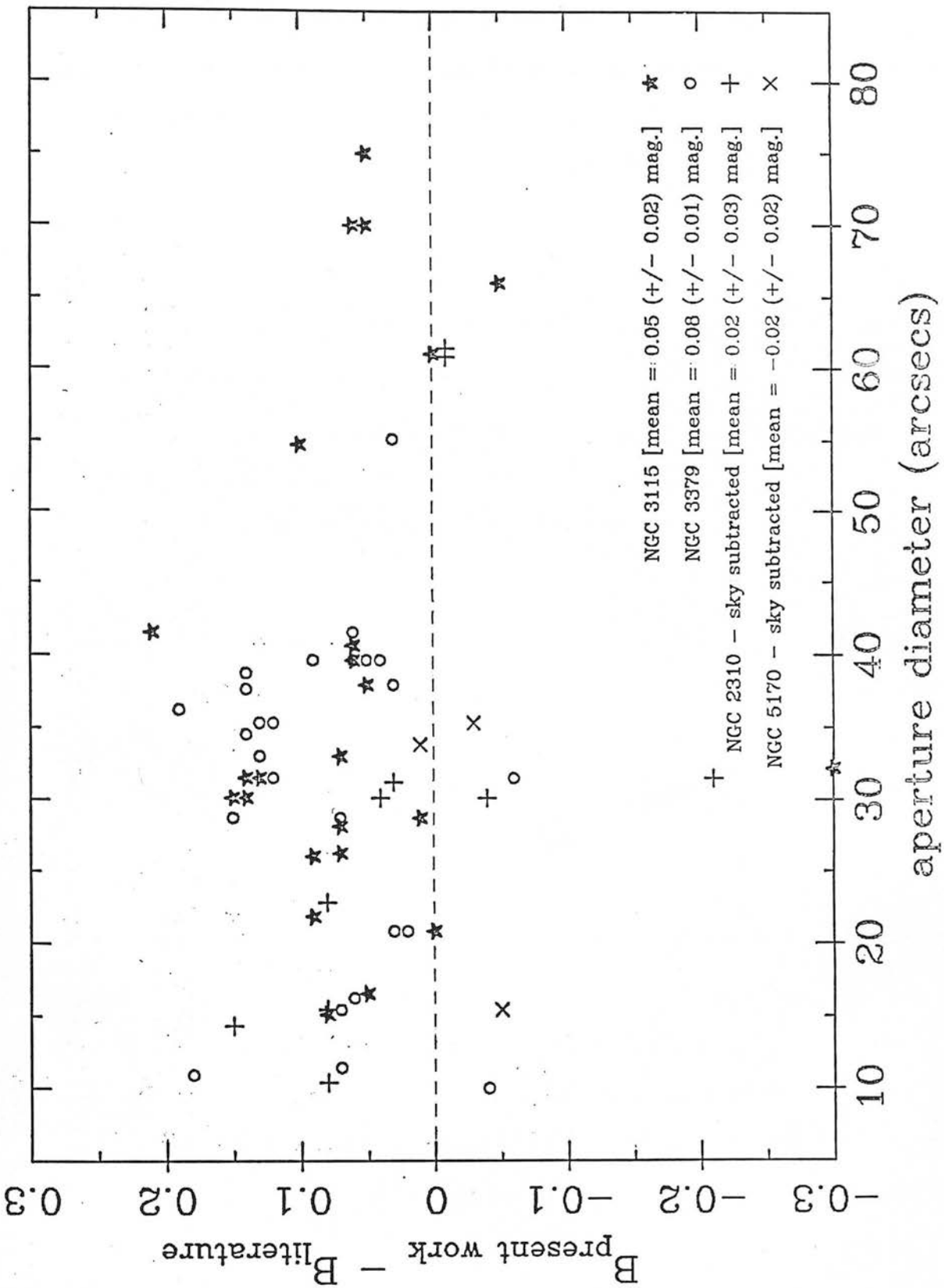
B present work − B literature
aperture diameter (arcsecs)
NGC 3115 [mean = 0.05 (+/− 0.02) mag.]
NGC 3379 [mean = 0.08 (+/− 0.01) mag.]
NGC 2310 − sky subtracted [mean = 0.02 (+/− 0.03) mag.]
NGC 5170 − sky subtracted [mean = −0.02 (+/− 0.02) mag.]

figure 2.16

reliablity of the zeropoints defined using the above procedure. As a result, there is every reason to expect that, for object frames taken throughout the night, photometry can be achieved to within the accuracies of the standard star frames used - giving estimates to ~ ±0.06 mag. in R and ~ ±0.04 mag. in B based on the quoted errors of Graham (1982).

- Chapter III -

A two-dimensional model for the light distributions in edge-on spiral galaxies and its application to NGC 891 and NGC 4565

III.1 Introduction

In this chapter I address the problem of devising a consistent means for evaluating fundamental galaxy properties from the available observational surface brightness data, fundamental meaning those underlying stellar populations contributing to the light we observe from the system being investigated.

Since the pioneering studies of Hubble (1930), de Vaucouleurs (1953) and King (1978), the general methodology by which this goal is attempted has been to describe the object of interest in terms of a number of unique components, each one of which is modelled using an intensity distribution/luminosity law. In this context the present study follows identical precepts.

Firstly one has to define the number of individual components the galaxy under study might be expected to contain. This is of fundamental importance to such a technique (and as such may be seen as its first, and possibly most important, limitation). Choosing too many components may well produce a fit of the prescribed accuracy but will almost certainly lead to meaningless results because of "non-uniqueness". However, in the case of spiral galaxies the situation is, in general, pre-defined. A cursory inspection commonly reveals the

presence, to a greater or lesser degree, of a highly flattened disc component superposed on an underlying bulge. In such situations one simply assumes a luminosity profile for each of these distinct populations. In cases where only one of them predominates, the procedure is to begin by using only the luminosity profile considered to be most relevant to that particular situation. If this fails to yield "satisfactory" results (a point I return to below) the next step is the addition of a further component, whose form depends largely on the nature and size of the discrepancies encountered using the previous combinations. From the point of view of describing the global nature of the galaxy under study, one is rapidly reaching the point of "non-uniqueness". Global in this context is meant to exclude such features as bright (i.e. "starlike") nuclei, bars, rings and the like - although it is certainly true that one can find many objects in which these forms are seen to dominate the light distribution over equally large scales to those under investigation here.

In the present study, the unsatisfactory situation of "non-uniqueness" is obviated by curtailing the investigation at this point, thus ensuring that in "disc + bulge" spirals the existence of no more than 3 components is being investigated at any one time (and $\leqslant$ 2 in the apparently exclusive disc or bulge objects). In reality, constituent stellar populations the models are intended to describe may well smoothly merge with others in the galaxy, to which I may be assigning a completely different luminosity law. Because of this, it is difficult to justify the use of any more than $\sim$ 3 model components on the basis of the "global" data currently available.

The next major question one must address is, having defined what populations are thought to be present, what form does one adopt for describing the form of their luminosity profiles? This is an equally unsatisfactory aspect, and has been so since such investigations were first undertaken. The problem arises because many of the model forms devised are exclusively empirical, i.e. they were simply chosen as the most convenient mathematical description of the observed data. However, from the point-of-view of simply gaining an insight into the overall structural parameters of the population under study, the models of greatest simplicity and value are an exponential disc profile (Freeman, 1970) and either the $r^{1/4}$ law form of de Vaucouleurs (1953) or the function proposed by King (1962, 1966). A description of those models adopted in the present study is deferred until section III.3.1 below.

For previous studies in this field, the most usual approach has been to fit (visually) a combination of these models to the derived surface brightness distributions, my own study of the 2D luminosity distributions in the "archetypal" edge-on spirals NGC 891 and NGC 4565 (Shaw & Gilmore, 1986) being a case in point. However, these methods are often inconclusive. Even when producing seemingly consistent results they have to be treated with caution since a variety of often widely varying model parameters can all yield equally good fits to the data, with no well-defined means of discriminating one set from any other. This is the "non-uniqueness" referred to previously and is a result of the strong correlation between the components modelled. Equally, concern arises from any inbuilt biases which may result from one's preconceived expectations of the stellar populations of which the object is comprised.

Evidently to make any progress in analysing the luminosity distributions of spiral galaxies in general, and edge-on candidates in particular, requires the use of unbiased techniques. These should hopefully allow one to deconvolve the individual contributors to the profile concerned whilst minimising the uncertainties which arise from the correlation between their parameters. This chapter presents the results of an algorithm designed with these aims in mind.

III.2 Previous modelling techniques

With a view to placing the algorithm discussed below in the context of modelling galaxy surface photometry in general, this section briefly reviews previous studies undertaken with a similar motivation.

It is investigations of elliptical galaxies which have most benefited from techniques such as those mentioned above - presumably because of their seeming simplicity of form. Jedrzjewski (1985) has outlined the previous methods in the study of such systems. I will only focus on those schemes involving algorithms which make use of best-fitting ellipse techniques to the isophotal contours [Mihalas & Binney (1981, chapter 5) give a more comprehensive review of the field]. This method is now taken as a standard technique and has been used in recent studies such as those of Jedrzjewski, Lauer (1985) and Davis et al (1985). The basic methodology involves fitting a series of concentric ellipses to the intensity contours in a particular galaxy image (usually by least-squares means). A Fourier analysis of the resulting residuals between the model and the galaxian isophotal shapes thence yields the errors or quality of the fit and thereby indicates the degree to which the object concerned departs from a

true ellipse. The modelling procedures are of interest here since recent methods of deriving photometric properties of spiral galaxies have made use of variants on this theme.

One study adopting such an "elliptical averaging" method is that of Boroson (1981) involving analysis of 26 spiral galaxies via photographic surface photometry (the objects primarily being of moderate inclinations or approaching a face-on aspect). After scaling each one of the 36 radial profiles (i.e. slices running at 10 degree opening angles from the centre of the galaxy) by the ratio of the ellipse radius at that specified angle to that of the major axis, a single mean co-added profile of the object concerned was derived. Subsequent deconvolution of such a profile followed the precepts of the work by Kormendy (1977a) outlined below.

A more recent analysis using similar techniques was made by Kent (1984, 1985) in his CCD photometry of 105 field spirals, lenticulars and ellipticals of widely varying inclination angles. In this case the position angle and ellipticity of each figure were allowed to vary as a function of radial distance until the difference between model and actual galaxian isophotal shapes are minimised. The luminosity profiles were thus extracted, and variations of major and minor axis surface brightness were evaluated. Subsequent modelling involved the use of nonlinear least-squares fits using a 2-component model combination of an exponential disc and the standard de Vaucouleurs $r^{1/4}$ law, all convolved with a Gaussian seeing profile.

There are considerable advantages in the application of these algorithms to ellipticals : the full information contained in a galaxy

can be retained but with greatly enhanced S/N obtained in the less well-defined outermost regions. However, there are drawbacks which result from the extension of such a modelling scheme to spiral galaxies. In the case of face-on systems to which the method has so far been most frequently applied, the evaluated parameters of any particular ellipse are clearly not unique to a specific stellar population as they are likely to be sampling light from all other components within that specified radius. As a result, specific population decomposition, of the type intended here, is impossible using this scheme. This problem is particularly well illustrated in figure 1 (c) of Kent (1984).

Once the luminosity distributions themselves have been obtained, the method initially proposed by Kormendy (1977a), which effectively makes two nonlinear least-squares fits to such profiles, is most often used to derive structural details of the constituent populations. By specifying regions of the profile where the disc and non-disc light are expected to dominate, the algorithm evaluates the least-squares fit for the disc over its range, subtracts it from the total profile and then fits the non-disc light in its dominant regime - iterations between the two continuing until convergence is achieved. The technique was used to effect by Burstein (1979a), and a variant on this theme was also adopted by Boroson (1981). The scheme is meritorious in that it indicates the validity of the components adopted even over the intermediate regions from which no information relevant to the fit is derived. It also allows one to vary the range over which the constituent populations are expected to dominate (unlike a more traditional least-squares fitting procedure). However, it is often extremely difficult to define such ranges. This has to be coupled with

the restriction of needing to specify a functional form which, whilst being required to fit over the specified range of the luminosity profile concerned, must also be valid globally. These limitations often make the use of such a procedure inapplicable or interpretation of the results as very unreliable.

A further method has been devised by van der Kruit & Searle (1981a,b and 1982a,b) which is more applicable to the current investigation as their analyses are of edge-on spirals. They adopt fitting models which are no longer simply functions of radial distance ($\mathbb{R}$) but also of height (Z) above the disc plane. The scalelength of any disc component is defined by considering those luminosity profiles (specifically chosen to be well away from potential dust contamination in the plane) parallel to the major axis - the parallel profiles. Cuts perpendicular to the plane are used to specify the scaleheight. By fitting over the whole galaxy, after suitable binning to improve S/N, a subtraction of the disc component should allow modelling of the residual light (or vice-versa in the case of bulge dominated galaxies such as NGC 7814 as studied in van der Kruit & Searle, 1982b).

Since any particular component is modelled over the whole galaxy in $\mathbb{R}$ and Z at any one time, this immediately overcomes the major limitation inherent in the analysis of Kormendy. The only precaution in using this scheme is that one must ensure the parallel profiles are unaffected by dust contamination. This is not a problem to those analyses of van der Kruit & Searle but is certainly of concern for the modelling of systems covered by fewer resolution elements.

III.3 Outline of the present modelling procedure

As a result of the limitations to the alternative schemes outlined above, the principle of global, nonlinear least-squares fitting to the luminosity profiles of the present sample objects (of a form similar to that of van der Kruit & Searle) was adopted. However, a limitation in the latter studies result from the need to model each component independantly. The present algorithm was written in such a way as simultaneously to include the effects of all components thought to be extant in the galaxy under investigation. As a result, the procedure adopted is quite similar to the scheme outlined by Bahcall & Kylafis (1985) in their analysis of NGC 891. The present method is, of course, limited by any correlations between the various parameters of a particular model component, and also by that between the separate components being fitted. Both problems are unfortunately inherent features of all such least-squares fitting routines (those of Kormendy, van der Kruit & Searle and Bahcall & Kylafis being no exceptions). Their effects must be borne in mind in the subsequent analyses.

III.3.1 The models adopted

Section III.1 above has already outlined limitations to population studies of external systems - in particular those resulting from the empirical nature of many of the models generally used. This is certainly true of the exponential disc (Freeman, 1979), the $r^{1/4}$ law and also the King models as they were first introduced (King, 1962). The latter were, however, subsequently placed on a more physical footing in King (1966).

This section details the functional forms adopted in the present fitting algorithm to model the stellar populations within the sample galaxies of table 1.1.

(i) The "old disc" :

The principal functional form made use of to model this stellar population was that initially adopted in the work of van der Kruit & Searle, in particular their paper I (1981a). It is assumed that one can approximate the density distribution $\rho(R,Z)$ within a disc by a self-gravitating isothermal sheet (the stellar velocity dispersion being independent of Z-height). In this particular case, the gravitational force at any point in the disc of this (stratified) system can be separated into a product of the radial (R) and perpendicular (Z) components. By requiring the stellar distribution function to satisfy the equation of continuity (and that the density distribution follows Poisson's equation) leads, through a separation of the (R,Z) variables, to a solution in which

$$\rho(Z) \propto \mathrm{sech}^2 Z$$

(Spitzer, 1942, and Camm, 1950).

The radial dependence is assumed to be exponential, based on the (purely empirical) luminosity distribution adopted by Freeman (1970). Nevertheless, because of the (albeit simplified) physical basis behind the Z-dependence in the present model, coupled with the results of limited earlier studies which suggest it is a reasonable fit to the data, it is adopted in the present investigations. Its form, as used here, is

$$\mu(\mathbb{R},Z) = \begin{cases} \mu(0,0) - 2.5\log_{10}([1 + (\mathbb{R}^2/2h_R^2)\log_e(\mathbb{R}/2h_R)] \, \mathrm{sech}^2(Z/Z_o)) \\ \mu(0,0) - 2.5\log_{10}([(\pi\mathbb{R}/2h_R)^{\frac{1}{2}} \exp(-\mathbb{R}/h_R)] \, \mathrm{sech}^2(Z/Z_o)) \end{cases}$$

where $\mu(0,0)$ is the central surface brightness (in mag. arcsec^{-2}), Z_o the scaleheight and h_R the scalelength (both in kpc). The first relation is applicable when $\mathbb{R} \ll h_R$ and the second is valid for $\mathbb{R} \gg h_R$. The model is henceforth referred to as the "sech^2" distribution.

However, because the sech^2 form has been used in relatively few previous studies which have sought to model galaxian light distributions in this way, a double-exponential form (in both $\mathbb{R}$ and Z) is also adopted here to allow a more detailed comparison with these earlier investigations :

$$I(\mathbb{R},Z) = I(0,0) \exp -[\, \mathbb{R}/h_R + Z/h_Z \,]$$

which, in terms of surface brightness (μ), gives

$$\mu(\mathbb{R},Z) = \mu(0,0) + 1.0857[\, \mathbb{R}/h_R + Z/h_Z \,] \quad \text{mag. arcsec}^{-2}$$

where h_R the scalelength of this population and h_Z the scaleheight (being half the scaleheight of the sech^2 model above). At large ($\mathbb{R}$,Z), however, these respective models become essentially indistinguishable. For completeness it is also noted that an alternative function, allowing for the effects of varying inclination angles to the line-of-sight, has been proposed by Jensen & Thuan (1982). I did not make use of this model form in the following analysis.

An analysis of the "young" disc population was precluded in the modelling scheme used here because its luminosity distribution is likely to be heavily affected by obscuration along the line-of-sight from dust lanes in the edge-on galaxies considered.

(ii) The "intermediate" population :

Any such "thick disc" component was modelled using identical functional forms to those outlined above in the case of the thin disc. However, in using the $sech^2$ form, I have adopted a disc scaleheight parameter of Z_1 (rather than the Z_o given above) in subsequent analyses.

(iii) The bulge :

The most widely used model form taken to describe the total non-thin disc light, and the one principally used in the present investigations, is the standard $r^{1/4}$ law of de Vaucouleurs (1953). Such a model is purely empirical, and is of the form

$$\log_{10} (I/I_e) = -3.33 \left[(\theta/\theta_e)^{1/4} - 1 \right]$$

or in surface brightness,

$$\mu(R,Z) = \mu_e + 8.325\left[(\theta/\theta_e)^{1/4} - 1 \right] \text{ mag arcsec}^{-2}$$

where,

$$\theta = \sqrt{q^2 R^2 + Z^2}$$

q being the axis ratio, θ_e the effective radius (inside which half the total light of the galaxy is found), and μ_e the surface brightness of the model profile at that radius.

As an alternative to the above, however, an exponential fitting function was also adopted as in the two previous cases. In the context of the component being modelled, the applicability of such an (isothermal) form may be called into question, as it is merely another attempt to fit the data by using a convenient fitting function. However, Binney (1982) has presented evidence of an alternative form to the $r^{1/4}$ law which is non-empirical and is claimed to describe the

light distribution in the standard elliptical NGC 3379 better than does the form of de Vaucouleurs (1953). In particular, Binney's assumption of a luminosity component describable in terms of a self-gravitating, isothermal and spherically symmetric stellar population leads to a (Boltzmann) model distribution and gives a better fit to the photometry of NGC 3379 over the innermost regions of the surface brightness distribution. I note the existence of such a form for completeness as it was not explicitly included in the models tested for this component in the present analyses.

Although there are clearly a large number of other potential analytic functions one could use, it was decided to restrict the present study to the two model forms already described. This was because, in the cases where more than 2 components may be required to describe the light distribution seen in the galaxy under study, one will be unable to distinguish between alternative functional forms on the basis of the available data. Such situations are obviated by using the simplest model considered applicable in that particular case. Differences in model form are, in any event, purely arbitrary as the $r^{1/4}$ law and the models of Hubble (1930, but see also Kormendy, 1977b) are all essentially empirical in nature. In addition, they all measure similar structural details within the galaxy concerned - there being a direct (albeit not a one-to-one) correspondence between the scalelength parameters in each case. Further, as it is also the most commonly adopted form in the current literature, use of the $r^{1/4}$ law facilitates an easier comparison between previous and present investigations than would, for example, the use of a King profile.

III.4 Features of the least-squares fitting routine

Having outlined the model components used within this algorithm, I now detail the salient characteristics of the present routine. As input, it requires a 2D array (in (R,Z) space) of surface brightness measures across the galaxy under investigation. A number of NAG routines (principally the nonlinear minimisation fitting function E04FCF) are then used to seek an unconstrained minimum in the sum of squares of the residuals between these (real) data values and the ones calculated on the basis of the combination of models adopted for that particular iteration. Each surface brightness measure in the input array is weighted on the basis of the associated error at that point.

When running the program, the user must provide initial estimates of those parameters relevant to the components being modelled in the fit. These values are used by the program to derive the basic model surface brightness data array to be used in the subsequent minimisation. Within the program, there exists a facility for monitoring the progress of the fit at each iteration, with measures such as the sum of squares of residuals, the χ^2, the reduced χ^2 and the actual parameter values derived during that particular iteration, being output to the user (and to a hardcopy file for future inspection). The latter is often of considerable value in defining the validity of a particular fit.

There are 3 principal parameters within the routine which serve to maintain the problem within reasonable bounds and thereby ensure rapid convergence to a solution. They are as follows :

(i) MAXCAL :

This is a parameter used to specify the total number of times the array of sums of squares of residuals is calculated. By choosing a relatively small value for this factor (~ 400 x the number of free parameters was adopted here) helps to ensure that the process does not become prohibitively expensive in terms of computer time.

(ii) Accuracy :

The program requires that, before any iteration can take place, a value is assigned for the accuracy of the required solution. Although a small input value for this parameter may lead to increased accuracy in the final result, this again has to be countered with the correspondingly increased computer time required to obtain a solution. Tests indicated that changing these tolerance limits (within which the fit was considered reasonable) had little effect either on the final output values themselves, or on the speed and direction with which convergence to this result was achieved. It was thus decided to perform a relatively low accuracy fit (with a correspondingly increased tolerance level) of ~ 50 %. All the following discussions centre on fits derived using this value alone.

(iii) Stepsize :

Finally, the user is required to specify an estimate of the total "distance" allowed between the starting point (as defined on the basis of the user-supplied initial input parameters) and the final solution. A careful choice of this factor helps to prevent mathematical overflow problems during calculation and also ensures that the minimum found is a "local" one - "distant" minima may well have a smaller overall sum of squares of residuals but experience indicates that the output

values thus generated are usually invalid. Of course, care has to be adopted in the choice of this parameter since restricting the fit to a very small step size may result in the routine being unable to find a minimum at all. On balance it was decided that, since the point of the "local" minimum is, by definition, unknown, the default value for the stepsize would be chosen. As with (ii) above, this parameter is also unchanged in all subsequent discussions.

Timing tests revealed that MAXCAL was first exceeded after 35 mins of CPU time had been used when incorporating a model combination of 6 free parameters to a data array of some 500 surface brightness measures.

Similar methods have recently been described by Kodaira et al (1986) and by Schombert & Bothun (1987), which aim to minimise the sums of squares of residuals or the χ^2 respectively over the available parameter space of a two-component (exponential + $r^{1/4}$ law) model combination using least-squares techniques. The latter method is found to recover the structural parameters of interest with variations in input estimates of up to ± 20 %, but differs from the present technique in adopting an extension of the iterative "disc + bulge" scheme developed by Kormendy (1977a) and is therefore expected to be constrained by the limitations of that scheme as outlined in section III.2 above. It also differs from my routine in that explicit boundaries are imposed for the region of parameter space to be searched, these being defined on the basis of the expected ranges in such parameters thought to be physically realistic. In the present method I do not adopt any such bounds as it was considered that such limits could not be reliably defined. Furthermore, their methods do not seek to

investigate the existence of a possible "intermediate" component in spiral galaxies and lenticulars as is intended here.

III.5 Testing the program on a "model" galaxy

I now outline the first of a series of tests conducted with a view to determining the operating characteristics of the modelling algorithm. The "model" galaxy concerned was constructed by producing an array of "surface brightness" values as a function of galactocentric distance and Z-height, specified on the basis of a number of desired components and the model parameters adopted for these components. In addition, errors were assigned to each point on the basis of the following expected uncertainties (as a function of surface brightness) :

$20 < \mu < 23$	mag arcsec^{-2}	assigned error	=	0.02 mag. arcsec^{-2}
$23 < \mu < 25$	"	"	=	0.04 mag. arcsec^{-2}
$25 < \mu < 27$	"	"	=	0.08 mag. arcsec^{-2}
$27 < \mu$	"	"	=	0.20 mag. arcsec^{-2}

Such values correspond quite closely to the actual scatter in μ typically found in studies of this kind. The above errors are assigned at each point to allow one to perform weighted least-squares fits to the model data.

An additional feature of the program allowed the possibility of "skipping over" specified rows of input model data before the program was run. This enabled one to simulate the decreased contribution from a thin disc to the resultant profiles - and hence test the viability of the program in discerning not only the parameter values assigned to each component, but more generally the number of components actually thought likely to exist in the data being used.

The effect of systematic errors :

Systematic errors (as might result from an incorrect choice of sky value) were simulated by simply adding the adopted errors set out above to the model data values themselves. Modelling then proceeded as follows :

a). Using all the available model data, fits were run based on the set of parameters used to generate the initial dataset. This served to ensure that the fitting program would generate the initial input parameters used to define my "model" galaxy, and results showed that this was indeed found to be the case.

b) A follow-up series of iterations were then performed by sequentially changing the initial estimates for the parameters to be minimised. These were of considerable value in defining the reliability of the program to generate the same output parameters from a (widely varying) set of input estimates.

c). Varying amounts of thin disc contribution were sampled (using the method described above) and step (b) was then repeated.

The latter two steps were continued, systematically changing the input parameters after each successful iteration, until the routine failed to converge.

The results of such tests showed the algorithm to be very robust to a wide variety of input measures. For example, in the case of a simple "exponential model + $r^{1/4}$ law profile" combination, identical output values were recovered (within the rounding errors) from variations in the input central surface brightness in both models of ~ ± 2 mag. arcsec^{-2}; in exponential scaleheight of ~ ± 14 arcsecs (± 80

%); exponential scalelength ~ ± 34 arcsecs (± 30 %); $r^{1/4}$ law axis ratio ~ ± 0.2 (± 30 %); and $r^{1/4}$ law scalelength ~ ± 20 arcsecs (± 33 %). Several series of iterations run at each step generated final output parameters which were consistent between one run and the next, and testify to the reliability of the values thus produced. In addition, the model was clearly able to define runs in which the "wrong" model combinations were being applied to the data - wrong in this sense meaning attempts to describe a "model" galaxy made up of a two-component model combination by a three-component fit and vice-versa. Excessively large sums of squares of residuals, reduced χ^2 and, less reliably, number of iterations required before convergence, were all good diagnostics of such an inappropriate model or the use of insufficient data (as occured when the thin disc contribution was removed entirely).

The addition of random noise :

Random noise at any point in the model data array was generated by the use of a random number generator (RNNORM), based on a mean of zero and a σ equal to the error assigned to that particular point in the array. Such noise was then added to the calculated surface brightness, a visual inspection of the result indicating close resemblance to actual profiles in terms of the typical scatter observed at any particular μ.

The same fitting precepts outlined above were adopted here. The most notable feature was a considerably increased sum of squares of residuals derived when incorporating such errors (typically 0.1 to 1.0 compared to ~ 10^{-6} or 10^{-7} as found previously). It was noted that to achieve a fit, certain parameters had to be fixed at specified

values. Experimentation indicated that when an $r^{1/4}$ law profile was used, it was generally the parameters for this component which were the most difficult to constrain, in particular the scalelength θ_e. Once the latter was fixed, repeatable fits were generated to within the rounding errors of ~ one part in 10^5, and with equally accurate output estimates for the input parameters to those found previously.

Again the program was found to be extremely successful at isolating cases in which inappropriate components were being fitted to the data being used. In such cases bad fits were evidenced either by the failure of convergence (i.e. the number of iterations exceeding ~ 50), premature exits from the fit because of simple arithmetic errors, or reduced χ^2 values a factor of ~ 2 to 5 greater than before.

In addition, the reproducibility of the final output values were again confirmed by running a series of fits with large variations in input, identical results being given in all cases when good fits to the data were initially obtained. The quality of the fits were never improved by altering the initial estimates of the parameters to be minimised. The modelling also proved to be very sensitive to the amount of thin disc removed from the test data before the fit was made, as one would expect. It is, however, important to note that the routine explicitly seeks to minimise the sum of squares of residuals, rather than the χ^2. Preliminary tests indicated that the endpoints of a particular iteration did not necessarily yield the smallest χ^2 values. For this reason, subsequent discussion will principally focus on results deduced from comparisons of the sum of squares, the importance of the χ^2 (or reduced χ^2) only being noted in cases when the former was unable to distinguish between respective model

combinations.

III.6 Application of the modelling to NGC 891

In this section I describe the results of tests carried out using existing literature data for the edge-on spiral galaxy NGC 891. The data concerned are the J, F and U' passband photographic material of van der Kruit & Searle (1981b, herafter KS81) and kindly made available by the first author. Their use in this context are of particular value in allowing one to compare directly with those parameters derived by van der Kruit & Searle using their own technique, as well as contrasting with the method (and the results) of Bahcall & Kylafis (1985) who make use of the same data set. An adopted distance to this galaxy of 9.5 Mpc is taken from KS81.

One is first required to define the error distribution for the data being modelled. Such errors were typically defined by the scatter in the measures of μ at any particular position on the galaxy between the plates used (see figure 4 of KS81). This procedure was followed by taking all the available surface brightness profiles in a particular band and normalising them at a Z-height above the plane of 32 arcsecs (i.e. scaling each profile such that the surface brightnesses were equal at that Z). The resultant scatter in μ was taken as the typical uncertainty except in the region of normalisation and over the faintest levels where too few data points existed to define a reliable error. In these cases I simply interpolated the errors across such regions - from Z $\sim$ 20 to 40 arcsecs at the point of normalisation, and smoothly extrapolated faintward from the last Z-height at which a sufficient number of individual surface brightness measures existed to

define such scatter.

III.6.1 Results

A methodology was adopted whereby I tested the applicability of all possible two- and three- component model combinations adopting the forms detailed in section III.3.1 above. Table 3.1 gives the models tested in these series of fits, and outlines their statistical quality (in terms of the sum of squares of residuals, the reduced χ^2 and their associated significance limits based on estimates given in standard tables), whilst table 3.2 shows the resultant parameters derived in each particular case. An inspection of table 3.1 indicates that the data for this galaxy, in all colours, can be well approximated by a simple two-component model. These parameter values are again "input estimate invariant" i.e. they result from a series of fits run with widely varying input parameters and as such are very reproduceable in all cases.

In terms of the sum of squares of residuals alone, it is clear that an equally good description of this galaxy can be achieved by the adoption of either the exponential or $sech^2$ form for the thin disc - the sum of squares differing by no more than 2 % when comparing such models within each photometric band. A similar "fit-by-fit" comparison of the corresponding reduced χ^2 estimates yields a similarity at ~ 93 %. In addition, although the sum of squares fail to differentiate the most appropriate model form for the non-thin disc light, an inspection of table 3.1 indicates a marginal improvement in the reduced χ^2 estimates with the adoption of the $sech^2$ form. However, a more detailed comparison of these reduced χ^2 values

MODELS ADOPTED	J BAND			U' BAND			F BAND		
	FSUMSQ	red. χ^2	P (%)	FSUMSQ	red. χ^2	P (%)	FSUMSQ	red. χ^2	P (%)
(a) Two-component combinations (ν = 6) :									
$sech^2$ thin disc +									
exp. thick disc	1.4×10^{-4}	0.63	>99.5	1.7×10^{-4}	0.63	>99.5	2.6×10^{-4}	0.82	>99.0
$sech^2$ thick disc	1.2×10^{-4}	0.55	>99.5	1.7×10^{-4}	0.64	>99.5	2.4×10^{-4}	0.71	>99.0
$r^{1/4}$ law profile	2.1×10^{-4}	1.09	>97.5	1.9×10^{-4}	0.73	>99.0	3.1×10^{-4}	1.12	>97.5
exp. thin disc +									
exp. thick disc	1.5×10^{-4}	0.76	>99.0	1.9×10^{-4}	0.72	>99.0	2.9×10^{-4}	0.99	>97.5
$sech^2$ thick disc	1.2×10^{-4}	0.65	>99.5	1.7×10^{-4}	0.70	>99.0	2.4×10^{-4}	0.85	>99.0
$r^{1/4}$ law profile	2.0×10^{-4}	0.91	>97.5	1.9×10^{-4}	0.74	>99.0	3.0×10^{-4}	1.09	>97.5
(b) Three-component combinations (ν = 9) :									
$sech^2$ thin disc +									
$sech^2$ thick disc +									
$r^{1/4}$ law profile	1.2×10^{-4}	0.55	>99.5	1.6×10^{-4}	0.74	>99.5	DID NOT FIT DATA		
exp. thick disc +									
$r^{1/4}$ law profile	1.3×10^{-4}	0.66	>99.5	1.6×10^{-4}	0.70	>99.5	2.5×10^{-4}	0.92	>99.5
exp. thin disc +									
$sech^2$ thick disc +									
$r^{1/4}$ law profile	1.1×10^{-4}	0.65	>99.5	1.6×10^{-4}	0.77	>99.5	2.3×10^{-4}	0.89	>99.5

Table 3.1 : Statistical "quality of fit" parameters for the modelling of the NGC 891 data using the error distribution of van der Kruit & Searle (1981b), modified as described in the text. The parameters listed are the sum of squares of residuals (FSUMSQ); the reduced χ^2; and the probability level of acceptance (P) based on values given in standard tables. The number of degrees of freedom (ν), taken as the number of parameters to be minimised, is also shown. Note that no other three-component model combinations, aside from the ones shown, were found to converge for any input estimates tested.

MODELS ADOPTED	THIN DISC MODEL			THICK DISC MODEL			$r^{1/4}$ LAW PROFILE		
	J	U'	F	J	U'	F	J	U'	F
(a) Two-component combinations :									
$sech^2$ thin disc + exp. thick disc	μ_o = 21.15 h_R = 4.2 Z_o = 0.92	22.07 4.4 1.17	20.14 4.1 0.92	μ_o = 22.04 h_R = 5.9 h_Z = 1.55	23.41 6.8 2.44	21.39 5.4 1.68			
$sech^2$ thin disc + $sech^2$ thick disc	μ_o = 21.05 h_R = 4.3 Z_o = 0.97	21.96 4.5 1.15	20.06 4.2 0.95	μ_o = 23.21 h_R = 4.5 Z_1 = 2.79	24.16 5.0 3.71	22.52 4.1 2.99			
$sech^2$ thin disc + $r^{1/4}$ law profile	μ_o = 21.48 h_R = 4.6 Z_o = 1.26	22.18 4.8 1.32	20.45 4.5 1.13				μ_e = 22.25 θ_e = 2.8 q = 0.57	24.50 7.9 0.57	20.65 2.1 0.56
exp. thin disc + exp. thick disc	μ_o = 19.96 h_R = 5.4 h_Z = 0.51	21.10 5.8 0.75	19.05 5.2 0.54	μ_o = 22.07 h_R = 5.8 h_Z = 1.56	23.88 7.0 2.95	21.56 5.4 1.76			
exp. thin disc + $sech^2$ thick disc	μ_o = 19.93 h_R = 5.6 h_Z = 0.56	20.99 6.0 0.70	19.00 5.3 0.56	μ_o = 23.31 h_R = 4.5 Z_1 = 2.86	24.33 5.0 3.90	22.68 4.1 3.11			
exp. thin disc + $r^{1/4}$ law profile	μ_o = 20.51 h_R = 5.8 h_Z = 0.78	21.25 6.3 0.81	19.41 5.6 0.69				μ_e = 23.17 θ_e = 3.8 q = 0.61	24.45 7.1 0.54	21.30 2.6 0.59
(b) Three-component combinations :									
$sech^2$ thin disc + $sech^2$ thick disc + $r^{1/4}$ law profile	μ_o = 21.04 h_R = 4.5 Z_o = 0.88	22.14 4.8 1.24	—— —— ——	μ_o = 22.87 h_R = 4.4 Z_1 = 2.32	24.91 5.0 4.13	—— —— ——	μ_e = 25.28 θ_e = 6.6 q = 0.71	23.83 3.0 0.34	—— —— ——
$sech^2$ thin disc + exp. thick disc + $r^{1/4}$ law profile	μ_o = 21.25 h_R = 4.4 Z_o = 0.90	22.15 4.7 1.14	20.30 4.4 0.93	μ_o = 21.90 h_R = 5.7 h_Z = 1.38	23.49 6.3 2.04	21.45 5.2 1.45	μ_e = 24.23 θ_e = 3.4 q = 0.54	24.60 4.8 0.45	21.65 2.1 0.53
exp. thin disc + $sech^2$ thick disc + $r^{1/4}$ law profile	μ_o = 19.92 h_R = 5.7 h_l = 0.52	21.04 6.2 0.68	19.05 5.5 0.56	μ_o = 23.07 h_R = 4.3 Z_1 = 2.51	24.50 4.5 3.56	22.68 4.0 2.86	μ_e = 26.69 θ_e = 10.9 q = 0.65	24.49 4.0 0.38	23.52 3.5 0.53

Table 3.2 : Resultant "best-fit" output parameters derived from the modelling of NGC 891 for all model combinations from which convergence was achieved. The quoted parameters are the central surface brightness (μ_o, μ_e) in mag arcsec^{-2}; the scalelength (h_R, θ_e) in kpc; the scaleheight (h_Z, Z_o, Z_1) also in kpc; and the axis ratio q. The conversion to kpc for all scale parameters is based on an assumed distance to NGC 891 of 9.5 Mpc (such that 1 arcsecs = 46.1 pc).

(either on a "fit-by-fit" basis or by forming averaged values) indicates that such an improvement is not statistically significant. To illustrate the quality of the results thus obtained, figure 3.1 shows a representative selection of model fits to individual (J band) profile cuts adopting the double $sech^2$ model combination of table 3.2.

A notable point from section (a) of table 3.2 is the high degree of reproduceability of the final model parameters between the various model combinations. There is also a large degree of similarity between respective scale parameters in the J and F passbands, as evidenced by the ratios of the averaged parameters given in table 3.3. The (J-F) colour index of the thin disc model as given in table 3.3 compares favourably with the estimate of 0.99 quoted by KS81 for this galaxy.

However, pronounced differences are found in all parameters when one compares results for the J or F bands with those obtained in U' - particularly so when comparing U' and F band results. The distribution of associated errors is very different in the U' band than in either J or F, a point probably only giving rise to differences in the statistical "quality-of-fit" parameters given in table 3.1. An additional reason for the parameter differences in table 3.3 may stem from the colour gradient noted by van der Kruit & Searle. The existence of such a gradient, seen as a bluer colour of the disc light at larger galactocentric distance, would be expected to have some effect on a comparison of the derived model parameters between each passband, but particularly so between U' and F (as is seen to be the case in table 3.2) where the difference in effective wavelengths is greatest. Furthermore, those derived thin disc colour indices shown in table 3.3 incorporating the U' band are considerably redder than the

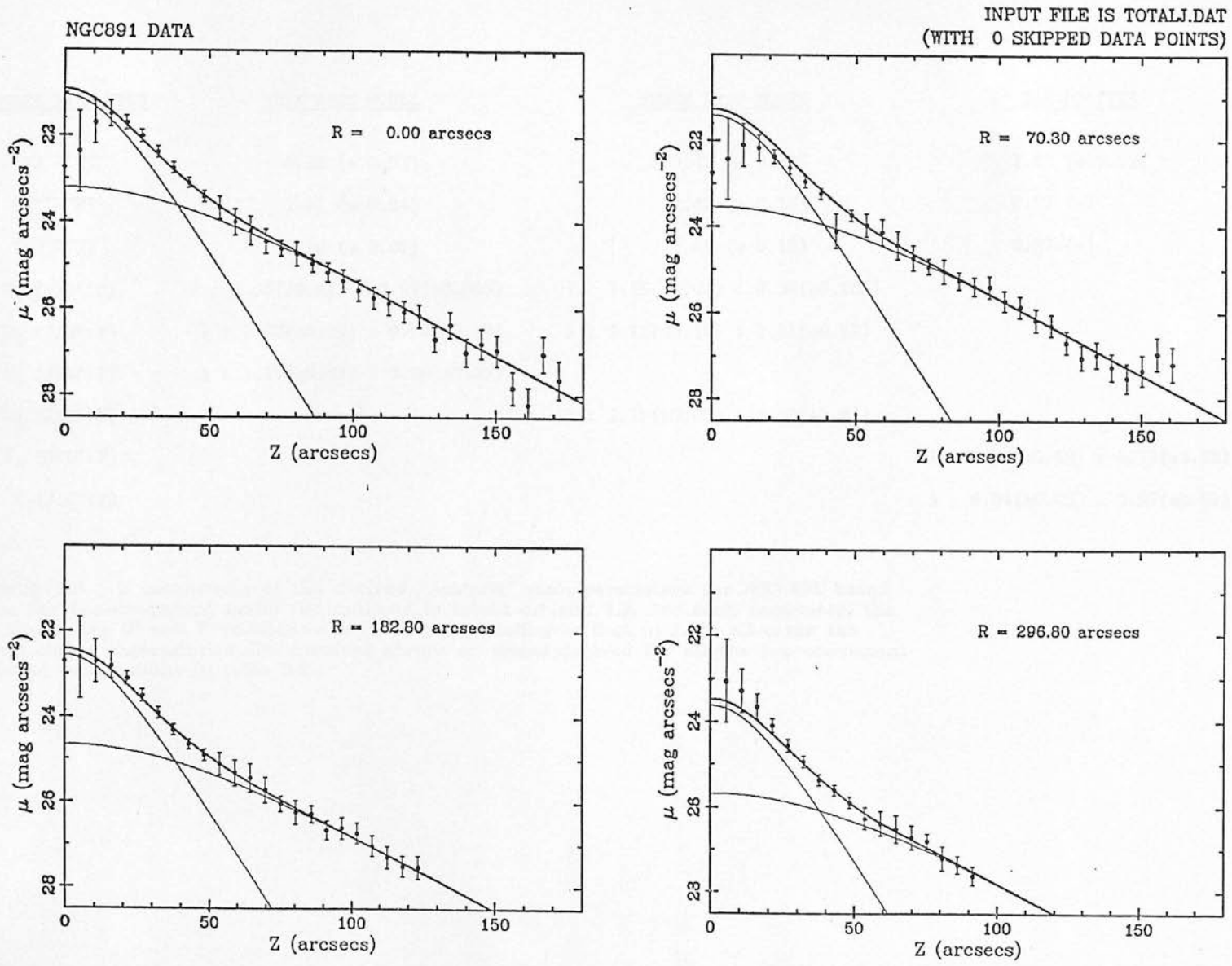

Figure 3.1 : Resultant model fits to the J band data of NGC 891 after adopting a double $sech^2$ model combination. Only a representative subset of the fits derived are illustrated here.

MODEL PARAMETER	THIN DISC MODEL	THICK DISC MODEL	$R^{1/4}$ LAW PROFILE
$\overline{(J-F)}$	0.92 (± 0.03)	0.43 (± 0.03)	1.02 (± 0.03)
$\overline{(U'-F)}$	1.71 (± 0.04)	1.43 (± 0.13)	0.97 (-)
$\overline{(U'-J)}$	0.78 (± 0.07)	0.99 (± 0.15)	0.97 (-)
$\overline{h}_R$ (J:U':F)	1 : 1.06(±0.01) : 0.97(±0.005)	1 : 1.15(±0.02) : 0.92(±0.005)	
$\overline{h}_Z$ (J:U':F)	1 : 1.25(±0.12) : 0.98(±0.05)	1 : 1.73(±0.16) : 1.11(±0.02)	
$\overline{Z}_o$ (J:U':F)	1 : 1.17(±0.07) : 0.96(±0.03)		
$\overline{Z}_1$ (J:U':F)		1 : 1.35(±0.02) : 1.08(±0.01)	
$\overline{e}_e$ (J:U':F)			1 : 2.34(±0.48) : 0.72(±0.03)
$\overline{q}$ (J:U':F)			1 : 0.94(±0.06) : 0.97(±0.01)

Table 3.3 : A comparison of the derived "best-fit" scale parameters for NGC 891 based on the two-component model fits outlined in tables 3.1 and 3.2. For each parameter, the ratio in the U' and F passbands is given after scaling to that in J. In all cases the associated uncertainties are standard errors on means derived for all the two-component model combinations in table 3.2.

values quoted by van der Kruit & Searle (for which (U'-F) = 1.15 and (U'-J) = 0.16). The reason for this is almost certainly due to the inclusion in the present modelling scheme of all the expected thin disc light - KS81 only consider data taken at $Z \gtrsim 32$ arcsecs to avoid contamination of the luminosity profiles by dust obscuration. An inspection of the distribution in (U'-F) (their figure 3) shows that interior to $Z \sim 1$ kpc and $R \sim 10$ kpc, the disc is dominated by sources with (U'-F) redder than 1.6 - 1.8. This conclusion is confirmed when progressively larger amounts of the thin disc are removed from the profiles before fitting. I find that removal of data to a Z-height of 21 arcsecs has very little effect on the derived model colour indices in all bands (because the data points being removed are assigned a very low weight on account of their very large associated errors), whilst the removal of more thin disc contribution to $Z \approx 32$ arcsecs results in a reduction of all colour indices (i.e. a progressive trend towards bluer colour), the form of which is identical to that seen in the KS81 data.

The results of KS81 suggest a far larger colour gradient in (U'-F) in the non-thin disc component than is seen in the disc, together with one in, to a lesser degree, (U'-J). One might, therefore, expect there to be significantly larger differences in scale parameters between U' and J or F passbands than was found to be the case for the model thin disc - an inspection of table 3.3 confirms this prediction. Indeed, on the basis of the standard errors quoted in that table, the differences in scaleheights in both exponential and $sech^2$ thick disc model forms are in excess of 10σ (J:U') and 14σ (U':F). Such a colour gradient, coupled with the effects of including all the thin disc photometric data as noted previously, is also likely to

account for any discrepancies which might exist between the (U'-F) and (U'-J) colour indices found here and those quoted by van der Kruit & Searle. Again the available evidence indicates a very small, if any, gradient in (J-F) - precisely the result one would expect on the basis of the great similarity in all thick disc model components between these photometric passbands seen in table 3.3. Table 3.4 compares the "best-fit" parameters of the two-component "exp./sech^2 + exp./sech^2" model combinations (culled from table 3.2) with the currently available parameter values for this system as given in the literature. In all cases the agreement with the results of van der Kruit & Searle is reasonably good, although differences are apparent between the present values and those of Bahcall & Kylafis (1985) - a point I return to below.

It is also of interest to investigate the results of superposing a two-component model combination of exponential or sech^2 thin disc model and an $r^{1/4}$ law profile to the NGC 891 data. Table 3.1 shows that the adoption of any such combination gives a somewhat poorer fit to this galaxy based on comparisons of either the sum of squares or the reduced χ^2. A "fit-by-fit" comparison of the respective reduced χ^2 estimates yield statistical degradations in the goodness-of-fit from 99.5 % (with the adoption of a sech^2 model) to 97.5 % (with an $r^{1/4}$ law profile) in J, 99.5 % to 99.0 % in U' and 99.0 % to 97.5 % in F. Thus, were one to exclude all model combinations at either the 99.5 % or 99.0 % confidence levels, a two-component model comprising a "sech^2/exponential disc + $r^{1/4}$ law" combination would be rejected in favour of the "exp./sech^2 + exp./sech^2" set. However, in view of the strong dependance of such probabilities on the adopted error distribution (see section III.7 below), a more meaningful comparison

Adopted model		J			U'			F		
		present study	KS2 + vdK	BK	present study	KS2 + vdK	BK	present study	KS2 + vdK	BK
$sech^2$ thin disc	μ_o =	21.2 (±0.1)	22.0		22.1 (±0.1)	22.2		20.2 (±0.1)	21.0	
	h_R =	4.4 (±0.1)	4.9		4.6 (±0.1)	4.9		4.3 (±0.1)	4.9	
	Z_o =	1.05 (±0.11)	0.99		1.21 (±0.05)	0.99		1.00 (±0.05)	0.99	
exponential thick disc	h_R =	5.9 (±0.05)	5.0	2.7-2.9	6.9 (±0.1)	5.0	2.7-2.9	5.4 (-)	5.0	2.7-2.9
	h_Z =	1.56 (±0.01)	1.5	1.0-1.3	2.7 (±0.3)	1.5	1.0-1.3	1.72(±0.04)	1.5	1.0-1.3

Table 3.4 : A comparison of the present "best-fit" resultant parameters for NGC 891 to those existing in the literature. As in table 3.2, zeropoints are quoted in mag. arcsec^{-2} and scale parameters in kpc. The adopted errors for these values in the current analysis are as given in table 3.3. Zeropoints for the exponential thick disc model are not available in the literature sources. The parameter ranges quoted for the Bahcall & Kylafis results are those calculated on the basis of the disc measures taken from van der Kruit & Searle.

SOURCES OF DATA

BK : Bahcall & Kylafis (1985)
KS2 : van der Kruit & Searle (1981b)
vdK : van der Kruit (1984)

results from an inspection of changes in the sum of squares between the respective fits. A "fit-by-fit" comparison from table 3.1 yields the following :

FSUMSQ (exp. model : $sech^2$ model : $r^{1/4}$ profile)
= 1.21 (±0.04) : 1 : 1.71 (±0.04) in J,
= 1.06 (±0.06) : 1 : 1.12 (-) in U',
= 1.15 (±0.06) : 1 : 1.27 (±0.02) in F,

which, on the basis of the quoted standard errors, amount to $\gtrsim 3\sigma$ effects in J or F.

When one studies the resultant model parameters given in table 3.2 it is evident that, while the thin disc model parameters are in good agreement with all these values in alternative two-component model combinations, μ_e and e_e for the $r^{1/4}$ law show very large discrepancies between the respective photometric bands. Only the axis ratio q, for which I find a mean of 0.57 (±0.01), appears to be invariant from one model combination to the next and between the various passbands. Thus, whilst the derived significance levels indicate only a marginal difference between the model fits to the NGC 891 data which use an exponential or $sech^2$ profile over those adopting the $r^{1/4}$ law form, a comparison of both the derived sum of squares and reduced χ^2 in each case indicate considerable improvement with the use of the former over the latter. If the derived fits are also required to reproduce the available literature data for this object, the above conclusion is strengthened by the implausibly discordant model parameters between passbands which result when adopting the $r^{1/4}$ law profile.

This result is of some importance in the light of the main conclusions derived by Bahcall & Kylafis (1985) who argue that such a

distinction between model forms cannot be made, in this or any other galaxy, on the basis of currently available photometry. Since there is no evidence to the contrary, it is assumed for present purposes that the study of Bahcall & Kylafis adopts an error distribution akin to that of van der Kruit & Searle and hence essentially identical to that used here. The reason for the differences in the present conclusions and those of Bahcall & Kylafis may lie in the nature of the model forms adopted.

In figure 3.2a I plot the difference in derived surface brightness distributions between the $r^{1/4}$ law (labelled $\mu_{de\ Vauc}$) and an exponential (μ_{exp}) model along a parallel profile calculated at a Z-height of 1.5 kpc - a value which, at the distance of NGC 891, corresponds to a profile unaffected by likely dust contamination from the galactic plane based on the expectations of KS81. The model parameters used in each case are those derived from the present modelling results in the F bandpass for the non-thin disc component of NGC 891 and quoted in table 3.2. The associated error bars are calculated on the basis of the error in this magnitude difference (which in turn are derived from the adopted error distribution in F outlined in section III.6 above). Evidently to an $\mathbb{R} \sim 3$ kpc ($\approx 1.3\ e_e$ or $0.7\ h_R$ assuming the average values given in table 3.2), the two models appear to be essentially identical within the quoted errors. Beyond this point they diverge (in the sense of the $r^{1/4}$ law profile becoming progressively fainter than the exponential form as $\mathbb{R}$ increases) out to $\mathbb{R} \sim 12$ kpc, beyond which a constant difference of $\sim$ 1.2 mag. is predicted.

However, figure 3.2b is of more value in this regard as it plots

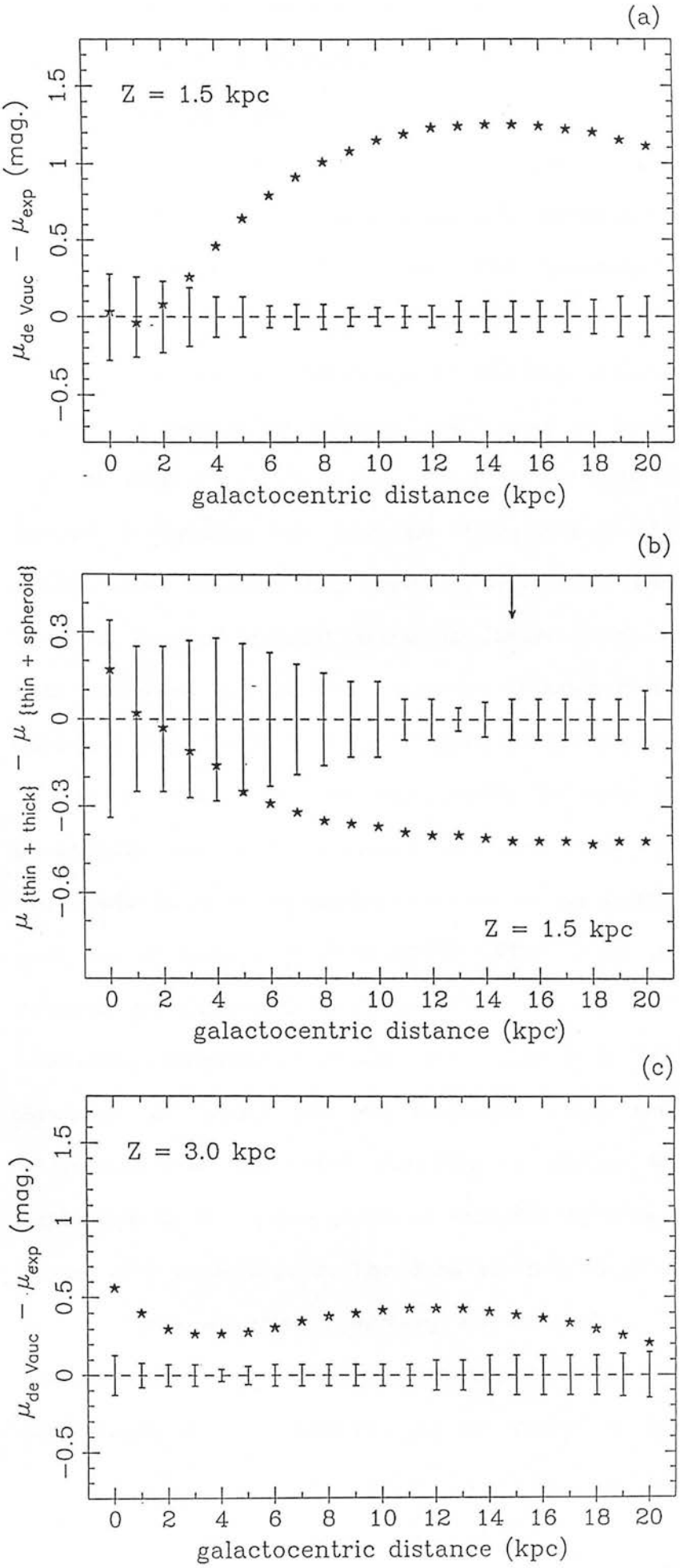
(a)
Z = 1.5 kpc
$\mu_{de\ Vauc} - \mu_{exp}$ (mag.)
galactocentric distance (kpc)
(b)
$\mu_{\{thin + thick\}} - \mu_{\{thin + spheroid\}}$
Z = 1.5 kpc
galactocentric distance (kpc)
(c)
Z = 3.0 kpc
$\mu_{de\ Vauc} - \mu_{exp}$ (mag.)
galactocentric distance (kpc)

figure 3.2

the *overall* discrepancy along such a parallel profile with the effect of the thin disc taken into account. The thin disc model concerned is of $sech^2$ form and is characterised by the *same* constituent parameters (again culled from table 3.2) in both combinations, with the error bars calculated as in figure 3.2a. From this plot it is seen that the model form describing the non-thin disc light essentially cannot be defined, within the errors, for $R \lesssim 8$ kpc. The (constant) difference of $\sim$ 0.4 mag. between the two combinations beyond this point is significant at the $\sim$ 3-4 σ level for all R out to the last measured point at 20 kpc (where the calculated surface brightness in both model combinations is $\sim$ 26 mag $arcsec^{-2}$). Hence, from figure 3.2b it is concluded that Bahcall & Kylafis may find no difference in the respective model combinations because they impose a magnitude limit of 25 mag $arcsec^{-2}$ (marked by the vertical arrow in figure 3.2b) and do not consider data faintward of this limit. Adoption of such a limit will lead to their sampling only $\sim$ 4 kpc of R in figure 3.2 (corresponding to $\sim$ 1.7 θ_e or $\sim$ 0.9 h_R) over which to distinguish between these model forms - potentially too small a range for any real differences to become apparent. Such a conclusion is also to be found in the star count analyses of Gilmore & Reid (1983). They were unable to distinguish between an exponential and an $r^{1/4}$ law profile for the non-thin disc luminosity distribution in our own Galaxy to Z $\sim$ 5 kpc and R $\sim$ 3.5 θ_e. However, in using all the available data, the present modelling procedure overcomes the inability to define the model form most applicable to the outer parts of NGC 891 by sampling data to an R in excess of 7 scalelengths. The data at such large R ($\sim$ 18 kpc), despite having large associated errors, are crucial in this regard as their inclusion places a sufficient constraint on the modelling process to allow such a discrimination to be made. It is important to note,

however, that only data at small Z-heights are required for this goal to be achieved since the exponential and $r^{1/4}$ law models become essentially indistinguishable at larger Z - as evidenced by figure 3.2c which shows differences in respective forms, as in figure 3.2a, but evaluated at a Z-height of 3 kpc ($\sim$ 1.7 h_Z on the basis of the values given in table 3.2).

Differences in the conclusions between respective studies of this galaxy may also arise from the criteria adopted in determining the acceptability of a particular model fit to the data. Bahcall & Kylafis (1985) not only rely on a comparison between the sum of squares of residuals, but also on a visual inspection of the degree of agreement with the actual galaxian isophotal contours. The latter criterion is clearly highly subjective.

Hence, on the basis of the arguments presented above, and despite the fact that the present modelling procedure was unable to distinguish between the respective model forms in the case of the thin disc, it would seem that the conclusions of Bahcall & Kylafis are unduly pessimistic. Existing data *are* sufficiently accurate to define the most likely model applicable to the non-thin disc light in this particular system based on the statistical "quality-of-fit" estimators thus derived. Presently available data in this system extend to the point at which one would expect the respective two-component models to differ by $\sim$ 0.4 mag. This magnitude difference is indeed reflected in the statistical fit parameters of table 3.1 - it thereby precludes the necessity for the observations of this galaxy to be accurate to $\sim$ 0.1 mag. at 1 % of the adopted sky brightness level (i.e. a surface brightness of $\mu_F \sim 26.0$ mag arcsec^{-2} in this particular case) as

required by Bahcall & Kylafis. This discussion, of course, assumes no zeropoint errors in the data. The existence of any such systematic uncertainties will be the predominant cause of any differences in the "quality-of-fit" parameters between the respective passbands, although they will not affect the "fit-by-fit" comparisons within each band as used previously.

Use of a three-component model :

I tested the possible existence of a three-component structure to NGC 891 primarily with the intention of defining whether the adoption of an additional component gives a statistically significant improvement to modelling of this system, but also to define the reliability of the fitting routine itself. Such tests also facilitated a comparison to published work on this galaxy, in particular the study of van der Kruit (1984) which presents the effects on the model fits of the inclusion of three-components (his figure 3). He concludes that such a combination gives a somewhat better fit to the data than does the simple two-component combination of a $sech^2$ thin disc and $r^{1/4}$ law model form, but this point was not addressed in a statistically meaningful way.

In the present modelling, I assume only an $r^{1/4}$ law profile for the non-thin disc component in this galaxy, a procedure which essentially limits the present investigation to one involving four possible model combinations (namely the "$sech^2$/exponential thin disc + $sech^2$/exponential thick disc + $r^{1/4}$ law" sets). As table 3.1 shows, only 3 of these possible combinations achieved convergence, whilst a further model combination was unable to achieve a fit for the F band data, regardless of input parameters tested. These parameters are

again considered to be very reproduceable in the light of the wide variety of such input estimates which were still found to yield the output values given in table 3.2.

From a detailed comparison of the fit parameters outlined in table 3.1 for those model combinations which were able to converge to a result, it is clear that no significant improvements result from the adoption of an additional model component. For example, I find that a comparison of the resultant sum of squares between the respective ("sech^2/exp. thin + sech^2/exp. thick disc) two-, and their corresponding three, -component combinations, yields

$$\overline{\text{FSUMSQ}}\ (2\ \text{component} : 3\ \text{component}) = \begin{array}{ll} 1 : 0.95 & \text{in J,} \\ 1 : 0.94 & \text{in U',} \\ 1 : 0.96 & \text{in F.} \end{array}$$

Aside from the failure of convergence in all but the 3 combinations shown in table 3.2, and from the inability of one such combination to model the F band data, the three-component models show pronounced differences in derived model parameters. The latter is clearly seen in table 3.5 which indicates that, aside from the thin disc parameters (which are found to be very comparable to those of table 3.3 previously), large fluctuations are present in all other corresponding values between the photometric bands. This point is very evident for both $\overline{\theta}_e$ and $\overline{q}$ in table 3.5 (for reasons noted above we would expect such parameters to be essentially identical in J and F although this table clearly precludes such a result) and in the mean colour indices which are mostly excluded on the basis of the results of KS81, particularly those for the exp./sech^2 thick disc component. Based on a visual inspection of the fits thus derived, the cause for the large degree of similarity in fit parameters in table 3.1

MODEL PARAMETER	THIN DISC MODEL	THICK DISC MODEL	$R^{1/4}$ LAW PROFILE
$\overline{(J-F)}$	0.87 (± 0.08)	0.24 (±0.01)	1.12 (± 0.42)
$\overline{(U'-F)}$	1.72 (± 0.01)	1.59 (± 0.03)	0.92 (± 0.24)
$\overline{(U'-J)}$	0.89 (± 0.06)	1.49 (± 0.14)	-0.05 (± 0.19)
$\bar{h}_R$ (J:U':F)	1 : 1.07(±0.01) : 0.98(±0.02)	1 : 1.10(±0.03) : 0.92(±0.01)	
$\bar{h}_Z$ (J:U':F)	1 : 1.31(-) : 1.08(-)	1 : 1.48(-) : 1.05(-)	
Z_o (J:U':F)	1 : 1.34(±0.07) : 1.03(-)		
Z_1 (J:U':F)		1 : 1.60(±0.18) : 1.14(-)	
$\bar{e}_e$ (J:U':F)			1 : 0.74(±0.33) : 0.47(±0.15)
$\bar{q}$ (J:U':F)			1 : 0.63(±0.11) : 0.90(±0.08)

Table 3.5 : As table 3.3 but for all those three-component model combinations in the present fitting procedure found to achieve convergence. The associated uncertainties are again standard errors.

between the two- and three-component sets arises because the outermost component in the latter is always suppressed to such an extent that these combinations essentially comprise of only two model constituents - a point confirmed by the similarity in thick disc parameters between table 3.2(a) and (b), and graphically illustrated in figure 3.3 which shows model fits to a representative subset of the J band profiles using the "sech^2 + exp. + $r^{1/4}$ law" model combination of table 3.2. From this figure, it is clear that the inclusion of the additional component only becomes significant in the very outermost regions of any perpendicular surface brightness profile (where the associated errors are likely to be in excess of ~ 0.25 mag.), and only becomes dominant (in terms of its effect on the overall shape of the summed model profile) beyond the last measured point.

III.7 Modelling NGC 891 using an alternative error distribution

With a view to defining the reliability of the present algorithm as a function of the error distribution used, I performed an additional series of tests incorporating a much more restrictive distribution than that adopted previously. The errors given by Jensen & Thuan (1982) and derived from their B and R passband photometry of NGC 4565 were taken, after "magnitude weighting" as outlined in section III.8 below, and were suitably modified to the present investigations of NGC 891 by using the conversions between the respective photometric systems as outlined in KS81. This alternative error distribution is much more restrictive because Jensen & Thuan claim small random errors in their data set after plate-stacking and binning.

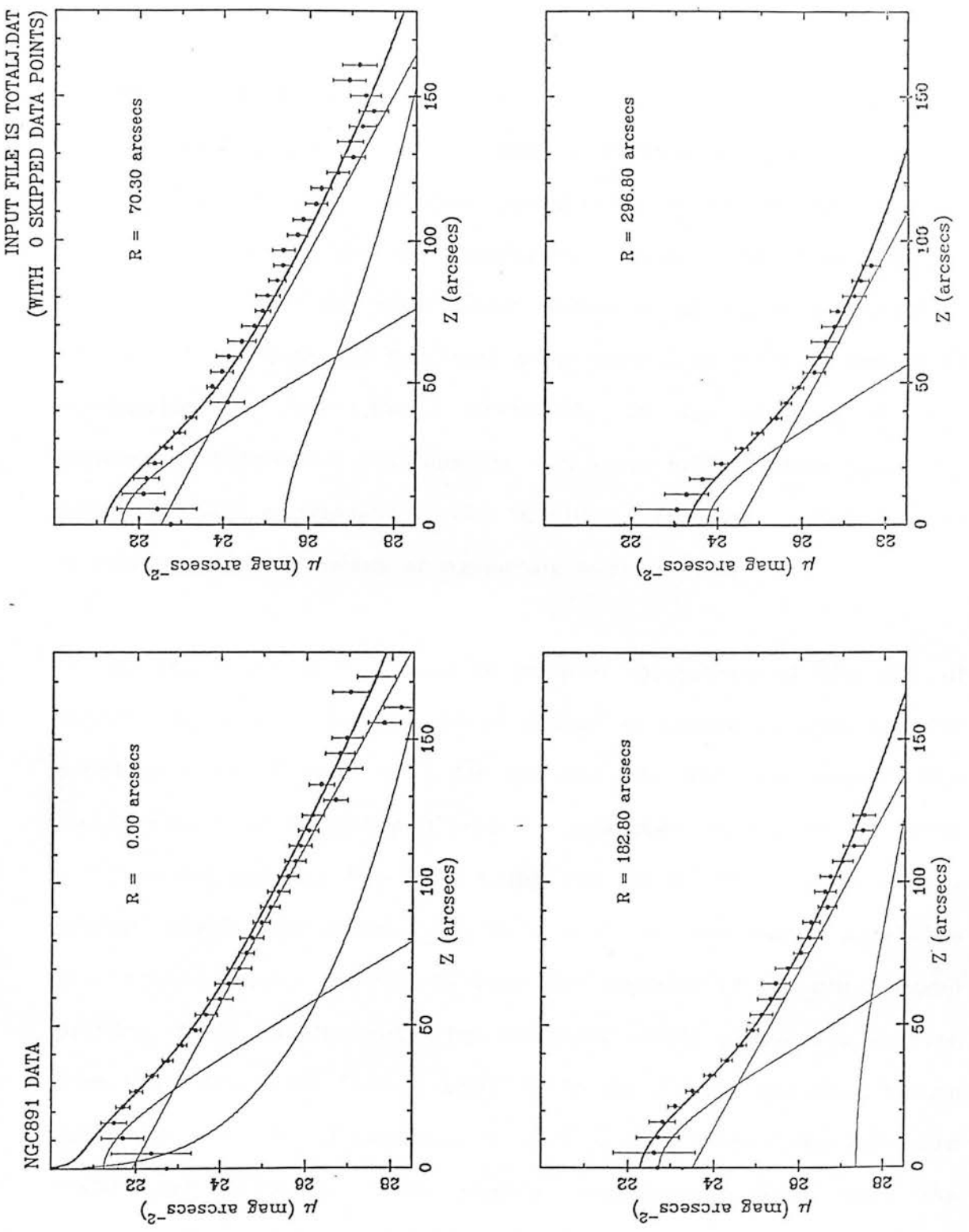
INPUT FILE IS TOTALJ.DAT
(WITH 0 SKIPPED DATA POINTS)
NGC891 DATA
R = 0.00 arcsecs
R = 70.30 arcsecs
R = 182.80 arcsecs
R = 296.80 arcsecs
μ (mag arcsecs⁻²)
Z (arcsecs)
0
50
100
150
22
24
26
28

figure 3.3

III.7.1 Results

In the light of the results noted previously, the present series of fits focussed on two-component model combinations alone. As a result of adopting such a restrictive distribution of errors, the present statistical fit parameters are considerably larger than those obtained previously - table 3.6 gives their values in all model combinations tested. Nevertheless, the resultant parameters thus obtained should be comparable to those found previously in the absence of any systematic differences between the two error distributions presently adopted, and a comparison of the "quality-of-fits" on a relative basis is still a justifiable means of comparing such models.

On the basis of just such a relative comparison of the sum of squares (or indeed the reduced χ^2 estimates) quoted in table 3.6, the adoption of an $r^{1/4}$ law profile for the non-thin disc data consistently yields a superior fit in the U' and F bands over the alternative forms - figure 3.4 showing fits in F using the "$sech^2$ thin disc + $r^{1/4}$ law profile" combination of table 3.7. Only in J does the use of an $r^{1/4}$ law give a significantly inferior fit than the majority of the other model profiles. Table 3.7 illustrates the resulting model parameters derived from these fits - the "exp. + exp." fit to the J band produces values particularly worthy of comment. In such a combination, the thin disc model has evidently been heavily suppressed such that the superposed model is essentially a single exponential. The discordant "quality-of-fit" resulting from using such a combination is also evident in table 3.6, in which a reduced χ^2, larger by a factor of $\sim$ 20

MODELS ADOPTED	J BAND			U' BAND			F BAND		
	FSUMSQ	red. χ^2	P (%)	FSUMSQ	red. χ^2	P (%)	FSUMSQ	red. χ^2	P (%)
$sech^2$ thin disc +									
exp. thick disc	4.5×10^{-4}	11.67	> 5.0	2.3×10^{-4}	10.14	>10.0	2.5×10^{-4}	11.17	> 5.0
$sech^2$ thick disc	4.6×10^{-4}	10.21	>10.0	2.2×10^{-4}	10.77	> 5.0	2.2×10^{-4}	9.25	>10.0
$r^{1/4}$ law profile	5.6×10^{-4}	15.37	> 1.0	1.4×10^{-4}	7.64	>25.0	9.0×10^{-5}	6.14	>25.0
exp. thin disc +									
exp. thick disc	6.0×10^{-4}	19.57	> 0.1	2.4×10^{-4}	10.53	>10.0	2.7×10^{-4}	11.67	> 5.0
$sech^2$ thick disc	4.2×10^{-4}	9.48	>10.0	2.2×10^{-4}	10.66	> 5.0	2.3×10^{-4}	10.01	>10.0
$r^{1/4}$ law profile	4.6×10^{-4}	12.30	> 5.0	1.4×10^{-4}	7.91	>10.0	1.2×10^{-4}	6.94	>25.0

Table **3.6** : As table **3.1** but using an alternative error distribution adapted to the NGC 891 data, as described in the text, from a "magnitude weighted" version of that given by Jensen & Thuan (1982) in their study of NGC 4565. The relevant statistical parameters are as given in table **3.1**.

MODELS ADOPTED		THIN DISC MODEL			THICK DISC MODEL			$R^{1/4}$ LAW PROFILE		
		J	U'	F	J	U'	F	J	U'	F
$sech^2$ thin disc + exp. thick disc	μ_o =	19.78	21.12	19.40	21.86	23.35	21.82			
	h_R =	3.6	3.6	3.0	6.9	8.4	7.0			
	Z_o =	0.58	0.94	0.92	h_Z = 1.45	2.26	1.85			
$sech^2$ thin disc + $sech^2$ thick disc	μ_o =	20.77	21.16	20.15	23.07	24.14	22.89			
	h_R =	4.4	3.9	3.8	5.0	6.0	5.0			
	Z_o =	0.80	0.95	1.04	Z_1 = 2.67	3.57	3.26			
$sech^2$ thin disc + $r^{1/4}$ law profile	μ_o =	21.78	21.45	21.01				μ_e = 20.74	22.11	19.13
	h_R =	5.6	4.7	4.8				θ_e = 1.7	2.7	1.3
	Z_o =	1.15	0.94	1.29				q = 0.48	0.44	0.54
exp. thin disc + exp. thick disc	μ_o =	75.23	19.97	18.98	21.66	23.55	21.97			
	h_R =	6.2	4.6	4.1	7.4	9.0	7.1			
	h_Z =	1.26	0.54	0.59	1.33	2.42	1.92			
exp. thin disc + $sech^2$ thick disc	μ_o =	20.50	20.02	19.62	23.54	24.32	23.32			
	h_R =	6.4	4.9	5.1	4.9	6.3	5.2			
	h_Z =	0.62	0.55	0.72	Z_1 = 3.04	3.78	3.63			
exp. thin disc + $r^{1/4}$ law profile	μ_o =	21.03	20.31	20.01				μ_e = 22.40	22.73	20.42
	h_R =	7.2	5.7	5.8				θ_e = 3.0	3.5	1.9
	h_Z =	0.84	0.55	0.81				q = 0.59	0.44	0.57

Table 3.7 : As table 3.2 but for the alternative error distribution of Jensen & Thuan (1982) derived as described in the text. The parameters have the same meanings as in table 3.2.

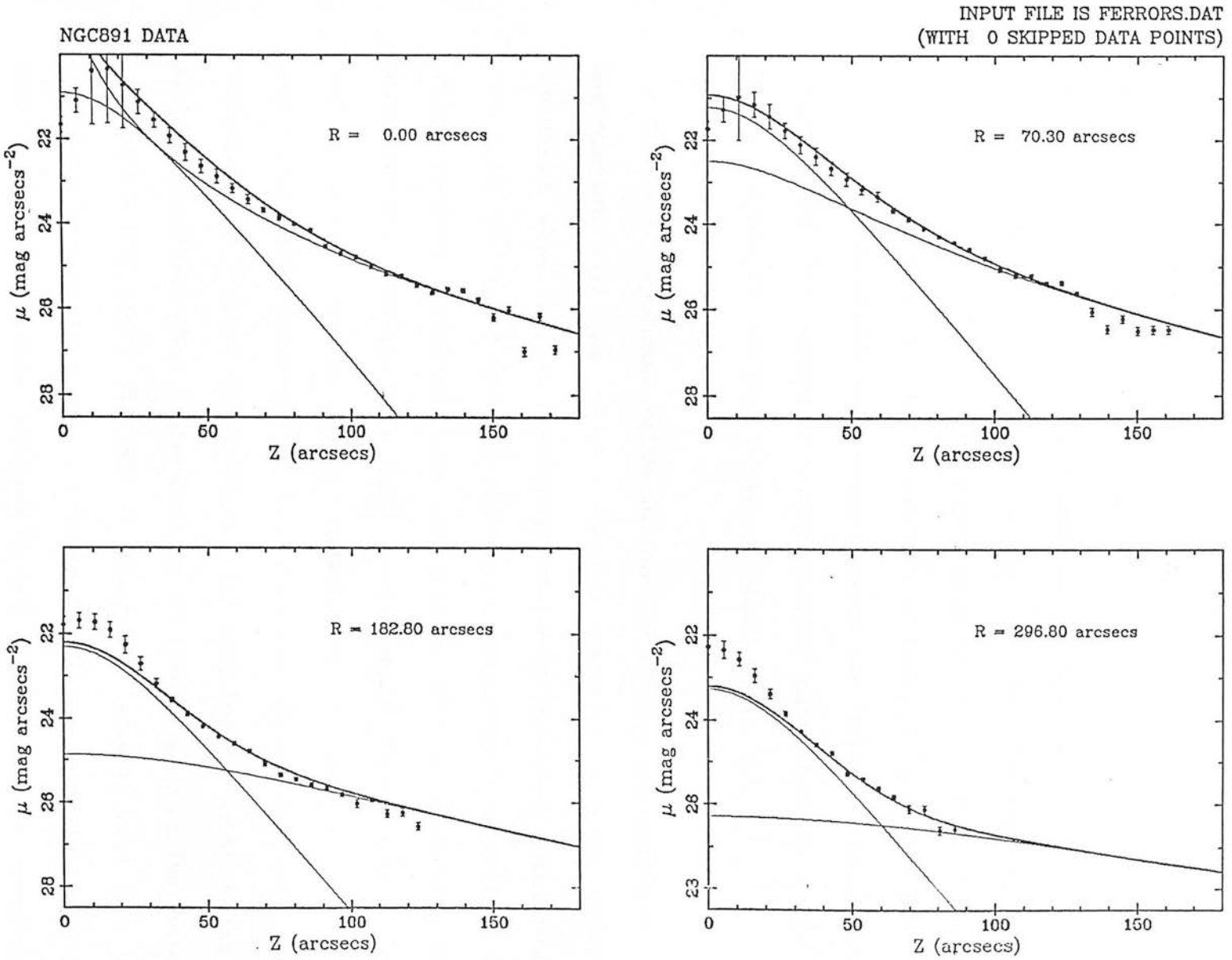
NGC891 DATA
INPUT FILE IS FERRORS.DAT
(WITH 0 SKIPPED DATA POINTS)
R = 0.00 arcsecs
R = 70.30 arcsecs
R = 182.80 arcsecs
R = 296.80 arcsecs
μ (mag arcsecs⁻²)
Z (arcsecs)
0
50
100
150
22
24
26
28
23

figure 3.4

than any other set in that particular passband, is found.

Nevertheless, a comparison of the derived "best-fit" parameters reveal a good agreement between tables 3.7 and 3.2 - particularly so for those models invoking a $sech^2$ form for the thin disc. The agreement is indeed suprisingly good in the light of the considerably different error distributions adopted in the present modelling procedures. A detailed comparison between the respective model parameters of table 3.7 (i.e. a corollary to tables 3.3 and 3.5) fails to indicate any significant differences between the respective passbands. In particular, the marked similarity between parameters in J and F bands confirms the findings of section III.6.1 above.

The most significant result in the use of this alternative error distribution, and one which therefore warrants a more careful discussion than does a detailed parameter-by-parameter comparison from table 3.7, is the fact that the above conclusions are contrary to those obtained previously (i.e. in section III.6.1). Evidently the solutions one derives from such least-squares fitting procedures depend largely on the error distribution one adopts. This is particulary well illustrated if one compares figure 3.4 with the corresponding F band fits in figure 3.5 adopting a "$sech^2$ + exp." model combination. The degradation in fit resulting from the latter combination (for which the sum of squares is greater than that in figure 3.4 by a factor $\gtrsim$ 2.5) is entirely due to the very small errors, and thence large weights, assigned to data points within the range 24 $\lesssim \mu_F \lesssim$ 26 mag. $arcsec^{-2}$ on the basis of the present "magnitude weighted" error distribution. The "exp./$sech^2$ disc + $r^{1/4}$ law profile" combinations are able to fit these points to a considerably better

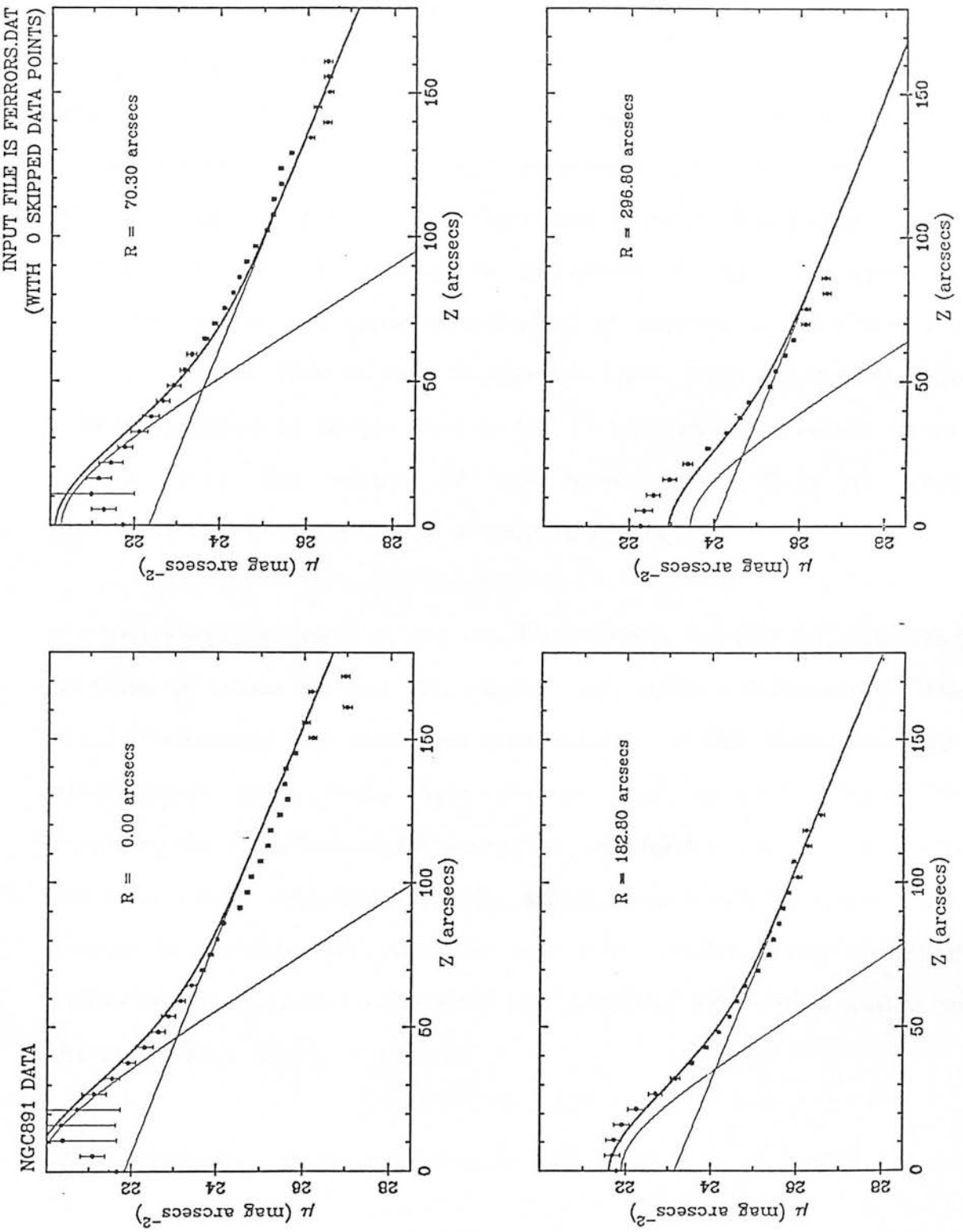
NGC891 DATA
INPUT FILE IS FERRORS.DAT
(WITH 0 SKIPPED DATA POINTS)
R = 0.00 arcsecs
R = 70.30 arcsecs
R = 106.80 arcsecs
R = 182.80 arcsecs
μ (mag arcsecs⁻²)
Z (arcsecs)
22
24
26
28
0
50
100
150

figure 3.5

degree than are alternative combinations, although this result is often found not to be the case at both the brighter and fainter ends of each luminosity profile. The $r^{1/4}$ law is, however, specifically excluded in the previous analyses because the associated errors in section III.6 assign less weight to the μ_F = 24 - 26 mag. arcsec^{-2} range, and thus correspondingly more so to the outermost parts of each profile. [Although figures 3.1 and 3.3 show the J band distribution, those errors in F are very similar in magnitude at each corresponding Z-height.] Using the error distribution of figures 3.1 and 3.3, the exp./sech^2 model form is able to describe these outer regions of each profile considerably better than is the $r^{1/4}$ law profile, primarily owing to the very flat nature of the latter model form at large galactocentric distances (as is evident in figure 3.4).

The weight attached to the results of tables 3.6 and 3.7, compared to those in tables 3.1 and 3.2, clearly reduces to a discussion of the error distribution one considers most suitable in this particular case. Nevertheless, these tests have proved their worth not only by verifying the resultant model parameters obtained in III.6.1 previously (to some extent regardless of the assigned uncertainties), but have served to indicate the value in *any* such least-squares modelling procedure of adopting a realistic and accurate error distribution to the data being fitted.

III.8 Application of the modelling to NGC 4565

A further test of the value of the present fitting algorithm was facilitated by using the (B and R passband) data of NGC 4565 presented by Jensen & Thuan (1982). However, in the light of the

results of section III.7.1 above, it was decided *not* to use their quoted errors for this dataset. Such errors are derived from standard deviations in surface brightness at a particular (R,Z) resulting from the stacking of individual profiles in the respective quadrants of the galaxy. Whilst this procedure often results in the co-adding of 4 separate profiles at any position, in the worst cases only 2 are used, thus giving rise to assigned errors of very variable reliability as a cursory inspection of their figure 18 and table 10 shows. This situation was undesirable in the context of the present testing since certain points would be given erroneously large weights resulting from two independant estimates of $\mu(R,Z)$ which happened to agree particularly closely.

It was reasoned that an improved estimate of the associated error would result if it was considered to be a function of surface brightness rather than spatial (R,Z) position on the galaxy. I therefore derived an error distribution over all surface brightness' seen in the data (binned in 1/2 mag. intervals), and formed a mean error which was then adopted as the uncertainty within that particular surface brightness range. A comparison of this ("magnitude weighted") distribution to that of Jensen & Thuan shows reasonable agreement between the two, with the former smoothing over areas of the literature data within which the quoted errors were considered too uncertain. In general, the points in their table 10 most affected by the present alternative error distribution are those with Z-heights in excess of 85 arcsecs in both B and R passbands.

III.8.1 Results

(a) Two-component v three-component models :

From table 3.8 I derive a mean sum of squares for the two-component models of 0.9 (±0.1) x 10^{-4} in B and 1.0 (±0.1) x 10^{-4} in R, whilst the three-component combinations yield a mean of 4.4 (±0.2) x 10^{-5} in B and 5.8 (±0.1) x 10^{-5} in R. Hence, a significant improvement (at the ~ 5σ level if one assumes an overall uncertainty in FSUMSQ of 10^{-5} based on these standard error estimates) results in the present modelling of NGC 4565 with the adoption of a three-component model. This conclusion is confirmed if one undertakes a more detailed "fit-by-fit" comparison of either the sum of squares or reduced χ^2 values in this table. Further, on the basis of the tabulated χ^2 statistic, one finds the two-component models to be accepted at only ~ 50 % or ~ 75 % levels (depending upon the choice of thin disc model) whilst the three-component fits are accepted at > 99.5 % in virtually all possible combinations. Although the absolute values of such probability limits are not meaningful in the context of comparing model forms, the pronounced differences in their relative values serves to confirm the significance of the improved fit quality found from the inspection of the sum of squares measures.

The reason for the inapplicability of the two-component fits are illustrated in figure 3.6, which shows representative "best-fit" model profiles in the R passband data using the "sech^2 disc + $r^{1/4}$ law profile" model combination of table 3.9. The very "flat" nature to the surface brightness distribution in the outermost regions of each

MODELS ADOPTED	B BAND			R BAND		
	FSUMSQ	red. χ^2	P (%)	FSUMSQ	red. χ^2	P (%)
(a) Two-component combinations (ν = 6) :						
$sech^2$ disc +						
exp. disc	5.9×10^{-5}	1.59	>95.0	6.3×10^{-5}	2.24	>75.0
$sech^2$ disc	1.2×10^{-4}	2.32	>75.0	1.2×10^{-4}	3.53	>50.0
$r^{1/4}$ law profile	5.4×10^{-5}	1.49	>95.0	7.5×10^{-5}	2.32	>75.0
exp. disc +						
exp. disc	9.5×10^{-5}	4.46	>50.0	1.2×10^{-4}	4.72	>50.0
$sech^2$ disc	1.0×10^{-4}	4.35	>50.0	1.0×10^{-4}	4.75	>50.0
$r^{1/4}$ law profile	8.9×10^{-5}	3.57	>50.0	1.3×10^{-4}	4.10	>50.0
(b) Three-component combinations (ν = 9) :						
$sech^2$ disc +						
$sech^2$ disc +						
$r^{1/4}$ law profile	4.4×10^{-5}	1.78	>99.0	5.9×10^{-5}	2.38	>97.5
$sech^2$ disc +						
exp. profile	4.1×10^{-5}	1.33	>99.5	5.5×10^{-5}	1.99	>99.0
exp. disc +						
$r^{1/4}$ law profile	3.9×10^{-5}	1.61	>99.5	5.8×10^{-5}	1.63	>99.5
exp. disc +						
exp. disc	4.1×10^{-5}	1.46	>99.5	5.8×10^{-5}	1.55	>99.5
exp. disc +						
$sech^2$ disc +						
$r^{1/4}$ law profile	5.4×10^{-5}	1.54	>99.5	5.8×10^{-5}	1.63	>95.5
$sech^2$ disc +						
exp. disc	4.7×10^{-5}	1.70	>99.5	DID NOT FIT DATA		

Table 3.8 : Statistical "quality of fit" parameters for all the model combinations for which convergence was achieved for the data of NGC 4565 by Jensen & Thuan (1982). The relevant parameters are detailed in table 3.9. The error values used in these iterations were the "magnitude weighted" distribution described in the text.

MODELS ADOPTED	1st DISC MODEL		2nd DISC MODEL		$R^{1/4}$ LAW MODEL	
	B	R	B	R	B	R
(a) Two-component combinations :						
$sech^2$ disc + exp. disc	μ_o = 20.94	19.58	μ_o = 23.70	22.58		
	h_R = 5.2	4.9	h_R = 8.3	8.1		
	Z_o = 0.84	0.86	h_Z = 1.92	2.26		
$sech^2$ disc + $sech^2$ disc	μ_o = 21.01	19.55	μ_o = 24.91	23.68		
	h_R = 5.2	4.8	h_R = 6.5	6.9		
	Z_o = 0.90	0.85	Z_1 = 3.51	3.93		
$sech^2$ disc + $r^{1/4}$ law profile	μ_o = 21.22	19.82			μ_e = 22.06	22.51
	h_R = 6.0	5.1			e_e = 1.8	3.9
	Z_o = 0.88	0.87			q = 0.34	0.37
exp. disc + exp. disc	μ_o = 20.01	18.83	μ_o = 24.04	22.96		
	h_R = 7.4	6.7	h_R = 7.9	7.4		
	h_Z = 0.49	0.51	h_Z = 2.20	2.73		
exp. disc + $sech^2$ disc	μ_o = 20.05	18.74	μ_o = 25.20	23.96		
	h_R = 7.3	6.4	h_R = 6.4	7.0		
	h_Z = 0.52	0.51	Z_1 = 3.89	4.35		
exp. disc + $r^{1/4}$ law profile	μ_o = 20.31	19.07			μ_e = 23.41	24.37
	h_R = 8.9	7.5			e_e = 3.2	11.1
	h_Z = 0.56	0.58			q = 0.44	0.59
(b) Three-component combinations :						
$sech^2$ disc + $sech^2$ disc + $r^{1/4}$ law profile	μ_o = 20.89	19.43	μ_o = 24.26	22.38	μ_e = 22.50	23.89
	h_R = 5.5	4.8	h_R = 8.9	6.3	e_e = 2.1	7.1
	Z_o = 0.83	0.78	Z_1 = 1.57	1.58	q = 0.37	0.36
$sech^2$ disc + $sech^2$ disc + exp. disc	μ_o = 21.47	19.46	μ_o = 21.89	21.61	μ_o = 24.28	23.25
	h_R = 7.3	4.7	h_R = 4.3	5.2	h_R = 10.7	10.3
	Z_o = 0.76	0.74	Z_1 = 1.12	1.31	h_Z = 2.36	2.92
$sech^2$ disc + exp. disc + $r^{1/4}$ law profile	μ_o = 20.87	19.53	μ_o = 23.46	22.16	μ_e = 22.97	26.26
	h_R = 5.2	4.8	h_R = 14.9	8.9	e_e = 2.5	24.1
	Z_o = 0.84	0.83	h_Z = 1.05	1.51	q = 0.46	0.69
$sech^2$ disc + exp. disc + exp. disc	μ_o = 21.10	19.58	μ_o = 22.07	22.00	μ_o = 25.31	26.50
	h_R = 6.0	4.9	h_R = 5.4	7.6	h_R = 15.2	26.6
	Z_o = 0.84	0.84	h_Z = 0.94	1.63	h_Z = 3.21	29.67
exp. disc + $sech^2$ disc + $r^{1/4}$ law profile	μ_o = 24.34	22.16	μ_o = 21.52	19.53	μ_e = 22.18	26.26
	h_R = 66.6	8.9	h_R = 6.3	4.8	e_e = 1.9	24.03
	h_Z = 0.33	1.51	Z_1 = 0.94	0.83	q = 0.34	0.69
exp. disc + $sech^2$ disc + exp. disc	μ_o = 22.77	-----	μ_o = 21.06	-----	μ_o = 23.94	-----
	h_R = 157.83	-----	h_R = 4.6	-----	h_R = 9.2	-----
	h_Z = 0.46	-----	Z_1 = 0.93	-----	h_Z = 2.18	-----

Table 3.9 : Resulting model output parameters for both two-component (a) and three-component (b) fits to the NGC 4565 data of Jensen & Thuan (1982) using the "magnitude weighted" error distribution. As in table 3.2, all central surface brightness' are quoted in mag. arcsec^{-2}, and scale parameters in kpc. From an assumed distance to this galaxy of 10 Mpc, 1 arcsec translates to 48.5 pc.

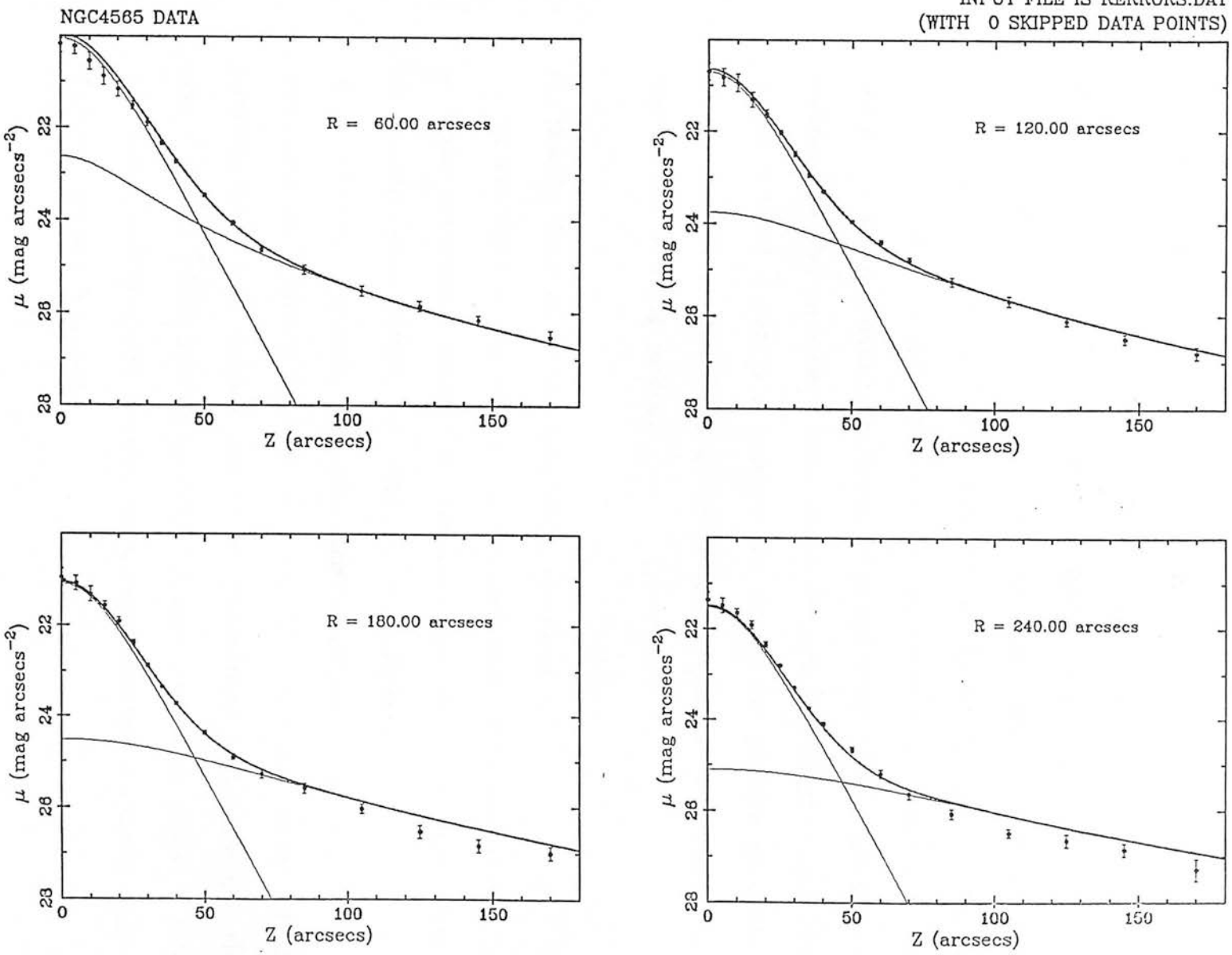
NGC4565 DATA
INPUT FILE IS RERRORS.DAT
(WITH 0 SKIPPED DATA POINTS)
R = 60.00 arcsecs
R = 120.00 arcsecs
R = 180.00 arcsecs
R = 240.00 arcsecs
μ (mag arcsecs^{-2})
Z (arcsecs)

figure 3.6

profile proves to be very difficult to model using any two-component combination - particularly at larger galactocentric distances as evidenced in that figure - despite the larger assigned errors at such positions. The extent to which an outer model in such two-component fits has to "flatten" to fit the data is clear from the uniformly large scalelengths in both colours seen in table 3.9, and is equally evident in the three-component fits such as the "sech^2 + exp." model combination shown in figure 3.7. In addition, the reason for the correspondingly larger statistical fit parameters in table 3.8 when using this R band data arise because of the very much smaller errors assigned to the outermost data points of each profile than are found in the B band - clearly a point which places far greater restrictions on the modelling procedure, particularly when a two-component model combination is being tested.

(b) Results from the three-component modelling :

In the light of the above results, therefore, it is considered that a three-component model is required to describe the surface brightness distribution in this galaxy. However, a number of three-component models can immediately be excluded from further consideration before inspection of table 3.8. They are three (of the possible four) sets making use of an exponential model for the thin disc - two of which fail to converge in any passband, whilst a third fails when modelling the R band data, regardless of the (wide variety of) input estimates tested.

Within those (5) combinations which were found to converge for both the B and R data, table 3.9 provides no set of models which are a statistically significant improvement over any others. An inspection

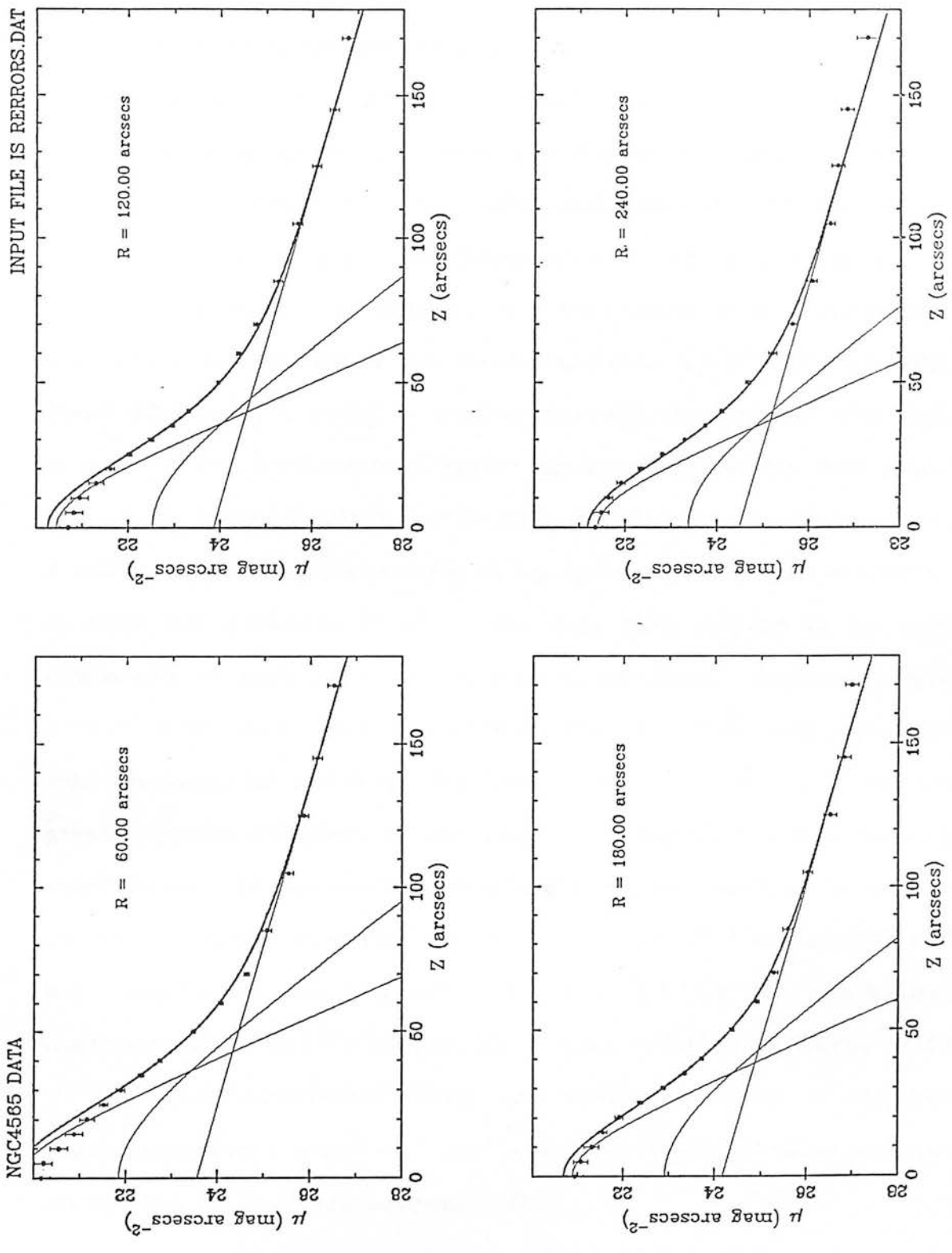
INPUT FILE IS RERRORS.DAT
NGC4565 DATA
R = 120.00 arcsecs
R = 240.00 arcsecs
R = 60.00 arcsecs
R = 180.00 arcsecs
μ (mag arcsecs⁻²)
Z (arcsecs)
0
50
100
150
22
24
26
28

figure 3.7

of table 3.8 shows that the only indications of changes in the "quality-of-fit" parameters within the 4 "sech^2 thin disc" combinations are found in the reduced χ^2 and indicate that a moderately improved fit in the R band results from the adoption of an exponential (as opposed to a sech^2) form for the thick disc. An inspection of the model output parameters in table 3.9 clearly indicates that for all model combinations, the scalelength parameter (h_R or θ_e) is not well-defined. Considerable variability, either between passbands in a particular model fit or between the alternative model combinations themselves, is also evident for the scaleheight (h_z) of the exponential model when such a model is used to describe the non-thin disc light in this system. A pronounced colour gradient in the thin disc (noted by Jensen & Thuan, 1982) may explain the discrepancies between the B and R parameters, particularly in h_R. However, the other parameters in table 3.9, primarily those of the thin disc, appear to be quite comparable between passbands in a particular model component, whilst a mean (B-R) colour index of the thick disc of 1.13 is quite consistent with the value (of 1.2) found by Jensen & Thuan. However, by far the greatest constraint posed by the results of this table is that for only those model combinations incorporating a double sech^2 model set are the (B-R) colours considered realistic - the "sech^2 + exponential + $r^{1/4}$ law" combination yields a colour index of 0.1 for the intermediate component, the "sech^2 + exponential + exponential" set a colour of 0.0 for the fainter exponential profile, and a thin disc colour of -2.2 from the "exponential + sech^2 + $r^{1/4}$ law" set. This result therefore excludes all but two of the three-component fits.

Those fits detailed in table 3.9 showing "unrealistic" resultant model parameters are worthy of further comment as they give an

added insight into the nature of the present modelling procedure. The "exp. + sech^2 + exp." combination has only been able to model the B band data by heavily suppressing the thin disc component, resulting in an effective two-component model fit of the form found in section (a) of table 3.9 (compare the derived sech^2 and fainter exponential parameters here to the thin disc and thick disc values in the two-component fits). A visual inspection of the model fits confirms that the same conclusion also applies to the previous combination in table 3.9 (b). Note that the more restrictive R band error distribution is a likely cause of the greatly increased $r^{1/4}$ law parameters required to fit the data in such an effective two-component model. The greatly increased scale parameters of the fainter exponential model profile in the 4th model combination of table 3.9 (b), and particularly those for the R passband, are further evidence that two-component combinations suffice to describe the light distribution in this galaxy only to a Z-height of ~ 100 arcsecs, beyond which point the third component is required. The representative fits in R for this combination shown in figure 3.8 clearly illustrate, however, that to model these outermost points requires such a third component to be very flat - hence the large scale-parameters of the exponential form in this combination, and for almost all other such combinations in table 3.9. The latter point is also pertinent to the third model combination of table 3.9 (b), although the intrinsically flat nature of the $r^{1/4}$ law profile requires the thick disc model to contribute to the fit out to much larger Z-heights than is necessary when the exponential profile is used for this component. It is for this reason that the scalelength of the exponential thick disc model is correspondingly increased over that shown in figure 3.8.

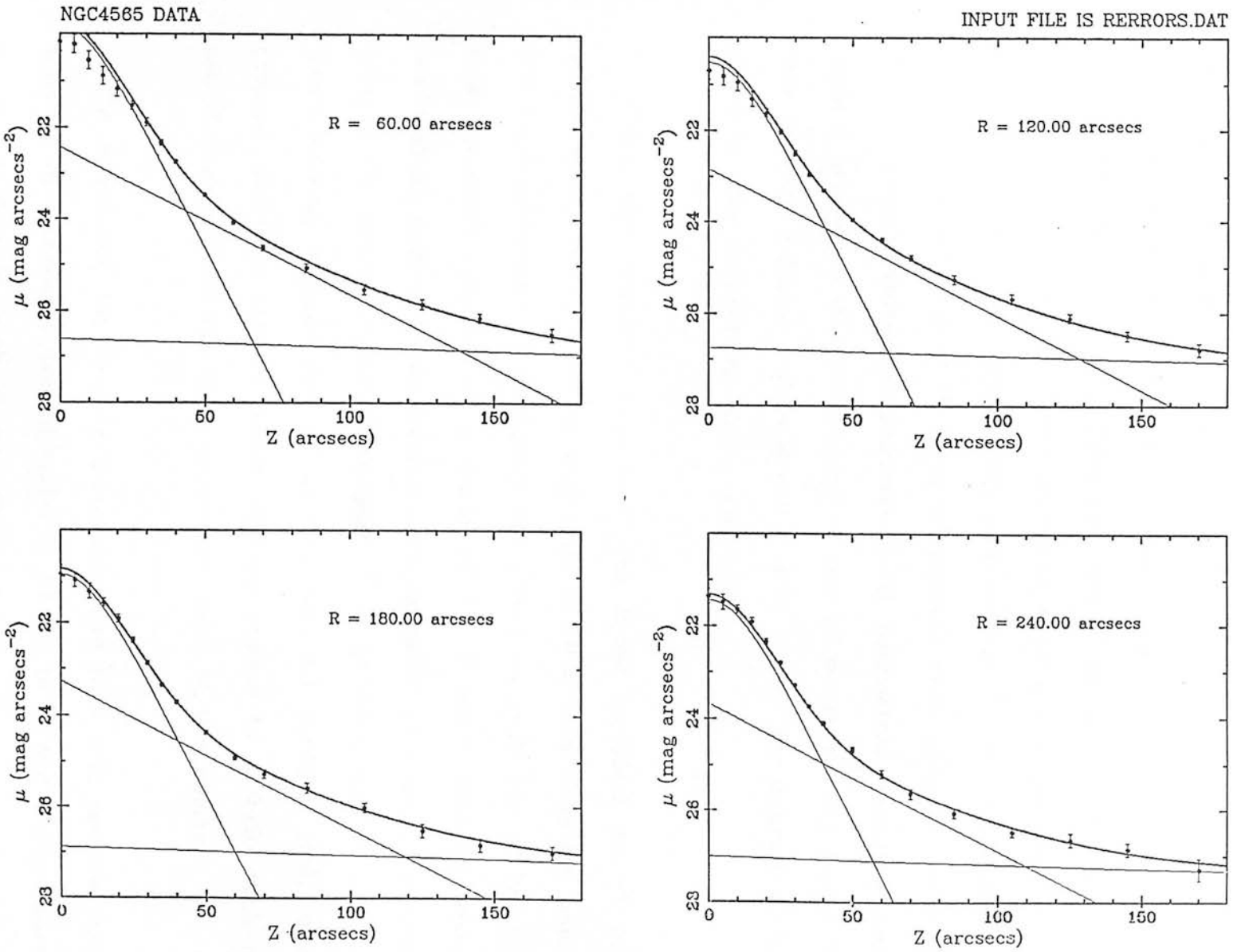
NGC4565 DATA
INPUT FILE IS RERRORS.DAT
R = 60.00 arcsecs
R = 120.00 arcsecs
R = 180.00 arcsecs
R = 240.00 arcsecs
μ (mag arcsecs^{-2})
Z (arcsecs)
0
50
100
150
22
24
26
28
23

figure 3.8

In the light of the generally poorly defined scalelengths which could be assigned to all components in table 3.9, a series of iterations was run to test whether improvements could be gained by forcing h_R in both thin and thick disc models to be equal (although the parameter itself was not held constant). No statistically significant differences were found in either the sum of squares or the reduced χ^2 values for model fits obtained under such a process. However, a further series of tests specifically excluded any model combinations in which the scalelength of all three components were equal on the basis of the greatly increased goodness-of-fit parameters resulting from such a procedure (the corresponding sum of squares being larger in this case by a factor ~ 2 in R and ~ 3 in B over the equivalent fits when no such restrictions on h_R were made).

Since the modelling procedure was found to yield an $r^{1/4}$ law profile with a very consistent axis ratio in all combinations for which fits were achieved, I investigated the effect on such fits of holding this parameter constant at a value of 0.7. I found that no model combinations achieved convergence using such an axis ratio, and that even at the point of failure a reduced χ^2 of 3.7 (±0.4) was found (the corresponding average sum of squares was 9.3 (±0.3) x 10^{-5}). The present modelling process would thereby appear to exclude such a round component in any three-component model of this galaxy.

In conclusion, the current investigation of NGC 4565 requires the adoption of a three-component model to fit the light distribution seen in this system in both B and R passbands, although the added requirement of the derived (B-R) colour index being considered "realistic" excludes all but two of these models. Table 3.10 compares

model used	present work	KS1	JT	H80	H82
sech^2 thin disc	h_R = 6.0 (±0.5) in B 4.8 (±0.1) in R	5.5	6.8 (B) 6.2 (R)	4.9	5.4
	Z_o = 0.82 (±0.02) in B 0.80 (±0.02) in R	0.79			
sech^2 thick disc	h_R = 6.0 (±1.1) in B 5.4 (±0.5) in R		6.8		
	Z_1 = 1.14 (±0.15) in B 1.24 (±0.22) in R		1.3		
exponential non-thin disc	h_Z = 2.58 (±0.32) in B 2.92 (-) in R		3.3		3.1

Table 3.10 : A comparison of present results for NGC 4565 to data existing in the literature. Such values are taken from those "best-fit" three-component models found in table 3.9 (b) which incorporate a double sech^2 disc combination. All scale parameters are quoted in kpc assuming a distance to NGC 4565 of 10 Mpc.

SOURCES OF DATA

KS1 : van der Kruit & Searle (1981a)
JT : Jensen & Thuan (1982)
H80 : Hamabe et al (1980)
H82 : Hamabe (1982)

the output parameters for these model combinations to existing data in the literature. On the whole, the agreement appears to be good indicating that, even in a system as complex as NGC 4565 (which is known to possess a "box/peanut" bulge and also a disc warp), the present algorithm was still able to generate reproduceable results. No allowance has been made in the current analyses for the effects of this disc warp on the luminosity distribution of the galaxy as a whole, and it is conceivable that the presence of such a feature could lead to the "unrealistic" values for some parameters in table 3.9. Based on the data of van der Kruit & Searle, the disc warp first becomes evident at a surface brightness ~ 25 μ in J, translating to ~ 26 μ in R adopting the appropriate colour indices from their work and Jensen & Thuan (1982). This corresponds to a Z-height in excess of 100 arcsecs for all profiles modelled. Thus, the presence of the warp is most likely to influence the model parameters for the faintest of the model profiles adopted here.

No attempt was made to investigate the detailed nature of the "box/peanut" bulge along the minor axis. The perpendicular profiles given by Jensen & Thuan (their figure 18) show that such a feature only becomes evident interior to Z ~ 20 arcsecs or so. The errors over such regions are sufficiently large, and the number of individual surface brightness measures sufficiently few, that no detailed investigation of these data was undertaken. Nevertheless, a general point can be made concerning this component on the basis of the present modelling results. It was found that an inward extrapolation of the $r^{1/4}$ law profile to these regions would *not* be able to account for the luminosity distribution seen in the region $5 \lesssim Z \lesssim 20$ arcsecs. For example, adopting such a profile with mean parameters (culled

from table 3.9b) of $\overline{\mu}_e$ = 22.51 mag arcsec^{-2} and $\overline{\theta}_e$ = 2.17 kpc implies a μ_B ~ 21.54 mag arcsec^{-2} at a Z-height of 5 arcsecs - some 2 mag. fainter than the actual value quoted by Jensen & Thuan at this minor axis position (see their table 10). This discrepancy is a ~ 10σ effect assuming an assigned uncertainty at this point from the "magnitude weighted" error distribution adopted above (a more striking discrepancy is, of course, found when adopting the "best-fit" exponential model given in table 3.9b which yields a μ_B of 24.38 mag arcsec^{-2} at Z = 5 arcsecs). The reason for such a disparity in the case of the mean $r^{1/4}$ law profile is that the well-known peak in this model at small Z-heights only becomes important interior to ~ 3 arcsec or so. This is true even when convolving such a model form with the seeing profile adopted by Jensen & Thuan (see, in particular, their figure 22). Hence, contrary to the expectations of Jensen & Thuan, the innermost "box/peanut" bulge component would seem to be distinct from the fainter model component defined here.

III.9 Conclusions

In this chapter I have presented an alternative iterative least-squares fitting algorithm with a view to modelling the light distributions specifically (but not exclusively) for edge-on spiral galaxies. This scheme allows one to model the complete spatial data array across a galaxy at one time, and also allows incorporation of as many model combinations as required. After extensive testing (involving ~ 180 runs) to determine the reproduceability of the derived results from such an algorithm it was concluded that when the program is able to fit the data within the pre-defined tolerance limits, it is able to do so repeatedly (and in the process generate

identical output model parameters) to within the rounding errors of one part in ~ 10^5, and also for a large variation in initial input estimates for these parameters.

The procedure defines the model combinations most appropriate to the test data being fitted on the basis of the sum of squares of residuals, the reduced χ^2 and, to a lesser degree, the number of iterations needed before convergence is achieved. These criteria can be further supplemented by requiring the resulting "best-fit" model parameters to be "realistic" on the basis of available photometry existing for the objects under study. However, the fact that such literature estimates are either rarely available, or are in themselves derived by less rigorous means than the current procedure, dictates that requiring agreement between data sets is of secondary importance to the statistical "quality" parameters defined using the present modelling scheme.

An important conclusion resulting from modelling the existing literature data of NGC 891 is the strong dependance of the derived model parameters on the adopted error distribution. Thus, it is very important to be aware of such a limitation when making use of any such least-squares technique - be it the present form or any of those used in the studies outlined in section III.2 above. Because the results of these modelling procedures rely to such an extent on the assigned errors means that the absolute values of reduced χ^2, and their associated probabilities, are meaningless. For this reason, the statistical "quality-of-fit" parameters detailed in tables 3.1, 3.6 and 3.8 are used to differentiate between model combinations by "ranking" their associated sum of squares (and also reduced χ^2) in a relative

sense only.

The present scheme still has certain flaws. In the case of three-component fits to NGC 4565 data, for example, it proves difficult to define the scalelength parameters (h_R and/or θ_e), between passbands or between alternative model combinations, with any degree of reliability. Nevertheless, application of the program to "model galaxies" (with and without the superposition of both random and systematic photometric errors) have testified as to its reliability. Use of existing data for both NGC 4565 and NGC 891 have also served to verify these expectations, even to the point of considerably changing their associated errors in surface brightness. On the basis of such results, the present algorithm therefore appears to be the most relevant (and one of the most powerful) means currently available for investigating the constituent luminosity distributions in external galaxies. It is one which is able to give information concerning the data being used at two levels : most fundamentaly what combination of model components are required to best fit the data and, at a more detailed level, to define the values of parameters within the fitted models. The latter is clearly the main goal in the application of such a method.

Use of the quoted literature data has also allowed me to investigate the conclusions of recent alternative investigations of both systems. The present results are, for example, found to be in excellent agreement with those of Shaw & Gilmore (1986) - even though the latter study was limited to a visual fitting procedure alone and not a least-squares process as adopted here. This compatibility is clearly shown by comparing their table I to table 3.2 and 3.10 in the

present study.

Specific conclusions for these systems on the basis of the present results are as follows :

(a). In the present analysis of NGC 891, I find an improvement in the model fits resulting from the adoption of a two-component "$sech^2$/exp. + $sech^2$/exp." model set when compared to those combinations incorporating the $r^{1/4}$ law profile - deduced from both the sum of squares and the reduced χ^2 parameters. In only 2 cases are three-component model combinations found to converge to a solution in J, F and U' bands, and in both cases I find that the extra component does not serve to reduce either the sum of squares or the reduced χ^2 by a significant factor. Indeed, a visual inspection of the model fits indicate that when adopted, the third component is suppressed in the model fitting to the point where it only becomes an important contributor to the overall model profile over the outer few points of each profile - as is clearly evident in figure 3.3. On the basis of the indistinguishability of the "quality-of-fit" parameters outlined in table 3.1, I thus conclude that the use of such an additional component is unwarranted in describing the luminosity distribution seen in this system.

(b). Adoption of the alternative ("magnitude weighted") error distribution outlined in section III.7 yields completely contrary results to those in (a) in that the use of the $r^{1/4}$ law profile is favoured (in preference to a $sech^2$ or exponential model form) for the non-thin disc component, a result which indicates the importance of the adopted error distribution. However, inspection of fits such as those

in figure 3.4 indicate that the very small assigned errors to the range $24 \lesssim \mu_F \lesssim 26$ mag. arcsec^{-2} bias the modelling to such a degree that the $r^{1/4}$ law profile in this case fails to describe the outermost points of each profile as well as does the sech^2/exp. model using the previous error distribution.

(c). A comparison of the derived model parameters for NGC 891 indicate good agreement with a variety of literature sources, and thus confirms the similarity of this system to that of our own Galaxy, previously alluded to by van der Kruit (1984). This point is amplified in table 3.11 which compares the currently available parameters for our own Galaxy and my "best-fit" estimates for NGC 891 - the respective values are seen to be reasonably consistent between the two.

(d). The inability to distinguish between a variety of model forms for the non-thin disc component in this object, found by Bahcall & Kylafis (1985), may be a result of their sampling over too small a range of galactocentric distance for differences between such models to become evident (owing to their self-imposed magnitude limit to the data being used). The very existence of data faintward of their magnitude limit is found to be a sufficient constraint on the present analysis to allow a distinction in model forms to be made, despite the large associated errors in such data. Indeed, at the limit of the present dataset, the predicted surface brightness estimates from exponential and $r^{1/4}$ law models differ by $\sim$ 0.4 mag., an amount sufficient to negate the requirement of Bahcall & Kylafis that this dataset be accurate to $\pm$ 0.1 mag. at a surface brightness $\sim$ 26.0 mag arcsec^{-2}.

Model adopted	the Galaxy	NGC 4565	NGC 891
thin disc :			
	μ_o = 22.5 (±0.3)	21.1 (±0.1)	21.4 (±0.1)
	h_R = 4.0 - 4.5	6.0 (±0.5)	4.4 (±0.1)
	Z_o = 0.65 (±0.05)	0.82 (±0.02)	1.05 (±0.11)
	h_Z = 0.33	0.40 (±0.07)	0.54 (±0.03)
thick disc :			
	h_R = 4.0	6.0 (±1.1)	4.5 (-)
	h_Z = 1.3	1.00 (±0.06)	1.56 (±0.01)
$r^{1/4}$ law profile :			
	θ_e = 2.7	2.2 (±0.2)	

Table 3.11 : A comparison of the present "best-fit" B passband resultant parameters for both NGC 891 and NGC 4565 to those currently available for our own Galaxy. Parameters, derived from the use of the $sech^2$ model form in all cases except in quoting h_l values, are as in table 3.2, and the magnitude zeropoint for NGC 891 has been corrected from the J band to the B using the colour equations given by van der Kruit & Searle (1981b). The range in h_R quoted for our Galaxy reflect the variations of a particular measure as given in the literature sources used.

SOURCES OF DATA FOR THE GALAXY :

Gilmore (1984)
van der Kruit (1984)
van der Kruit (1987a)

(e). On the basis of the "fit quality" parameters given in table 3.8, the present modelling of NGC 4565 shows that the adoption of a third component results in a considerable reduction in the sum of squares of residuals, and the reduced χ^2, in all cases tested. However, the scalelength parameters prove to be poorly constrained in all two- and three-component model combinations, whilst in only two of the three-component fits are the derived (B-R) colour indices considered to be "realistic". No improvements result from forcing the scalelength parameters to be equal in the thin and thick disc models, whilst equal values for all three components are explicitly excluded on the basis of the greatly inferior quality-of-fits which result from such a procedure. The use of a standard de Vaucouleurs $r^{1/4}$ law precludes axis ratios rounder than 0.4 when q is allowed to vary as a free parameter. This value is entirely consistent both with previous estimates for this system (e.g. ~ 0.4 at a surface brightness of 27μ from van der Kruit & Searle (1981a); 0.5 as found by Jensen & Thuan (1982) and 0.46 from Hamabe et al (1980)). A fixed axis ratio of 0.7 is specifically rejected in the present results by the factor of 3 increase in both reduced χ^2 and sum of squares which result. The existence of a relatively flat $r^{1/4}$ law profile, coupled with the existence of a disc warp, may argue in favour of a considerable greater similarity between NGC 4565 and our Galaxy than has recently been argued in van der Kruit (1984) - a result again consistent with the findings detailed in table 3.11.

(f). Contrary to the conclusions of Jensen & Thuan (1982), the central "box/peanut" bulge does not appear to be an inward extrapolation of the outermost component. Despite the fact that the $r^{1/4}$ law profile possesses an intrinsic peak towards the centre, it still

underestimates the light distribution seen in the region dominated by the "box/peanut" by > 2 mag. at a Z-height of 5 arcsecs. Since it is seen to extend over ~ 40 arcsec of the minor axis profile of Jensen & Thuan, this feature would appear to be a specific component photometrically distinct from an exponential or $r^{1/4}$ law model form.

- Chapter IV -

Resulting observations of the programme galaxies

Introduction

The primary aim of this thesis is to (statistically) test the validity of using standard fitting functions when describing the luminosity distributions of galaxies, in a more systematic way then has been attempted to date. In this chapter, therefore, are presented the results of investigations of those galaxies noted in table 1.1 for which CCD photometry was obtained. For the sake of clarity, only the conclusions appropriate to each case are discussed here - the more general implications of the results obtained being deferred until chapter V.

In addition to this main goal I have also attempted to define the extent to which those galaxies within the present dataset which show clear "box/peanut" morphologies can be described by means of the same standard fitting functions. By determining the quality of the fits exterior to the disc component in such systems, I have therefore proceeded to test whether the box/peanut bulges can be viewed merely as the bright, central regions of the data at larger (R,Z), or whether they are an additional (i.e. distinct) contributor to the total luminosity distribution in each case.

The means by which these aims were undertaken was to apply the nonlinear, least-squares fitting technique described in chapter III. A

systematic investigation, incorporating single, double or triple model combinations, was adopted in each galaxy to define that particular fitting function (or set thereof) for which the smallest sum of squares of residuals was obtained when compared to the actual data.

In the following sections, the term "bulge" (as used in an attempt to describe the visual appearance of each system being studied) is defined to mean the total non-thin disc light within the galaxy. To improve the clarity of section IV.2, the tables of model parameters derived for each galaxy are to be found in appendix A. For distance estimates, H_o = 100 km s^{-1} Mpc^{-1} is assumed in all cases. Photographs of the galaxies being modelled here are presented in appendix C.

IV.1 Derivation of the error distributions

In the light of the results of chapter III, considerable care was taken when assigning an error to each measure being modelled. The error on a "mean" μ derived over 1 mag. $arcsec^{-2}$ bins of each data set being modelled was calculated in the same way as that adopted for the "model galaxy" in section III.5, and was used for those points for which only a single μ measure was available. In all other cases, the uncertainty assigned to that particular point was either this calculated measure appropriate to such a particular surface brightness or the standard error on the mean value derived from the binning procedure in section II.3.8, whichever was the larger. Such a procedure yields smoothly varying error distributions, and greatly reduces the liklihood of an unrealistically large weight being assigned because of the chance similarity of the surface brightness at that

point after folding about both major and minor axes.

IV.2 Application of the algorithm to the programme galaxies

IV.2.1 NGC 2295 (α = 06^h 45^m 23^s, δ = -26^o 40' 48")

NGC 2295 is one of several of the galaxies observed here for which no entry could be found in either the RC2 or RSA catalogues. Despite its very small apparent dimension (some 2.2' on the SERC J plate 5552) its appearance is of an intermediate galaxy possessing both a conspicuous disc and a clear central bulge. The ~ 7^o offset from an exactly edge-on aspect gives rise to partial obscuration of the bulge in the NW. Because of the prominance of this disc, the Sab[?] classification assigned by Corwin et al (1985) is adopted for the present work, although an S0/a morphology is quoted in the ESO catalogue.

The derived R band co-added CCD frame was obtained with the chip long axis orientated N-S to allow complete spatial coverage of the galaxy together with an excellent estimate of the local sky background at the time of observation. Of order 48 stellar and non-stellar objects were removed from this final image frame prior to extraction of the surface brightness profiles. The presence of 2 relatively bright stars due north and south of the galaxy itself was particularly notable on this frame, but a detailed comparison of the profile cuts showed no residual structure after their removal when compared to equivalent data in the other 3 quadrants of the galaxy (a testimony to the bright star removal procedure of section II.3.3). Any contamination from the major axis dust lane was removed in this, as in all the

programme galaxies, by a point-by-point inspection of each surface brightness profile at small Z-heights, together with a trial inspection of model fits. Those data found to become progressively fainter with decreasing Z were assumed to be affected by obscuration and were thus set to zero prior to the generation of the final data array to be adopted in the modelling. In the case of NGC 2295, a visual inspection of those profiles taken SE and NW of the major axis show the dust lane to affect data only for which $Z \lesssim 5''$.

There is only one nearby system seen on the CCD frames and the SERC/ESO plate material - a diffuse galaxy some 1.1' NW of centre - although NGC 2295 itself is located only 5.6' west of the pronounced interacting S0/E complex NGC 2292/93. Indeed, the ESO catalogue assigns a common group membership to the program galaxy and to the interacting system, although no distance estimates were found for any of these galaxies.

Results of the modelling

The derived model parameters, together with the corresponding statistical "quality-of-fit" estimators appropriate to that particular fit, are given in table A.1. [To re-iterate from chapter III, such results correspond to the minimum sum of squares of residuals (FSUMSQ) obtained for that particular model combination, rather than in the associated reduced χ^2 parameter.]

As is evident from an inspection of this table, single component model combinations are inapplicable in this particular case owing to the significantly poorer fits obtained (by ~ an order-of-magnitude in the sum of squares of residuals) when compared to the two component

sets. Furthermore, a statistically significant improvement in the goodness-of-fit does not accrue when adopting a triple component combination - the largest reductions found over those previously being only ~ 1.1 % in FSUMSQ and ~ 2.6 % in red. χ^2. The reason for this similarity arises because, in all cases, one of the three components being adopted is suppressed to such an extent (either as a result of excessively faint central surface brightness and/or very large scalelength parameters) that the final model fits comprise two components alone.

The essentially identical quality-of-fits for all two-component combinations in that table which iterate to a solution indicates that the non-thin disc light in this system can be equally well-described by any of the fitting functions adopted.

In the light of the poorly defined scalelength parameters found when modelling NGC 4565 in chapter III, additional iterations were conducted specifically with the intention of defining the reproduceability of h_r and θ_e. By undertaking tests in which both surface brightness estimates and scaleheight (or, where appropriate, axis ratio) parameters were held constant at their respective values in table A.1, only the parameters of interest were allowed to remain as variables. For a wide variety of input (typically ~ 2" to 500" in h_r and 20" - 500" in θ_e) identical output values were obtained to those of that table, thus indicating the excellent repeatability of all the scale parameters thus defined. The same conclusion was derived for fits conducted with the scaleheight as the free parameter.

Figure 4.1 illustrates the results obtained when using the "exponential + $r^{1/4}$ law" set before full allowance was made for dust contamination from the thin disc at small Z-heights (to illustrate the importance of allowing for such contamination). In figure 4.1 (a) are shown the model fits to a representative subset of the surface brightness profiles extracted across this galaxy, whilst figure 4.1 (b) illustrates the associated (unweighted) residuals for this model combination (such residuals being defined as the difference between the predicted and observed surface brightness measures) as a function of surface brightness (labelled a), galactocentric distance (b) and Z-height (c).

A significant feature of this figure (particularly clearly seen in the residuals diagram) is the apparent systematic trend of a progressively fainter model than data at faint surface brightnesses. The decreasing ($\mu_{model} - \mu_{data}$) seen here may either result from a systematic error in the data being modelled, or the inapplicability of the modelling profile being adopted. A further discussion of this point, which proves to be common to many of the galaxies studied here, is deferred until chapter V, but for the present it is assumed that the former is the case. An inspection of the above residuals diagram therefore indicates that the estimate of the local sky background has to be reduced by ~ 0.3 % of the value quoted in table 2.2.

Figure 4.2 shows the results of adopting a double exponential model combination after correction has been made for the contamination effects and the systematics at faint μ, the model parameters thus derived being given in table 4.1. The sum of squares

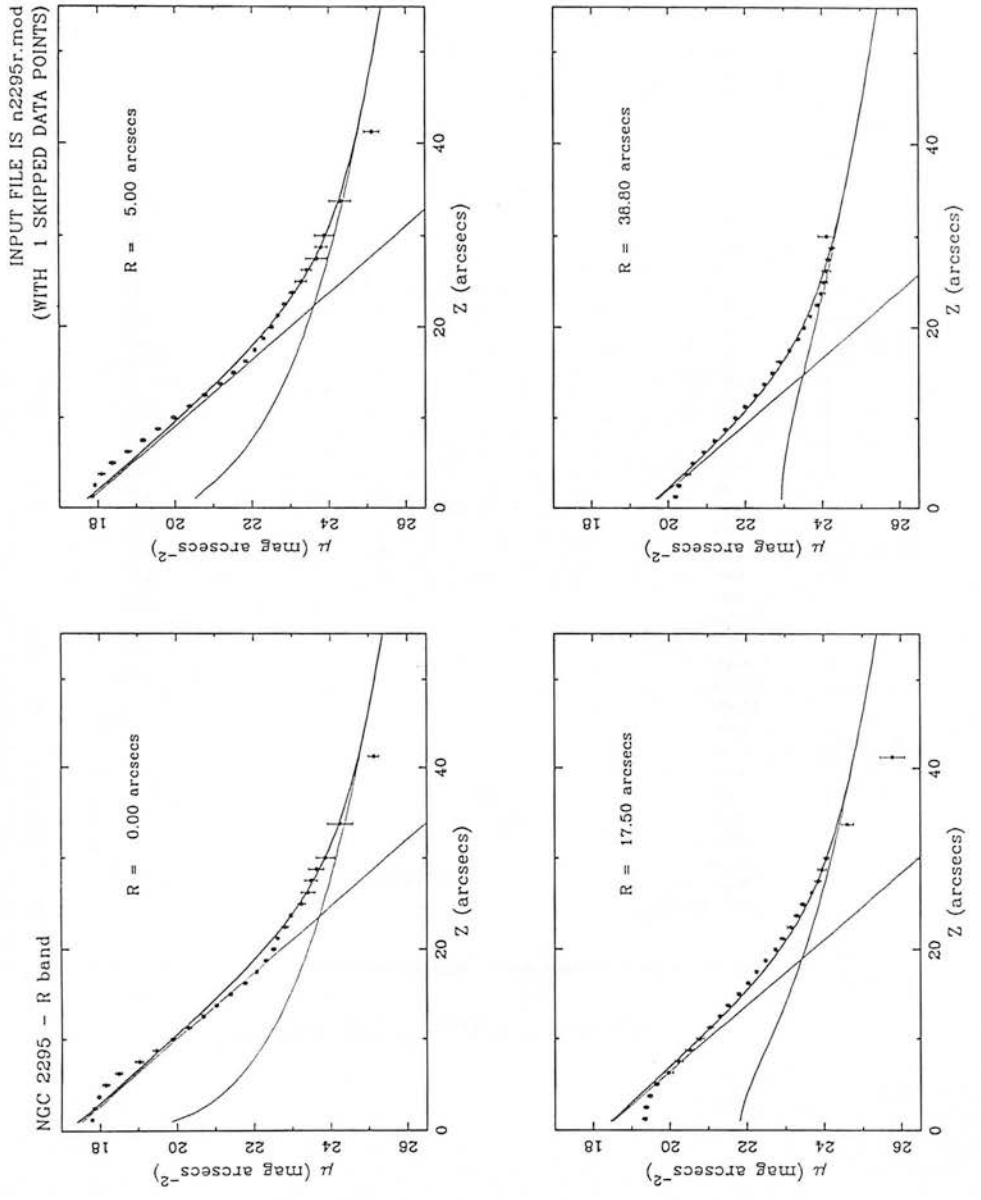

Figure 4.1 (a) : Model fits to a representative subset of the surface brightness profiles extracted across NGC 2295. The ordinate is surface brightness and the abscissa Z-height (arcsecs) above the assumed major axis. The galactocentric distance of each surface brightness profile is labelled R and shown in the upper right of each plot (in arcsecs). The summed model profile illustrated (thick full line) is that resulting from a superposition of exponential disc and $r^{1/4}$ law model profiles (both thin full lines). The assigned error bars were derived as described in the text.

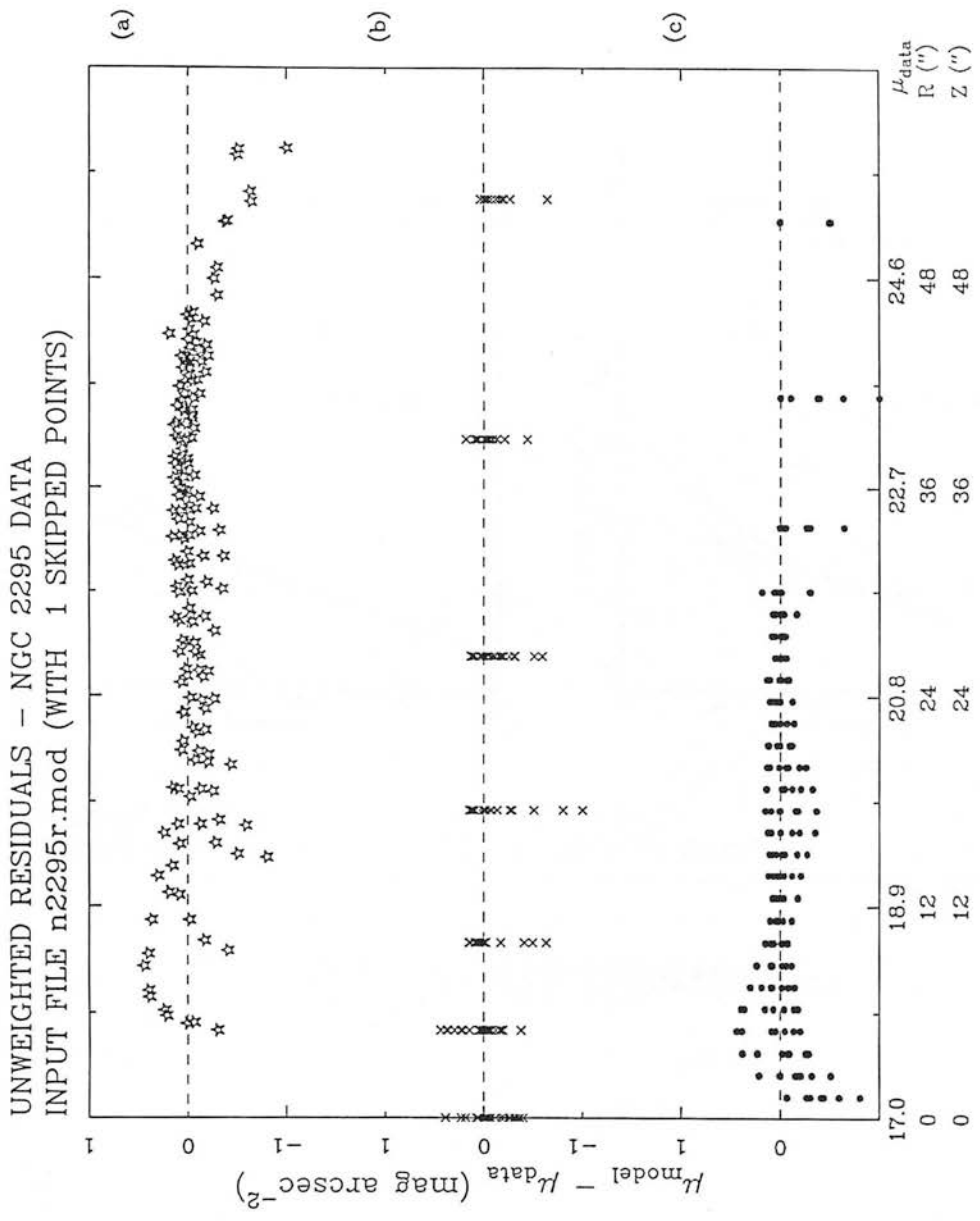

Figure 4.1 (b) : The distribution of unweighted residuals (defined as the difference between the predicted and observed surface brightness) for the model fits shown in figure 4.1 (a). These residuals are plotted as a function of observed surface brightness (labelled (a) and plotted as stars), of galactocentric distance (labelled (b) and plotted as crosses) and of Z-height (labelled (c) and represented by filled circles). The corresponding scales (μ_{data}, R and Z) are given along the lower axis, and lines of zero residuals are also shown in each case. All scale parameters are given in arcsecs and surface brightnesses in mag. arcsec^{-2}.

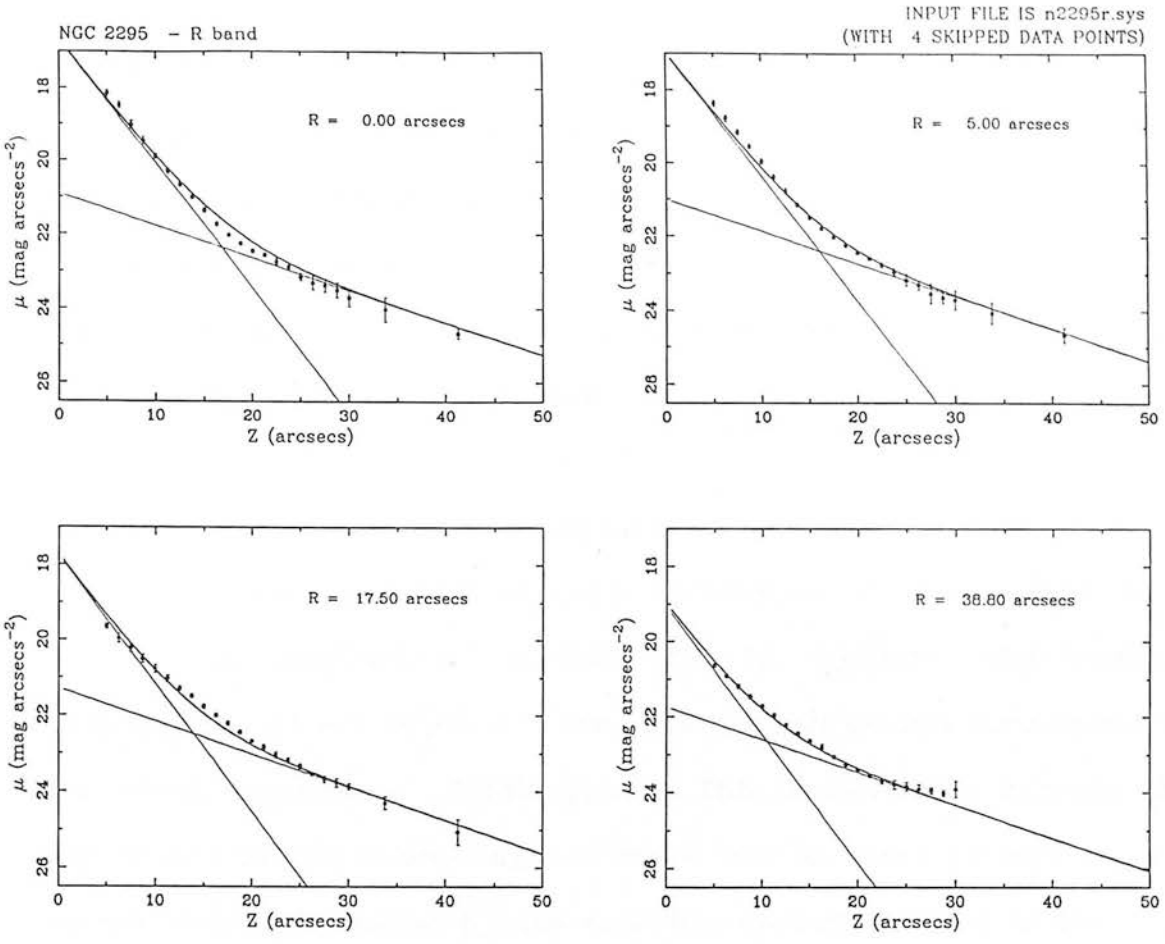
NGC 2295 - R band
INPUT FILE IS n2295r.sys
(WITH 4 SKIPPED DATA POINTS)
R = 0.00 arcsecs
R = 5.00 arcsecs
R = 17.50 arcsecs
R = 38.80 arcsecs
μ (mag arcsecs⁻²)
Z (arcsecs)

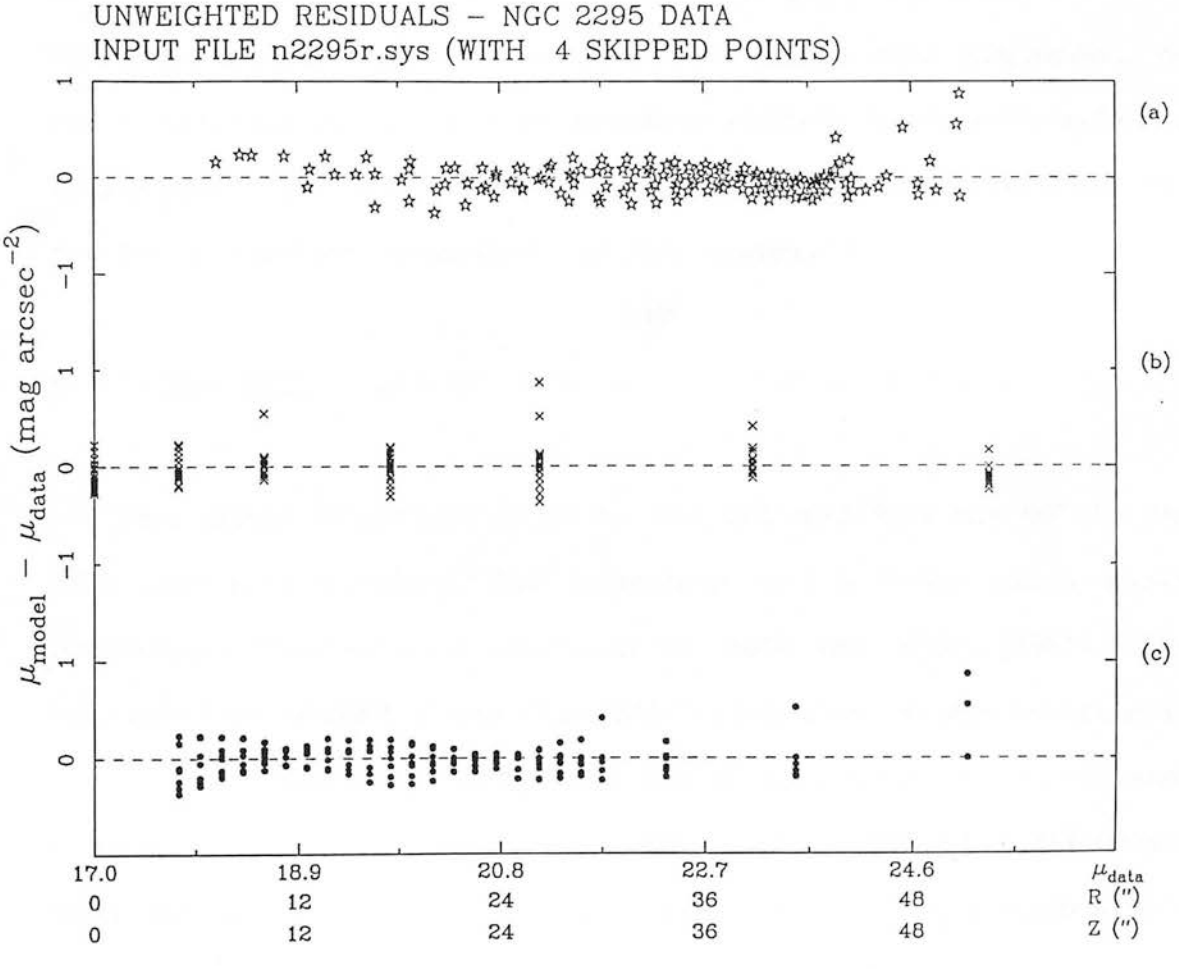
UNWEIGHTED RESIDUALS - NGC 2295 DATA
INPUT FILE n2295r.sys (WITH 4 SKIPPED POINTS)
(a)
(b)
(c)
μmodel - μdata (mag arcsec⁻²)
17.0
18.9
20.8
22.7
24.6
μdata
R (")
Z (")

figure 4.2

of residuals in this case is reduced by > 40 % over those "best-fit" combinations in table A.1. A visual comparison of the fits derived to the appearance of this galaxy in appendix C suggests that the first exponential model describes the luminosity distribution of the non-thin disc, whilst the fainter (but spatially more extended) second profile describes the thin disc component.

Despite the statistically improved fit, however, such a model combination only provides a good description of this galaxy to a typical rms residual of ± 0.25 μ_R. In addition, the relative contributions of the model profiles thus defined do not correspond to the visual appearance of this galaxy. This is primarily because the exponential profile dominating the minor axis at small Z-heights (in a region clearly dominated by the non-thin disc component) is the same as that model dominating those profiles at $R \gtrsim 30"$ where the non-disc influence is substantially less than that of the disc component. All model combinations tested here reveal a similarly implausible solution. This would imply that no set of model combinations tested here can provide a "realistic" description of this system.

IV.2.2 NGC 2310 ($\alpha = 06^h\ 52^m\ 16^s$, $\delta = -40^o\ 47'\ 54"$)

This galaxy (classified as S0 by the RC2 and ESO but $S0^+$ by the RSA) possesses a strong disc component and a bulge which shows pronounced "box"-shaped isophotes on both the SERC (J5747, field 309) and ESO (R3530) plates. The latter plate also reveals evidence of a weak major axis dust lane, whilst the strong, centrally concentrated nucleus is particularly clear on the ESO B plate 1776. The CCD frames show strong boxy isophotes to the very centre of this system, and

also reveal a warp at the NE end of the major axis (appendix C). Digital unsharp masking (appendix B, in particular figure B.2) reveals that the bulge may, in fact, be strongly "peanut"-shaped at the very brightest isophotal levels and that the clear major axis dust lane extends close to the central regions in the present data.

The local environment of NGC 2310 is sparse, with one smaller galaxy ~2.2' to the S and one ~9.0' W - it is assigned a field classification in the present work. The local stellar density is, however, quite high (with in excess of 35 stellar and non-stellar objects removed from each final co-added frame). In particular, one very bright star ~1.1' SE of the galaxy centre, whilst not falling on the frames obtained, contaminates the fainter galaxy surface brightness profiles SE of the major axis. All data contained within the affected areas were removed if, by comparing with the corresponding values in the NW profile, a discrepancy in excess of twice the assigned error at that point was encountered. The high degree of symmetry in the brighter galaxy profiles NW and SE of the major axis vindicates such a procedure.

The derived (single position) co-added frames obtained provide spatial coverage across almost the whole disc component - whose dimension on J5747 is ~3.1', corresponding to 8.5 kpc assuming a distance to this galaxy of 9.5 Mpc (calculated from the recessional velocity published by Sandage (1978), corrected for motion of the local group). Such a distance translates to a scale factor of 0.046 kpc/arcsecs.

Results of the modelling

Upon inspection of the surface brightness profiles being modelled, it was immediately evident that all profiles in B at galactocentric distances in excess of 9" are strongly affected at small Z by contamination from the major axis dust lane - particularly those between 9" and 32". To remove these effects requires the removal of at least the inner 3 data points in each profile. Thus the subsequent discussion will focus on fits derived after the removal of data interior to this Z-height. Interestingly, the inner profile cuts (the minor axis and R = 2.7" profiles) show no sign of dust contamination - and indeed the central 3 points along the minor axis show a rise of ~0.5μ towards the centre although such contamination must still be present in such regions. The much improved success found in the R band when modelling the full data array implies that at longer wavelengths the effect of the dust lane is considerably reduced (a point confirmed by a visual inspection of the data obtained). However, to maintain consistency with the data in B, the inner 3 data points at the smallest Z-heights were removed prior to the modelling procedure.

All single component models can immediately be rejected on the basis of the factor ~ 5 or more increase in the associated sum of squares of residuals when compared to the two-component fits in table A.2. In addition, those limited number of triple-component sets for which a solution of any form could be achieved are all found to have heavily suppressed one model profile in favour of the other two (thence yielding identical model parameters and statistical fit estimators to those of the corresponding two-component sets). Of the two-component combinations themselves, those incorporating the $r^{1/4}$ law fit the data considerably better than does any other model

combination tested.

Identical tests to those conducted for NGC 2295 again indicate that the scalelength parameters h_r and θ_e in the "best fit" two-component combinations appear to be very well-defined in both B and R. Furthermore, I also attempted to define whether the scaleheight of the disc component varies as a function of galactocentric distance by modelling each surface brightness profile independantly of the rest, using a model combination in which all parameters other than the scaleheight itself were held constant at their values in table A.2. Any variations in the light distribution perpendicular to the plane would thus be manifested by variations in h_z with $\mathbb{R}$. No evidence was found in either passband for any systematic variation in this parameter across the entire array of perpendicular profiles modelled - mean scaleheights of 0.294 (±0.004) kpc in B and 0.257 (±0.003) kpc in R being found (in very good agreement with those in table A.2). Evidently the assumption of a constant disc scaleheight in this galaxy is a good one. In particular, the lack of any trend seen at larger $\mathbb{R}$ indicates that the presence of the disc warp has a minimal effect on the parameters characterising the disc component. Were the light distribution in the disc significantly altered by the presence of the warp, one might have expected the scaleheight to increase at larger $\mathbb{R}$ from the "flaring" which would result in such profiles after reflection about both major and minor axes.

However, a comparison of the model parameters thus obtained reveals differences of ~ 45 % between the disc scalelengths in B and R. Indeed, a visual comparison of model fits graphically illustrates

that the relative contributions of the model disc profile are quite different in the two datasets. A possible cause of this disparity may result from the fact that the luminosity profiles being modelled are all very "flat" (as a function of Z) exterior to those galactocentric distances dominated by the box-shaped feature. It appears that the modelling routine is unable to unambiguously differentiate between the available model components adopted.

Such discrepancies are implausible, and as a result I undertook to test whether possible dissimilarities in the respective error distributions adopted would account for these effects. To this end, I imposed a lower limit on the error assigned to each data point used, and tested the similarity of the derived model parameters in the two passbands at equivalent lower limits. Such a procedure was indeed found to reduce the disparity between all scale parameters in the B and R data - imposing a minimum error of ± 0.10 μ reducing the difference in disc scalelengths to 28 % and in θ_e to 13 %. The results obtained by applying the "best-fit" exponential + $r^{1/4}$ law combination to the present data after allowance for such parameter differences are illustrated in figures 4.3 (B) and 4.4 (R).

In conclusion, NGC 2310 is best described by a combination of a disc component and an $r^{1/4}$ law profile. The figures indicate that after applying a minimum error to the dataset used, a typical residual between the predicted and observed luminosity distribution is ~ ± 0.5 μ in the B band and ~ ± 0.4 μ in R. Interestingly, the box-shaped isophotes appear well-described by the same $r^{1/4}$ law profile which is a major contributor to the summed model profile at larger Z-heights. The luminosity contained within the box regions therefore appears to

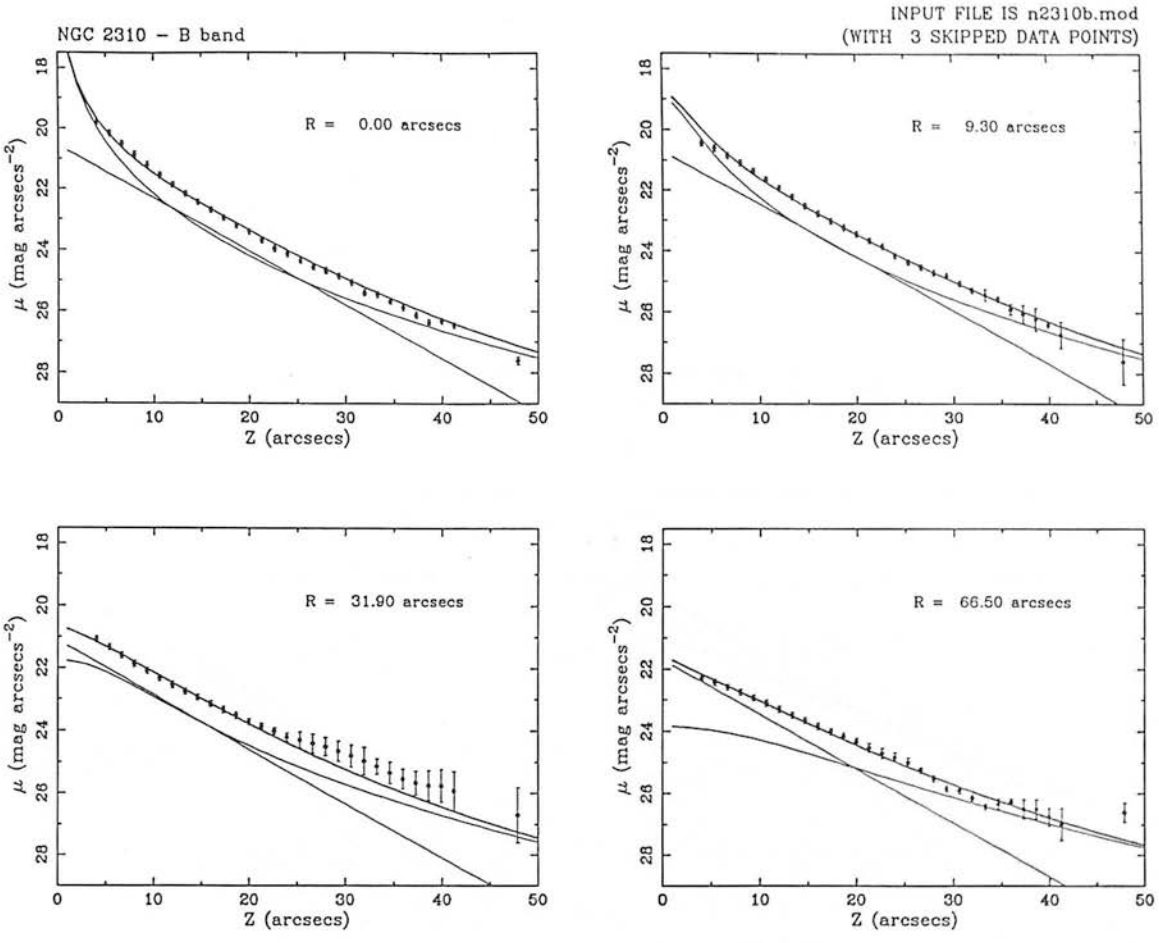
NGC 2310 – B band
INPUT FILE IS n2310b.mod
(WITH 3 SKIPPED DATA POINTS)
R = 0.00 arcsecs
R = 9.30 arcsecs
R = 31.90 arcsecs
R = 66.50 arcsecs
μ (mag arcsecs⁻²)
Z (arcsecs)

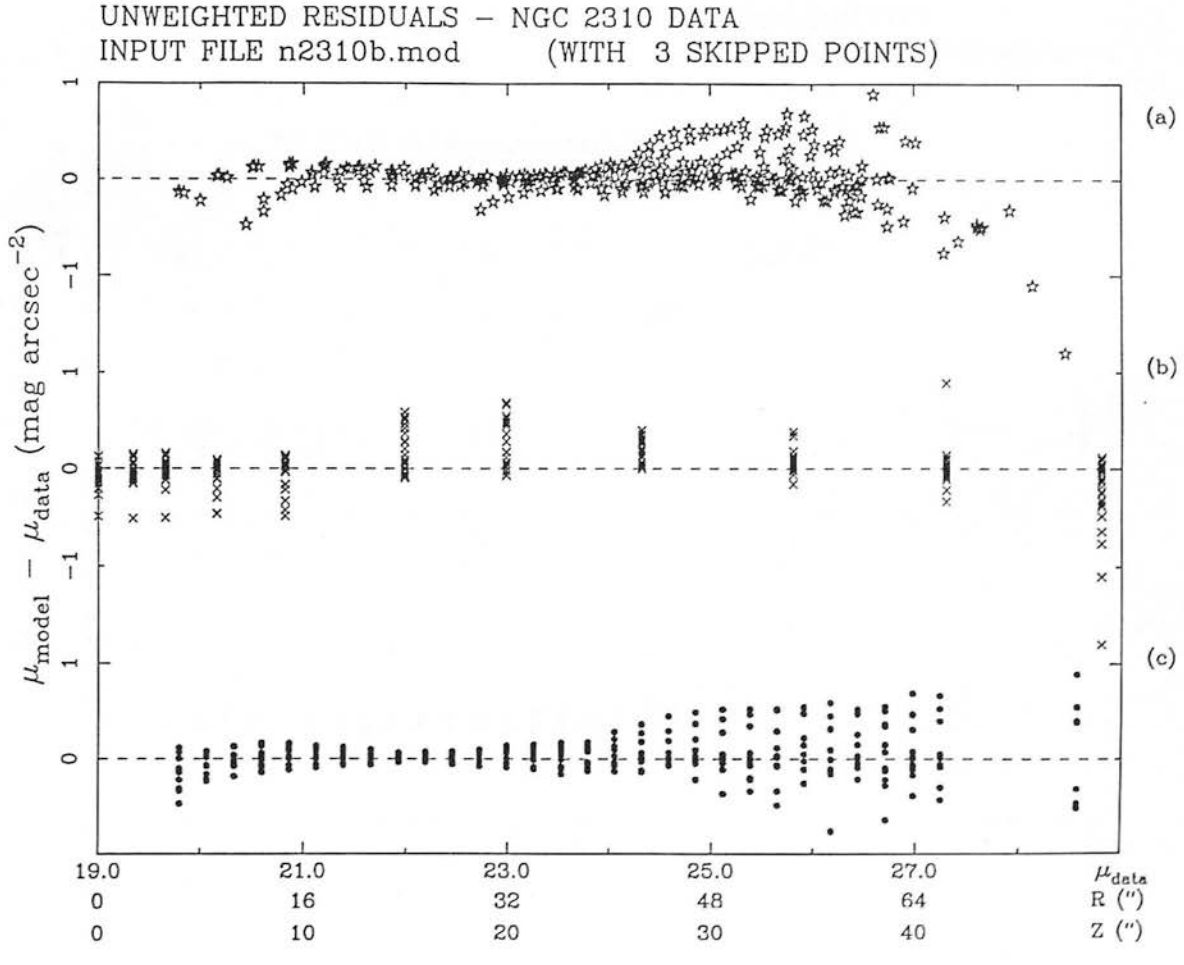
UNWEIGHTED RESIDUALS – NGC 2310 DATA
INPUT FILE n2310b.mod (WITH 3 SKIPPED POINTS)
(a)
(b)
(c)
μmodel – μdata (mag arcsec⁻²)
19.0 21.0 23.0 25.0 27.0 μdata
0 16 32 48 64 R (")
0 10 20 30 40 Z (")

figure 4.3

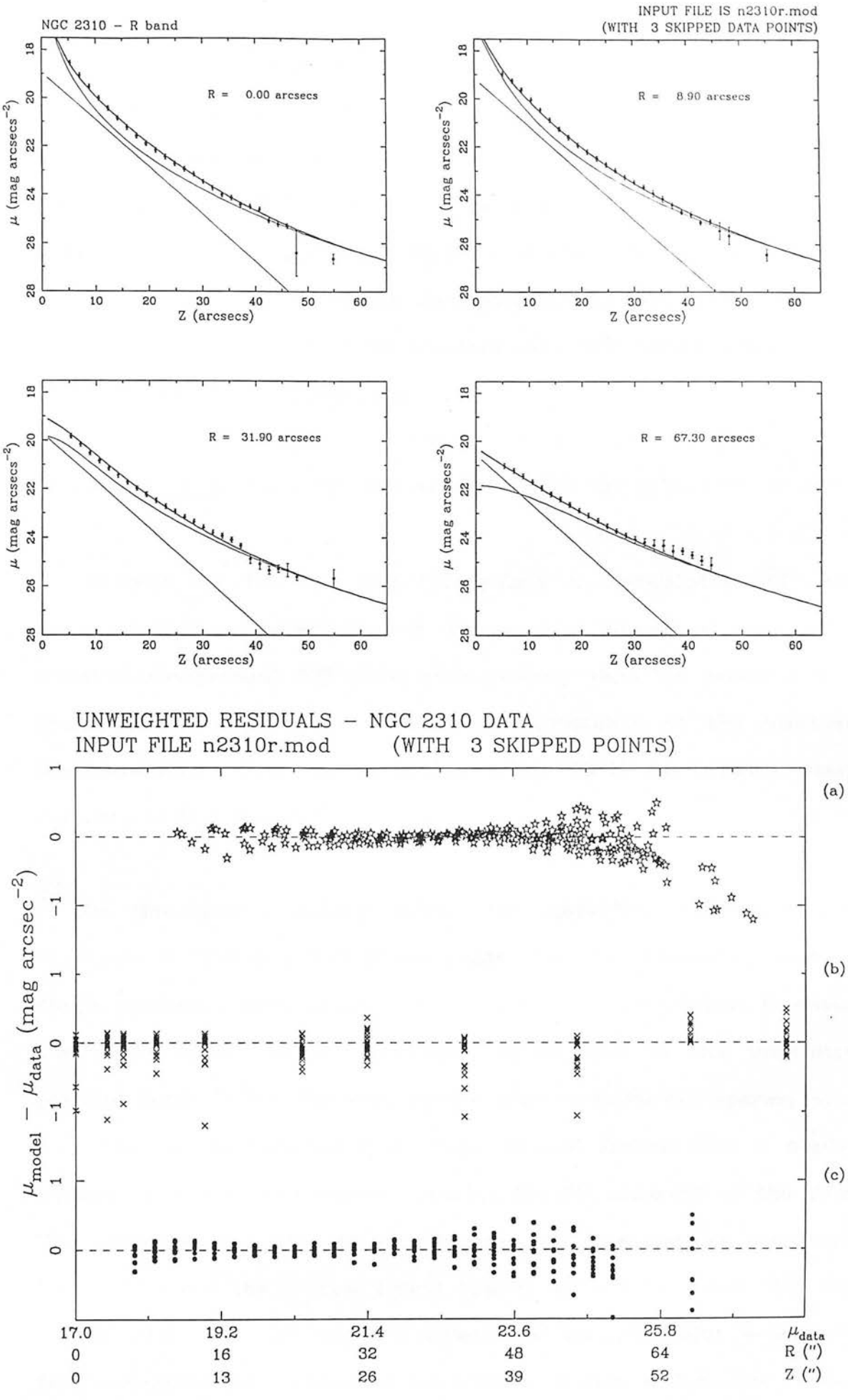
NGC 2310 – R band
INPUT FILE IS n2310r.mod
(WITH 3 SKIPPED DATA POINTS)
R = 0.00 arcsecs
R = 8.90 arcsecs
R = 31.90 arcsecs
R = 67.30 arcsecs
μ (mag arcsecs⁻²)
Z (arcsecs)
UNWEIGHTED RESIDUALS – NGC 2310 DATA
INPUT FILE n2310r.mod (WITH 3 SKIPPED POINTS)
μmodel – μdata (mag arcsec⁻²)
(a)
(b)
(c)
17.0 19.2 21.4 23.6 25.8 μdata
0 16 32 48 64 R (")
0 13 26 39 52 Z (")

figure 4.4

be precisely that expected from the central concentration of the fainter non-disc component in this system. This result was confirmed upon inspection of image frames for NGC 2310 from which the exponential and $r^{1/4}$ law model luminosity distributions had been subtracted. The residual light exterior to the dust lane (but in an area noted as being previously dominated by the box morphology) is only ~ 10 (± 5) % of the total non-thin disc light within the original image frames in both passbands.

IV.2.3 NGC 3115 ($\alpha = 10^h\ 02^m\ 44.8^s$, $\delta = -07^o\ 28'\ 27''$)

In both the RC2 and RSA this galaxy is classified as SO^- i.e. there appears to be an absence of any dust along the major axis. However, the present CCD observations clearly show the presence of a pronounced, but very thin, inner disc component at the brighter isophotal levels (see also Tsikoudi (1977, 1979) for equally clear evidence of this feature).

On the SERC J survey (plate 8438, field 781) the major axis dimension is ~5.6' and that of the minor axis ~1.7'. Thus the co-added single position frames centred on the nucleus are sufficient to cover the whole galaxy to such isophotal levels (due to the associated position angle ~45°). The local stellar field is relatively sparse, with only ~20 images removed from these central frames, and a similar number on the R band frames covering the SW extremity of the disc. The galaxy environment is also sparse, with the nearest neighbour being ~5' E and the nearest bright system (a face-on spiral) ~16' SSE of NGC 3115 itself. An adopted distance of 4.8 (±0.2) Mpc is derived from a mean of the recessional velocities of Morton & Chevalier (1973),

Rubin et al (1980) and Williams (1975) corrected for solar motion relative to the local group. This translates to an image scale of 0.023 kpc/arcsec.

IV.2.3 (a) Results of the modelling

A pronounced turnover in surface brightness is seen between the innermost data points of the minor axis profile of this system. This is unlikely to be due to dust obscuration (as such an effect is not seen in the immediately adjacent profiles) but it may arise from some undefined saturation/nonlinearity effects at the very centre because of the relatively long (1500 secs) exposure of the brightest galaxy in the sample. Initial tests were conducted with up to 3 points removed to define the significance of such an effect on the model parameters obtained, although in the light of the degree of reproduceability between parameters in these tests, the present analysis focusses on the modelling results derived when the single data point along the major axis was removed from each profile prior to modelling.

The detailed discussion undertaken by Tsikoudi (1977) of the principal axes (and equivalent) profiles of this galaxy obviates the need for similar observations here, although it is noted in passing that none of the "fine structures" seen in her major axis profile are found in the present data. The most obvious of these features (at R ~1.5') may result from the presence of an unremoved faint star - the CCD frames show a number of such stars superimposed on the very brightest isophotal regions of this galaxy.

Table A.3 summarises the results obtained from each single and two component model fit to this system. I did not undertake

three-component fits in this case as they appeared unwarranted in the light of the visual appearance of this system and because the limited spatial and dynamic range of the current observations were considered inadequate to apply a further component. As is evident from these results, the simple $r^{1/4}$ law profile provides a substantially better fit than any other single, and most double, component combinations. However, inspection of the representative fits and the corresponding residuals diagram for this model - figure 4.5 shows its application to the data in B - reveals discrepancies at both small and large Z-heights. The former are most in evidence over those profiles at larger galactocentric distances (~40 to 80"), and are considerably reduced by the inclusion of an additional disc profile - either using a $sech^2$ model (preferred in the R band and reducing FSUMSQ by 22 % over the single $r^{1/4}$ law profile), or an exponential model (in B where the improvement in FSUMSQ is 53 %).

A more detailed study of the disc components in such two-component fits show no trends of scaleheight with R to ~ 2 % in B and ~ 4 % in R. The clear systematic overestimation of the observed light distribution seen at fainter μ in figure 4.5, however, persists with the inclusion of the disc profile. Assuming, as previously, that such an effect is a result of an incorrect assessment of the sky requires those values in table 2.2 to be reduced by ~ 11 % and ~ 2 % in B and R respectively. Such changes are substantially larger than those required for almost all other galaxies in the present sample, but the sky measures for this dataset are very much less certain owing to the limited number of pixels in the image frames obtained which are likely to be free from contamination by light from the galaxy itself. The change required in the B band is reasonably consistent

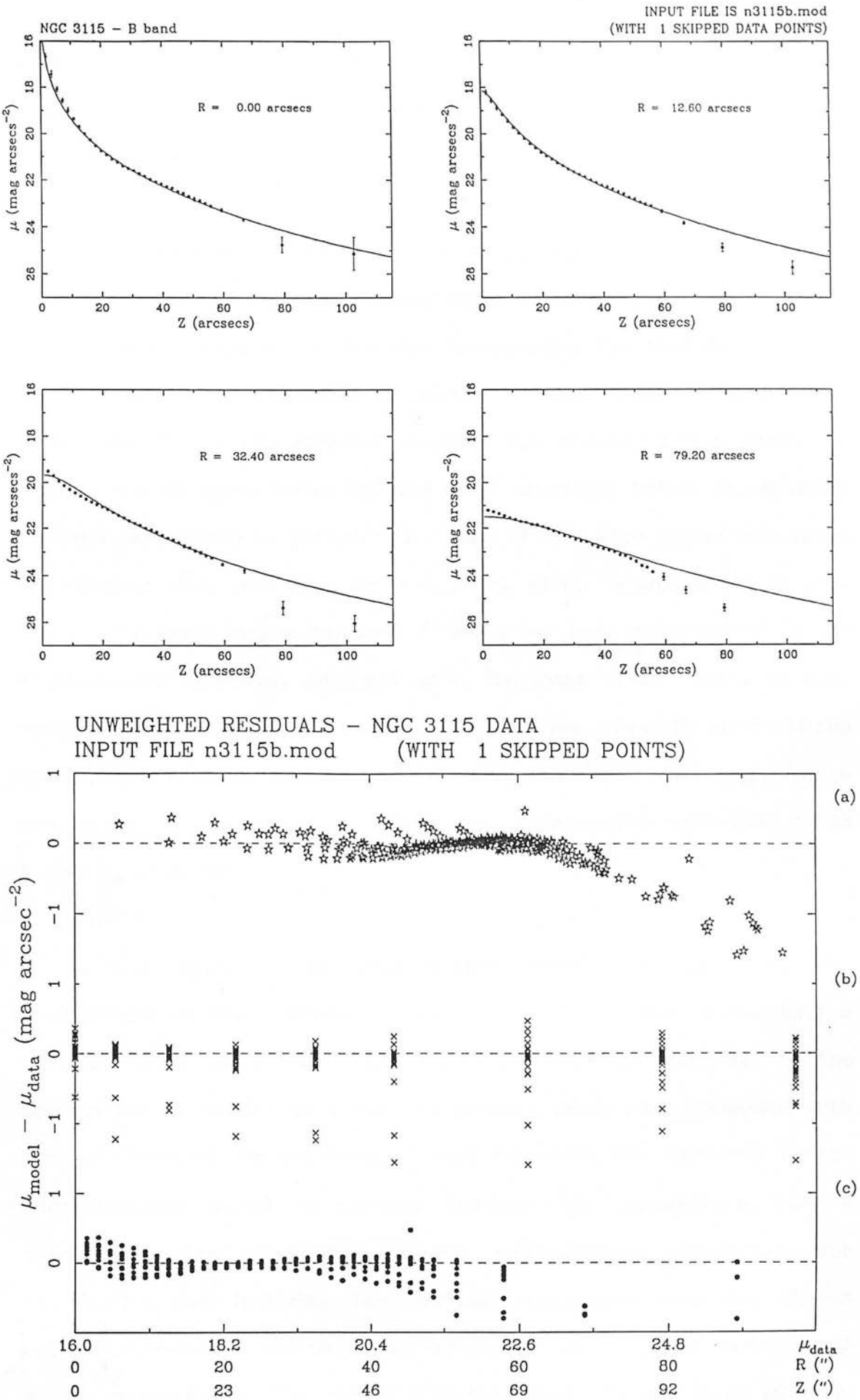
NGC 3115 – B band
INPUT FILE IS n3115b.mod
(WITH 1 SKIPPED DATA POINTS)
R = 0.00 arcsecs
R = 12.60 arcsecs
R = 32.40 arcsecs
R = 79.20 arcsecs
μ (mag arcsecs⁻²)
Z (arcsecs)
UNWEIGHTED RESIDUALS – NGC 3115 DATA
INPUT FILE n3115b.mod (WITH 1 SKIPPED POINTS)
μmodel – μdata (mag arcsec⁻²)
(a)
(b)
(c)
16.0 18.2 20.4 22.6 24.8 μdata
0 20 40 60 80 R (")
0 23 46 69 92 Z (")

figure 4.5

with the 14 % required in chapter II to bring the major and minor axis profiles into agreement between the present work and that of Tsikoudi (1977).

After allowance for such systematics, the derived model parameters again show unphysically large disparities between B and R passbands particularly for the disc components. The fact that none of the two-component combinations in the R band iterate to a solution within the fit criteria imposed (despite the quoted output parameter values in such cases being defined many iterations before the MAXCAL factor is exceeded) is probably a result of the more restrictive error distribution than that used in B (a point which is also likely to give rise to the much larger reduced χ^2 estimates than encountered in the B passband). However, adoption of a "minimum error" leads to only marginal improvement in this case. Of all the possible combinations tested, the most consistent results were obtained when imposing a minimum error of ± 0.15 μ, yielding disc scalelengths equivalent to 43 % and e_e to 31 %.

In the light of the present uncertainties in the local sky background on these frames, I also tested the results of adopting a minimum error procedure after correcting the sky measure by the amount (14 %) needed to bring the present work into agreement with that of Tsikoudi. No improvement was found in the similarity of the corresponding model parameters between the present B and R passbands. The "best-fit" model combinations, corrected for systematics and bringing the derived parameters into the closest possible agreement, are shown in figures 4.6 and 4.7 applied to B and R data respectively. The values defining these fits are given in table

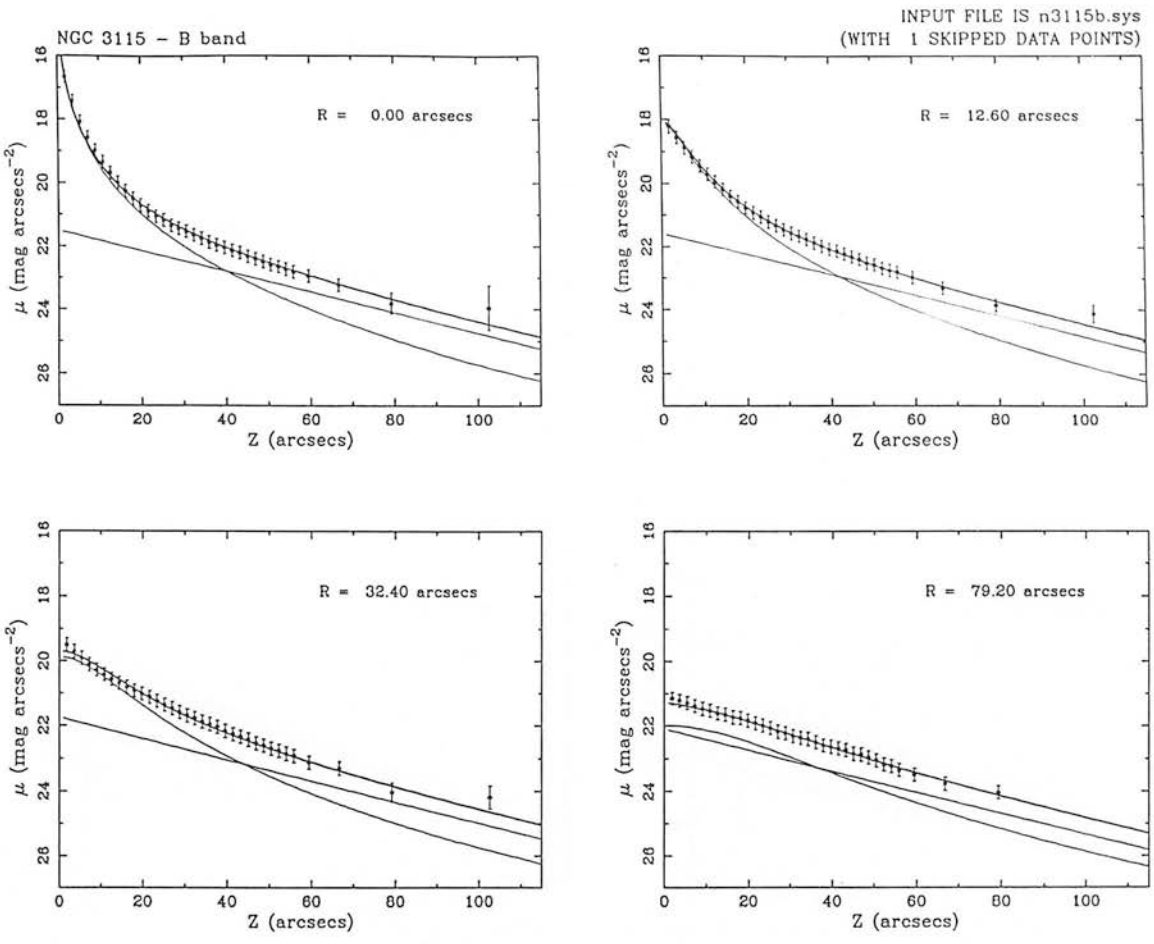
NGC 3115 – B band
INPUT FILE IS n3115b.sys
(WITH 1 SKIPPED DATA POINTS)
R = 0.00 arcsecs
R = 12.60 arcsecs
R = 32.40 arcsecs
R = 79.20 arcsecs
μ (mag arcsecs⁻²)
Z (arcsecs)

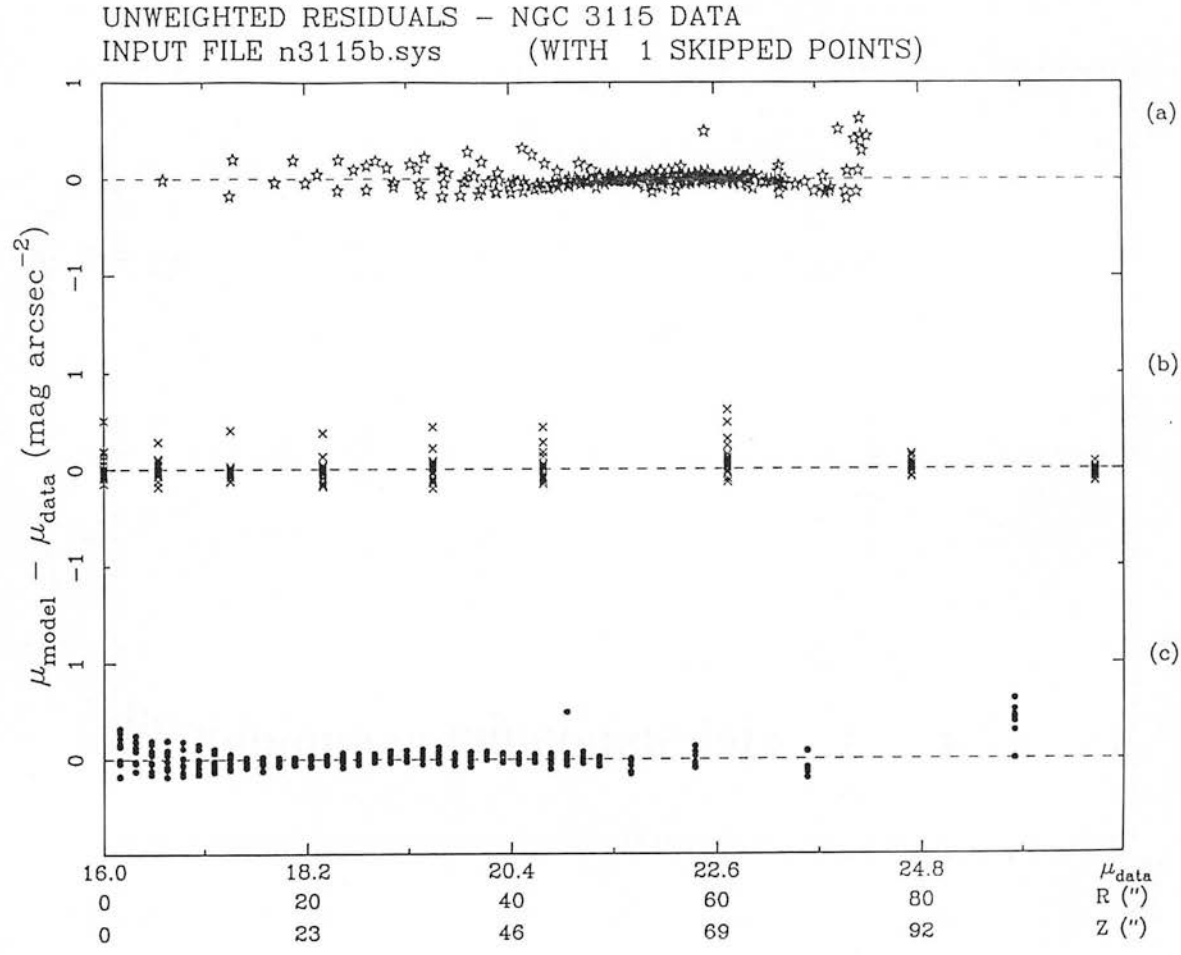
UNWEIGHTED RESIDUALS – NGC 3115 DATA
INPUT FILE n3115b.sys (WITH 1 SKIPPED POINTS)
(a)
(b)
(c)
μmodel – μdata (mag arcsec⁻²)
16.0 18.2 20.4 22.6 24.8 μdata
0 20 40 60 80 R (")
0 23 46 69 92 Z (")

figure 4.6

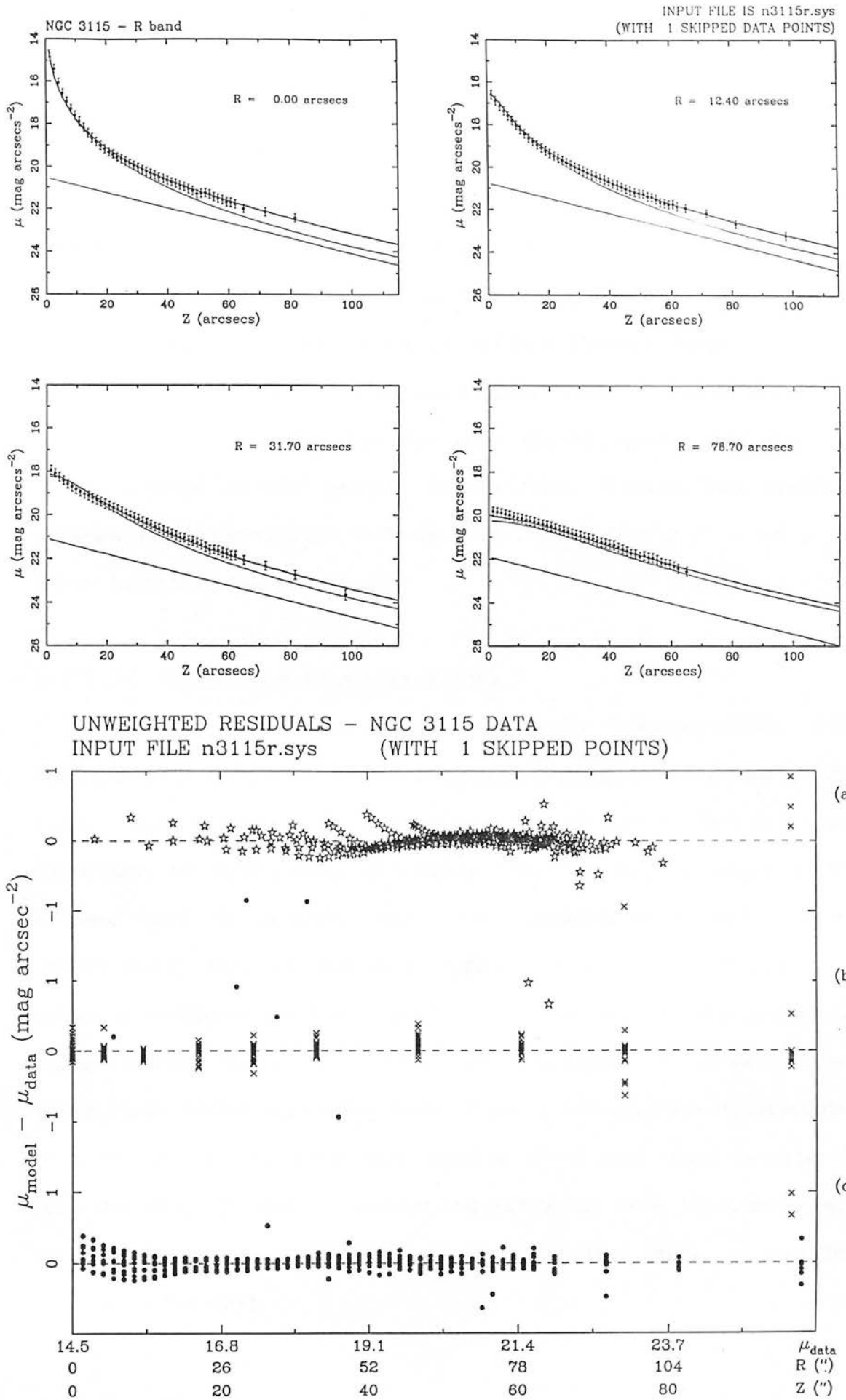
NGC 3115 – R band
INPUT FILE IS n3115r.sys
(WITH 1 SKIPPED DATA POINTS)
R = 0.00 arcsecs
R = 12.40 arcsecs
R = 31.70 arcsecs
R = 78.70 arcsecs
μ (mag arcsecs⁻²)
Z (arcsecs)
UNWEIGHTED RESIDUALS – NGC 3115 DATA
INPUT FILE n3115r.sys (WITH 1 SKIPPED POINTS)
μmodel – μdata (mag arcsec⁻²)
(a)
(b)
(c)
14.5 16.8 19.1 21.4 23.7 μdata
0 26 52 78 104 R (")
0 20 40 60 80 Z (")

figure 4.7

4.1 at the end of this chapter.

The cause of such parameter differences may be likened to the case of NGC 2310 previously in that a visual fit to the surface brightness profiles extracted at large R would suggest that a simple exponential profile would be all that is required to model the galaxy over all Z-heights - the modelling routine thereby being unable to delineate unique contributions from each model in such situations. Alternatively, it may be due the very limited spatial, and dynamic, range covered in the present observations. Typical rms residuals between the observations and the best model fits of ~ ± 0.2 μ are found in both colours.

IV.2.3 (b) Comparison to previous work

Confirming the conclusions arrived at by Tskioudi (1977, 1979), the modelling results in the B passband contain clear evidence of a faint disc component whose relative contribution becomes most significant at intermediate Z-heights (~20 to 100") at small R. The present work is, however, more than a simple confirmation of the earlier study because this is the first attempt to differentiate the model contributors to the total light distribution in this galaxy by using purely statistical means. The analysis of Tsikoudi was particularly limited in basing most of its conclusions on deconvolution of major, minor and equivalent profiles alone and, more importantly, from modelling of each component independantly from the others (with all the limitations, noted in chapter III, that such a modelling procedure invokes).

A detailed comparison between the present B band results and those of Tsikoudi (1977) is not possible owing to the limited spatial coverage in the present work compared to that of the earlier (photographic) study. Nevertheless, some useful comparisons can still be made. Based on table 5 of Tsikoudi (1977), I note that all surface brightness profiles modelled in the present B passband data correspond to semi-major axes of $\lesssim$ 60", the point at which the integrated luminosity is ~ 75 % of the total. Indeed, 2/3 of the model profiles modelled here are interior to ~ 40", where Tsikoudi suggest that half of the total luminosity of this system is contained. Her results given over regions of 25 % to 50 % of L_{tot}, show a range in μ_e of 18.15 to 20.26 mag. arcsec^{-2}, a θ_e of 7.8" - 21.6" and an axis ratio of 0.42 to 0.31. The values approximately encompass the parameters defined in the present work (the θ_e of 0.26 kpc derived here corresponding to 11.5") when due account is also taken of the zeropoint difference between the respective studies noted in chapter II. The present axis ratio also compares well with the value of 0.40 (±0.01) found by Strom et al (1977) from their iterative ellipse fitting to data in the V band interior to a semi-major axis ~ 100".

An equivalent comparison of the disc is not possible for the same reasons noted above (Tsikoudi models such a component to Z-heights ~150" - considerably beyond the extent of the present surface brightness array). Nevertheless, a visual inspection of her minor axis profile indicates that the exponential disc first becomes a significant contributor to the summed model profile at a Z-height ~ 60", in reasonable agreement with the corresponding model fit in figure 4.6. Furthermore, adopting the modelling results of Tsikoudi's 3 perpendicular profile cuts at 44, 50 and 74 arcsecs yields a mean μ_o

of 21.32 μ in reasonable agreement with the present results. However, her corresponding scaleheight, corrected for the different assumed distances between the two studies, of 1.7 kpc is considerably larger than the present estimate. A possible source of this difference may again result because the present data cover such a small range in Z as to make a definition of the disc scaleheight uncertain, and because her results are uncertain as they apply to an independant modelling procedure for each of these 3 surface brightness profiles mentioned.

IV.2.4 NGC 3573 (α = 11^h 09^m 01^s, δ = -36^o 35' 49")

This bulge dominated system, which also possesses a pronounced dust lane obscuring the lower centre of the galaxy, is classified as SA0 (pec?) in Corwin et al (1985), and S0 in the ESO catalogue (although it is not contained in either the RC2 or RSA). Inspection of both the SERC J survey plate 3993 (field 377) and the current CCD data reveals evidence of complex (but faint) structure at the extremities of the major axis within the disc component. The total major axis dimension on this plate is ~ 4.5' such that the (single position) B band frames, for which a chip orientation EW was adopted, cover the central bulge but only ~1/3 of the total disc extent. In R, however, the current data samples an area considerably beyond that of the faintest isophotes on J3993 as it comprises a mosaiced composite of 3 pairs of co-added frames.

The local stellar environment on these frames is sufficiently dense as to require the removal of ~ 27 images from both B and R frames centred on the nucleus. However, only one bright star is found to fall on the galaxy itself - lying on the southern end of the obscuring

dust lane - and as such had no effect on the derived surface brightness profiles taken across such a region. The immediate galaxian density is also quite rich, the nearest system being only ~ 2.2' west of NGC 3573 itself. An assigned cluster membership is taken from the ESO catalogue. However, the cluster is unidentified in this source, and no distance estimates for this galaxy could be found.

The notably "disturbed" nature of the dust lane, particularly at large galactocentric distances, was of some concern when extracting profiles at such positions. A comparison of the corresponding E and W profiles was used to determine the excess contamination in the latter over the former - those measures clearly affected by obscuration effects being discarded. Such a procedure required the removal of between 3 to 6 inner data points in B - fewer in R - but in addition all data along the major axis itself in both colours. The validity of the latter procedure was evidenced by the 10 % reduction in FSUMSQ (and 38 % in red. χ^2) compared to the fits derived when such data were retained. The data arrays finally adopted in both colours are as free from contamination by the major axis dust lane as a visual inspection of the data obtained would allow.

Results of the modelling

The results of modelling this system are given in table A.4. On the basis of a comparison between the statistical fit estimators, the best description of this galaxy is afforded by a combination of exponential disc and $r^{1/4}$ law profiles in the B band. In R, the triple combination of "exponential + $sech^2$ + $r^{1/4}$ law" profiles gives the smallest sum of squares of residuals (by ~ 45 % over the best two-component combination). However, an inspection of the parameters

derived highlights an unrealistically large scaleheight for the exponential profile, and an exceptionally small scalelength. Indeed, a visual study of the fits derived in this case shows such a model to possess a surface brightness roughly constant with Z over all profiles. The statistical improvement noted above results from the improved fit over the outermost 3 data points in each profile (i.e. those for which $Z \gtrsim 45"$).

Discounting such combinations on the strength of the implausible parameters obtained, a combination of $sech^2$ and $r^{1/4}$ law models fit the data best in R. However, table A.4 reveals similar unphysical disparities between the model parameters in B and R, whilst the fits obtained show such model combinations to be quite inadequate in describing the luminosity distribution in this galaxy. Evidence of a systematic overestimation of the observed light at large Z is seen in the R band, at least for those profiles interior to galactocentric distances ~ 50", whilst equally poor agreement, but seemingly not due to any "systematics", is also found over the same regions in the B band.

The 0.3 % reduction in the local sky background required to correct for the systematics at large Z in R, are found to change the resultant model parameters by minimal amounts, and certainly insufficient to improve the quality of those fits at larger R to the ones noted previously. The question therefore arises as to why these "best-fit" model combinations are unable to fit the observed luminosity distribution to better than ~ 0.4 μ in both colours, even after allowance has been made for any possible systematics in the data. Owing to the somewhat inclined aspect of the dust lane (a figure

of 7° is estimated from the present observations), and in the light of the varying amount of data removed to allow for contamination from such a feature, those parameters defining the thin disc component must be viewed with considerable uncertainty (particularly in B where the effects are most marked). As a result of the additional constraints placed on decomposition of the non-thin disc light with such uncertain disc parameters, therefore, values for the $r^{1/4}$ law profile must also be viewed as considerably less well-defined than for other galaxies in the current sample.

However, whilst the presence of the dust lane undoubtedly introduces complications when modelling this galaxy, this cannot be the reason for the poor fits obtained over all (R,Z). For example, the minor axis profile is poorly described in both B and R beyond Z ~ 40", although a visual inspection of the image frames concerned (appendix C) reveals relatively little obscuration along this profile beyond 20", and explicitly precludes the existence of dust lane contamination at such Z - particularly in the R band where the model fit is the poorest. Indeed, the whole galaxy to a surface brightness ~ 25 μ_R would have to be so affected were this hypothesis to be tenable.

In the light of the dissimilar parameters noted above, a minimum error procedure was again applied to the dataset after removal of the systematics in the R band. It was found that a substantial improvement in the reproduceability of all scale parameters (originally discordant by ~ 70 % in all cases) could be obtained by imposing a minimum error of ± 0.2 μ - the corresponding differences in scalelengths now being reduced to 29 %, the scaleheights to 37 % and

the effective radii to 21 %. No further improvements arose with the removal of more data at small Z-heights. The results of such a procedure are illustrated in the model fits shown in figures 4.8 (the "exponential + $r^{1/4}$ law" combination in B) and 4.9 (the $sech^2$ + $r^{1/4}$ law" set in R). Indeed, the goodness-of-fit parameters indicate a statistically considerable improvement in B over the corresponding model combination in table A.4 (FSUMSQ being reduced by ~ 50 %), although the improvement in R is only marginal (at ~ 5 %). However, in R the typical rms residual appears to be reduced to ± 0.25 μ.

In conclusion, therefore, NGC 3573 can be well-described by the model combinations adopted to ± 0.3 μ_B and ± 0.25 μ_R, and yield model parameters equivalent to ~ 30 % in B and R. However, to obtain this agreement requires a large change in the adopted sky background on the R frame, and a minimum error of ± 0.2 μ in both passbands.

IV.2.5 NGC 4289 (α = 12^h 18^m 27^s, δ = 04° 00' 06")

The striking appearance of this galaxy (classified as Sc in both RC2 and UGC) results from the dominant disc component, with the inclination ~4° from an edge-on aspect being deduced on the basis of the slight obscuration of the bulge seen on the western side of the galaxy. On both the POSS red and blue survey (plates 1560), and the current observations, no evidence of any disc warping is seen. The total disc dimension on this plate material is ~4.5', and is sufficient to require CCD frames oriented N-S (long axis parallel to the major axis of the galaxy) for full coverage to be achieved. The limited spatial coverage perpendicular to the major axis was not considered a restriction in obtaining sky in these frames because of the rapid

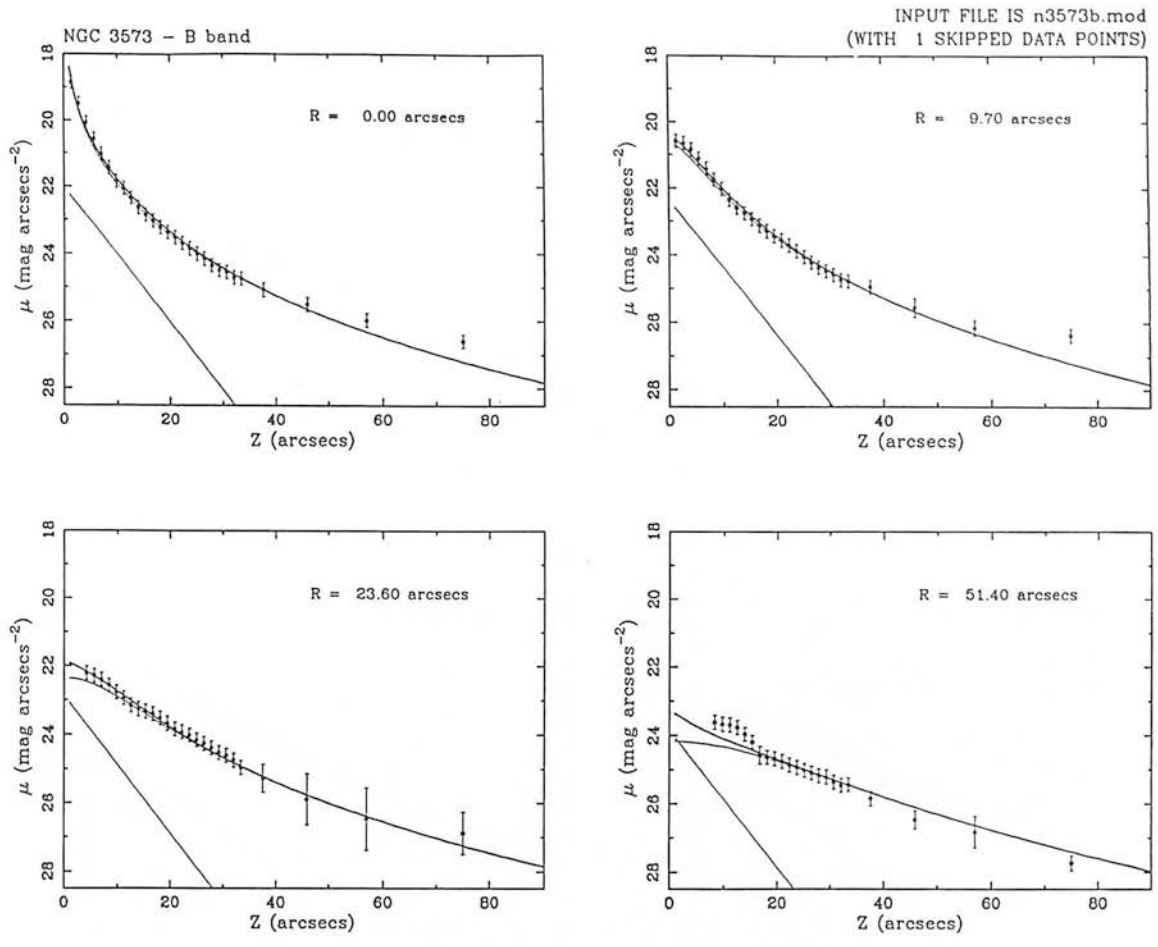
NGC 3573 – B band
INPUT FILE IS n3573b.mod
(WITH 1 SKIPPED DATA POINTS)
R = 0.00 arcsecs
R = 9.70 arcsecs
R = 23.60 arcsecs
R = 51.40 arcsecs
μ (mag arcsecs⁻²)
Z (arcsecs)

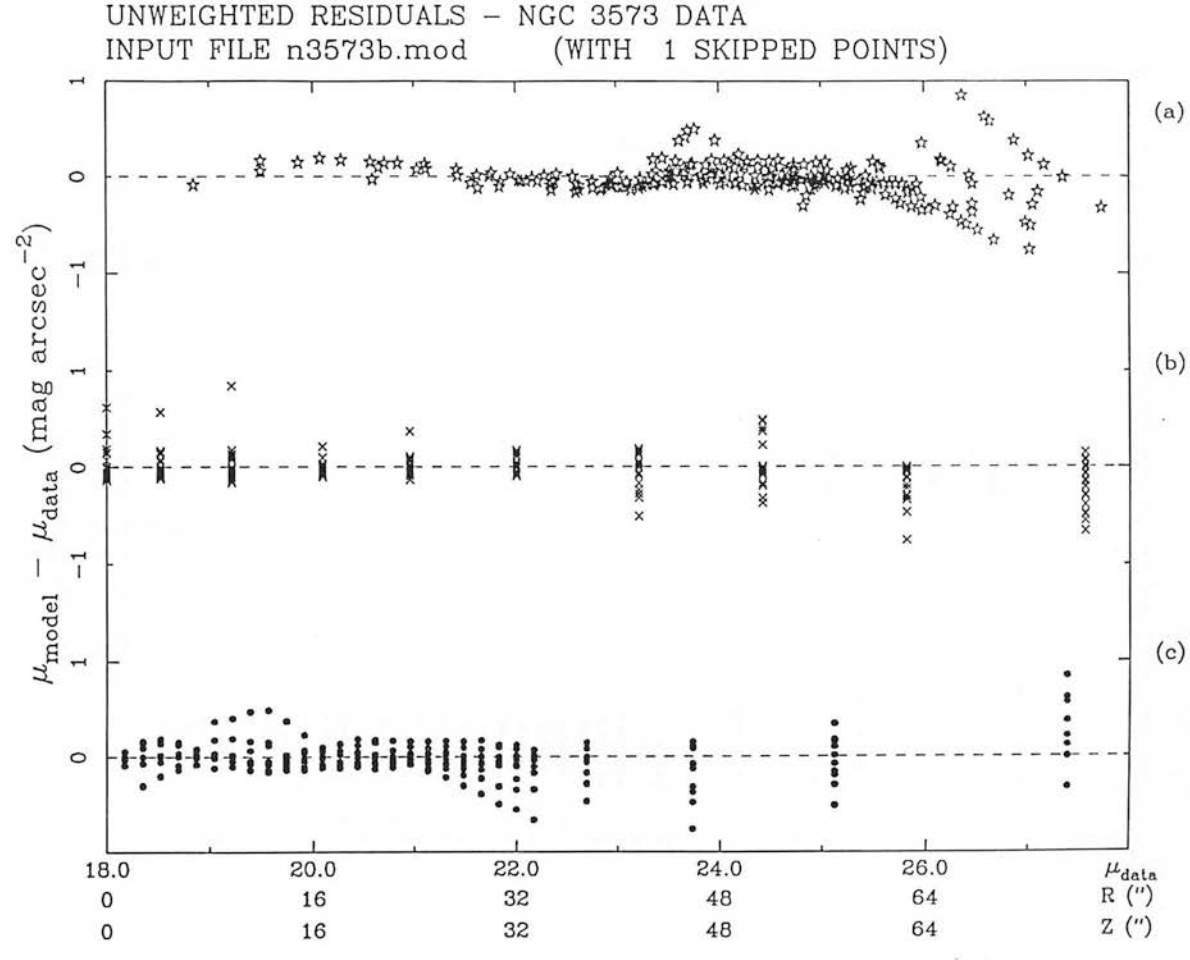
UNWEIGHTED RESIDUALS – NGC 3573 DATA
INPUT FILE n3573b.mod (WITH 1 SKIPPED POINTS)
(a)
(b)
(c)
μmodel – μdata (mag arcsec⁻²)
μdata
R (")
Z (")

figure 4.8

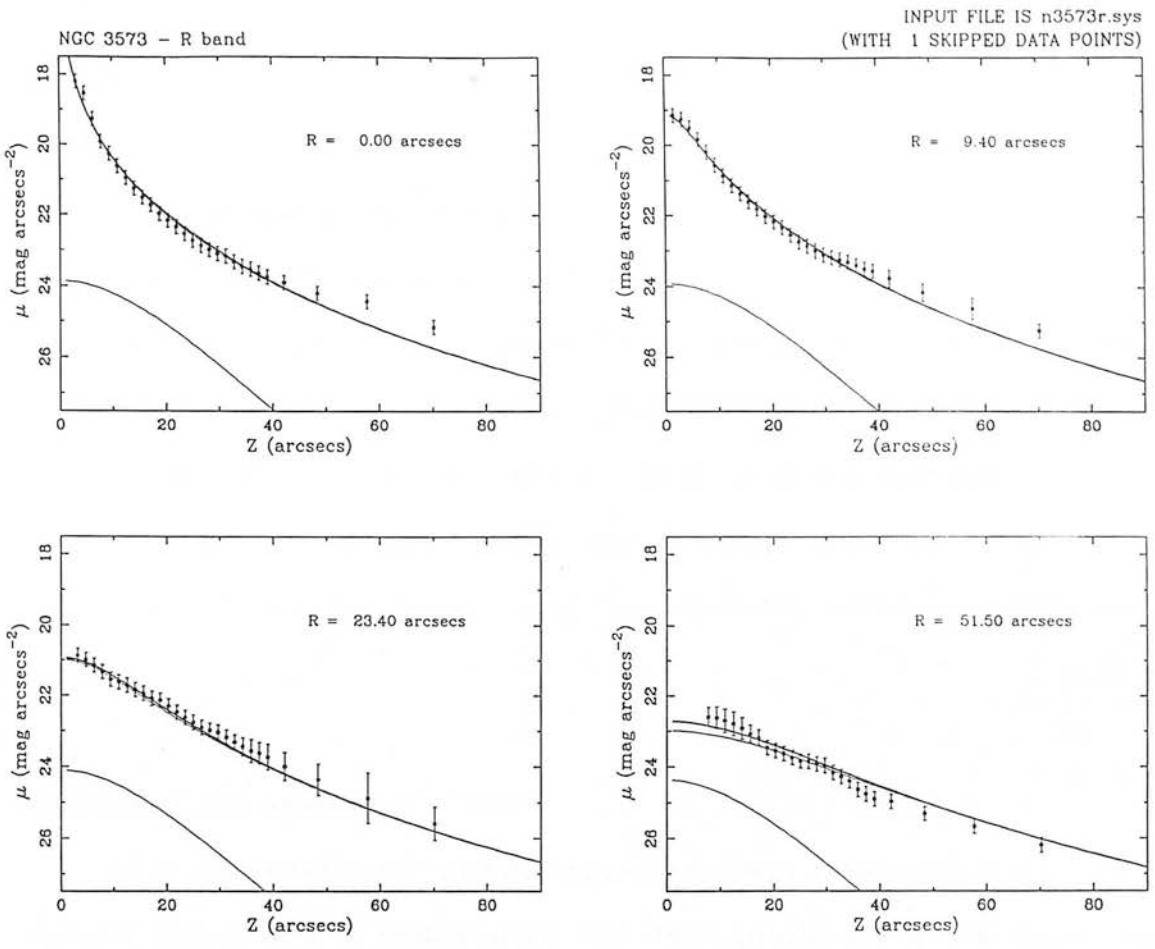
NGC 3573 – R band
INPUT FILE IS n3573r.sys
(WITH 1 SKIPPED DATA POINTS)
R = 0.00 arcsecs
R = 9.40 arcsecs
R = 23.40 arcsecs
R = 51.50 arcsecs
μ (mag arcsecs⁻²)
Z (arcsecs)

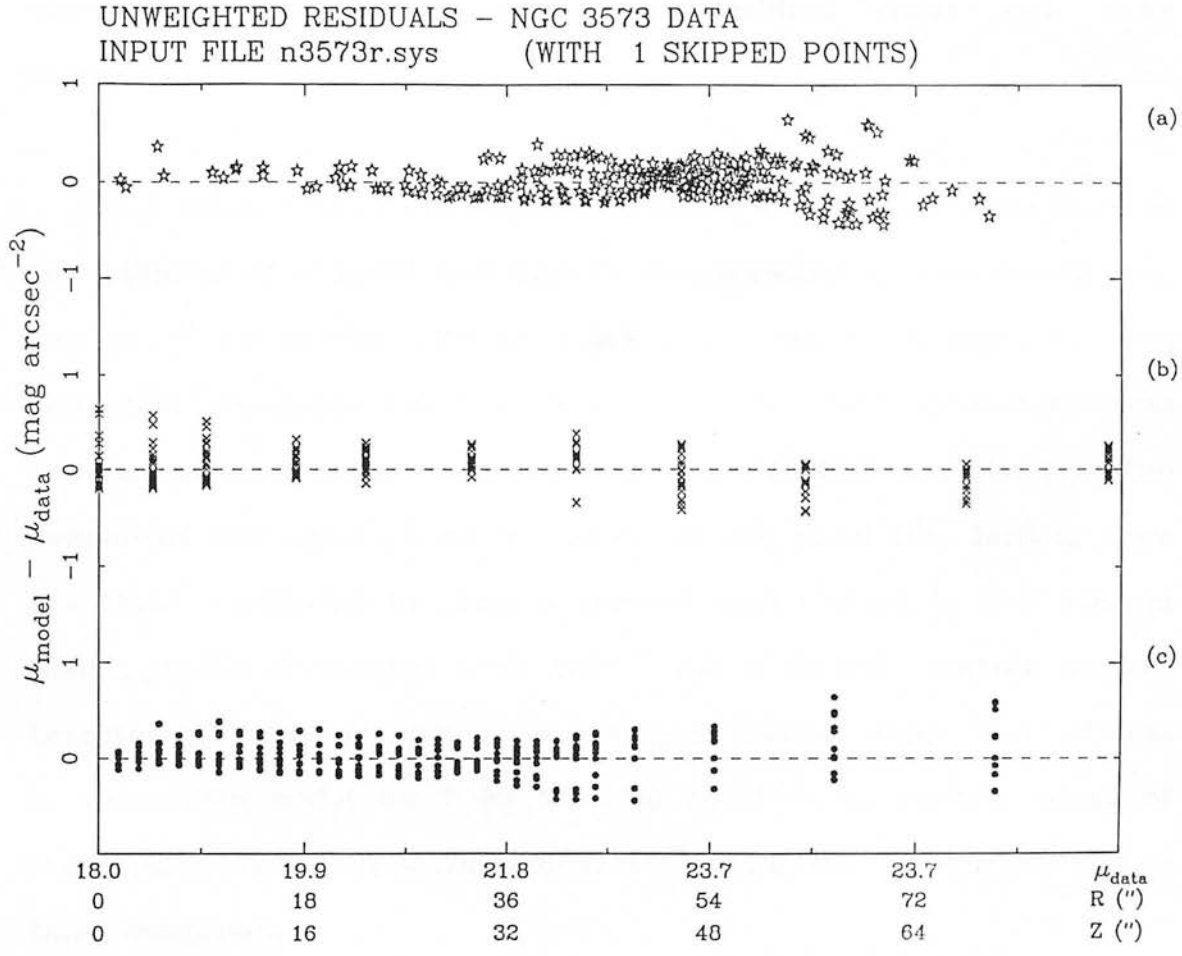
UNWEIGHTED RESIDUALS – NGC 3573 DATA
INPUT FILE n3573r.sys (WITH 1 SKIPPED POINTS)
(a)
(b)
(c)
μmodel – μdata (mag arcsec⁻²)
18.0 19.9 21.8 23.7 23.7 μdata
0 18 36 54 72 R (")
0 16 32 48 64 Z (")

figure 4.9

fall-off in the light distribution of the galaxy in such directions.

The local stellar density is sufficiently low that only ~9 bright, or moderately bright, stars required removal from the frames obtained (none were located on the galaxy image itself). The immediate galaxy environment is also quite sparse - the nearest system being ~ 5.6' to the W - but the larger scale environment (over an aperture of 1 or 2 square degrees) is very rich. However, no reference to cluster occupancy could be found, and no distance estimates were thus derived.

Results of the modelling

Table A.5 details the results obtained when modelling the array of surface brightness profiles after the data points along the major axis have been removed to allow for residual major axis dust contamination.

This table reveals the significant improvement which results from the adoption of a model combination incorporating an exponential disc and an $r^{1/4}$ law profile over all other single and two-component sets, and most three-component combinations. The best three-component combination provides a reduction ~ 15 % in FSUMSQ over the best two component set, although an inspection of the model fits derived show the third component to make a minimal contribution to the summed model profile (resulting from the ~ 2.5 μ fainter central surface brightness, coupled with a scaleheight smaller than that of the brighter disc model by ~ 30 % to 50 %). The implausible values of these parameters raises concern as to the physical reality of such a third component.

All scale parameters for the "best-fit" two-component combination were found to be very repeatable for a wide variety of input estimates. The scaleheight of the disc component is found to be constant to better than ± 3 % of the mean value of 3.12", with no evidence of a systematic trend with R over the whole array of profile cuts.

Despite the considerable degree of consistency in model parameters in table A.5, however, a visual inspection of all model fits derived using the combinations in that table show similar systematic trends at large Z as noted in the galaxies modelled previously. Allowance for such an effect requires a reduction in I_{sky} of ~ 0.3 %. The model fits obtained after such a correction has been applied to the "exp. + $r^{1/4}$ law" set are illustrated in figure 4.10 - this model combination is now found to describe NGC 4289 to ± 0.3 μ_R.

The relatively small change in many of these parameters from those in table A.5 indicates the rather limited significance of such an effect. A B/T ratio of 0.19 from the above results is in accord with that expected for such a late-type system (Simien & de Vaucouleurs 1986), whilst the very small scaleheight of the disc model corroborates the visual appearance of this system in appendix C.

IV.2.6 <u>NGC 4469</u> (α = 12^h 26^m $53^s.9$, δ = +09° 01' 2")

Probably one of the clearest examples currently known of a lenticular galaxy possessing "peanut shaped" isophotes is NGC 4469 - the depression in isophotal contours along the minor (rotation) axis giving the characteristic "bow-tie" appearance. This structure is

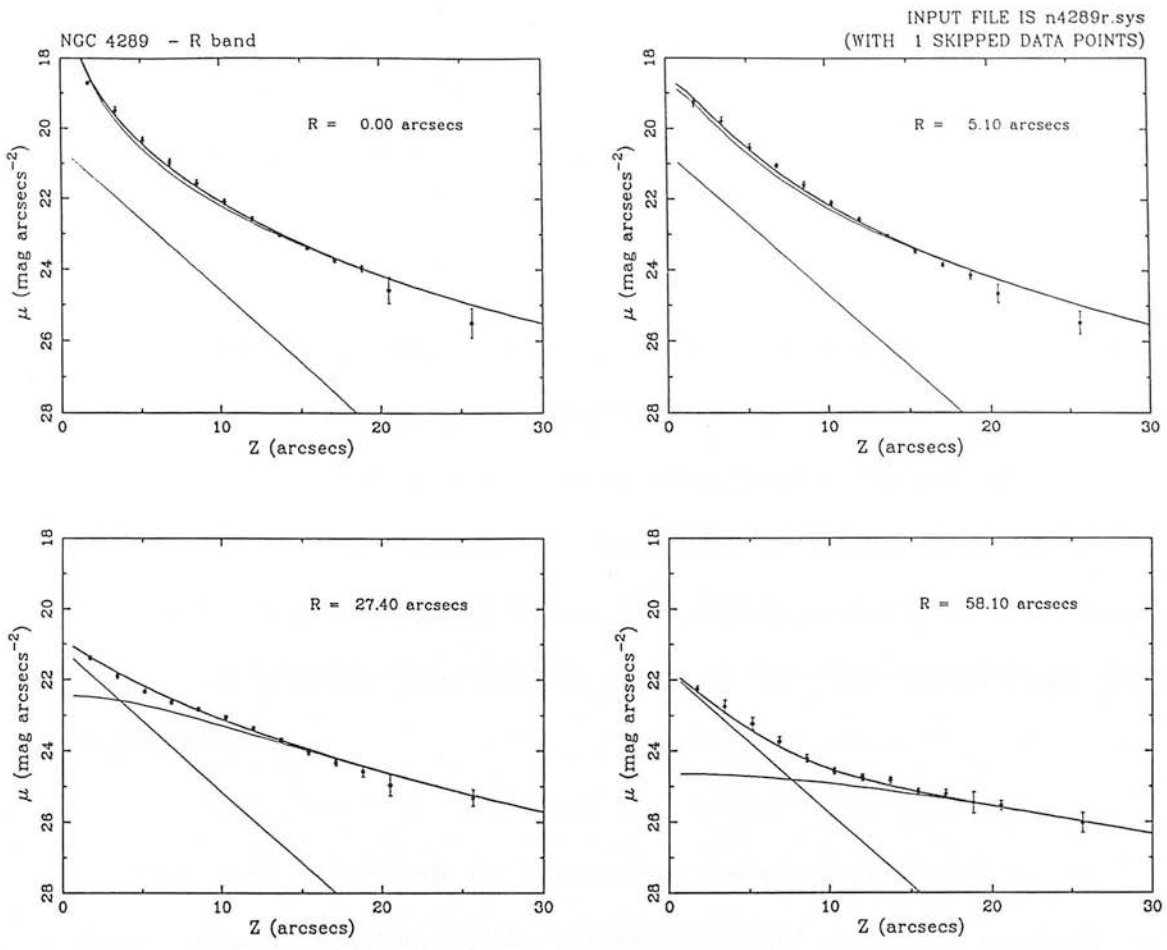
NGC 4289 - R band
INPUT FILE IS n4289r.sys
(WITH 1 SKIPPED DATA POINTS)
R = 0.00 arcsecs
R = 5.10 arcsecs
R = 27.40 arcsecs
R = 58.10 arcsecs
μ (mag arcsecs⁻²)
Z (arcsecs)

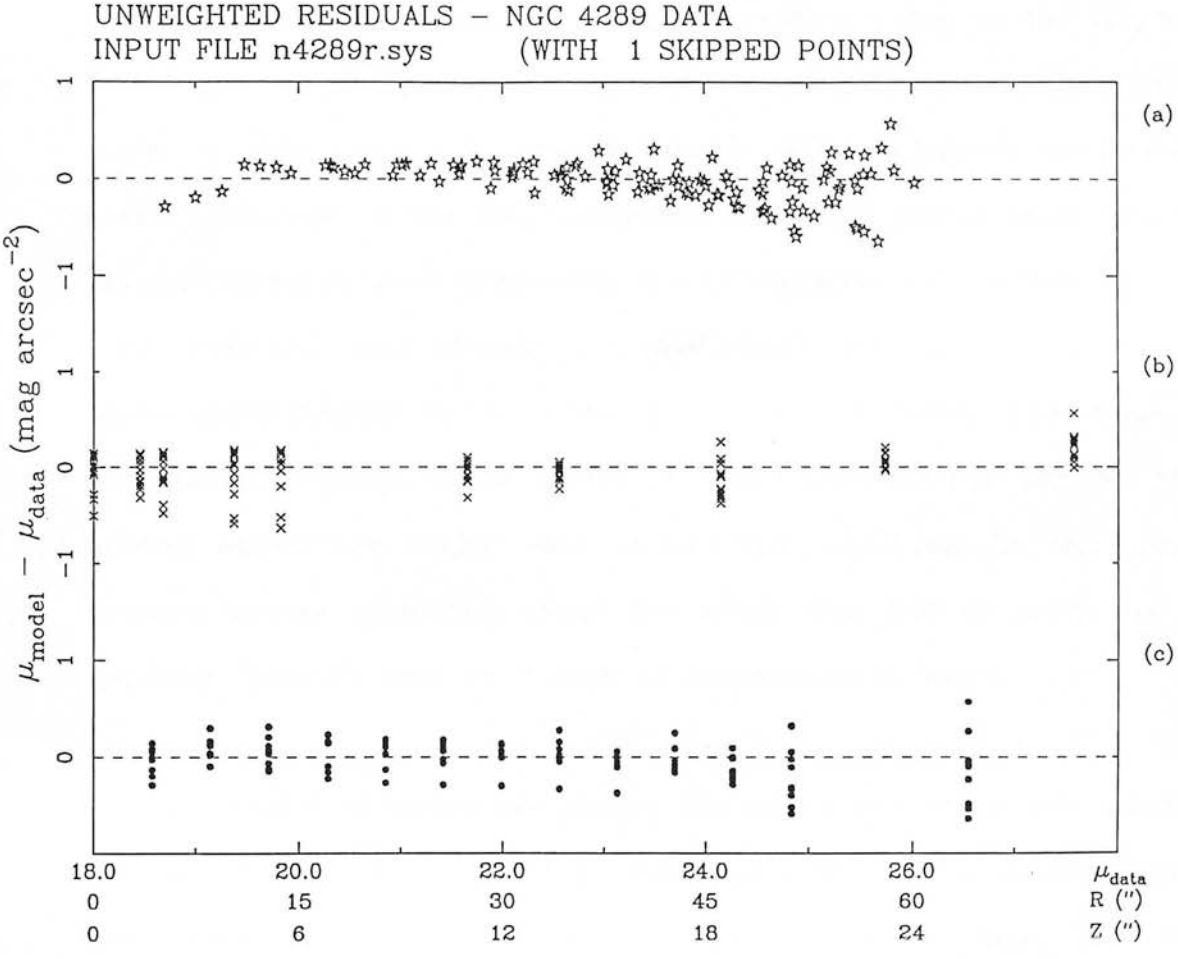
UNWEIGHTED RESIDUALS - NGC 4289 DATA
INPUT FILE n4289r.sys (WITH 1 SKIPPED POINTS)
(a)
(b)
(c)
μmodel − μdata (mag arcsec⁻²)
μdata
R (")
Z (")

figure 4.10

discussed in more detail in chapter VI and is particularly evident in figure B.2 of appendix B after the application of digital unsharp masking.

An S0/a morphology is assigned to this system in both the RC2 and UGC catalogues and is adopted in the present work. The major axis dust lane giving rise to this classification is evident on both B and R POSS plates (numbers 1563) and is particularly so in the B band CCD frame obtained here. Nevertheless, such a disc does not appear sufficiently dominant to suggest the Sab morphology adopted in the RSA.

The disc dimension on this plate material is found to be ~ 3.4'. Thus, single position CCD frames centred on the nucleus would provide information across virtually the entire bulge to the isophotal levels seen on the plates - even with the NS orientation (the position angle of this system is almost exactly 90^{o}). However, to maximise spatial coverage of the disc component, and the galaxy as a whole at fainter isophotal levels than this, the CCD frames were offset some 10" - 20" east and west of centre. Unfortunately time did not permit the easternmost frames to be obtained in the B band, and thus for galactocentric distances in excess of ~ 10" the data are derived after folding about the major axis alone. The modelling in this colour assumes galaxy symmetry about the minor axis but to judge by the spatially complete data in R such an assumption is valid.

The frames obtained are almost devoid of any stars and galaxies. However, NGC 4469 is only ~ 4^{o} south of M87, and its membership of the Virgo cluster is given in several sources (e.g. the RSA,

Kraan-Kortweg (1982), Geller & Huchra (1983)). Thus a distance of 10.7 Mpc is adopted - giving an image scale of 0.052 kpc/arcsec.

Results of the modelling

Whilst the adoption of a single $r^{1/4}$ law profile is found to provide a substantially improved quality-of-fit over most other combinations in table A.6, two principal sources of discrepancy which arise when using this profile indicate that the shape of the luminosity distribution in NGC 4469 is too complex to adopt a single-component fitting function. The form of such discrepancies is a systematic overestimation of the predicted luminosity at large Z-heights relative to that actually observed, and a failure to describe the "thicker" profiles at $R \sim 15"$ and $Z \lesssim 30"$ (attributed to the peanut-shaped morphology noted above).

The effect of adding an exponential disc to the $r^{1/4}$ law is to reduce FSUMSQ by ~ 51 % in B and ~ 23 % in R. This statistical improvement results from the contribution of the disc to the fit at $10" \lesssim Z \lesssim 40"$, thereby relaxing constraints placed on the $r^{1/4}$ law profile and thus leading to a somewhat improved fit over the intermediate and large R profiles.

The modelling results in table A.6 preclude the adoption of a three-component fit since those combinations found to iterate to a solution are only able to do so by the suppression of this third component. This result was also noted at the endpoints of all sets in that table for which a final solution could not be derived.

Despite the statistical improvements noted above, the "exponential + $r^{1/4}$ law" set still falls short of an adequate description of this galaxy owing to an inability to describe the peanut bulge at R ~ 15" and from the existence of systematics at large Z of the form noted previously. Removal of the latter effects require reductions in I_{sky} of 0.6 % in the B band and 0.3 % in R over the values quoted in table 2.2. Figures 4.11 (B) and 4.12 (R) show the fits obtained using this model combination after imposing such a change in the adopted sky level.

However, the disc scalelengths which result after correcting for these effects are discordant by ~ 60 % between B and R. Indeed, a visual inspection of the image frames (appendix C illustrating that in R) would suggest that the scalelength of the exponential profile in the R band is far too small since the disc being modelled clearly extends over an equivalent radial scale as does that in B. The parameters for the fit to the B band data are therefore considered to be more "realistic" in this sense.

The removal of the disparities between the model parameters in the respective passbands (evident in table A.6) required the incorporation of a minimum error of ± 0.1 μ. The effects of this procedure reduce the differences in h_r by an order-of-magnitude (although differences in θ_e increase to ~ 30 %). Such model combinations are still found to be less than optimal due to a poor fit at large Z over certain profiles and an underestimation of the light across the edge of the peanut isophotes (by ~ 0.25 μ_R and ~ 0.1 μ_B). These underestimations correspond to ~ 4 % of the total predicted luminosity over such regions in the B band and ~ 7 % in R. I find

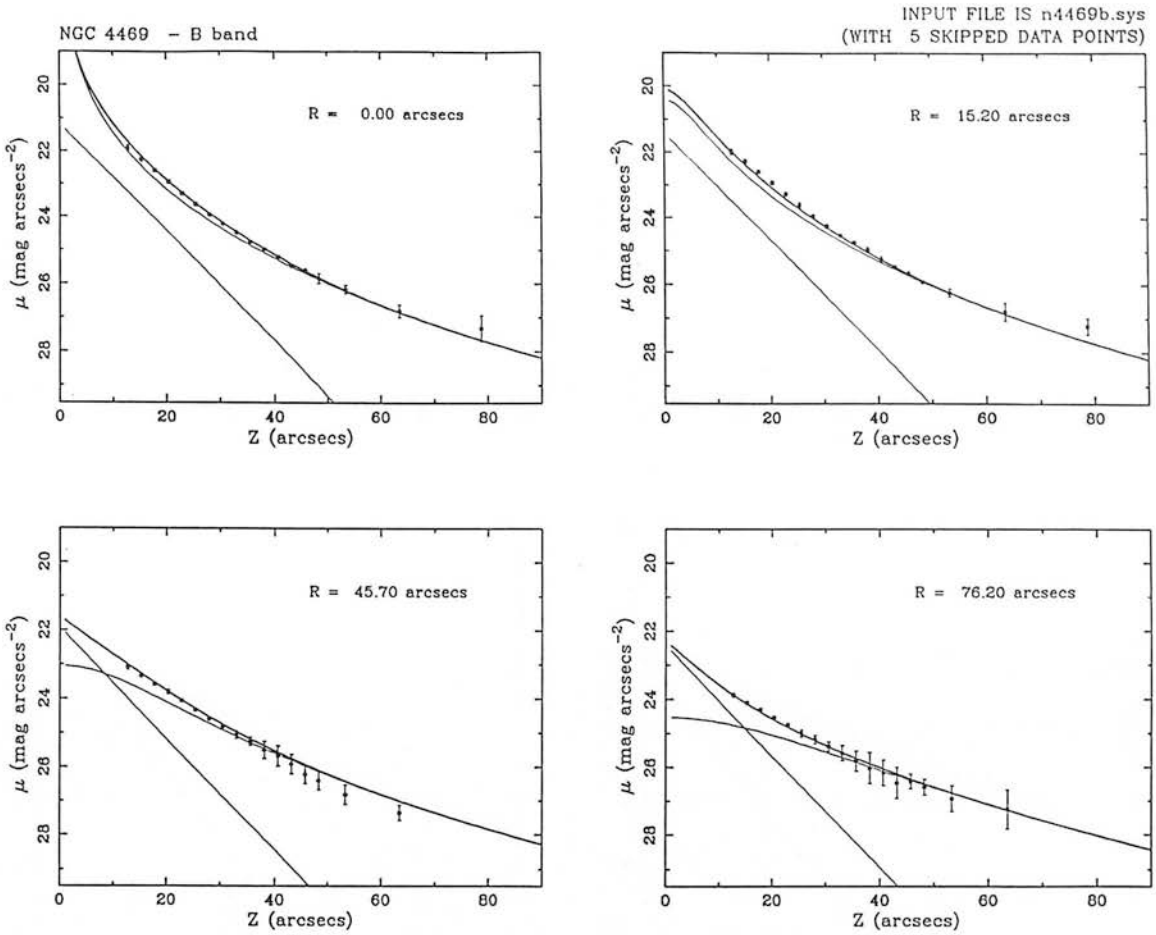
NGC 4469 – B band
INPUT FILE IS n4469b.sys
(WITH 5 SKIPPED DATA POINTS)
R = 0.00 arcsecs
R = 15.20 arcsecs
R = 45.70 arcsecs
R = 76.20 arcsecs
μ (mag arcsecs⁻²)
Z (arcsecs)

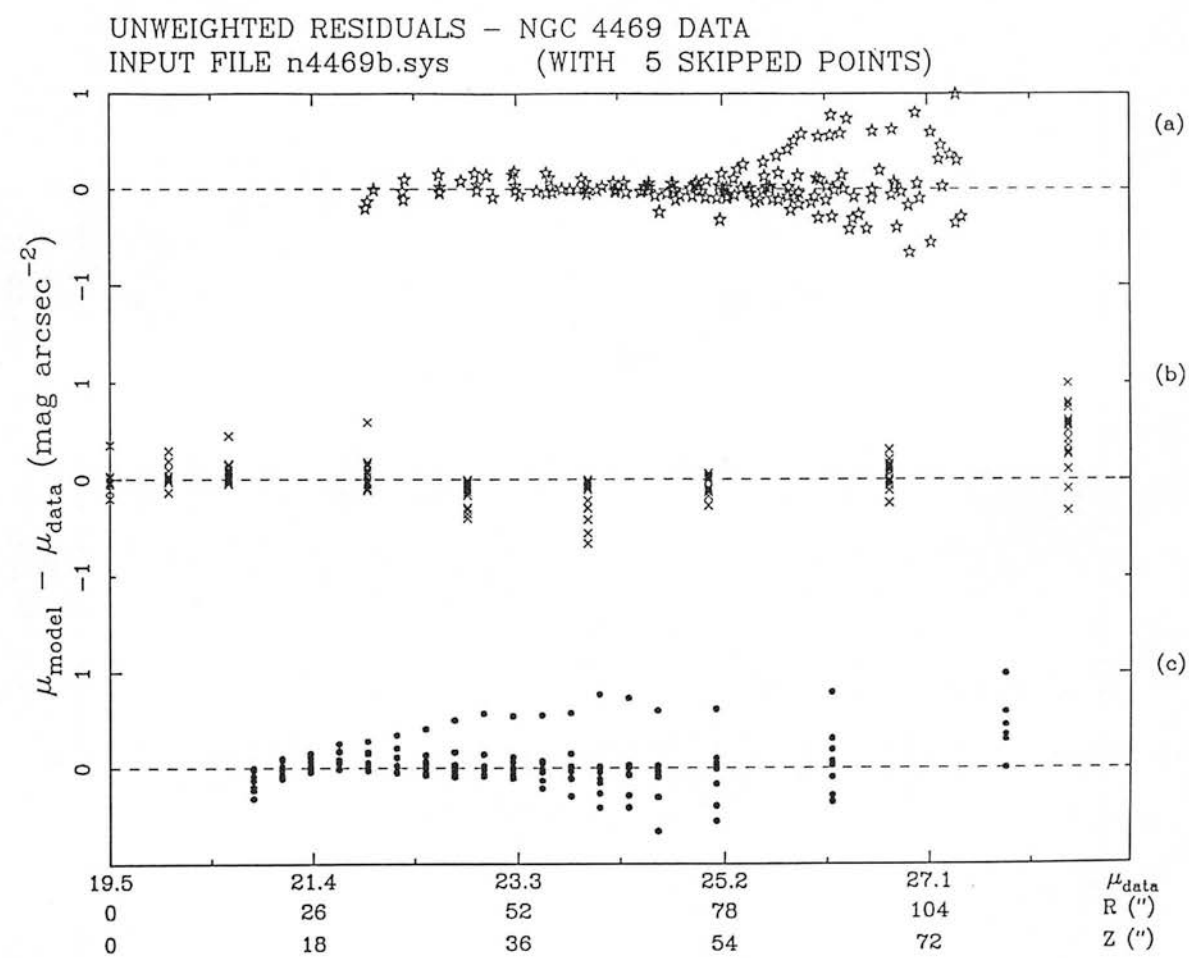
UNWEIGHTED RESIDUALS – NGC 4469 DATA
INPUT FILE n4469b.sys (WITH 5 SKIPPED POINTS)
(a)
(b)
(c)
μmodel – μdata (mag arcsec⁻²)
19.5 21.4 23.3 25.2 27.1 μdata
0 26 52 78 104 R (")
0 18 36 54 72 Z (")

figure 4.11

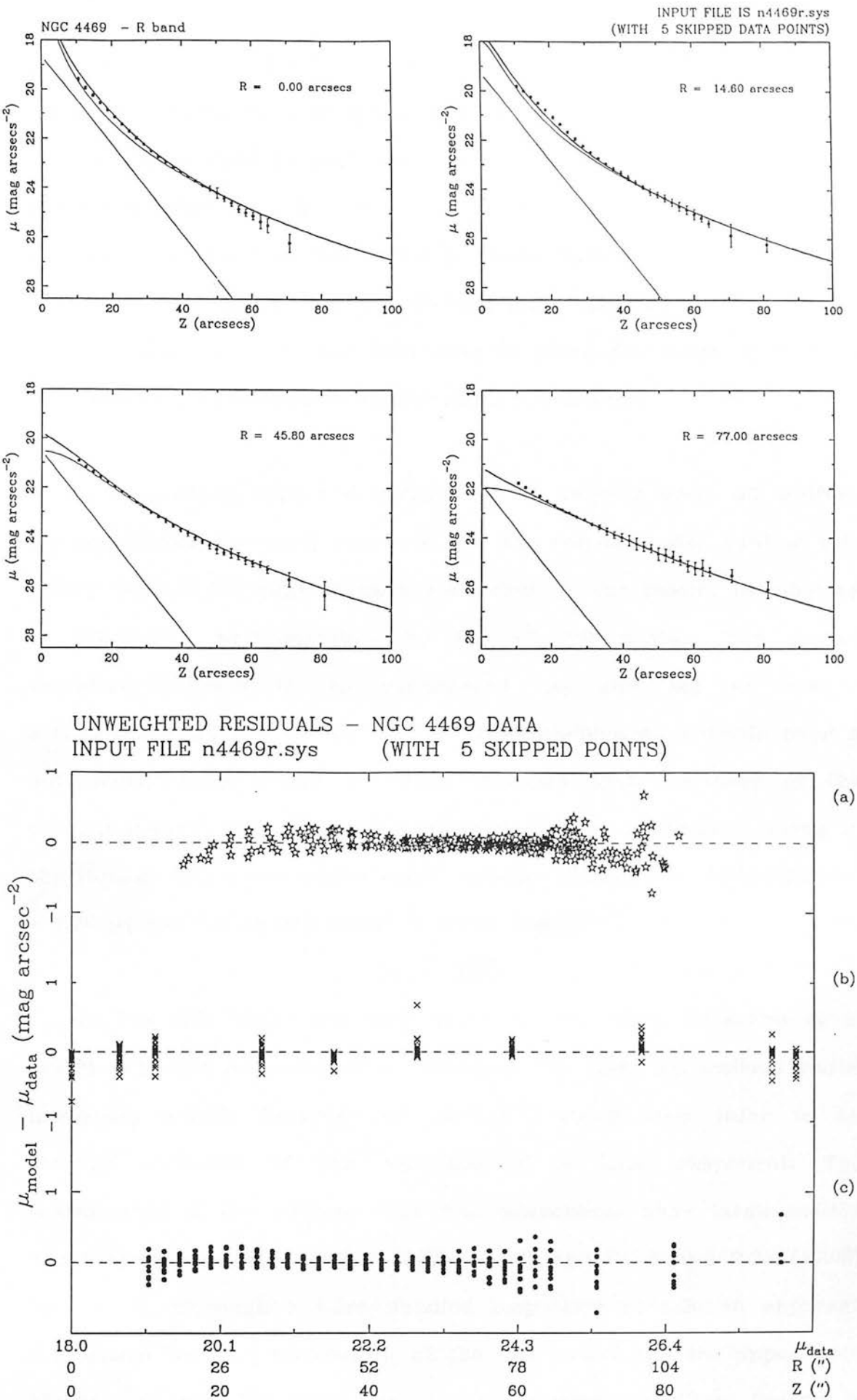
NGC 4469 – R band
INPUT FILE IS n4469r.sys
(WITH 5 SKIPPED DATA POINTS)
R = 0.00 arcsecs
R = 14.60 arcsecs
R = 45.80 arcsecs
R = 77.00 arcsecs
μ (mag arcsecs⁻²)
Z (arcsecs)
UNWEIGHTED RESIDUALS – NGC 4469 DATA
INPUT FILE n4469r.sys (WITH 5 SKIPPED POINTS)
μmodel – μdata (mag arcsec⁻²)
(a)
(b)
(c)
18.0 20.1 22.2 24.3 26.4 μdata
0 26 52 78 104 R (")
0 20 40 60 80 Z (")

figure 4.12

that subtraction of the summed "exponential + $r^{1/4}$ law" model luminosity distributions from the original image frames yield only ~ 15 - 20 % excess light in both passbands exterior to the dust lane and thus attributed to the presence of the peanut. Although such morphology is very evident upon a visual inspection of this galaxy, the peanut appears to be a less-significant contributor to the total non-thin disc light in NGC 4469 than is noted for other systems in the present sample showing similar isophotal shapes.

The generally improved description at large Z when *all* profiles are considered, however, indicates that the non-thin disc light in this galaxy beyond the regions most dominated by the peanut morphology is reasonably well-described by the $r^{1/4}$ law profile. The peanut therefore appears to be superposed on, and not an inward extrapolation of, the $r^{1/4}$ law profile. This morphology extends over a sufficiently large range of radial distance that modelling of the present dataset with the peanut removed was not undertaken owing to the limited data array which would remain. Typical rms residuals of ~ ± 0.25 μ_B and 0.2 μ_R are found in these fits.

In the only other previous study of NGC 4469, Watanabe et al (1982) note the existence of a "shoulder" in their generalised radial luminosity profile between 50" and 80", which they infer to be indirect evidence of the existence of a lens component. The scaleheights of the present thin disc components show large scatter about their associated means (0.38 (±0.02) kpc in B and 0.31 (±0.05) kpc in R), although a more detailed inspection reveals an apparent correlation between scaleheight of the disc model and the appearance of the non-thin disc isophotes at that particular position. Indeed, a

qualitatively similar trend is noted for all galaxies in the present sample containing clear peanut morphology. However, the decrease in disc h_z at 45" $\lesssim$ R $\lesssim$ 60" (more prominant in R than B due to the seemingly more pronounced peanut shapes at longer wavelengths) is not statistically significant in the light of the associated uncertainties in each measure. Equally, the inability within the present modelling scheme of distinguishing between a true variation of $h_z(R)$ and the "parameter coupling" (noted in chapter III) to the peanut isophotes means that such results cannot be taken as a confirmation of the findings of Watanabe et al (1982).

IV.2.7 NGC 5078 (α = 13^h 19^m 19.8^s, δ = -27^o 09' 08")

This galaxy is characterised by a dominant bulge on which is superposed a pronounced major axis dust lane whose internal structure becomes progressively more complex further from the galactic centre. The visual appearance is not dissimilar to that of the Sombrero galaxy (NGC 4594). The assigned morphological type of SA(s)a is taken from the RC2, although such a classification is also adopted by Corwin et al (1985). The ESO catalogue assigns it an S0 type, but such an estimate appears untenable on the basis of the scale of, and the pronounced structure seen in, the dust lane.

The inclined aspect of this dust lane leads to contamination of almost half of the SW extent of the bulge. The latter component appears quite flat over the outermost isophotal levels on both the current CCD frames and from the ESO R band survey plate 3185. On the SERC J survey (plate 2347, field 508) the total major axis dimension is ~ 5.6'. Thus, a single position CCD frame centred on the

nucleus (and with a N-S orientation) would sample almost the whole bulge component to the isophotal levels seen on this plate, but would include only half of the light along the major axis. As no sky would be obtained on such a frame, the present (R band) observations of this galaxy comprise a mosaic of 4 frames (each one a co-add of two 1000 secs exposures) taken at various positions across the system - one centred on the nucleus itself, one offset ~30" W of centre, a third covering the SE and a fourth the NW extemities of the major axis. The central frames were scaled to those outer ones where an adequate sky estimate could be defined.

Fortunately, the local stellar density in this field is very low, with only one moderately bright star (~30" SE of centre) located on the galaxy image itself. Particularly evident on this image, however, are a large number of faint galaxies - J2347 indicates as many as 9 systems within a 4.5' aperture centred on NGC 5078 itself. Two such galaxies are noteworthy for their effect on the surface brightness profiles extracted from this data, namely an elliptical ~40" due south and a very bright barred spiral only 2.2' SW of the nucleus. The latter in particular was found to significantly affect the SW extremities of the profiles obtained even though the brightest regions of the object itself did not fall in the area covered by the mosaic. However, the excellent degree of symmetry found in the brighter regions of all profiles obtained facilitated relatively straightforward definition and removal of the regions most contaminated by these neighbours. The point-by-point comparison of the corresponding measures NE and SW of the major axis also allowed the varying effects of the dust lane contamination to be suitably allowed for.

Despite being assigned cluster membership in the ESO catalogue, no distance estimates for this galaxy could be found.

Results of the modelling

As table A.7 shows, the adoption of an $r^{1/4}$ law profile provides a good description of this galaxy, although a further reduction of ~ 23 % in both FSUMSQ and red. χ^2 result from the addition of a disc model to the fit. The source of this improvement comes from the better fit to the data at $Z \lesssim 10"$ when the additional component is included.

However, a visual inspection of the model fits derived in such two-component combinations shows the exponential profile to make no contribution to the summed profile beyond Z ~ 5-10" (a result of the unrealistically small scale parameters shown in that table). An inspection of the image frame in appendix C confirms the unphysical nature of this solution. The adoption of a $sech^2$ disc model is equally unsatisfactory, in this case owing to the very faint central surface brightness and unrealistically large scaleheight with which such a component is assigned. These parameters combine to ensure that such a profile makes a minimal contribution to the summed profile - the differences between the latter and that of the $r^{1/4}$ law being ~ 0.2 μ_R over all R and Z. This result is indeed suggested by the similarity of both statistical fit estimators and the model parameters defining the $r^{1/4}$ law itself between the single and double component sets in that table. The use of a three-component combination is explicitly excluded in these data.

However, the $r^{1/4}$ law profile in table A.7 progressively overestimates the actual luminosity distribution at $Z \gtrsim 75"$ over all R (by as much as ~ 1.0 μ_R at a μ_R ~ 27 μ), the removal of such an effect requiring a reduction of ~ 0.2 % in the I_{sky} estimate in table 2.2. Figure 4.13 illustrates the resultant fits to this system.

In conclusion, the present modelling routine is unable to find evidence of any disc component within the present data, but is able to model the light distribution away from the dust lane by a single $r^{1/4}$ law profile to an rms residual of typically ± 0.2 μ_R. The inclined aspect of this system, the strong contamination from the dust lane and the fact that light from the $r^{1/4}$ law is so dominant over much of this galaxy, would all make the identification of any disc population very difficult were one to exist. The possibility also arises that this galaxy possesses nothing other than a dust lane superposed on the non-disc light distribution.

IV.2.8 NGC 5170 (α = 13^h 27^m 06.5^s, δ = -17^o 42' 17")

The Sc classification for this disc dominated galaxy is taken from the RC2. It is also given this type in the ESO catalogue, although an Sb[?] morphology is assigned in the RSA, whilst Corwin et al (1985) describe it as Sbc. The SW region of the bulge is partly obscured by the complex dust lane (the galaxy is an estimated 5^o from edge-on), whilst the disc component - for which a total dimension of ~8.4' is found from the SERC survey plate J8408 (field 576) - shows no sign of warping. On the ESO R band plate 5973 the very flat central bulge is particularly clear, whilst the corresponding B plate (1499) again highlights its very strong degree of central concentration towards the

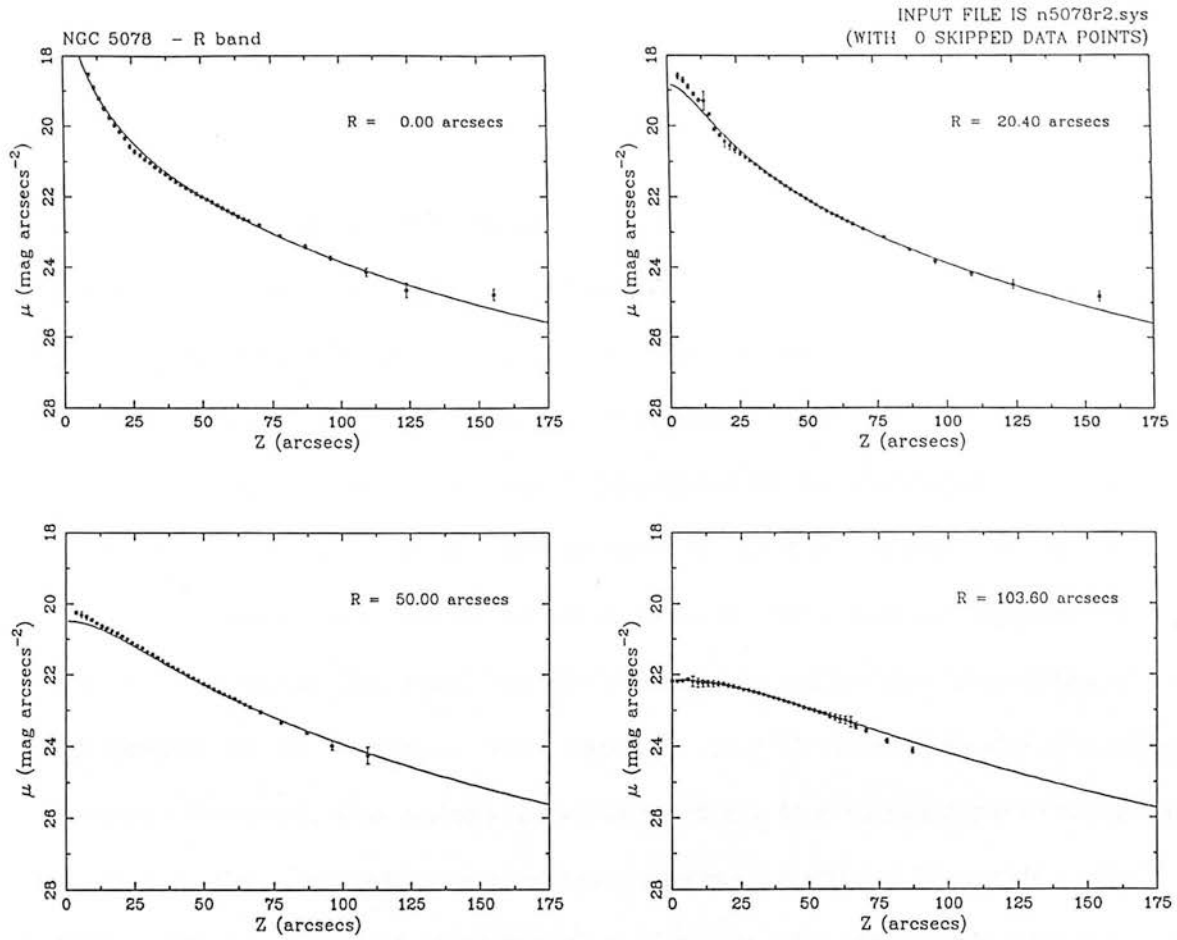
INPUT FILE IS n5078r2.sys
(WITH 0 SKIPPED DATA POINTS)
NGC 5078 - R band
R = 0.00 arcsecs
R = 20.40 arcsecs
R = 50.00 arcsecs
R = 103.60 arcsecs
μ (mag arcsecs⁻²)
Z (arcsecs)

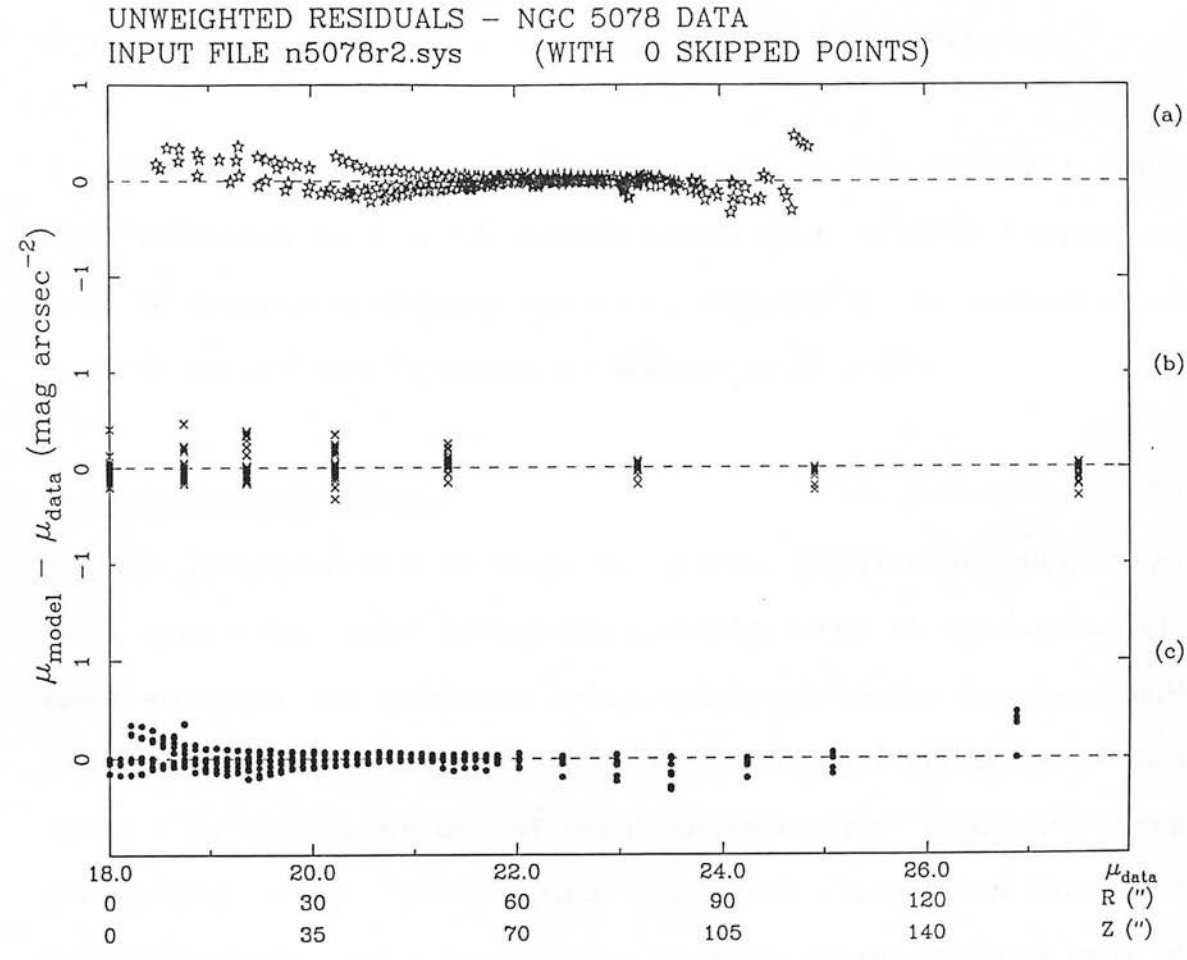
UNWEIGHTED RESIDUALS - NGC 5078 DATA
INPUT FILE n5078r2.sys (WITH 0 SKIPPED POINTS)
(a)
(b)
(c)
μmodel − μdata (mag arcsec⁻²)
μdata
R (″)
Z (″)

figure 4.13

nucleus.

With an adopted CCD long axis orientation N-S (to improve the estimate of the local sky background) three co-added frames were required to spatially map the total extent of the disc as seen on these plates. Although all three such positions were covered in B, time limitations only allowed two such positions to be obtained in R. Thus the modelling results in the latter assume perfect symmetry about the minor axis (although such an assumption does indeed appear valid from the B data). The local stellar density is quite low, requiring only ~20 images to be removed from those B and R frames centred on the nucleus. However, the galaxy environment on the survey plate material appears quite rich, with two adjacent systems only 2.8' north and 3.9' south. Indeed, the ESO catalogue assigns it the dominant membership of a group to which these fainter systems are also a part.

The adopted distance of 13.4 Mpc to this system (Fisher & Tully, 1981) translates to a corresponding image scale of 0.065 kpc/arcsec. Such an estimate is in good agreement with the 20 Mpc (assuming an H_o of 75 km s^{-1} Mpc^{-1}) quoted by Bottema et al (1987).

Results of the modelling

The results shown in table A.8 clearly discount all single and three component model combinations on the basis of the excessively large statistical fit estimators (when compared to the two-component sets) in the former, and the inability of the latter to converge to a solution for a wide variety of input estimates. The restrictive error distribution which places such stringent constraints on any three-component combinations is also likely to be the cause of most of

the two-component fits not achieving full convergence within the limit of the number of allowed iterations. Nevertheless, within these combinations, the "exponential + $sech^2$" model combination is marginally preferred over that of the "exponential + $r^{1/4}$ law" set in B, with the reverse being the case in R.

The reproduceability of all scale parameters in table A.8 has again been confirmed in both colours. For the "exponential + $sech^2$" combination in that table, a mean scaleheight (for the exponential model in B) of 0.535 (±0.001) kpc is found, whilst that of the same profile in the "exponential + $r^{1/4}$ law" fit to the R band data is 0.481 (±0.003) kpc over those profiles interior to $\mathbb{R}$ = 150" (i.e. 10 of the possible 13 profiles available). Equally small scatter about the corresponding means are found for the disc components in a variety of alternative two-component model combinations. The values are in excellent agreement with those in table A.8, and no systematic variation of scaleheight with $\mathbb{R}$ is noted in all cases.

However, a visual inspection of the model fits obtained in these cases reveal a severe underestimation of the observed luminosity interior to Z ~ 10" and a systematic overestimation at larger Z-heights. Since these models provide an adequate description of the data at such small Z only for those profiles at $\mathbb{R} \gtrsim 17.8"$ (or 1.16 kpc), this discrepancy is taken as evidence that the summed model is failing to account for the small bulge component particularly evident on the image frame shown in appendix C. Those iterations conducted when adopting three-component combinations never proceeded a sufficient "distance" from the starting points for one to define the reason for their inability to fit the data in either passband.

With a view to testing the result of imposing a three-component model combination to the data more specifically, I undertook a series of iterations incorporating a fixed contribution from either $sech^2$ or $r^{1/4}$ law profiles using the parameters in table A.8. The ~ 27 % reduction of FSUMSQ in the R band and ~ 19 % in B which result indicate the considerable improvement arising from the superposition of an additional exponential model to these original double component combinations. Once the parameters for the additional exponential profile had been defined using the above procedure, a further series of iterations was then conducted with such a component fixed. An "exponential + $r^{1/4}$ law" set was adopted in both passbands, and corrections of 0.4 % in B and 0.6 % in R were applied to remove systematics at large Z. The excess light at small Z appears well-modelled by an exponential profile which is bright but spatially quite small. Such a model form provides no contribution to the summed fit at $R \gtrsim 30"$, a position which a visual inspection of the images frames indicates is just that within which the small, bright component noted in the above description is found. This leads one to suspect that the bright exponential profile does indeed represent this component.

Despite the "realistic" nature of these solutions, however, differences in model parameters are again evident when comparing the results obtained in B and R - the most substantial being in θ_e (51 %) and h_r (22 %). The assumption of a minimum error of ± 0.1 μ reduces these to 16 % and 7 % respectively - figures 4.14 and 4.15 showing the resultant fits obtained after incorporation of all such corrections. The corrected model fits describe the observed luminosity distribution

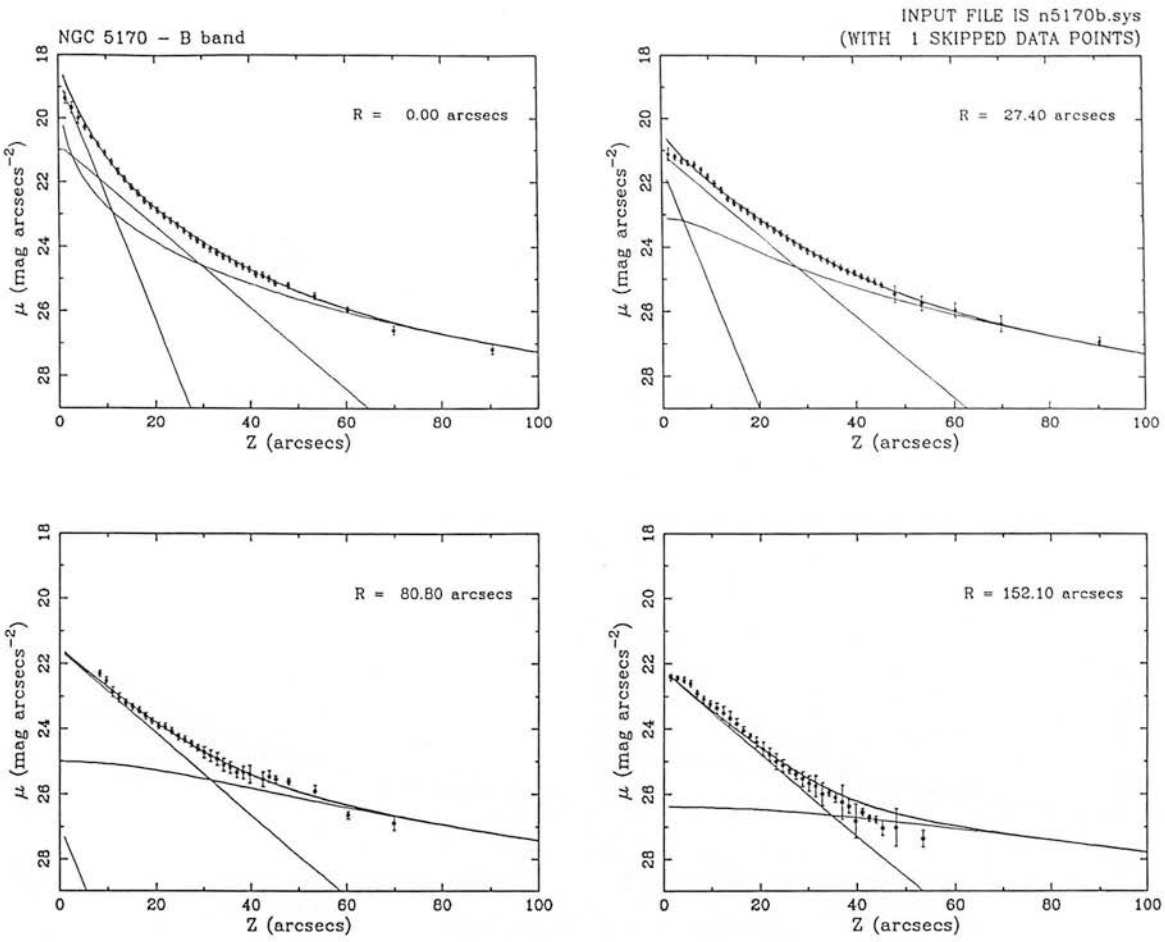
NGC 5170 – B band
INPUT FILE IS n5170b.sys
(WITH 1 SKIPPED DATA POINTS)
R = 0.00 arcsecs
R = 27.40 arcsecs
R = 80.80 arcsecs
R = 152.10 arcsecs
μ (mag arcsecs⁻²)
Z (arcsecs)

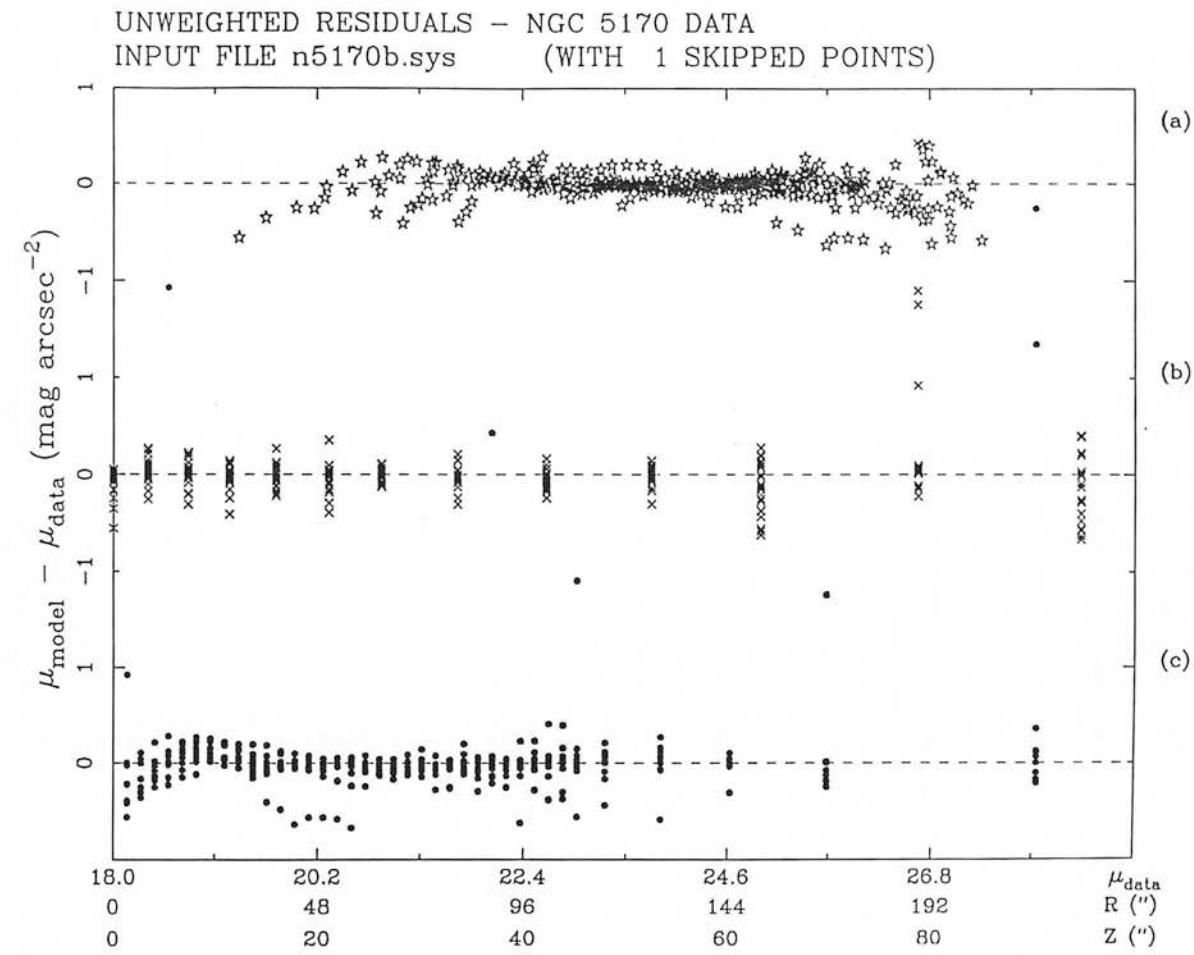
UNWEIGHTED RESIDUALS – NGC 5170 DATA
INPUT FILE n5170b.sys (WITH 1 SKIPPED POINTS)
(a)
(b)
(c)
μmodel – μdata (mag arcsec⁻²)
18.0 20.2 22.4 24.6 26.8 μdata
0 48 96 144 192 R (")
0 20 40 60 80 Z (")

figure 4.14

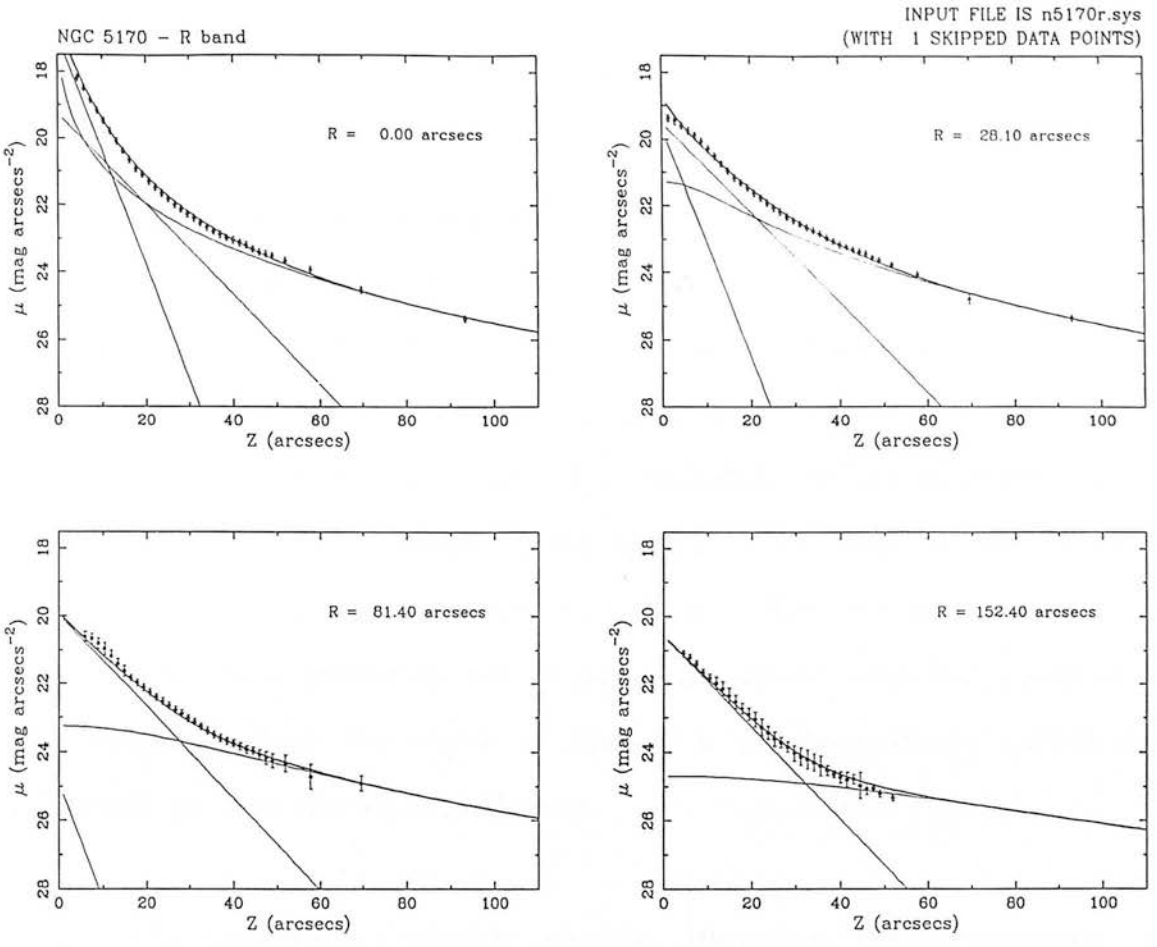
NGC 5170 – R band
INPUT FILE IS n5170r.sys
(WITH 1 SKIPPED DATA POINTS)
R = 0.00 arcsecs
R = 28.10 arcsecs
R = 81.40 arcsecs
R = 152.40 arcsecs
μ (mag arcsecs⁻²)
Z (arcsecs)

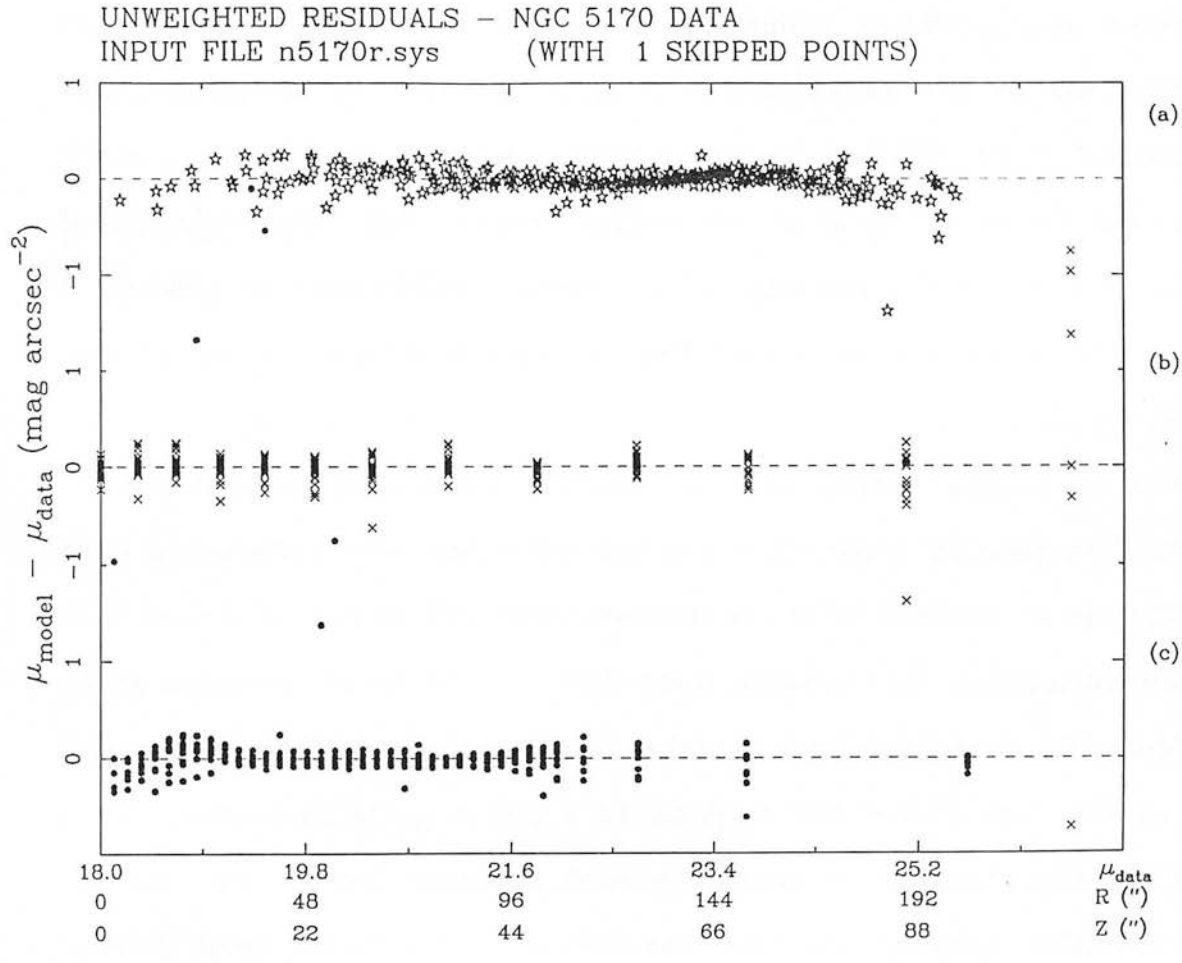
UNWEIGHTED RESIDUALS – NGC 5170 DATA
INPUT FILE n5170r.sys (WITH 1 SKIPPED POINTS)
(a)
(b)
(c)
μmodel – μdata (mag arcsec⁻²)
18.0
19.8
21.6
23.4
25.2
μdata
0
48
96
144
192
R (")
0
22
44
66
88
Z (")

figure 4.15

in this system to ~ ± 0.3 μ_B and 0.2 μ_R.

The model parameters for the second exponential component in these combinations are clearly in very good agreement with those quoted in table A.8, whilst their dominant contribution to the overall model fit at all $\mathbb{R}$ and 10" $\lesssim$ Z $\lesssim$ 30" suggests such a profile corresponds to the thin disc. An indication of the relatively minimal contribution to the total light output from this galaxy from the brighter exponential comes of the derived B/T ratios of 0.13 (B) and 0.14 (R). Such estimates are in good agreement with the value of 0.08 I calculate from the work of Simien & de Vaucouleurs (1986) for a galaxy of this morphological type.

The modelling results clearly discount the component best described by the brighter exponential above as being an inward extrapolation of the light at large Z well-fitted by the $r^{1/4}$ law - the latter underestimating the luminosity seen at Z = 10" by ~ 0.5 μ in both passbands. This would appear to designate the $r^{1/4}$ law as describing an intermediate component for which a colour index of 1.72 mag. is found - similar to that of the brighter exponential model.

No detailed photometric studies of this galaxy appear to have been undertaken with which the above results could be compared. The only source known is the (very limited) study of Bottema et al (1987) using digitised scans of the SERC plate material. By considering data brightward of 25.5 μ_B alone, they isolate a disc component with $sech^2$ model parameters of μ_o = 21.2 - 21.6μ; Z_o = 0.57 - 0.82 kpc; and h_r = 6.8 kpc (the ranges resulting from a varying inclination angle of 85° to 87°). Even allowing for the different distance estimates adopted in

this study and the present work, the agreement with the corresponding $sech^2$ thin disc model parameters in table A.8 is reasonable. Bottema et al also define a maximum disc radius of ~200". This is more than twice the spatial coverage available in the present data and therefore appears to vindicate the choice of not imposing such a disc cut-off in the present modelling procedure.

IV.2.9 IC 2531 (α = 09^h 57^m 42^s, δ = -29^o 22' 30")

The striking edge-on appearance of this galaxy is highlighted by a complex major axis dust lane from the dominant thin disc component. A central bulge (particularly clear on the current R band CCD frame and the ESO R survey plate 6359) is seen which, despite its small size, shows clear "peanut" shaped isophotes. On the SERC J plate 10012 (field 435) the total disc dimension is ~ 6.7' across which, assuming an object distance of 21.9 Mpc (Fisher & Tully 1981), corresponds to an actual dimension of ~ 63 kpc. Although no obvious warping of the disc is evident on the SERC J plate, a slight "flaring" at the eastern limit of the present frames is noted. On the current R CCD frame this very faint feature does indeed appear to be the start of a disc warp, although the major axis dust lane does not show any apparent change in geometry over such a region.

The present observations result from single-position, co-added B frames from run 1 and a mosaic of 3 co-added R frames from run 2. Insufficient time was available to complete the spatial mapping in B during the second run, and thus only ~ 1/2 of the disc seen on J10012 is covered in these observations (all frames were orientated N-S to improve the estimates of the local sky background). Such

reduced coverage has to be borne in mind for the modelling results discussed below, particularly its effect on the derived disc scalelength.

Although the local stellar density on the J survey plate appears quite small, some 33 objects were removed from both B and R frames centred on the nucleus. Three (relatively faint) stars fall on the bulge of IC 2531 itself, and a brighter one at the eastern arm of the major axis dust lane. Each object was satisfactorily removed by the routine outlined in chapter II. The galaxian density also appears quite low, with no systems seen within ~ 7.8', although over larger scales (~ 2^{o}) several much brighter systems are evident. IC 2531 is assigned cluster/group membership in the ESO catalogue.

Results of the modelling

A reasonable description of this galaxy can be afforded by adopting almost any two-component combination as table A.9 illustrates, with one incorporating an $r^{1/4}$ law profile being marginally preferred in all cases. The results derived using an "exponential + $r^{1/4}$ law" combination in R, and a "$sech^2$ + $r^{1/4}$ law" set in B are shown in figures 4.16 and 4.17 respectively. The profiles in B are seen to be reasonably well-fitted by the imposed model combination, at least in the sense of there being no obvious systematics, although there are clear discrepancies in the R band - particularly for those profiles at intermediate galactocentric distances and those coinciding with the edge of the dominant peanut feature at smaller R. In the case of the latter, the model combinations underestimate the actual luminosity distribution by $\lesssim$ 0.5 μ_R (and by ~ 0.25 μ_B) for those data in the range 10" $\lesssim$ Z $\lesssim$ 20" - corresponding to an excess ~ 11 % over the

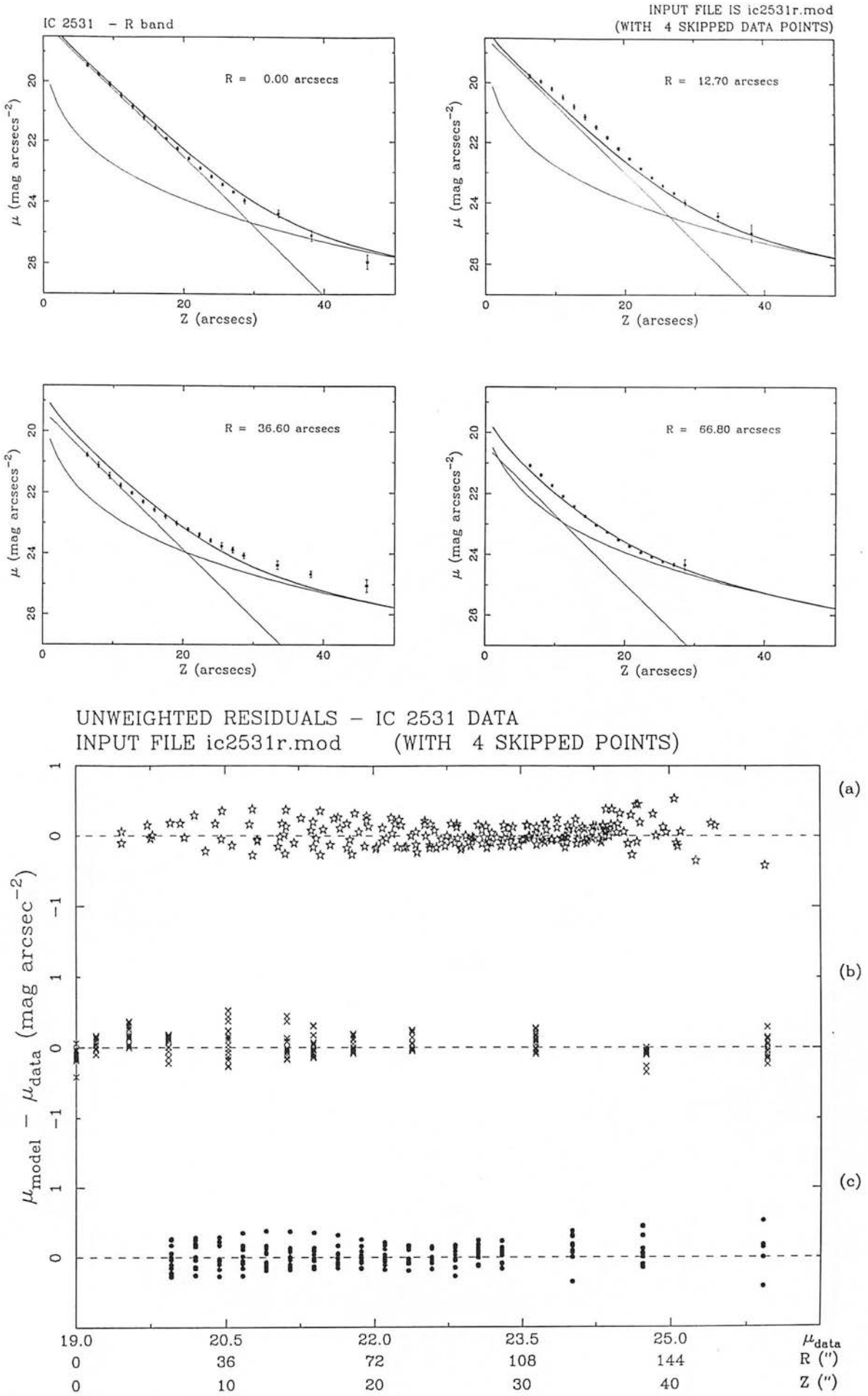
IC 2531 – R band
INPUT FILE IS ic2531r.mod
(WITH 4 SKIPPED DATA POINTS)
R = 0.00 arcsecs
R = 12.70 arcsecs
R = 36.60 arcsecs
R = 66.80 arcsecs
μ (mag arcsecs⁻²)
Z (arcsecs)
UNWEIGHTED RESIDUALS – IC 2531 DATA
INPUT FILE ic2531r.mod (WITH 4 SKIPPED POINTS)
(a)
(b)
(c)
μmodel – μdata (mag arcsec⁻²)
μdata
R (")
Z (")

figure 4.16

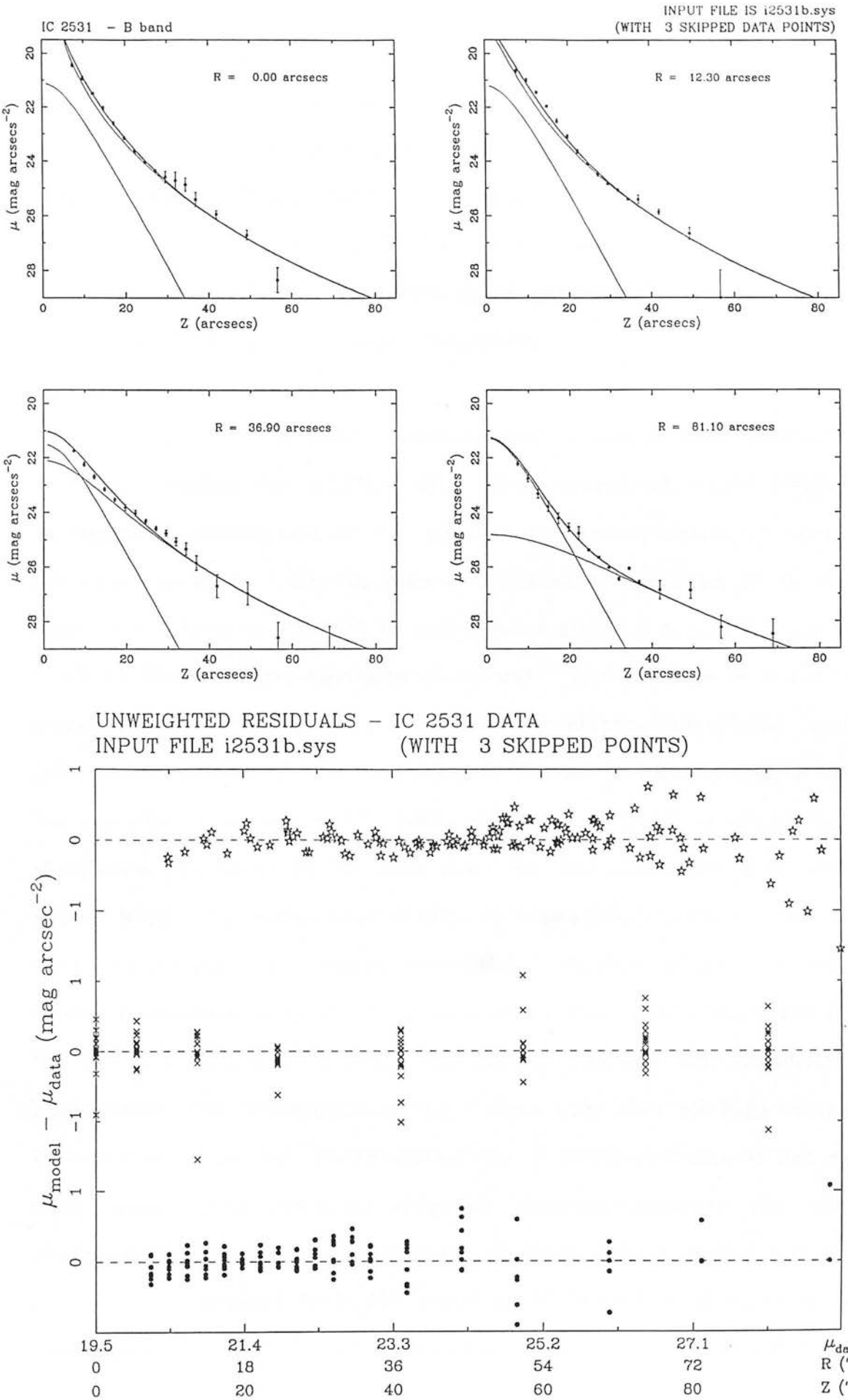
IC 2531 – B band
INPUT FILE IS i2531b.sys
(WITH 3 SKIPPED DATA POINTS)
R = 0.00 arcsecs
R = 12.30 arcsecs
R = 36.90 arcsecs
R = 81.10 arcsecs
μ (mag arcsecs⁻²)
Z (arcsecs)
UNWEIGHTED RESIDUALS – IC 2531 DATA
INPUT FILE i2531b.sys (WITH 3 SKIPPED POINTS)
μmodel – μdata (mag arcsec⁻²)
(a)
(b)
(c)
19.5
21.4
23.3
25.2
27.1
μdata
R (")
Z (")

figure 4.17

predicted luminosity in the R band and 6 % in the B. This is also graphically illustrated by the residual light seen at small (R,Z), but exterior to the dust lane which remains upon subtraction of the best-fit "disc + $r^{1/4}$ law" model combinations in each passband. I find that ~ 35 (±10) % of the total non-thin disc light in the R band for this galaxy, and 30 (±5) % in the B, is contained within the region dominated by the peanut-shaped isophotes.

In the light of the above discrepancies, it was of some interest to ascertain whether the addition of a third component would facilitate an improved description of the peanut. The incorporation of such a additional model is found to give a statistically improved fit in most cases (by $\lesssim$ 18 % in FSUMSQ in the B band and $\lesssim$ 8 % in R). However, ~ 1/2 of the model combinations in B, and ~ 2/3 of those in R can be immediately rejected in the light of the clearly unrealistic model parameters shown in table A.9. Of those remaining, only the "exponential + $sech^2$ + $r^{1/4}$ law" combination gives a statistically significant reduction in FSUMSQ over the two-component sets noted above. Whilst the exponential profile in these combinations makes the most significant contribution over those regions which the image frames themselves suggest are dominated by the peanut isophotes (i.e. $R \lesssim 30"$, $Z \lesssim 20"$), such a model still fails to describe this morphology. Furthermore, the description of the R band data over all (R,Z) appears little better than that found when only a double-component set was used (indeed the residuals diagrams derived suggests the model systematically overestimates the light at large Z to a degree not seen in the two component fits). The $sech^2$ model in this combination makes essentially no contribution to the summed profile over all R and Z.

A notable feature of all such model combinations in table A.9 are again the discordant model parameters between B and R passbands. In particular, both θ_e and q show differences ~ 100 %. The adoption of a minimum error in this case does not improve the agreement since more consistent $r^{1/4}$ law parameters are balanced by less consistent disc values. For example, a minimum error of ± 0.2 μ applied to the "$sech^2$ + $r^{1/4}$ law" combination reduces the disparities in θ_e to 17 % and q to 3 %, but Z_o and h_r show dissimilarities of 28 % and 78 % (previously 5 % and 18 % respectively). The best three-component model show discrepancies considerably larger than these values.

With a view to defining the quality-of-fit exterior to the region dominated by the peanut morphology, I undertook a series of fits but with the region of the galaxy dominated by the latter specifically excluded (as defined by a visual inspection of the image frames obtained). Note that IC 2531 is the only galaxy in the present dataset for which sufficient spatial coverage existed in the radial direction to allow such a procedure to be adopted (partly a result of the limited spatial extent of the peanut itself). Even so, the limited coverage in the B passband has to be borne in mind in the foregoing discussion.

The "$sech^2$ + $r^{1/4}$ law" combination proved to be the only set for which a solution could be derived, and the model parameters for the $r^{1/4}$ law profile were again found to be quite discordant between B and R passbands (θ_e by 99 % and q by 98 %). Such differences were reduced, to 95 % and 80 % respectively, by imposing a minimum error of ± 0.1 μ on both datasets. The resulting model fits obtained in R are illustrated in figure 4.18.

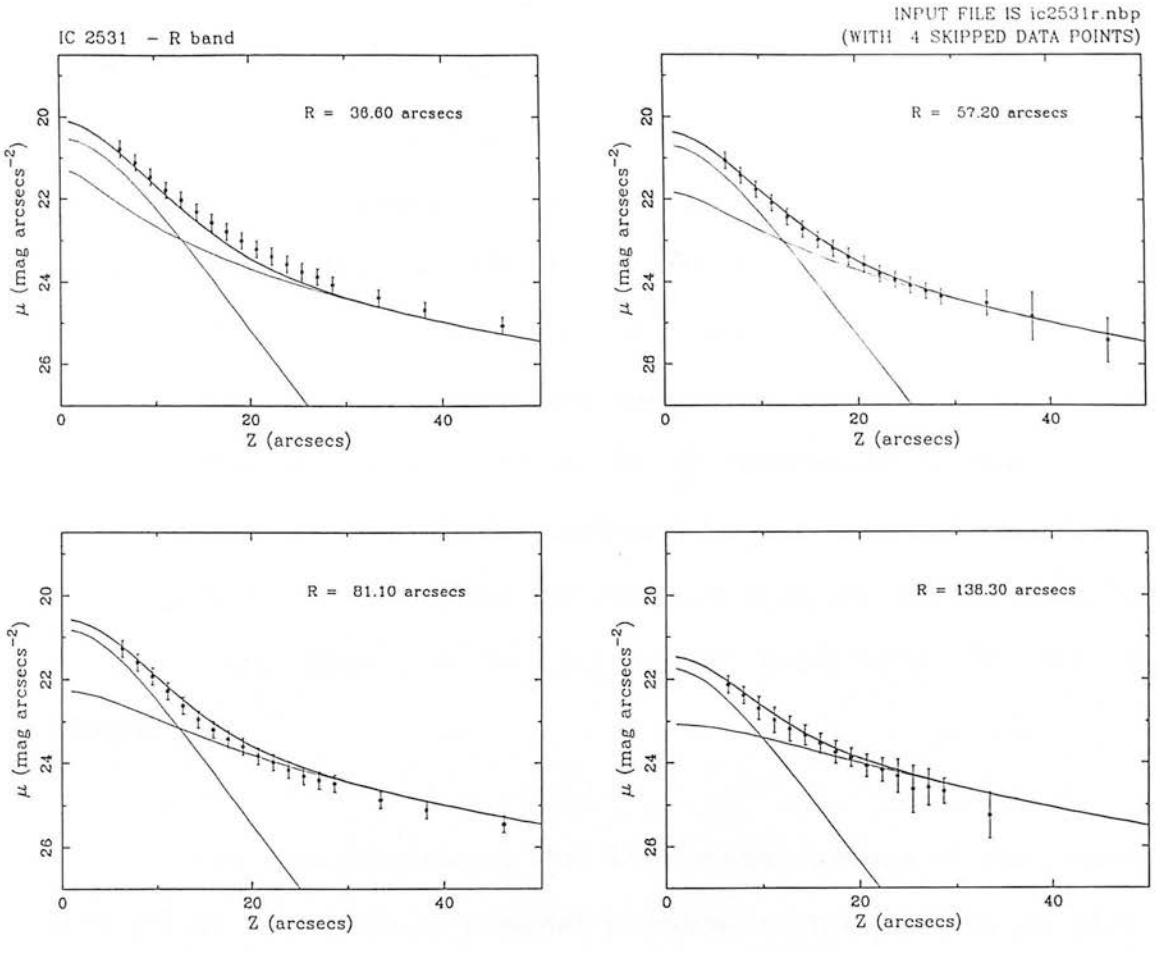
IC 2531 – R band
INPUT FILE IS ic2531r.nbp
(WITH 4 SKIPPED DATA POINTS)
R = 36.60 arcsecs
R = 57.20 arcsecs
R = 81.10 arcsecs
R = 138.30 arcsecs
μ (mag arcsecs⁻²)
Z (arcsecs)

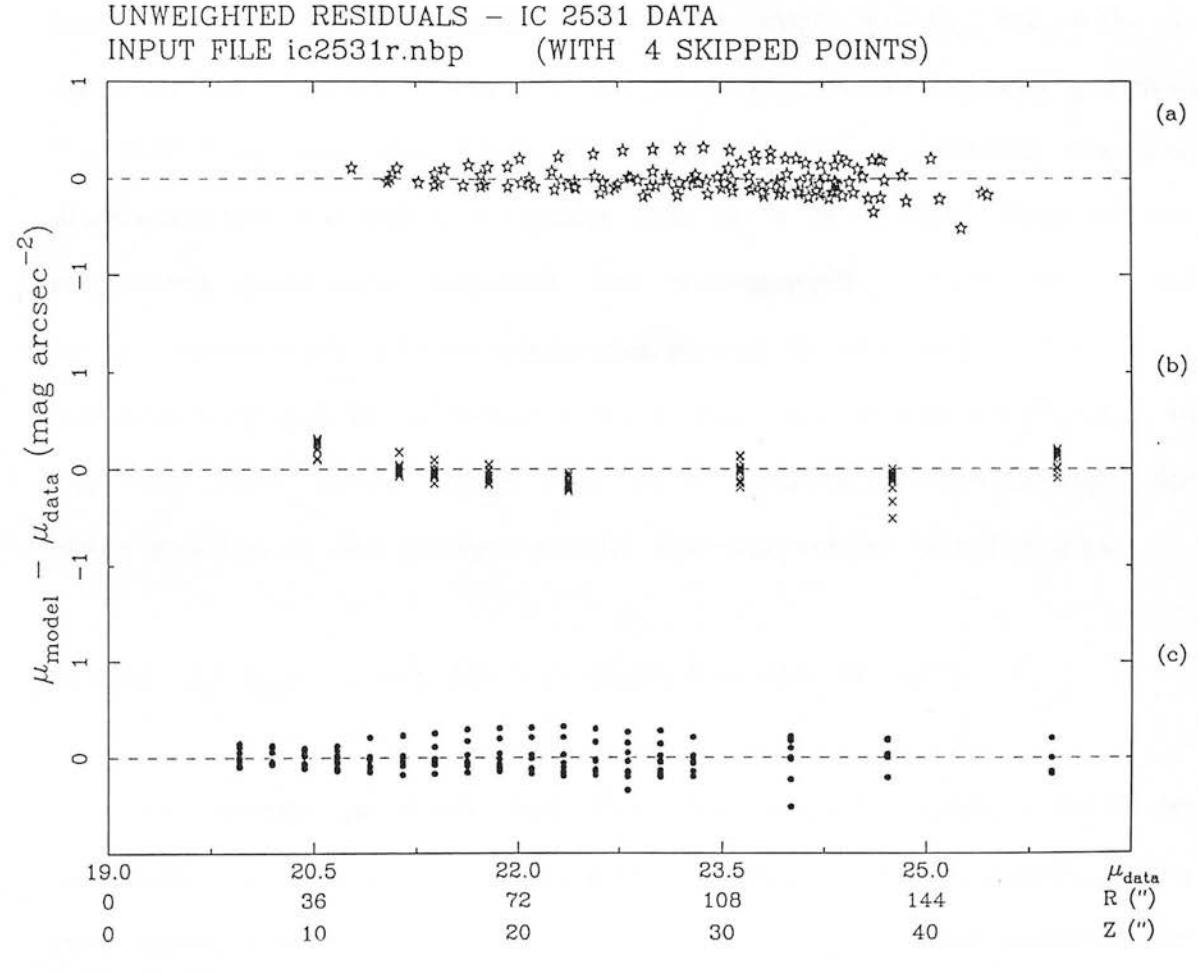
UNWEIGHTED RESIDUALS – IC 2531 DATA
INPUT FILE ic2531r.nbp (WITH 4 SKIPPED POINTS)
(a)
(b)
(c)
μmodel – μdata (mag arcsec⁻²)
19.0
20.5
22.0
23.5
25.0
μdata
0
36
72
108
144
R (")
0
10
20
30
40
Z (")

figure 4.18

The model fits illustrated in this figure show a reduction in FSUMSQ of 23 % in the B band and 3 % in R over the corresponding set in table A.9. However, the continued differences between those parameters defining the $r^{1/4}$ law almost certainly arise because too much high surface brightness data have been subtracted when removing the peanut to allow the parameters for such a profile to be reliably defined (particularly so in B). Nevertheless, the fact that such a reasonable fit can be obtained to the non-thin disc light in both passbands over regions far removed from the peanut itself again suggests the latter to be a distinct contributor to the light distribution.

In conclusion, it appears that the extreme nature of the peanut in this galaxy discounts any model combination tested here as being a good fit to the observations, although such models are able to describe the regions exterior to the peanut to within an rms residual $\sim \pm 0.25\ \mu$ in both passbands. The scale parameters defining the disc component are equivalent to better than 30 % in all cases between the respective passbands modelled. The substantially poorer fit to the longer wavelength dataset when the peanut is included in the fit is the result of the latter being a much more significant contributor to the total light output in R than in B, confirming the findings for other galaxies in the present sample showing similar morphologies.

IV.2.10 <u>IC 4351</u> ($\alpha = 13^h\ 55^m\ 03.8^s$, $\delta = -29^o\ 04'\ 16''$)

This galaxy is some way from an edge-on aspect (with an estimated inclination angle $\sim 85^o$) and the strong obscuration resulting from spiral arm structure in the disc poses considerable problems for

analyses of the bulge population to the eastern side of the major axis.

Although the disc is a prominant feature on the SERC J survey plate 1318 (field 445), the bulge is still sufficiently clear to warrant the intermediate Sb morphology assigned to this system in both the RSA and RC2 catalogues. Corwin et al (1985) adopt an Sbc form, whilst it is classed Sc in the ESO catalogue. The total major axis dimension of the disc on this plate material is ~5.4'. No warping is evident, although this is to be expected for data of such limited radial coverage.

The single position co-added R band CCD frame of this object (from run 1) was derived with the chip long axis oriented N-S. A position angle of 17° (table 1.1) therefore dictates that only ~1/3 of the disc dimension on J 1318 was covered in the present observations (i.e. to a surface brightness ~ 25 μ_B). In the light of the desire to obtain as much sky as possible this frame was centred on a region ~20" N and ~30" W of the galaxy nucleus. Thus, the surface brightness profiles extracted sample the light distribution westwards of the major axis alone.

The ESO catalogue assigns IC 4351 membership of a rich cluster of galaxies to the east on J1318. The galaxy also possess several adjacent fainter systems, the nearest being ~4.5' NW and SW of IC 4351 itself. The stellar density in this field (for which b^{II} ~30°) is also quite high as 25 objects required removal from the final image frame prior to extraction of the surface brightness profiles. Only one was found to contaminate the galaxy light - a star some 1.7' SW of centre. The surface brightness estimates for such a region were thus

based solely on those of the profile at an equivalent galactocentric distance NE of the nucleus after folding about the minor axis. An assumed distance of 24.9 Mpc (Fisher & Tully 1981) translates to an image scale of 0.121 kpc/arcsec, and thus a total dimension on J1318 of ~ 39 kpc.

Results of the modelling

As table A.10 shows, the statistical goodness-of-fit estimators discount all single-component fits to IC 4351 in favour of a two-component combination incorporating exponential and $r^{1/4}$ law profiles. In only two cases does the inclusion of a third component give a statistically significant improvement over the above set, and of these only the "exponential + $sech^2$ + $r^{1/4}$ law" combination yield parameters which are considered to be "realistic" in the context of the dataset used. The reduction in sum of squares of residuals is ~ 25 % over all two-component combinations, a result of the somewhat better description afforded to the data at $Z \lesssim 10"$ for those profiles interior to $R \sim 10"$ by the addition of the third component.

Tests conducted on this "best-fit" three-component set indicate excellent reproduceability in all the scale parameters quoted in table A.10, whilst the scaleheights of both disc components again show very small scatter about a derived mean in good agreement with the global estimates given in that table (I find h_z = 1.04 (±0.01) kpc for the exponential and Z_1 = 1.48 (±0.03) kpc for the $sech^2$ models). Indeed, tests conducted on the "exponential + $r^{1/4}$ law" set reveal even smaller scatter of ~ ± 0.9 % about the mean of 1.05 kpc for the disc profile.

However, a visual inspection of the fits derived show all model combinations to systematically overestimate the luminosity distribution at Z $\gtrsim$ 40" over all profiles. The removal of this effect requires the local sky background measure to be reduced by ~ 0.7 %. Figure 4.19 shows the results of adopting an "exponential + $r^{1/4}$ law" fit to the data so corrected.

A comparison of the fits in this figure to the image frame obtained (appendix C) confirms that the relative contributions from each model profile are "realistic", whilst the derived B/T ratio of 0.24 is quite consistent with the intermediate Hubble type to which this galaxy is assigned (I derive a typical value of 0.19 for an Sb system from the figures presented by Simien & de Vaucouleurs (1986)). A typical residual for this combination between the observed and predicted luminosity distributions is ~ $\pm$ 0.3 μ_R.

The incorporation of an additional ($sech^2$) model profile to the above gives rise to a very marginal reduction in FSUMSQ of only ~ 8 %. The reason for such a small improvement is due to the essentially negligible contribution (~ 1.4 % of the total integrated luminosity of the model combination) provided by this additional component over all (R,Z). Because the inclined aspect of this galaxy makes deconvolution of the data at Z $\lesssim$ 20" (the region over which the additional $sech^2$ model is of most importance to the summed profile) ambiguous, I conclude that IC 4351 is most realistically described by a two-component combination of exponential disc and $r^{1/4}$ law.

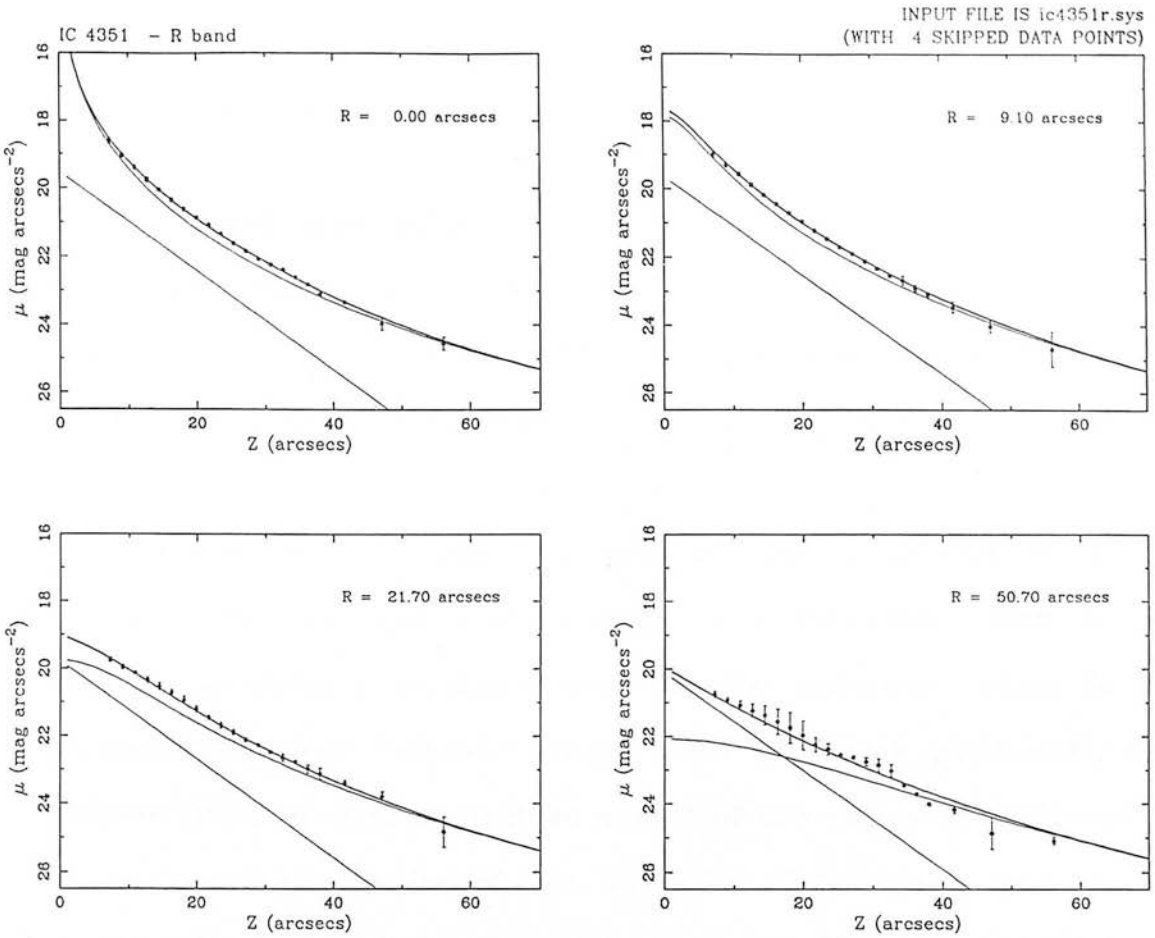
IC 4351 - R band
INPUT FILE IS ic4351r.sys
(WITH 4 SKIPPED DATA POINTS)
R = 0.00 arcsecs
R = 9.10 arcsecs
R = 21.70 arcsecs
R = 50.70 arcsecs
μ (mag arcsecs⁻²)
Z (arcsecs)

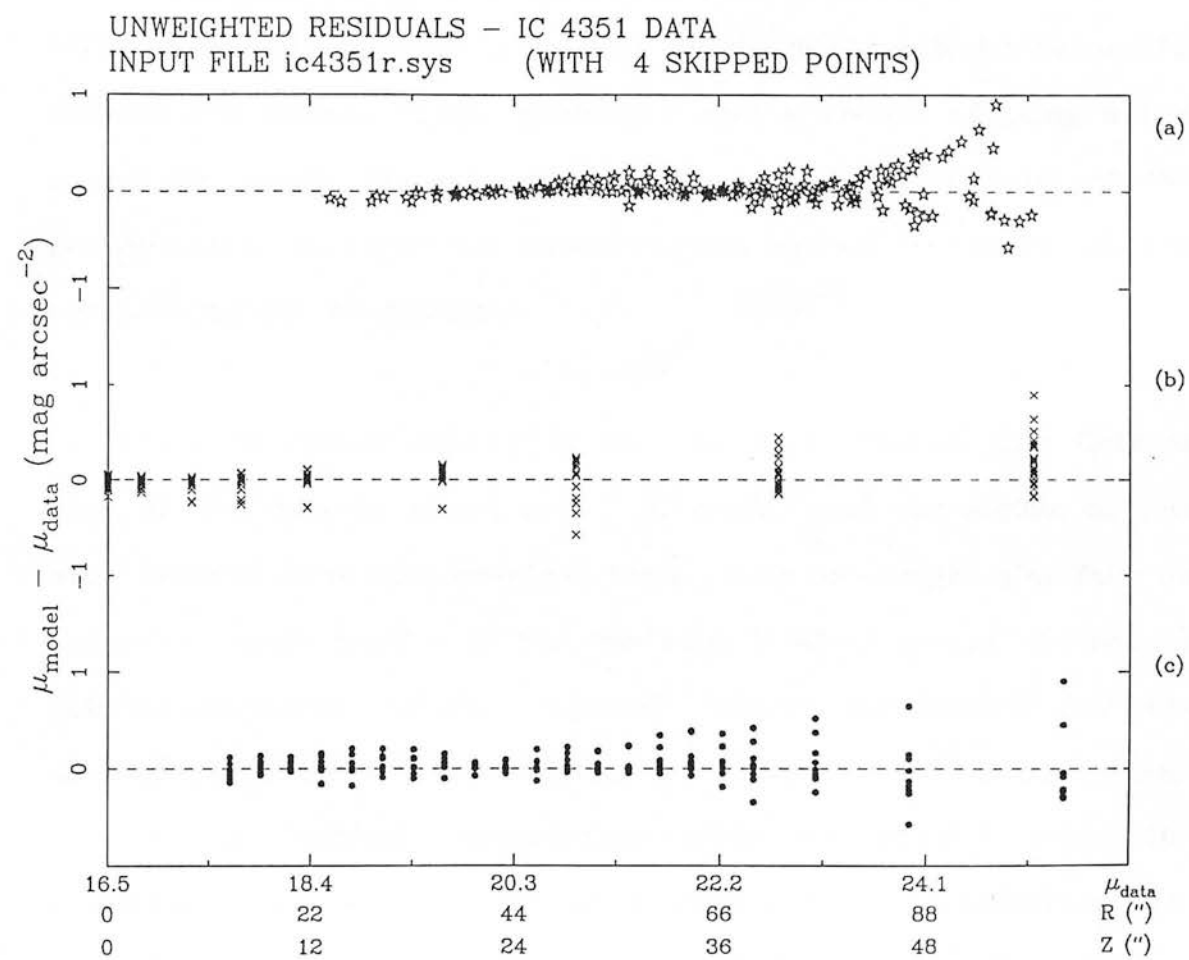
UNWEIGHTED RESIDUALS - IC 4351 DATA
INPUT FILE ic4351r.sys (WITH 4 SKIPPED POINTS)
(a)
(b)
(c)
μmodel - μdata (mag arcsec⁻²)
16.5
18.4
20.3
22.2
24.1
μdata
R (")
Z (")

figure 4.19

IV.2.11 A0902-68 (α = 09^h 02^m 03^s, δ = -68^o 01' 42")

This anonymous galaxy has no entry in either the RC2 or RSA catalogues, the assigned Sb morphology coming from the ESO catalogue and Corwin et al (1985). The latter source gives this galaxy the additional name NGC 2778A.

A0902-68 is very close to edge-on (an inclination of 87^o is adopted here) and has a clear major axis dust lane. Even so, the system also shows a prominant non-thin disc component which is seen to possess a clear "peanut" shape (SERC J survey plate 3901, field number 60). The slightly inclined aspect of the galaxy is evidenced by the central concentration of the bulge SE of the major axis as seen on the ESO R plate 1293. The total major axis dimension on J3901 is ~ 2.8' and no disc warping is evident on the plate material or on the current CCD frames. Single position B and R frames adopting a N-S orientation sample the whole galaxy to the isophotal limits of the survey plate as well as contain good spatial coverage of the surrounding sky background.

The local stellar density is high on these frames (the field is close to the galactic plane) and ~ 92 stellar and non-stellar objects were removed from each co-added frame. Only one bright star falls on the galaxy image itself - on the disc some 1' NE of centre. However, a detailed inspection of the isophotal contour distribution and the derived perpendicular surface brightness profiles did not reveal any evidence of residual contamination after its removal using the standard procedures. The galaxian environment is also relatively rich. A peculiar warped disc system lies some 4.5' SSW and a more diffuse

system ~ 5.6' NE of the sample object, and group/cluster membership is assumed based on its apparent link with the galaxy ESO 060-IG23 (West et al 1981).

A distance of 41.2 Mpc is adopted from West et al. This translates to an image scale on the sky of 0.20 kpc/arcsec, and to a total galaxy dimension of ~ 34 (± 7) kpc adopting an apparent dimension determined from J3901.

Results of the modelling

As table A.11 shows, there is no evidence in either passband for a statistically significant improvement in the goodness-of-fit by the incorporation of a three-component model combination. All such triple model sets converge to an endpoint comprising contributions from solely two-components for all possible combinations and all input parameter estimates tested (due to the physically implausible parameters defined for this additional component). A marginal preference is seen within the two-component sets for the "exponential + $r^{1/4}$ law" combination in B (by ~ 2 % in FSUMSQ over the next best double component set), and a more statistically significant one (of ~ 14 %) for the "exponential + $sech^2$" set in R.

Additional tests of all the "best-fit" combinations in A.11 again indicated the good repeatability of all scale parameters. Further, the scaleheights of the disc components in the "exponential + $r^{1/4}$ law" set in that table are found to be constant to ± 3.0 % (mean = 0.71 kpc) in the B band, and ± 3.9 % (mean = 0.70 kpc) in R. For the "exponential + $sech^2$" set in R, a mean scaleheight of 0.67 kpc (exponential model) and 1.97 kpc ($sech^2$ profile) show standard deviations of 1.9 % and

11.0 % respectively.

However, although no evidence was found of a systematic trend with Z or μ, an inspection of the fits thus obtained indicated that the "best-fit" model combinations are very poor descriptions of the luminosity distribution in this system, primarily due to an inability to model adequately the "peanut" bulge. The light at the edges of this feature is underestimated by ~ 0.8 μ over regions $10" \lesssim R \lesssim 20"$ and $9" \lesssim Z \lesssim 15"$, corresponding to 9 % of the predicted luminosity distribution in the B band over such regions, and ~ 13 % in R. The peanut morphology accounts for ~ 20 (±8) % of the total non-thin disc light in the B band and 17 (±10) % in R based on the residual luminosity distributions derived after removing exponential and $r^{1/4}$ law components from the original image frames.

Furthermore, particularly evident in table A.11 are substantial differences in both disc and $r^{1/4}$ law model parameters between the respective passbands (h_r being discordant by ~ 66 %, θ_e by 99 % and q by 27 %). By adopting an "exponential + $r^{1/4}$ law" combination in both colours, and imposing a minimum error of ± 0.05 μ, these discrepancies are reduced to 28 % in h_r and 33 % in θ_e, although dissimilarities in the axis ratios increase to ~ 70 %. The model fits derived are illustrated in figures 4.20 and 4.21, whilst the reductions in FSUMSQ of 55 % in the B band and 40 % in R are testimony to the greatly improved fits over the corresponding combinations in table A.11. On the basis of these figures, I estimate such model combinations to describe this galaxy to within ± 0.3 μ_B and 0.35 μ_R.

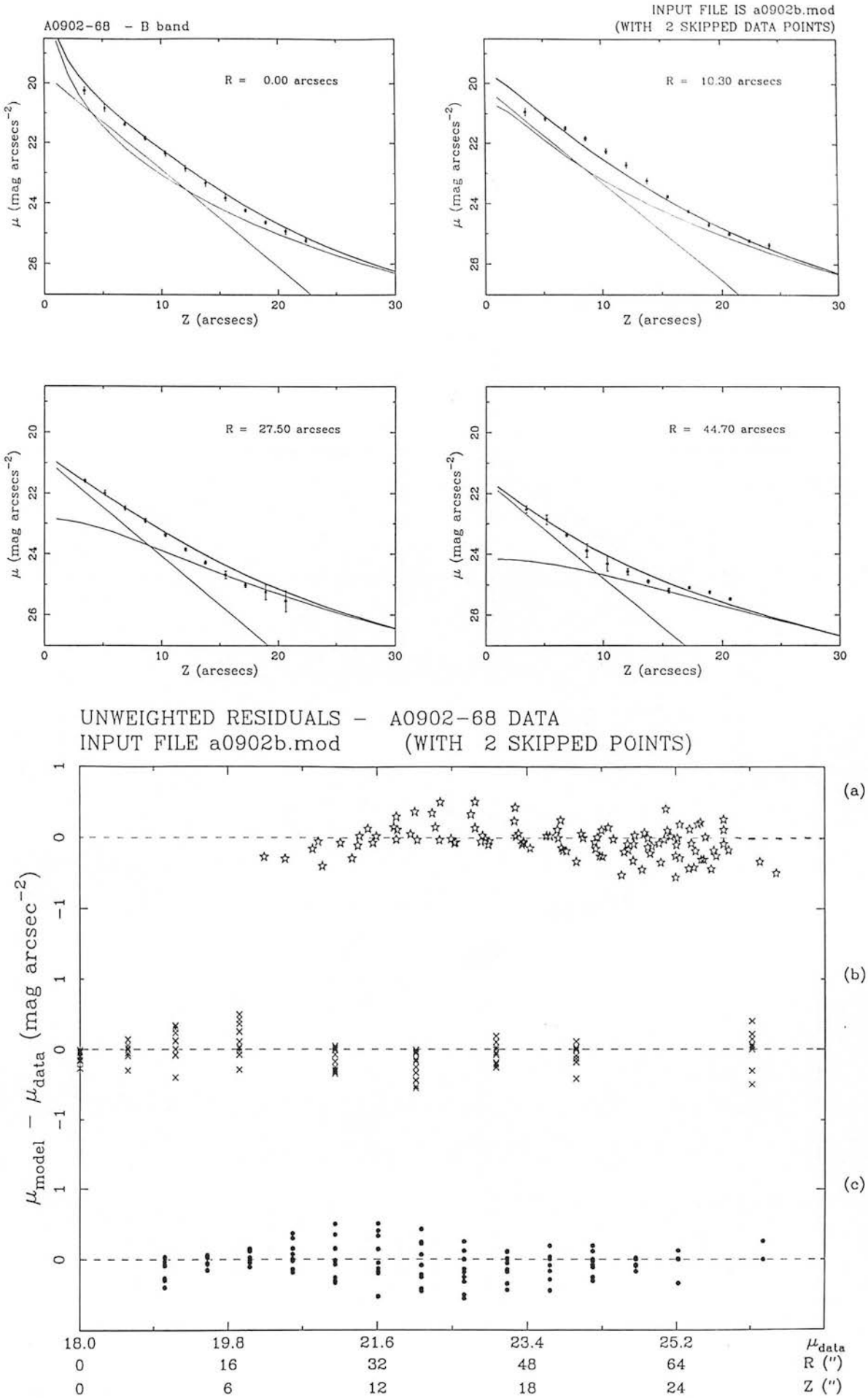
A0902-68 - B band
INPUT FILE IS a0902b.mod
(WITH 2 SKIPPED DATA POINTS)
R = 0.00 arcsecs
R = 10.30 arcsecs
R = 27.50 arcsecs
R = 44.70 arcsecs
μ (mag arcsecs⁻²)
Z (arcsecs)
UNWEIGHTED RESIDUALS - A0902-68 DATA
INPUT FILE a0902b.mod (WITH 2 SKIPPED POINTS)
μmodel − μdata (mag arcsec⁻²)
(a)
(b)
(c)
μdata
R (")
Z (")

figure 4.20

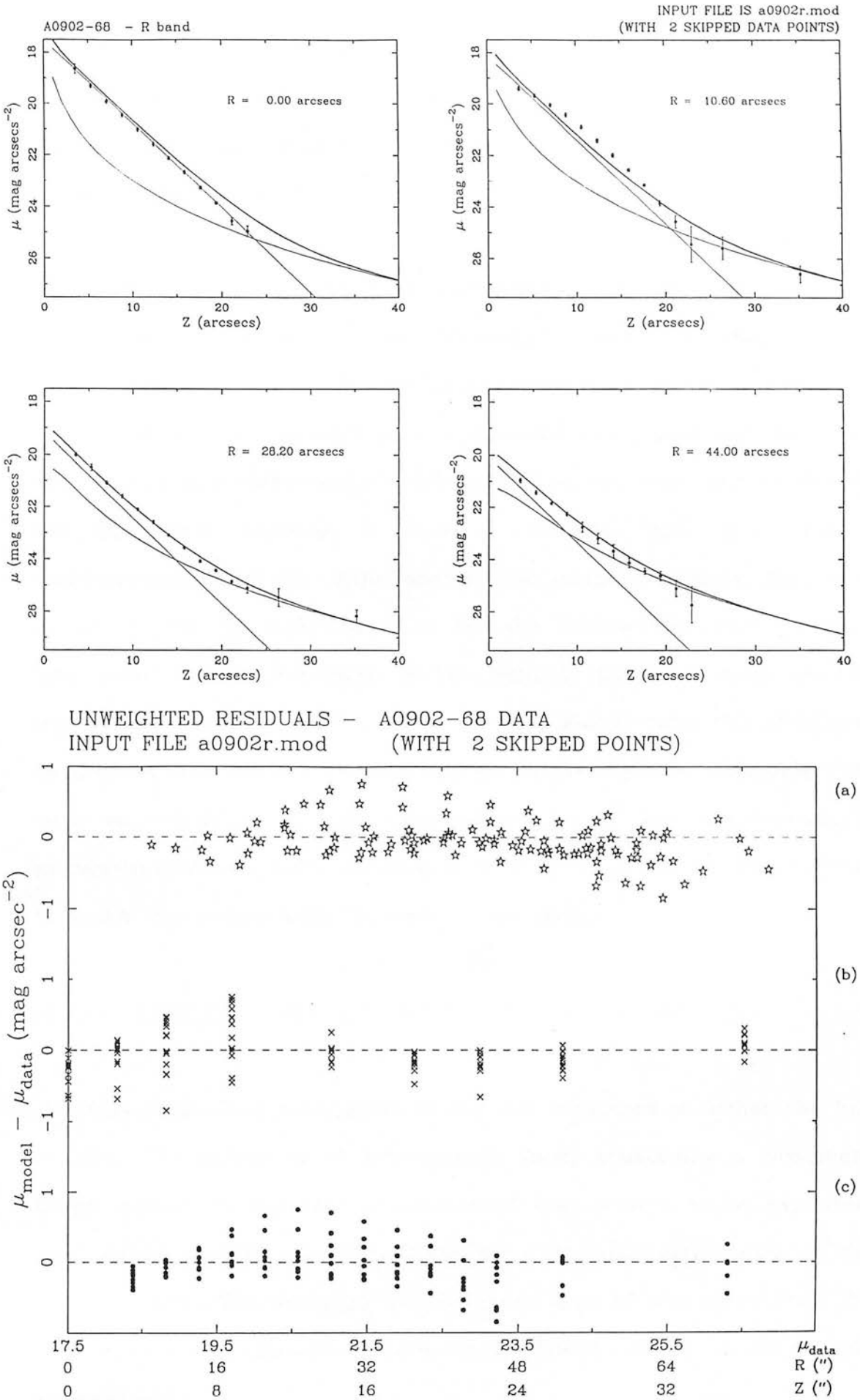
A0902-68 - R band
INPUT FILE IS a0902r.mod
(WITH 2 SKIPPED DATA POINTS)
R = 0.00 arcsecs
R = 10.60 arcsecs
R = 28.20 arcsecs
R = 44.00 arcsecs
μ (mag arcsecs⁻²)
Z (arcsecs)
UNWEIGHTED RESIDUALS - A0902-68 DATA
INPUT FILE a0902r.mod (WITH 2 SKIPPED POINTS)
μmodel - μdata (mag arcsec⁻²)
(a)
(b)
(c)
μdata
R (")
Z (")

figure 4.21

The reasonable fit evident at large Z-heights over all profiles again indicates that the clear peanut only appears to be a feature of the brighter isophotes of the galaxy (with such a morphology "fading" at large distances from the centre).

In conclusion, statistical fit parameters (and the requirement of the model parameters to be "realistic") serve to discount all three-component fits in favour of a combination of two components whose contributions depend on the passband being modelled. However, the considerable differences which remain in the axis ratio of the $r^{1/4}$ law component between B and R, coupled with a $\sim$ 0.8 μ underestimation of the light across the peanut, indicate that this system cannot be well-described by the fitting functions adopted. This result is not suprising in the light of the even more extreme peanut morphology than that of IC 2531, together with the additional restriction that such a feature dominates the light in this galaxy to such an extent as to make parameterisation of the disc component extremely difficult. Such domination at all (R,Z) precludes any attempt to model this galaxy with the peanut removed.

IV.2.12 A0919-33 (α = 09^h 18^m 55^s, δ = -32^o 58' 48")

This is another anonymous galaxy not contained in either the RC2 or RSA. The galaxy is of intermediate form, possessing a prominant bulge component but also a substantial disc with a major axis dust lane which partially obscures light over the southern region of the non-disc light. The assigned morphological type of Sbc comes from the ESO catalogue (although Corwin et al (1985) assign it an SAb[?] morphology).

The galaxy itself has a disc dimension of only ~2.8' on the SERC J survey plate 2982 (field 372). The adopted N-S orientation of the CCD chip long axis, even for the co-added single-position frames centred on the nucleus itself, are thus sufficient to allow spatial coverage of the disc (which shows no evidence of warping even to the faintest light levels).

As the local stellar density is very high, considerable care was adopted in this particular case in removing all such objects from the image frames (some 54 in total). In particular, a bright star located on the NE arm of the disc, some ~0.5' from the galactic centre, was particularly troublesome. A detailed inspection of the image frame and isophotal contour distribution indicated that the profiles N of the dust lane at R = 36" and 46" were both still affected by residual contamination after the removal process outline in section II.3.3. The northernmost regions of these particular profiles were thus discarded prior to generating the final surface brightness profile array - the profiles at these positions therefore comprising means of 3 individual slices rather than 4 as in all other cases. The galaxy environment is, however, relatively sparse, with the nearest system (an edge-on pure disc galaxy) being some ~12.3' E of A0919-33 itself. No magnitude or distance estimates were found for this system.

Results of the modelling

With all surface brightness profiles again affected by dust contamination from the disc component at small Z-heights ($\lesssim$ 2"), the following results are derived from fits made after the inner 2 data points of each profile were removed before the iterations were

conducted. Table A.12 details the results obtained.

Based on the statistical parameters for the model combinations in this table, I find a substantially improved fit to be obtained by the adoption of a double component combination incorporating an $r^{1/4}$ law profile. Although most three-component fits are to be preferred in the sense of their associated FSUMSQ values being ~ 17 % in B (~ 3 % in R) smaller than the two-component sets, placing the additional constraint of the results being "realistic" in either passband discounts all possible combinations in that table.

Particularly notable from an inspection of the fits derived are again systematic overestimations of the light at large Z by all model combinations adopted, whilst the derived scale parameters again show large discrepancies between B and R. Correction for the former effect requires the reduction of those sky estimates quoted in table 2.2 by 1.3 % in B and 0.2 % in R. The latter effect is, however, only partly alleviated by the adoption of the minimum error procedure - an "exponential + $r^{1/4}$ law" combination corrected for systematics and applied to data with a minimum error of ± 0.2 μ is found to reduce the disparities in disc scalelength to 14 % (from 63 %) and effective radius to 34 % (from 50 %), although the corresponding disc scaleheights become more discrepant (41 % compared to 25 % previously). The model fits obtained are illustrated in figures 4.22 (B) and 4.23 (R) - such combinations are able to describe this galaxy to within a typical residual of ± 0.2 μ in both passbands.

It is possible in this case that insufficient thin disc light (uncontaminated by the presence of the dust lane) exists to reliably

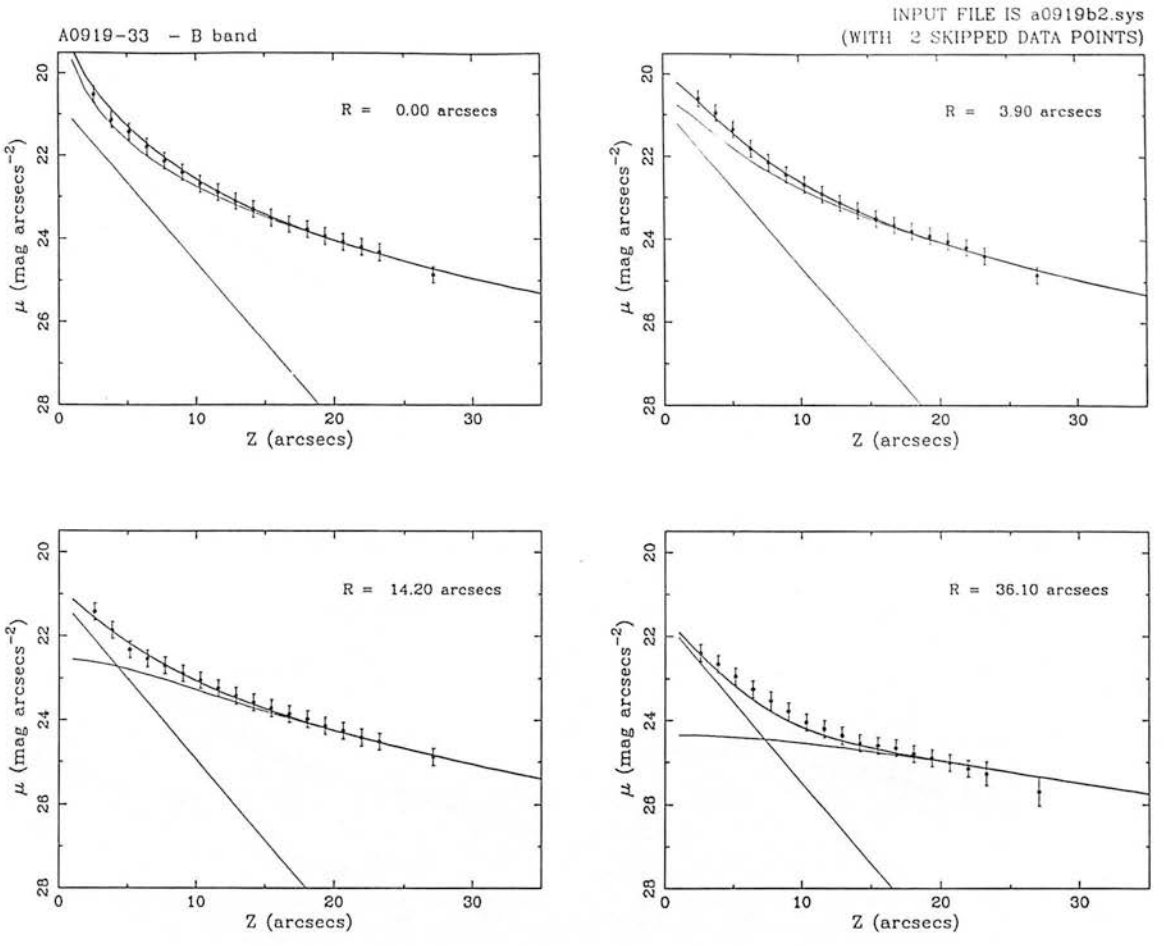
A0919-33 - B band
INPUT FILE IS a0919b2.sys
(WITH 2 SKIPPED DATA POINTS)
R = 0.00 arcsecs
R = 3.90 arcsecs
R = 14.20 arcsecs
R = 36.10 arcsecs
μ (mag arcsecs⁻²)
Z (arcsecs)

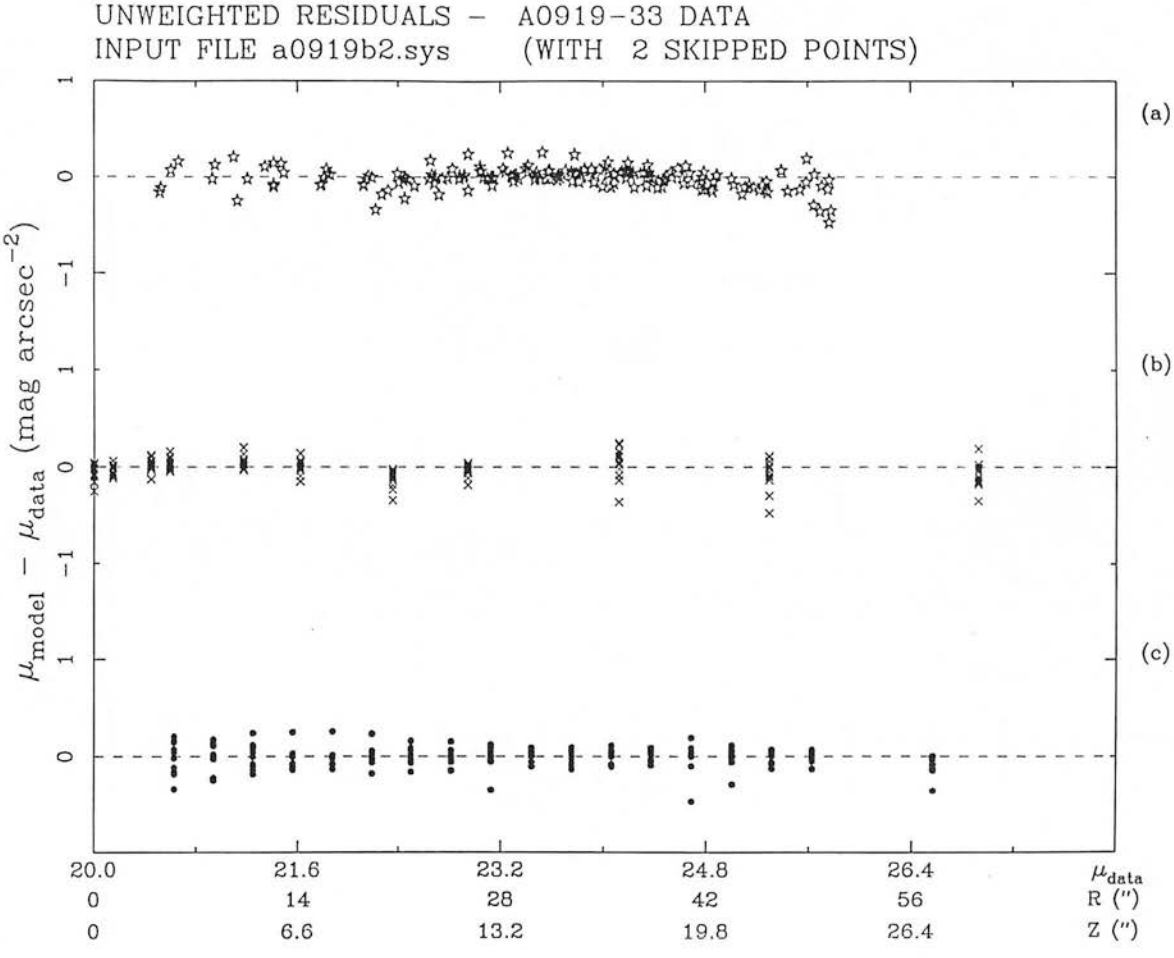
UNWEIGHTED RESIDUALS - A0919-33 DATA
INPUT FILE a0919b2.sys (WITH 2 SKIPPED POINTS)
(a)
(b)
(c)
μmodel − μdata (mag arcsec⁻²)
20.0 21.6 23.2 24.8 26.4 μdata
0 14 28 42 56 R (")
0 6.6 13.2 19.8 26.4 Z (")

figure 4.22

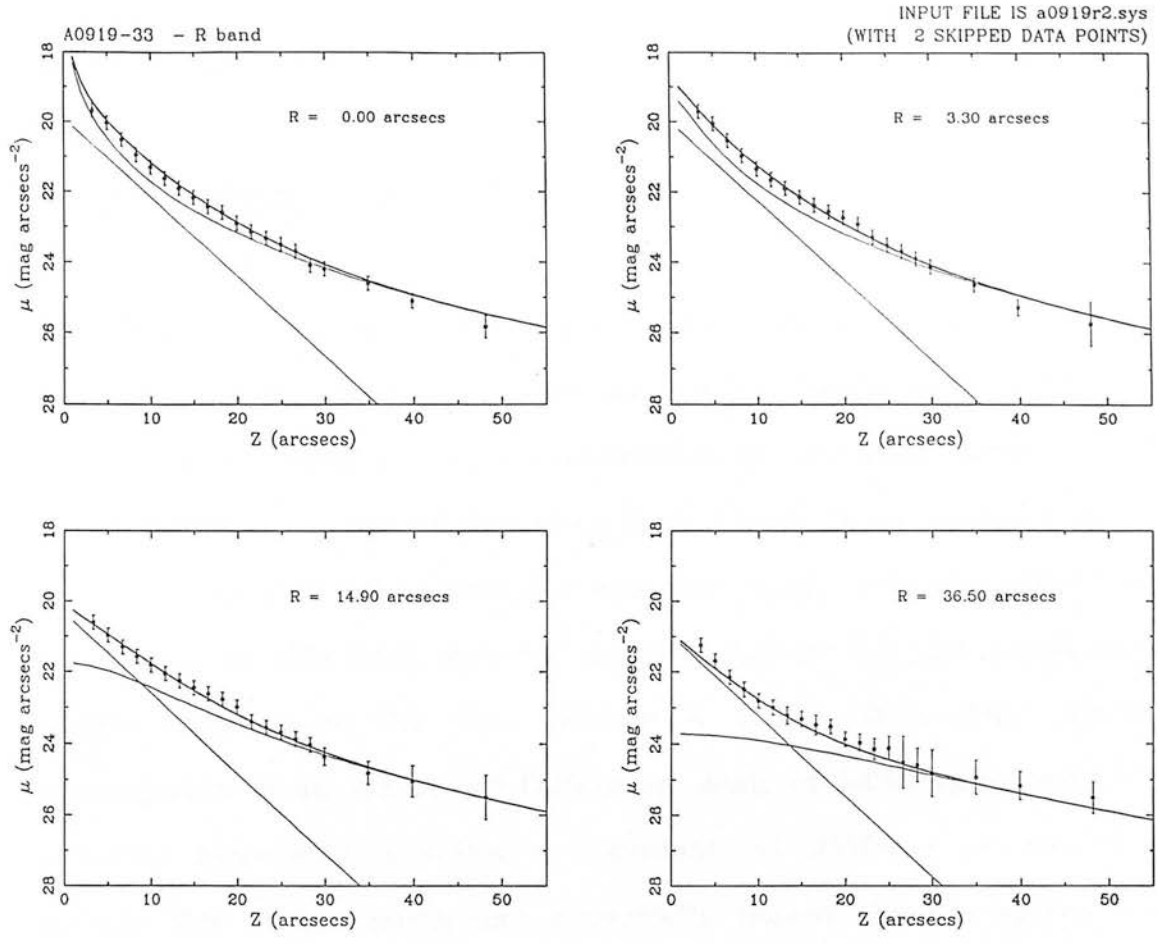
A0919-33 - R band
INPUT FILE IS a0919r2.sys
(WITH 2 SKIPPED DATA POINTS)
R = 0.00 arcsecs
R = 3.30 arcsecs
R = 14.90 arcsecs
R = 36.50 arcsecs
μ (mag arcsecs⁻²)
Z (arcsecs)

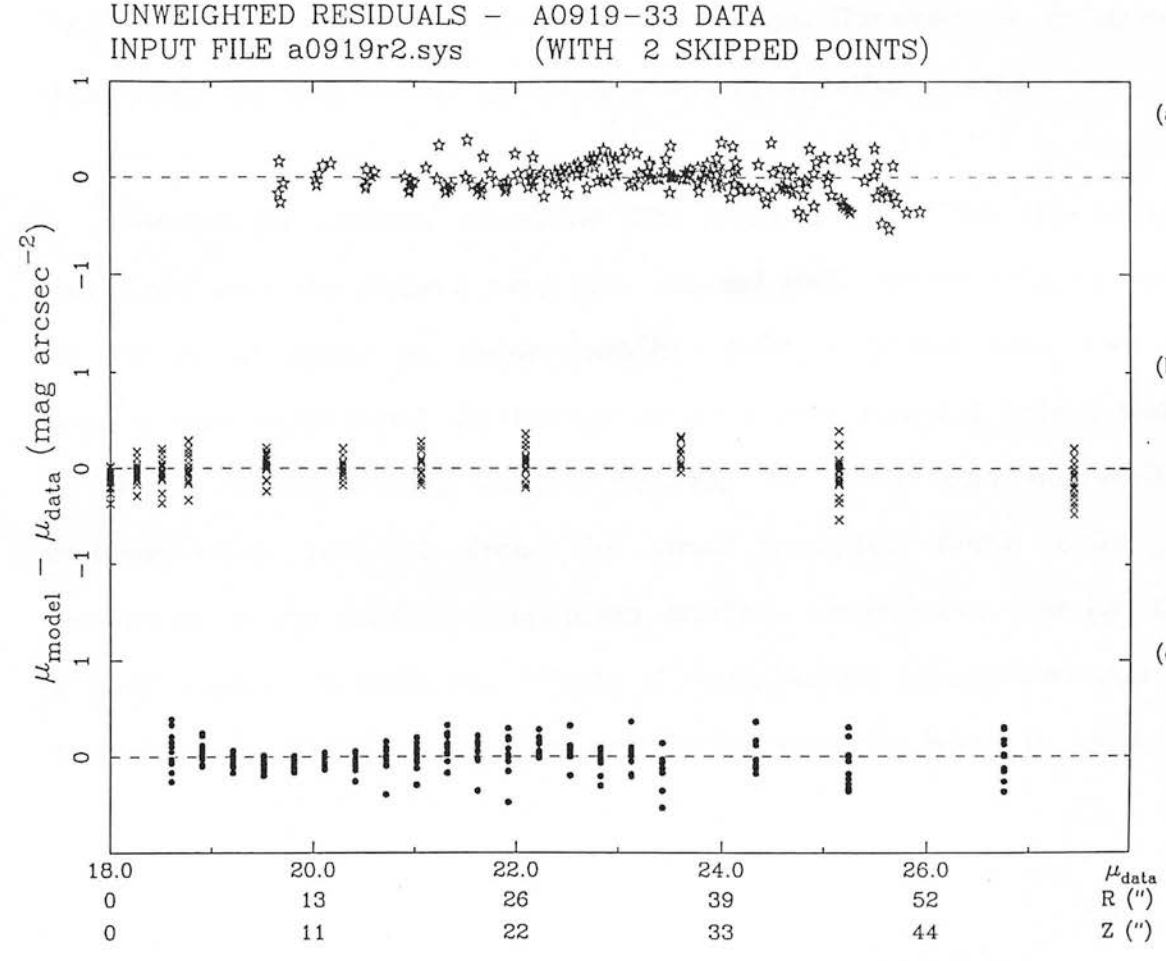
UNWEIGHTED RESIDUALS - A0919-33 DATA
INPUT FILE a0919r2.sys (WITH 2 SKIPPED POINTS)
(a)
(b)
(c)
μmodel - μdata (mag arcsec⁻²)
μdata
R (")
Z (")

figure 4.23

define the scaleheight in either or both datasets modelled here.

IV.2.13 A0931-32 (α = 09^h 31^m 13^s, δ = -32^o 48' 36")

Although not contained within the RC2 or RSA, this "disc dominated" galaxy is classified as an Scd by Corwin et al (1985). The ESO catalogue assigns it an Irr classification, probably because of the highly complex nature of the dust lane. There is no evidence on the SERC J plate 5580 (field 373) for any disc warp, with the overall disc major axis on this plate material being ~ 5.6' or 5.4 kpc based on an object distance of 3.2 Mpc (Fisher & Tully 1981). This distance corresponds to an associated CCD image scale of 0.016 kpc/arcsec. Two possibly associated systems are evident on J5580 - an amorphous galaxy ~3.9' to the north and a partially face-on barred spiral, some ~2.8' east and only ~1.1' above the disc plane. However, no reference was found for any cluster/group membership for this system.

The (single position) co-added CCD frame obtained for this object (obtained with the camera long axis aligned N-S) covers roughly half of the radial extent as determined on J5580, and was positioned in such a way as to avoid the barred spiral to the E and 2 bright stars to the W of the galaxy centre. Roughly 34 stellar and non-stellar objects were removed from the final co-added frame prior to extraction of the surface brightness profiles. As was the case for the B band data of IC 2531, the effects of such limited spatial coverage of these data on the derived model parameters must be borne in mind.

Results of the modelling

Because of the morphology of this galaxy, I only chose to describe it using either single or two-component model combinations. Despite the complex nature of the dust lane, the surface brightness profiles do not deviate from a smoothly decreasing μ with increasing Z-height beyond ~3.5". Thus, the foregoing modelling has been conducted after removal of those data in each profile for which $Z \lesssim 3.5$" (i.e. the innermost 3 data points).

As is immediately evident from the resulting parameters in table A.13, in choosing to describe this system by a single model, the use of a pure exponential yields a significant improvement over the sech^2 form (by ~ 30 % in FSUMSQ), and the $r^{1/4}$ law (by ~ 53 %). All two-component combinations in that table can be immediately rejected in the light of the physically implausible disc scalelength parameters thus defined (all of which are larger than the radial coverage in this data by a factor $>$ 20), and by the correspondingly larger goodness-of-fit parameters.

Use of the single exponential profile reveals no trend of scaleheight with $\mathbb{R}$, the derived mean of 0.10 kpc being constant to ± 3 % for $0 \leqslant \mathbb{R} \leqslant 1.2$ kpc. However, as is evident from the representative fits illustrated in figure 4.24, this profile shows significant discrepancies over the data at large galactocentric distances ($\gtrsim$ 50") and $Z \gtrsim 20$". An inspection of the image frame used reveals substantial patchy dust contamination at this $\mathbb{R}$ which appears to have an effect on all data to Z ~ 25", but it appears unlikely to extend to Z ~ 40". Thus the source of the disparities at large Z are unclear. They cannot be due to an incorrect assessment of the sky

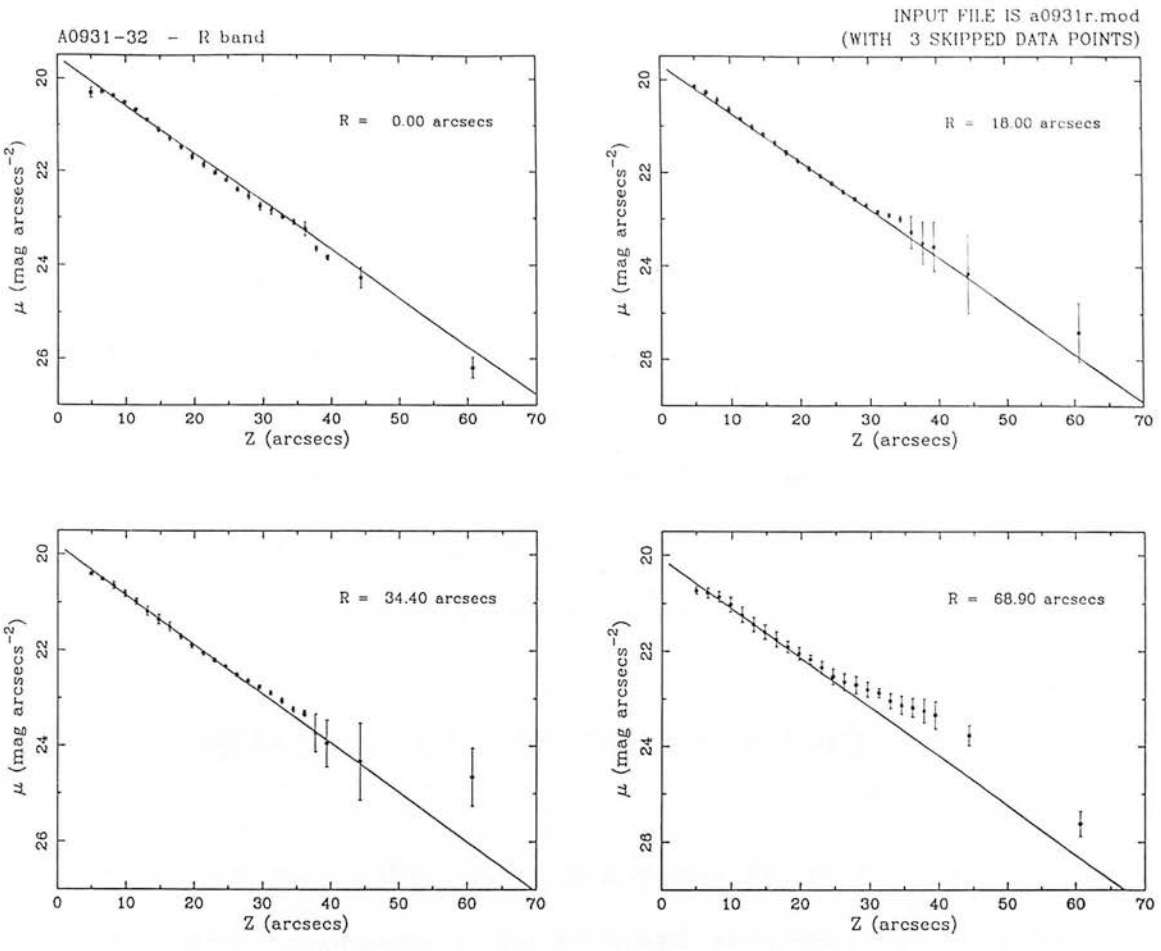
A0931-32 - R band
INPUT FILE IS a0931r.mod
(WITH 3 SKIPPED DATA POINTS)
R = 0.00 arcsecs
R = 18.00 arcsecs
R = 34.40 arcsecs
R = 68.90 arcsecs
μ (mag arcsecs⁻²)
Z (arcsecs)

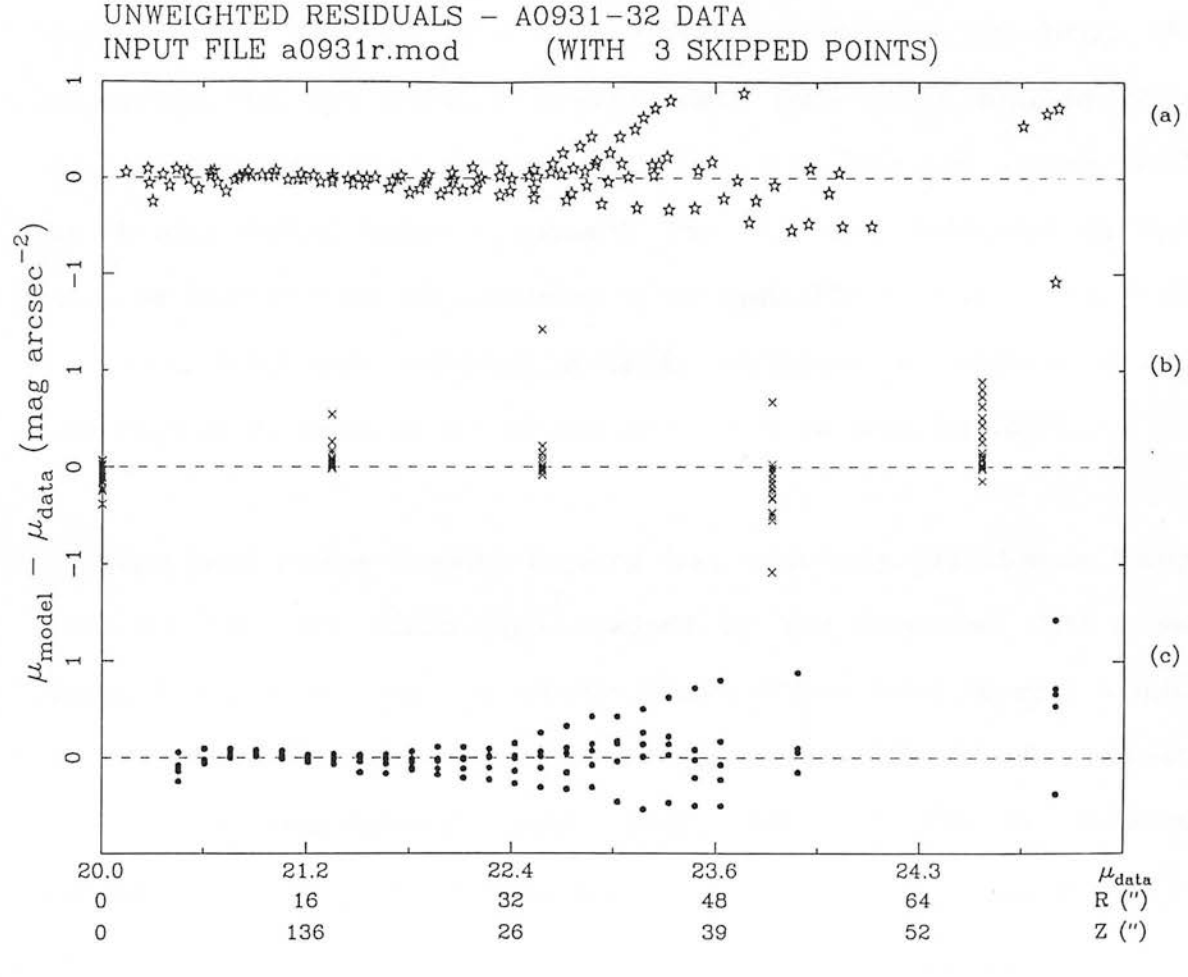
UNWEIGHTED RESIDUALS - A0931-32 DATA
INPUT FILE a0931r.mod (WITH 3 SKIPPED POINTS)
(a)
(b)
(c)
μmodel - μdata (mag arcsec⁻²)
20.0 21.2 22.4 23.6 24.3 μdata
0 16 32 48 64 R (")
0 136 26 39 52 Z (")

figure 4.24

level as no systematic trends are seen at large Z and/or faint surface brightness. Of course, the fact that all regions of the galaxy in the frame shown in appendix C are affected by dust contamination (i.e. Z $\lesssim$ 25") means that the model parameters for this system must be treated as very uncertain. Removal of all data thus affected, however, would leave too few points in each profile to allow extraction of meaningful results. This galaxy therefore appears to be described by a single exponential profile but only to an accuracy ~ $\pm$ 0.4 μ_R (based on the residuals diagram in figure 4.24).

IV.2.14 A1611-00 (α = 16^h 11^m 48^s, δ = -00^o 05')

This anonymous disc dominated galaxy is not contained within any of the major catalogues - the assigned morphological type Scd being derived from the lists of Corwin (private communication, 1981). Its appearance on the SERC J survey plate 5803 (field 872) is of a slightly inclined system possessing a clear dust lane and a very small but bright central bulge component. The total disc dimension on this plate is ~4.5' and no disc warping is evident. The CCD coverage (with the chip long axis oriented N-S) is sufficient to ensure spatial coverage of as much as 2/3 of the major axis as seen on J5803.

The local stellar density is very low, with only ~12 objects being removed from the whole area covered by the co-added CCD frame (none being located on the galaxy itself). There exist several bright and faint galaxies seen on the survey material within 1^o of A1611-00, the nearest (amorphous) system being some 3.3' SW. No distance estimate is available for this galaxy.

A point-by-point investigation of the surface brightness profiles at small Z-heights served to highlight those measures south of the major axis most affected by the obscuration. Such values were discarded and the surface brightness at these points were taken from the northernmost section of each perpendicular profile alone prior to generation of the final data array. Residual contamination seen along the major axis itself required the additional (global) removal of the Z = 0" data point in each one before the modelling was conducted.

Results of the modelling

As is seen in table A.14, this galaxy is best described by a combination of disc and $r^{1/4}$ law profiles - the single component fits all being excluded on the basis of their larger goodness-of-fit estimators (by > 57 % in the case of FSUMSQ) and the triple component combinations all converging to double component endpoints for all input. Indeed, an inspection of all tested three-component fits which failed to achieve convergence indicated that, at the point of arithmetic error (resulting from the excessive degree to which the third component had been suppressed), the same conclusions applied to those which were able to yield a solution within the imposed constraints. The mean scaleheight of the disc component in the "exponential + $r^{1/4}$ law" combination is 3.19 (±0.10)", the standard error being some 3.0% of the mean. Thus the assumption of a constant scaleheight with galactocentric distance for the disc component appears to be reasonable in this galaxy.

Again, however, a systematic overestimation of the light at large Z was noted and allowance for such an effect required a reduction of 0.2 % of the I_{sky} estimate in table 2.2. Figure 4.25 shows the results

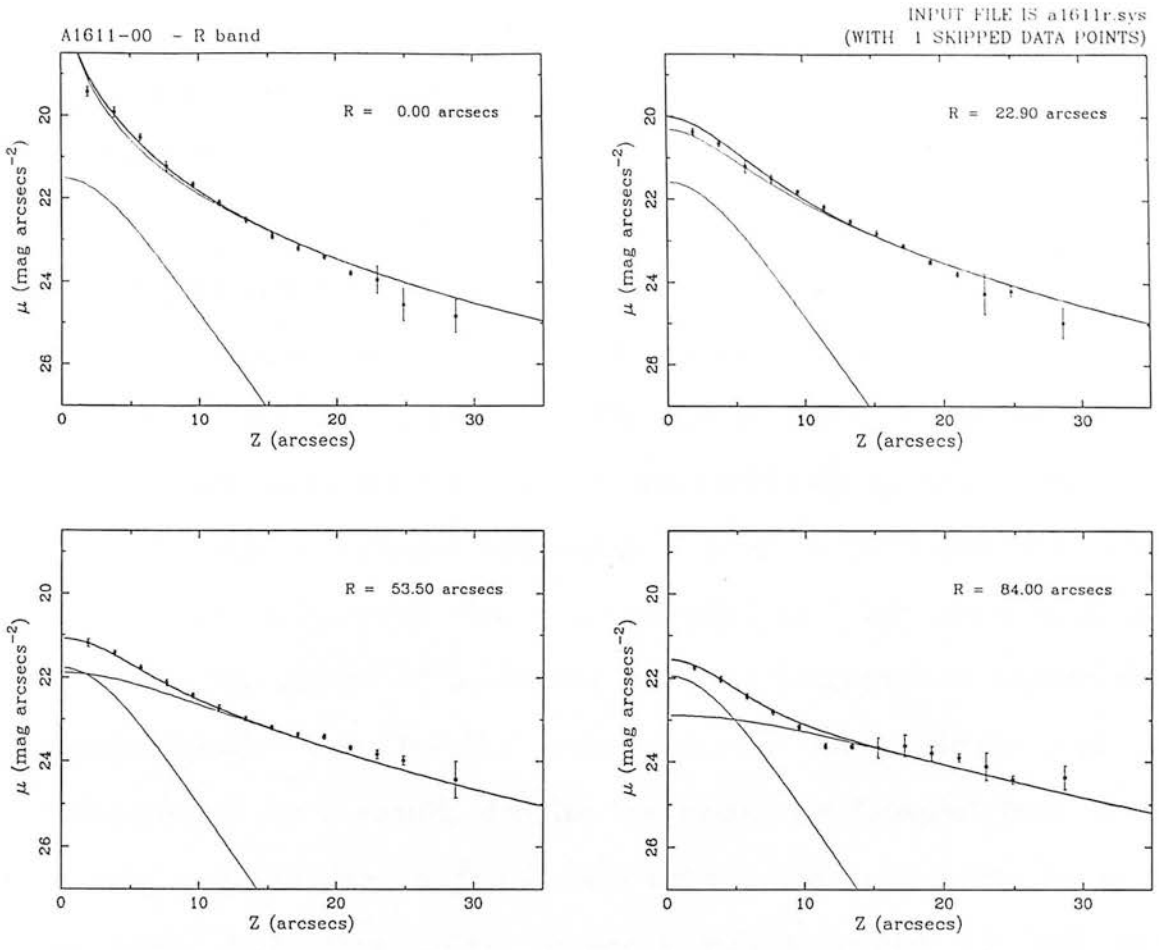
A1611-00 - R band
INPUT FILE IS a1611r.sys
(WITH 1 SKIPPED DATA POINTS)
R = 0.00 arcsecs
R = 22.90 arcsecs
R = 53.50 arcsecs
R = 84.00 arcsecs
μ (mag arcsecs⁻²)
Z (arcsecs)

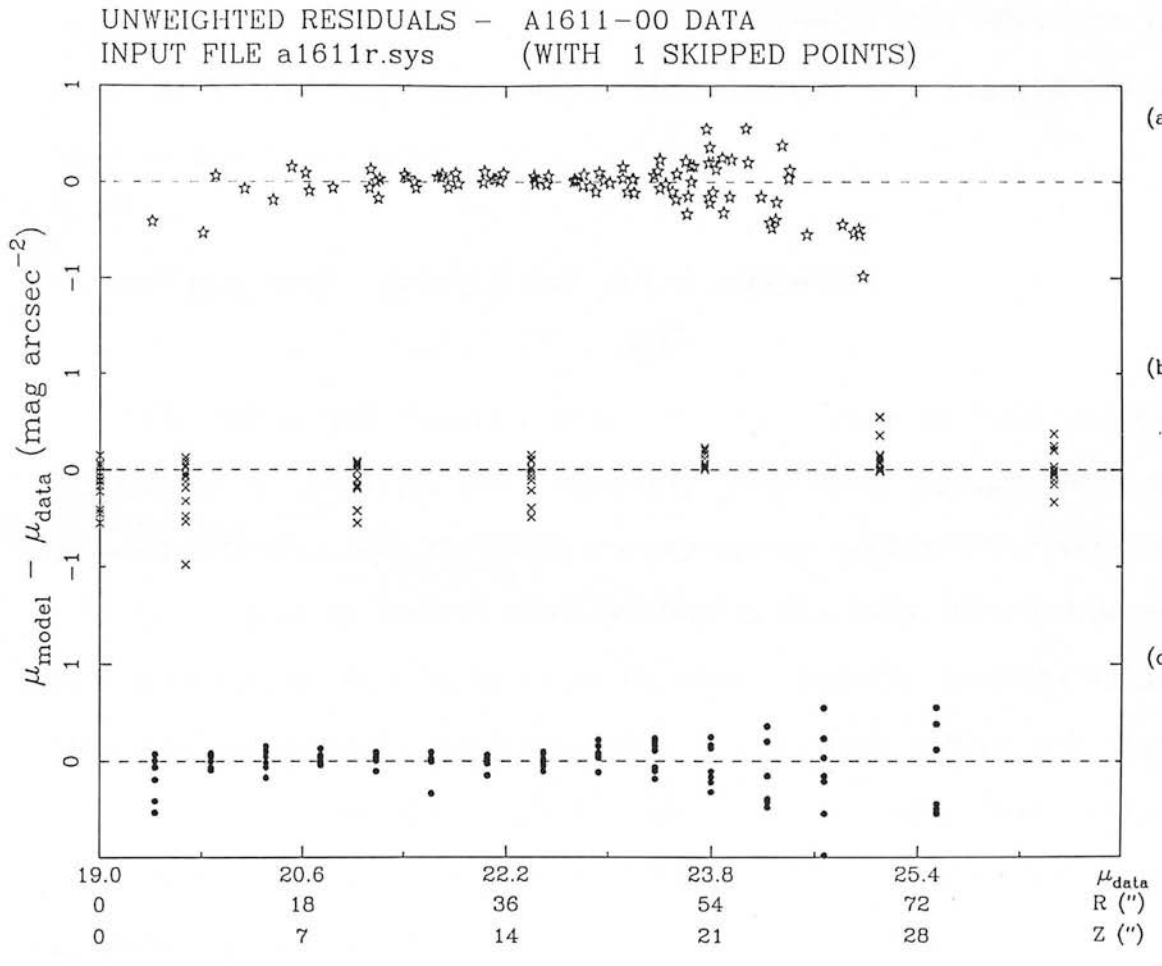
UNWEIGHTED RESIDUALS - A1611-00 DATA
INPUT FILE a1611r.sys (WITH 1 SKIPPED POINTS)
(a)
(b)
(c)
μmodel − μdata (mag arcsec⁻²)
μdata
R (")
Z (")

figure 4.25

of incorporating such a correction to the best-fit "sech^2 + $r^{1/4}$ law" combination.

Despite the allowance for such systematics, the $r^{1/4}$ law model is still a poor description of the data beyond Z ~ 20" over all profiles, whilst a comparison of the fits obtained to the image frame itself raises some concerns as to the relatively minimal contribution from the disc component beyond Z ~ 5-10" - an inspection of the actual frame suggesting that a contribution to ~ 20" might seem more realistic. The source of luminosity at these heights still appear to be predominantly due to the galaxy rather than simply the sky background. As a result, despite the seemingly "simple" form of this galaxy, and the clear differentation between the respective model fits in table A.14, this galaxy appears well-described by the model combinations only to within ± 0.35 μ - even after due allowance has been made for any systematic discrepancies at large Z-heights between model and data.

IV.2.15 UGC 7170 (α = 12^h 08^m 06^s, δ = +19° 06')

This galaxy was included in the current sample as being a prime example of a late-type, and seemingly pure disc, system. Both the present CCD data and the POSS survey (plate number 89) reveal only a limited degree of central concentration in the light distribution and the particularly thin nature of the disc. Indeed, Goad & Roberts (1981) interpret this system as being a superthin galaxy (for which axis ratios of typically $\lesssim$ 0.1 are encountered). The adopted classification of Sc comes from the UGC as this galaxy is not entered in either the RC2 or RSA.

An additional feature of this galaxy, however, is the pronounced warping of the northern and southern extremities of the disc - giving the galaxy the appearance of an integral sign and clearly evident on the isophotal contour plots shown in both B and R in figure 4.26. The present CCD data show the southernmost warp (turning to the SE) to be far clearer and slightly "sharper" than that at the northern end, i.e. showing a more rapid divergence from the disc plane. The latter is indeed barely visible on the POSS plates. Also notable in these frames (particularly in B) are numerous condensations along the disc plane which may be associated with spiral arm structure. Such condensations are also detectable in both warped regions of the disc.

An inclination angle of 90° is assumed in the present work, such a value being strongly implied by the striking clarity of the disc warps. The disc dimension as determined from plate R89 is ~ 2.2'. Thus, the single position CCD frames (chip long axis orientation N-S) cover not only the radial extent of the disc but also facilitate an excellent determination of the sky background. The local stellar density is very low in this field (l^{II} = 252°, b^{II} = 177°), although the number of galaxies within a 16.5' aperture centred on UGC 7170 itself is quite high (the UGC catalogue assigns this system membership of the NGC 4155 group). Thus a merger/interaction origin of the warp is a distinct possibility.

The distance of 23.9 Mpc to this galaxy is derived from Fisher & Tully (1981), agreeing well with the 32.0 Mpc (for an H_o of 75 kms^{-1} Mpc^{-1}) of Goad & Roberts (1981), and corresponds to an image scale of 0.116 kpc/arcsecs. The distance adopted here implies a maximum divergence of the warp from the southern end of the major axis of ~

1.0 kpc at ~ 25.5 μ_B (or ~ 24.7 μ_R). At such isophotal levels, the warp makes an angle of 17° with the disc plane on the southern end and 9° at the northern end.

Results of the modelling

Within the context of the present modelling, it is clearly difficult to assign global photometric parameters to a galaxy assumed to be axially symmetric but known to be strongly warped. Thus, in an attempt to counter the effects of the warp, only those surface brightness profiles with galactocentric distances interior to ~ 55" were used. Those profiles extracted from positions adjacent to the major axis will be only slightly affected owing to the fact that the line-of-nodes of the warp and the disc plane are almost coincident over such regions. This criterion therefore disposes of the outermost 2 profiles in both B and R in figure 4.26. No profiles interior to this point show any evidence of the effects of warping (such as a shift in the peak surface brightness of the profile away from the assumed major axis, or to that of its corresponding profile at the opposite end of the disc). At the extremities of the major axis where the warp is most in evidence, it is only detectable for those isophotes fainter than ~ 23.2 μ_B or ~ 22.8 μ_R.

As table A.15 illustrates, statistically improved model fits result from the adoption of a two-component model, and indeed all three-component sets, over the single exponential disc. Nevertheless, the very repeatable parameters for the dominant disc profile in all combinations in this table indicate that the same model component is being identified in both passbands and regardless of the model combinations adopted.

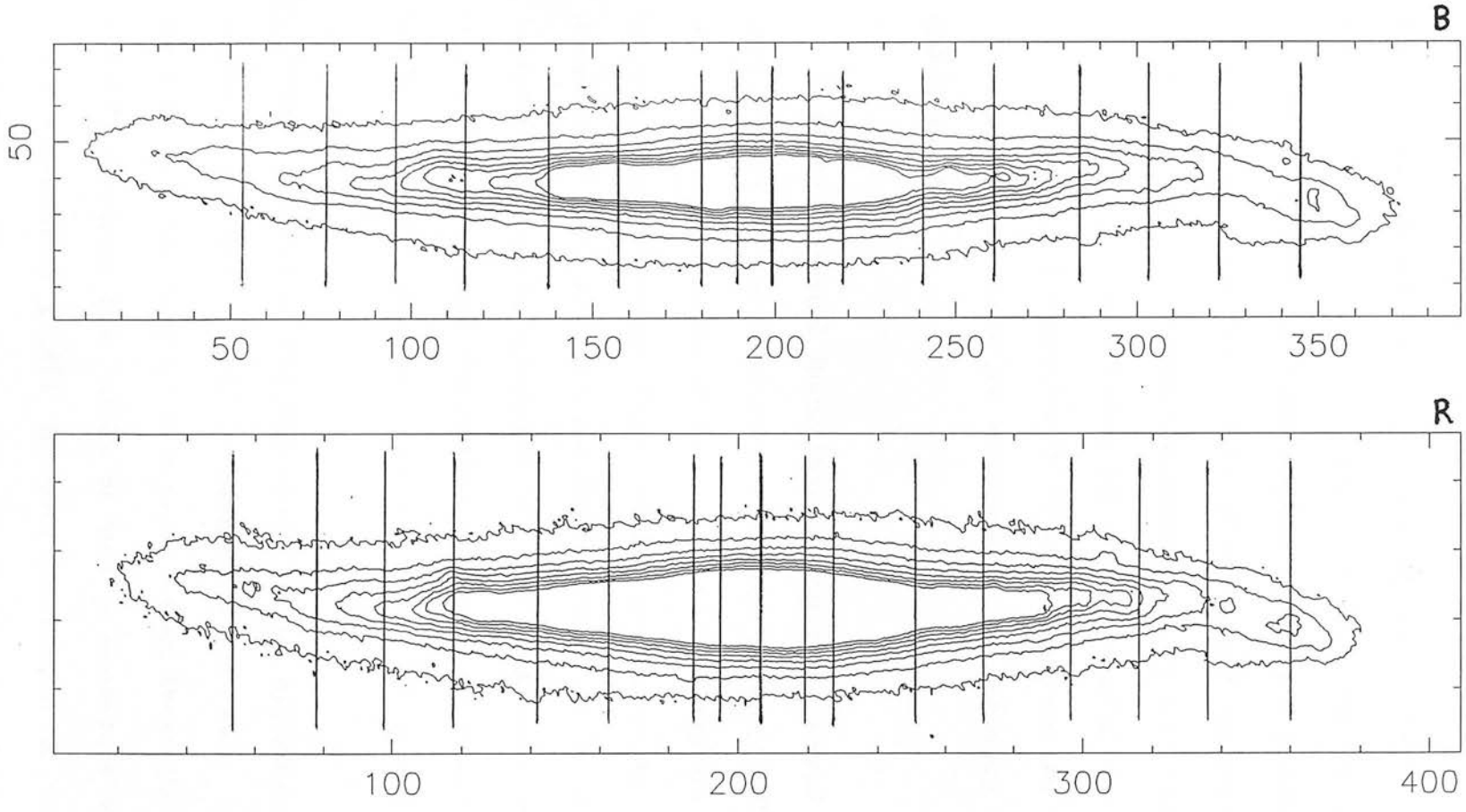

Figure 4.2**6** : Isophotal contour plots of subregions of the B and R band CCD frames of UGC 7170. The contours are set at intensity levels corresponding to ~ 21.8 to 24.7 μ_R and ~ 22.2 to 25.3 μ_B. Superposed are the surface brightness profiles extracted across this galaxy (the assumed minor axis is marked in bold).

Subsequent additional testing of a variety of model combinations in both B and R again attested to the reproduceability of all scale parameters in table A.15. It was of considerable interest, however, to analyse any variations in the scaleheight of the disc component(s) with galactocentric distance which may be attributed to the effects of the warp and thus not fully allowed for in the present modelling. In both passbands the scaleheight of the single exponential disc shows no evidence of a systematic variation with $\mathbb{R}$, with the derived means of 0.36 kpc (B) and 0.38 kpc (R) having associated errors of only ± 1.8 % and ± 1.9 % respectively. None of the (random) variations about the mean values could be assigned to any obvious features in the galaxy itself.

However, a visual inspection of the fits derived in these cases clearly show the model profiles to become systematically brighter than the observed luminosity at large Z - particularly for the profiles at larger radial distances. These effects are likely to result from the presence of the warp and not fully allowed for in the above scheme (despite the seeming constancy of h_Z ($\mathbb{R}$)). A close inspection of the fits obtained indicates the deviations from an exponential profile first become evident at surface brightnesses of ~ 26 μ_B and ~ 25 μ_R.

Thus, a series of fits was conducted by applying both single and double exponential model combinations to data arrays suitably corrected by removing all data fainter than these limits. Figures 4.27 and 4.28 illustrate the results of such a procedure when applying a single exponential profile to data in B and R respectively. The parameters defining these fits are essentially identical to those of table A.15 (with the disc (B-R) colour index of 0.95 mag. being only ~

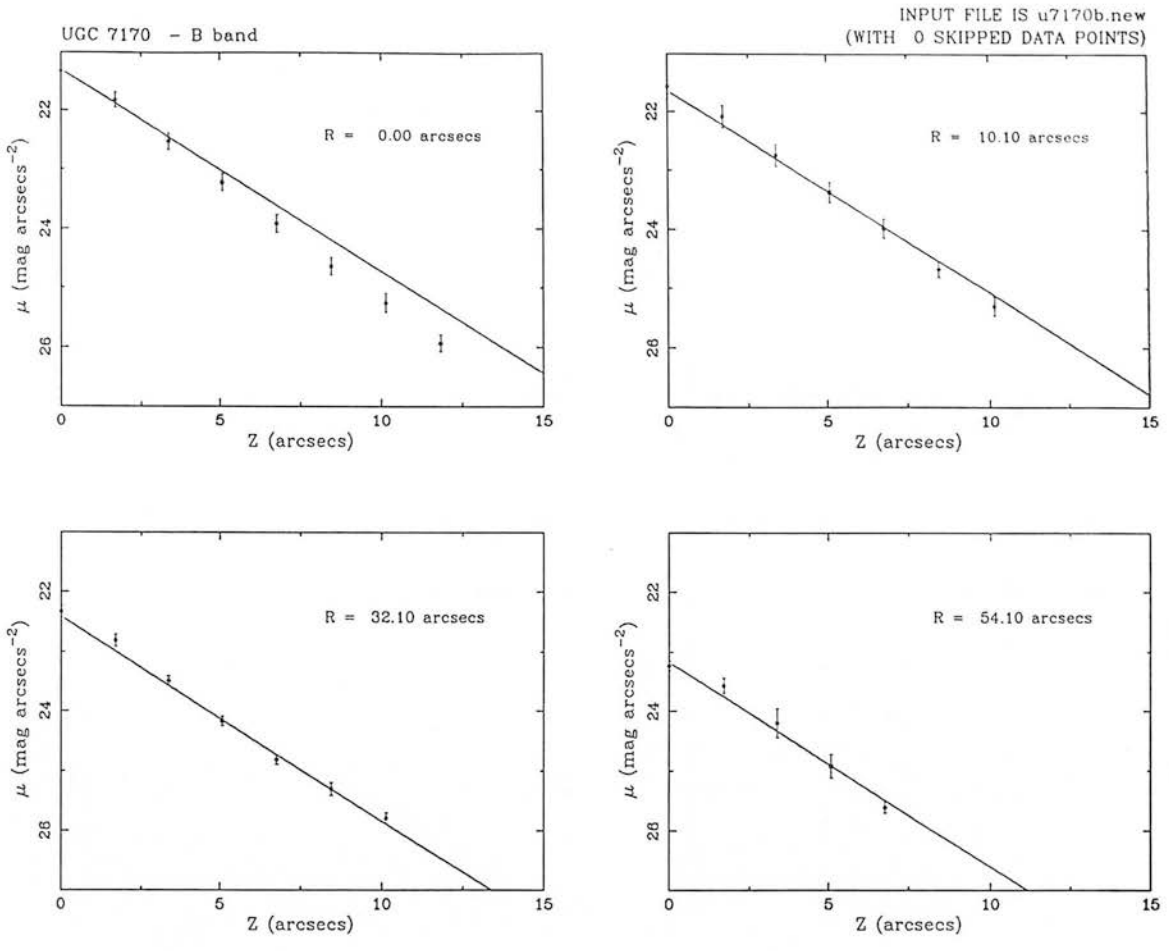
UGC 7170 - B band
INPUT FILE IS u7170b.new
(WITH 0 SKIPPED DATA POINTS)
R = 0.00 arcsecs
R = 10.10 arcsecs
R = 32.10 arcsecs
R = 54.10 arcsecs
μ (mag arcsecs⁻²)
Z (arcsecs)

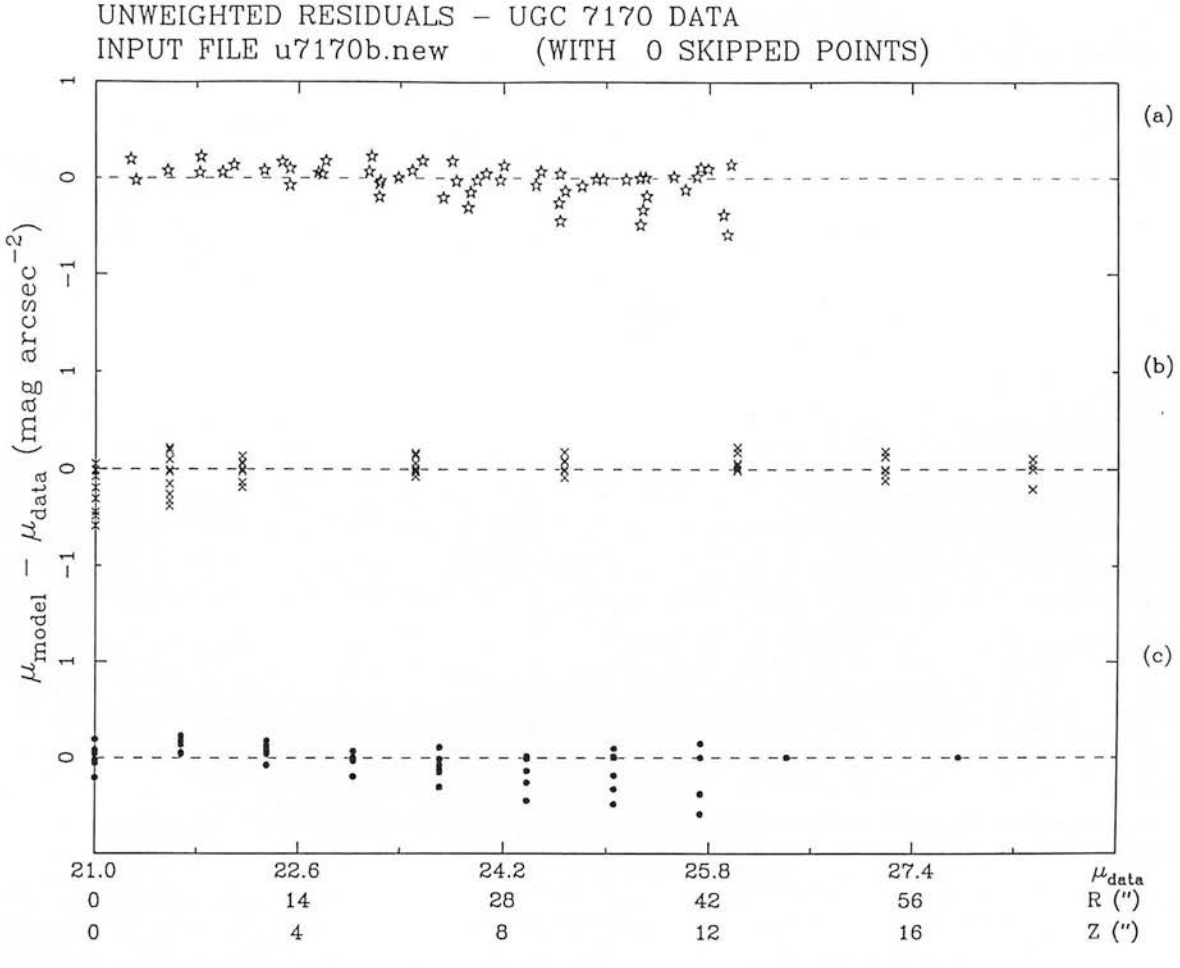
UNWEIGHTED RESIDUALS – UGC 7170 DATA
INPUT FILE u7170b.new (WITH 0 SKIPPED POINTS)
(a)
(b)
(c)
μmodel – μdata (mag arcsec⁻²)
21.0
22.6
24.2
25.8
27.4
μdata
R (")
Z (")

figure 4.27

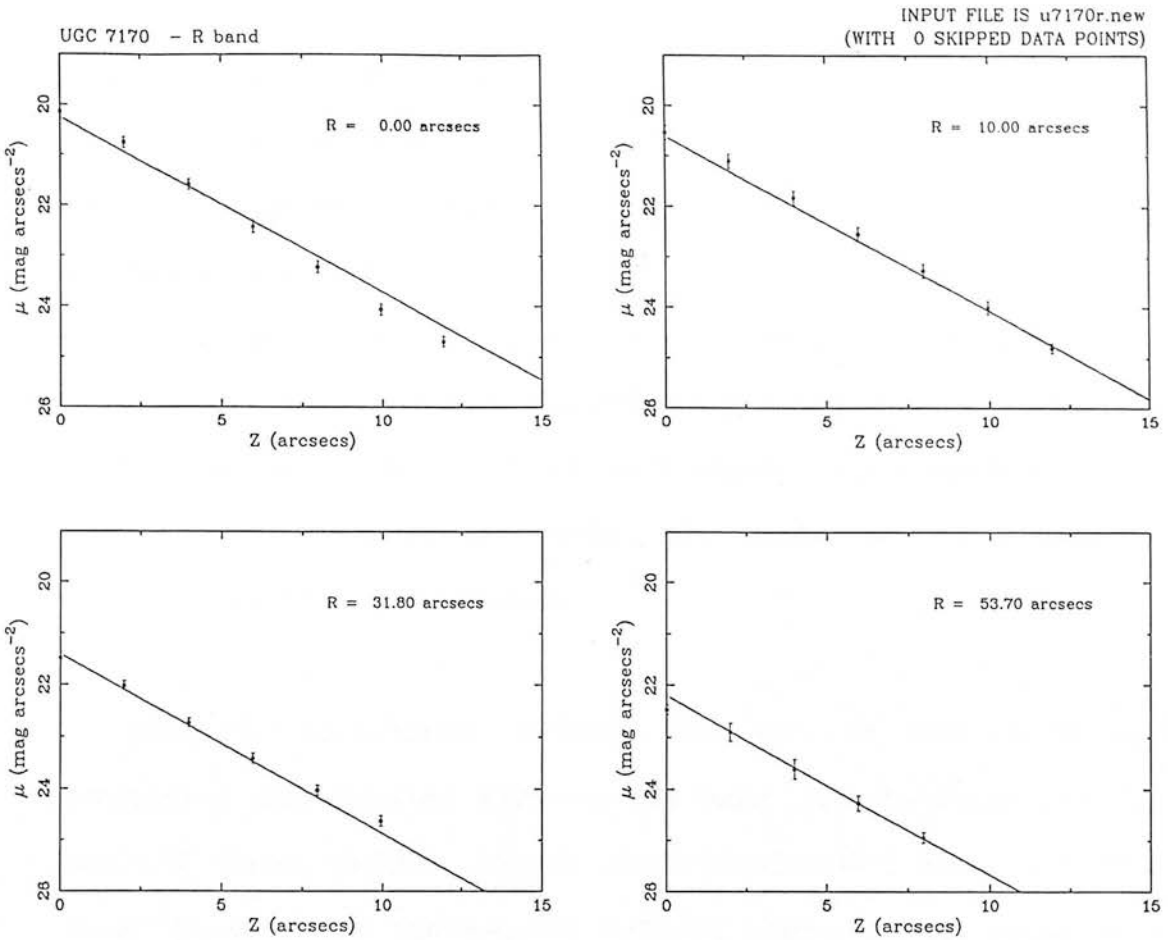
UGC 7170 - R band
INPUT FILE IS u7170r.new
(WITH 0 SKIPPED DATA POINTS)
R = 0.00 arcsecs
R = 10.00 arcsecs
R = 31.80 arcsecs
R = 53.70 arcsecs
μ (mag arcsecs⁻²)
Z (arcsecs)

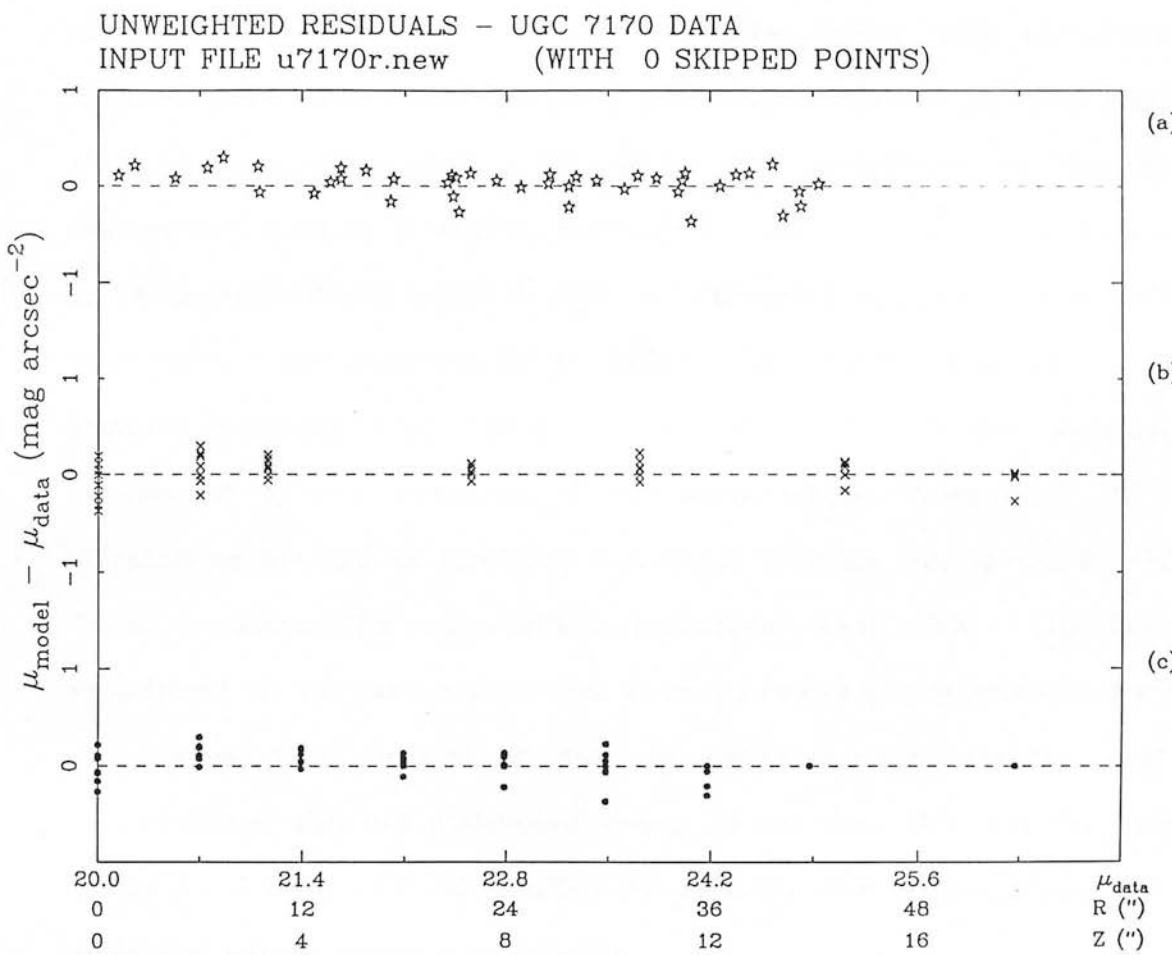
UNWEIGHTED RESIDUALS - UGC 7170 DATA
INPUT FILE u7170r.new (WITH 0 SKIPPED POINTS)
(a)
(b)
(c)
μmodel - μdata (mag arcsec⁻²)
20.0
21.4
22.8
24.2
25.6
μdata
R (")
Z (")

figure 4.28

3 % larger than that derived from parameters in the table), although the reduction in FSUMSQ by ~ 10 % in B and ~ 18 % in R indicate that an improved allowance for the warp has been achieved. The corresponding two-component fits still give a smaller FSUMSQ, indicating that residual light from the warp still contaminates the profiles modelled, although the effects are less severe than those in table A.15. This is most evident in R where the improvement from the addition of the second exponential disc profile is ~ 23 % in FSUMSQ compared to 42 % in table A.15.

What is particularly notable, however, is that such double component combinations give equally poor fits to those profiles at small $\mathbb{R}$. These profiles should show considerably less contamination from the warp for the reasons outlined above, so the cause of such poor fits may be due to all other profiles being more significantly affected then these. However, the residuals diagrams in both figures show those profiles at $\mathbb{R}$ ~ 10" to be very well-fitted by the single exponential profile, a region sufficiently close to the minor axis that an inspection of the image frames indicate such cuts are dominated by the central concentration of the disc over almost all Z. In short, it appears unlikely that those profiles at $\mathbb{R}$ ~ 6 " are completely unaffected by the presence of the warp whilst those at ~ 10" are affected as heavily as the very outermost profiles (for which $\mathbb{R}$ ~ 50"). There remains the possibility, therefore, that UGC 7170 is not well-fitted by an exponential disc even in regions less affected by the disc warp. The removal of data to progressively brighter surface brightnesses was not attempted owing to the fact that too few points would be found over all profiles to reliably define the properties of even the single exponential profile.

In conclusion, of all the model combinations tested here, UGC 7170 seems to be best described by a single exponential model which shows varying degrees of contamination from the disc warp. Removal of those surface brightness profiles exterior to a specified radial distance cannot allow for the affects of the warp, although significantly reduced discrepancies at large Z are facilitated by discarding data at a specific surface brightness level. However, these procedures generate exponential disc parameters which are highly reproduceable in all cases, suggesting that the disc parameters quoted in table A.15 closely approximate the "true" values for this system. Indeed, even a visual fit to the minor axis profile alone yields values for the central surface brightness and scaleheight of 21.25 μ and 0.32 kpc respectively in the B band, and 20.10 μ and 0.32 kpc in R - all estimates in very close agreement with those defined in the modified arrays above and the values in table A.15. The poor fits at R $\lesssim$ 10", however, imply that even if due account can be made of the effects of the warp, the adoption of an exponential profile may still be unable to describe this galaxy to better than the rms residuals of $\pm$ 0.15 μ_B and 0.2 μ_R found in the present analysis.

IV.3 General conclusions

In this chapter I have presented the results obtained when applying the nonlinear, least-squares modelling routine outlined in chapter III to those galaxies for which CCD photometry was obtained (table 2.2).

A combination of goodness-of-fit estimates and the requirement of the output parameters thus defined to be "realistic" (in the context of

the data being modelled) is found to isolate a particular model combination as being most appropriate to that data in all cases. This confirms the conclusions of chapter III and therefore does not support van der Kruit (1984) who infers that any differences in the quality-of-fit between two and three component model combinations is solely due to corresponding differences in their associated degrees of freedom. Furthermore, all parameters defined for each "best-fit" combination show excellent repeatability for each galaxy over a wide range of input estimates.

A number of specific conclusions emerge from the present investigation. For all those galaxies for which a thin disc component can be clearly defined, the scaleheight of this disc is found to be constant to better than ± 16 % (and typically ~ ± 4 %) of the derived mean in all cases, confirming the results found in the literature for smaller datasets than that studied here.

The candidate showing pronounced "box" shaped central isophotes (NGC 2310) appears well-described by the standard fitting functions adopted - the light contained within the central regions being consistent with that expected from an inward extrapolation of the non-thin disc component at large (R,Z). The ~ 10 % excess light at small (R,Z) noted in section IV.2.2 after subtraction of the "best-fit" model combinations is essentially a null-detection in the light of the accuracy with which such estimates can be defined. For example, a similar procedure applied to the non-box/peanut NGC 4289 reveals a ~ 5 - 10 % excess in the R band over the two-component model which is on the whole found to provide a very good description of this system.

However, in answer to the question posed at the start of this chapter, the "peanut" shaped isophotes cannot be well-fitted by any profile - the model combinations all underestimating the light at the edges of these features by ~ 0.25 μ_B and ~ 0.75 μ_R. These correspond to typically ~ 10 % of the predicted (model) luminosity in the R band over these regions and ~ 6 % in B. The inclusion of an additional model component does not reduce this disparity. The peanut morphologies typically contribute $\gtrsim$ 20 % (and as much as 35 % in IC 2531 - the most extreme case) of the total non-thin disc light in each passband for the galaxies concerned. The non-thin disc light at regions of large (R,Z), however, is reasonably well-described by the fitting functions adopted, suggesting that the peanut morphology is an additional contributor to the total luminosity of the galaxy and is not merely accounted for by a concentration of the "outlying" component to the central regions. This result is in accord with that found for NGC 4565 in chapter III.

Unfortunately in only one system (IC 2531) is the peanut shape sufficiently small, and does the data obtained cover a sufficiently large range in R, to allow a meaningful test of the fitting functions adopted after removal of those regions most affected by these isophotal "distortions". In so doing, I find the model combinations adopted can provide an adequate description of the data remaining to within an rms residual of ± 0.25 μ_R in both passbands.

The main aim of this chapter, however, was to determine whether the luminosity distributions of the galaxies studied, and in particular their non-thin disc regions, can be well-fitted by a suitable choice of fitting functions, and whether any discrepancies which result from

the addition of a particular set of components can be accounted for by the inclusion of an additional profile. In only two galaxies modelled here (NGC 5170 and IC 2531) is there any evidence of a third component, most systems being best described by the combination of a disc model (the exponential is statistically preferred to the $sech^2$ in almost all cases) and an $r^{1/4}$ law profile.

Two particular discrepancies appear common to most galaxies studied in this sample. The model combinations show a systematic overestimation of the light at large Z-heights in many cases, correction for which requires the sky estimates quoted in table 2.2 to be in error by typically 0.5 % in R and 3.3 % in B. Furthermore, even after correcting for these effects, substantial differences remain between the model parameters thus defined in the two passbands. Although the present least-squares algorithm performs a fit based on the weighting assigned to each data point, for such results to be meaningful the fits obtained are required to be adequate globally. Such highly discordant model parameters therefore appear unphysical, and their removal requires the error distributions to be modified accordingly (by imposing a typical minimum error to each data point of $\pm$ 0.2 μ). The implications of these, seemingly implausible, correction factors required to bring observations and predictions into satisfactory agreement are discussed in more detail in chapter V. However, after their application, the model combinations are found to describe the present galaxies to within a typical rms residual $\sim \pm$ 0.3 μ, with the derived parameters consistent to within $\sim$ 30 %, in both passbands. Table 4.1 summarises the "best-fit" parameters characterising each system after all corrections have been applied.

GALAXY	THIN DISC PARAMETERS		NON-THIN DISC PARAMETERS		
NGC 2295	μ_o = 20.91 μ (R) h_z = 12.49 " (R) h_r = 51.4 " (R)		μ_o = 16.69 μ (R) h_z = 3.21 " (R) h_r = 17.6 " (R)		
NGC 2310	μ_o = 20.55 μ (B) h_z = 0.29 kpc (B) h_r = 2.9 kpc (B)	18.94 μ (R) 0.26 kpc (R) 3.1 kpc (R)	μ_e = 17.18 μ (B) e_e = 0.16 kpc (B) q = 0.27 (B)	15.87 μ (R) 0.19 kpc (R) 0.24 (R)	
NGC 3115			μ_e = 17.25 μ (B) e_e = 0.26 kpc (B) q = 0.38 (B)	16.07 μ (R) 0.33 kpc (R) 0.38 (R)	μ_o = 21.50 μ (B) 20.56 μ (R) h_z = 0.77 kpc (B) 0.70 kpc (R) h_r = 3.3 kpc (B) 1.5 kpc (R)
NGC 3573	μ_o = 22.04 μ (B) h_z = 5.43 " (B) h_r = 30.6 " (B)	23.87 μ (R) Z_o = 17.16 " (R) 43.4 " (R)	μ_e = 19.72 μ (B) e_e = 11.47 " (B) q = 0.52 (B)	17.67 μ (R) 9.02 " (R) 0.56 (R)	
NGC 4289	μ_o = 20.59 μ (R) h_z = 2.71 " (R) h_r = 53.4 " (R)		μ_e = 17.62 μ (R) e_e = 4.08 " (R) q = 0.40 (R)		
NGC 4469	μ_o = 20.89 μ (B) h_z = 0.40 kpc (B) h_r = 1.9 kpc (B)	20.72 μ (R) 0.46 kpc (R) 2.0 kpc (R)	μ_e = 18.29 μ (B) e_e = 0.34 kpc (B) q = 0.33 (B)	15.00 μ (R) 0.23 kpc (R) 0.32 (R)	
NGC 5078			μ_e = 18.08 μ (R) e_e = 26.65 " (R) q = 0.51 (R)		
NGC 5170	μ_o = 20.84 μ (B) h_z = 0.56 kpc (B) h_r = 7.6 kpc (B)	19.27 μ (R) 0.53 kpc (R) 8.2 kpc (R)	μ_o = 18.74 μ (B) h_z = 0.19 kpc (B) h_r = 0.7 kpc (B)	16.94 μ (R) 0.21 kpc (R) 0.7 kpc (R)	μ_e = 22.81 μ (B) 20.61 μ (R) e_e = 2.80 kpc (B) 2.36 kpc (R) q = 0.46 (B) 0.48 (R)
IC 2531	μ_o = 21.03 μ (B) Z_o = 0.86 kpc (B) h_r = 5.5 kpc (B)	20.24 μ (R) 0.78 kpc (R) 7.9 kpc (R)	μ_e = 17.42 μ (B) e_e = 0.52 kpc (B) q = 0.44 (B)	23.87 μ (R) 9.54 kpc (R) 0.10 (R)	
IC 4351	μ_o = 19.53 μ (R) h_z = 0.91 kpc (R) h_r = 11.4 kpc (R)		μ_e = 15.81 μ (R) e_e = 0.73 kpc (R) q = 0.53 (R)		
A0902-68	μ_o = 19.69 μ (B) h_z = 0.68 kpc (B) h_r = 5.1 kpc (B)	17.50 μ (R) 0.66 kpc (R) 3.7 kpc (R)	μ_e = 18.62 μ (B) e_e = 0.86 kpc (B) q = 0.33 (B)	19.57 μ (R) 1.20 kpc (R) 0.10 (R)	
A0919-33	μ_o = 20.73 μ (B) h_z = 2.82 " (B) h_r = 42.8 " (B)	19.90 μ (R) 4.82 " (R) 36.6 " (R)	μ_e = 21.55 μ (B) e_e = 19.91 " (B) q = 0.63 (B)	19.75 μ (R) 13.06 " (R) 0.69 (R)	
A0931-32	μ_o = 19.61 μ (R) h_z = 0.17 kpc (R) h_r = 6.4 kpc (R)				
A1611-00	μ_o = 21.51 μ (R) Z_o = 4.59 " (R) h_r = 88.5 " (R)		μ_e = 19.46 μ (R) e_e = 10.32 " (R) q = 0.19 (R)		
UGC 7170	μ_o = 21.34 μ (B) h_z = 0.37 kpc (B) h_r = 3.8 kpc (B)	20.36 μ (R) 0.38 kpc (R) 3.7 kpc (R)			
NGC 891	μ_o = 21.20 μ (J) Z_o = 1.05 kpc (J) h_r = 4.4 kpc (J)				μ_o = 22.04 μ (J) h_z = 1.56 kpc (J) h_r = 5.9 kpc (J)
NGC 4565	μ_o = 21.47 μ (B) Z_o = 0.76 kpc (B) h_r = 7.3 kpc (B)	19.46 μ (R) 0.74 kpc (R) 4.7 kpc (R)	μ_o = 24.28 μ (B) h_z = 2.36 kpc (B) h_r = 10.7 kpc (B)	23.25 μ (R) 2.92 kpc (R) 10.3 kpc (R)	μ_o = 21.89 μ (B) 21.61 μ (R) Z_1 = 1.12 kpc (B) 1.31 kpc (R) h_r = 4.3 kpc (B) 5.2 kpc (R)

Table 4.1 : Resultant parameters for the programme galaxies after correction for all possible systematic effects and after imposing minimum errors in some cases to bring scale parameters between B and R data into agreement. All surface brightness estimates are given in mag. arcsec^{-2} (μ), and scale parameters in kpc or arcsecs (").

- Chapter V -

Photometric properties of the programme galaxies

V.1 The applicability of standard fitting functions

The principal goal of chapter IV was to determine how well the luminosity distributions of spiral and lenticular galaxies can be described by the adoption of standard fitting functions, and in particular the extent to which the non-thin disc light in each case departs from that of a single model profile. The most important result of this investigation is that, even after applying corrections to remove all possible systematic differences between the predicted and observed luminosity distributions (section V.2 below) and to reduce any possible disparities between the model parameters thus defined in the two passbands (section V.3), the result obtained still show typical rms residuals $\sim$ 0.25 - 0.3 μ in both colours. The question therefore arises as to whether this figure is an absolute limit to techniques of this type.

To place this conclusion in context, I have therefore compared the present results to those derived by van der Kruit & Searle (1981a,b and 1982a,b) - such literature studies being widely considered to be the best currently available. In their analysis of NGC 7814, van der Kruit & Searle (1982b) quote typical residuals of $\lesssim$ 0.2 μ between their predicted and the observed light distribution. However, an inspection of their model fits show that for any particular surface brightness profile, discrepancies considerably larger than this value (indeed of

as much as ± 0.75 μ) are evident. By way of illustration, I show in figure 5.1 a reproduction of their figure 8 in the above paper. In addition to the above random variations, systematic effects are also evident at both small and large Z-heights in all colours. In short, their quoted accuracy of ± 0.2 μ is only attained when taking the results *as a whole*, on a profile-by-profile basis the agreement is generally much worse than this. Such a conclusion is true for all their studies, even for the pure disc systems NGC 4244 and NGC 5907. The aim here is not to single out these studies *per se*, but merely to note that in general the analyses existing in the literature show discrepancies of the form, and of magnitudes equivalent to (and often greater than) those noted in chapter IV. This result should not, in fact, be too suprising - for photometrically "simple" systems such as ellipticals, the agreement between the data and model (even when considering only the radial range in which the fitting functions best describe the observed profiles) is not demanded to be better than ~ 0.1 - 0.2 μ (Kormendy, 1980).

From the quoted literature sources, the modelling techniques commonly adopted are so simplified as to make it impossible to ascertain whether the noted discrepancies are the result of poor quality data, of an inappropriate fitting procedure or because of the general inapplicability of using standard fitting functions (or indeed any combination of the above). In the case of van der Kruit & Searle the first option is considered unlikely as their data are anticipated to be of high quality. Since all the data acquired in this thesis were obtained under essentially identical observational conditions, and because the luminosity distributions were obtained by analysing the data in an identical fashion in each case, this limitation is considered

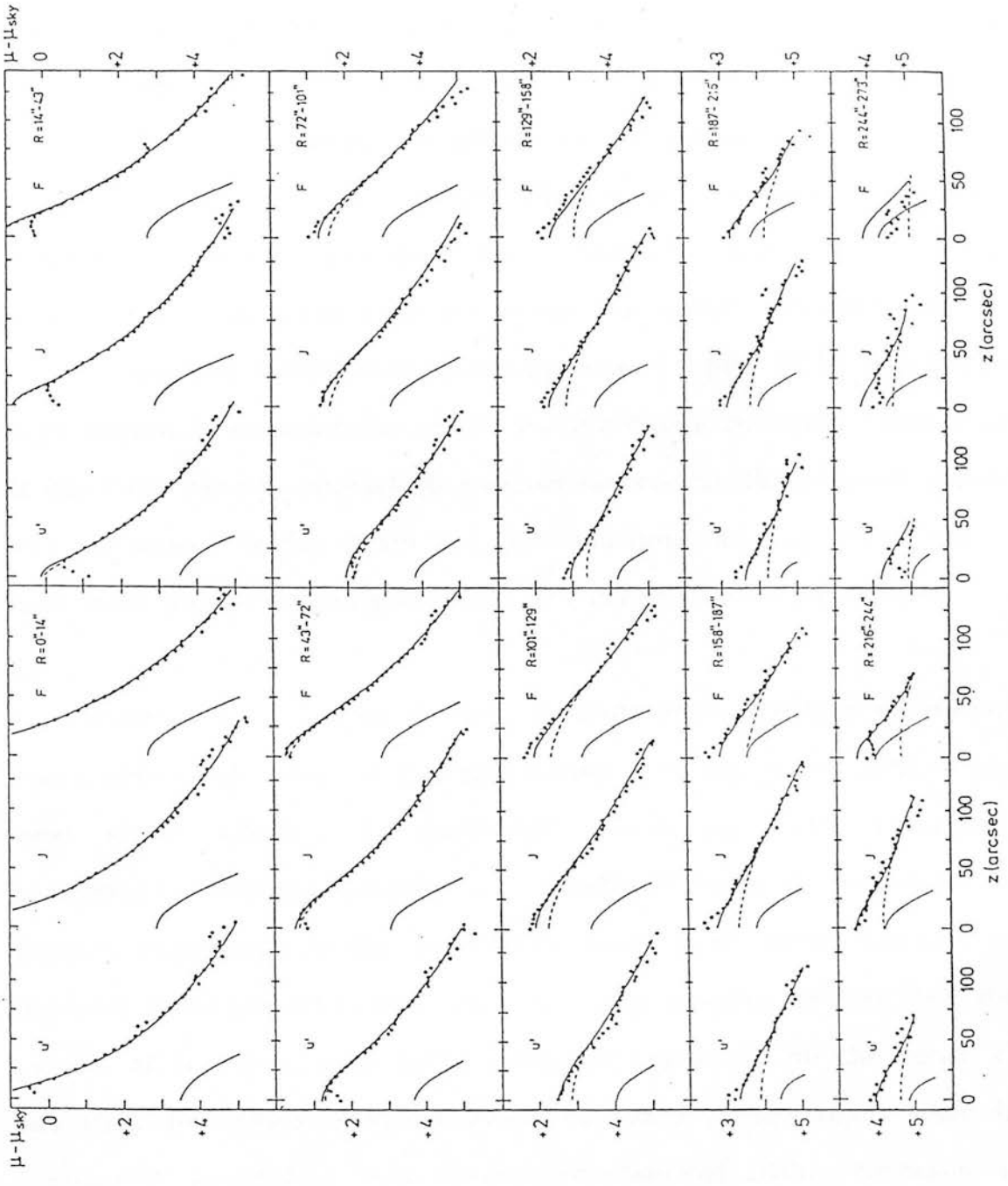

Figure 5.1 : The resultant fits obtained by adopting a two-component "sech^2 + r$^{1/4}$ law" model combination to the data in J, U' and F for NGC 7814. This figure is reproduced from fig. 8 of van der Kruit & Searle (1982b). Galactocentric distances and Z-heights are quoted in arcsecs, and the surface brightness is that relative to sky. The r$^{1/4}$ law profile is represented dashed, the sech^2 profile as the thin full line and the summed profile the bold line.

untenable when comparing the present B and R datasets.

The second point is a more distinct possibility, and any inadequacies in previous schemes have been explicitly determined here by the construction and application of the algorithm described in chapter III. Nevertheless, limitations to the present scheme remain despite the fact that the routine adopted here is one of the best methods currently available for studying galaxian luminosity distributions and is the only one primed for a full, systematic search of the luminosity components within galaxies. Chapter IV attests to the high degree of repeatability of the results obtained, whilst comparison to previous studies applied to galaxies common to the current sample has indicated results which are as consistent as one might expect from such widely differing datasets and decomposition techniques.

However, the fact that all such methods yield typically equivalent rms residuals of $\sim \pm 0.3\ \mu$ strongly implies that the last point is the most likely solution. In particular, since the quite discordant parameters obtained between the passbands studied are seen in galaxies regardless of the number of model components required to describe their non-thin disc luminosity distributions implies that the quality of the data used again does not appear to be the cause of any such disparities. Evidence exists in nearly all systems studied in chapter IV suggesting that the use of standard fitting functions is not an optimal means of elucidating the appearance of galaxies.

No allowance was made within the present modelling procedure for those galaxies in the present dataset which show clear evidence of box and peanut shapes at the brightest isophotal levels because I

aimed to specifically test whether these shapes could be described by the standard fitting functions adopted in all other cases. Although the single box-bulge candidate (NGC 2310) was well-described by the functions adopted, the peanut shapes could not be adequately modelled. In the latter systems, the discrepancies between predicted and observed luminosity distributions took the form of an underestimate of the actual light at the edges of the peanut (i.e. over the regions of greatest Z-height above the major axis) by ~ 0.25 to 0.75 μ. These values correspond to excesses ~ 6 % in B and 10 % in R over the model luminosity predicted in that particular region. The fainter isophotes were, however, well-fitted in most cases. This seems to concur with the study of NGC 4565 presented in chapter III in suggesting that the peanut is a feature quite distinct from the other non-thin disc constituents modelled here, and is not merely an inward concentration of the "outlying" components.

V.2 The form of "sky" systematics

One of the most notable aspects of the results in chapter IV is that, even after having defined the particular model combination found to be the most suitable in each particular case, fully 2/3 of the sample showed such models to systematically overestimate the actual luminosity distributions at large Z-heights over almost all profiles in one or both of the photometric passbands studied. This section, therefore, outlines an attempt to ascertain the extent to which these effects could be accounted for by systematic errors in the sky estimates used in each case.

By changing the sky estimates in each galaxy as appropriate, improved model fits (in terms of reduced sums of squares of residuals over those obtained previously for the same model combination) were derived in all cases. However, whilst it is certainly true that the sky measures for NGC 3115 and, to a lesser degree, NGC 5078 are likely to be poorly defined because of the limited number of pixels in each data array not contaminated by light from the galaxy, this limitation is considered unlikely in all other galaxies for which systematics are seen. Furthermore, removal of such effects requires the sky estimates to be reduced to bring data and model into agreement, although in the light of the methods by which the sky values were derived (section II.3.7), a reduction in I_{sky} seems highly unlikely (because the lower intensity region of the assumed Poisson distribution of pixel intensities is very well-defined). For the greater proportion of galaxies so affected, changes in $I_{sky} \sim 4$ times the assigned errors in table 2.2 are required (these errors being based on a visual estimation of the accuracy with which the modal peak can be determined). Thus, the systematic trends noted in chapter IV can only be accounted for by an implausibly large modification of the local sky estimate particular to each dataset being modelled.

It is, therefore, important to define whether an alternative source of such systematics exists other than from uncertainties in the adopted sky value. The possible inapplicability of the model profiles being adopted has already been alluded to above and was a further possibility to be investigated. Because the systematics occur over the region of the profiles for which the $r^{1/4}$ law was invariably the major contributor to the summed model luminosity distribution, I sought to test the above hypothesis by conducting iterations in a similar vein

to those used to define the variations in disc scaleheight with $\mathbb{R}$ in chapter IV, but in this case choosing the axis ratio to be the free parameter. Only those (4) galaxies for which clear non-thin disc components are seen (those showing box/peanut morphology being specifically excluded) were investigated. However, it is noted that for only 3 of these systems - NGC 3115, NGC 3573 and A0919-33 - is the $r^{1/4}$ law profile an adequate description of the non-thin disc light, an exponential profile being most appropriate for NGC 5170.

The results of such a procedure are illustrated in figure 5.2, which shows variations in axis ratio with $\mathbb{R}$ for the data in both passbands together with those for the ratio q(B)/q(R). The axis ratios used in this figure are those given in table 4.1. Any systematic variations of axis ratio with $\mathbb{R}$ appear precluded in all systems, although the highly disturbed nature of the dust lane in NGC 3573, and its corresponding effect on the model results derived for the non-thin disc component, is such that measures in this case are considerably less certain than those of the other three candidates. The shapes of the non-thin disc isophotes appear equal in both B and R for all galaxies in this figure.

Strom et al (1977) and Strom & Strom (1978) have undertaken a similar investigation of the correspondance between isochrome and isophote shapes for NGC 3115. These studies conclude that interior to a semi-major axis of 60", the isochromes are flatter than the isophotes, whilst from 60" $\lesssim$ b $\lesssim$ 120" they are equivalent in shape. However, the changes between U and R found by them are very small ($\lesssim$ 10 %). The differing spatial scales concerned in these studies compared to the present work are such as to make a detailed

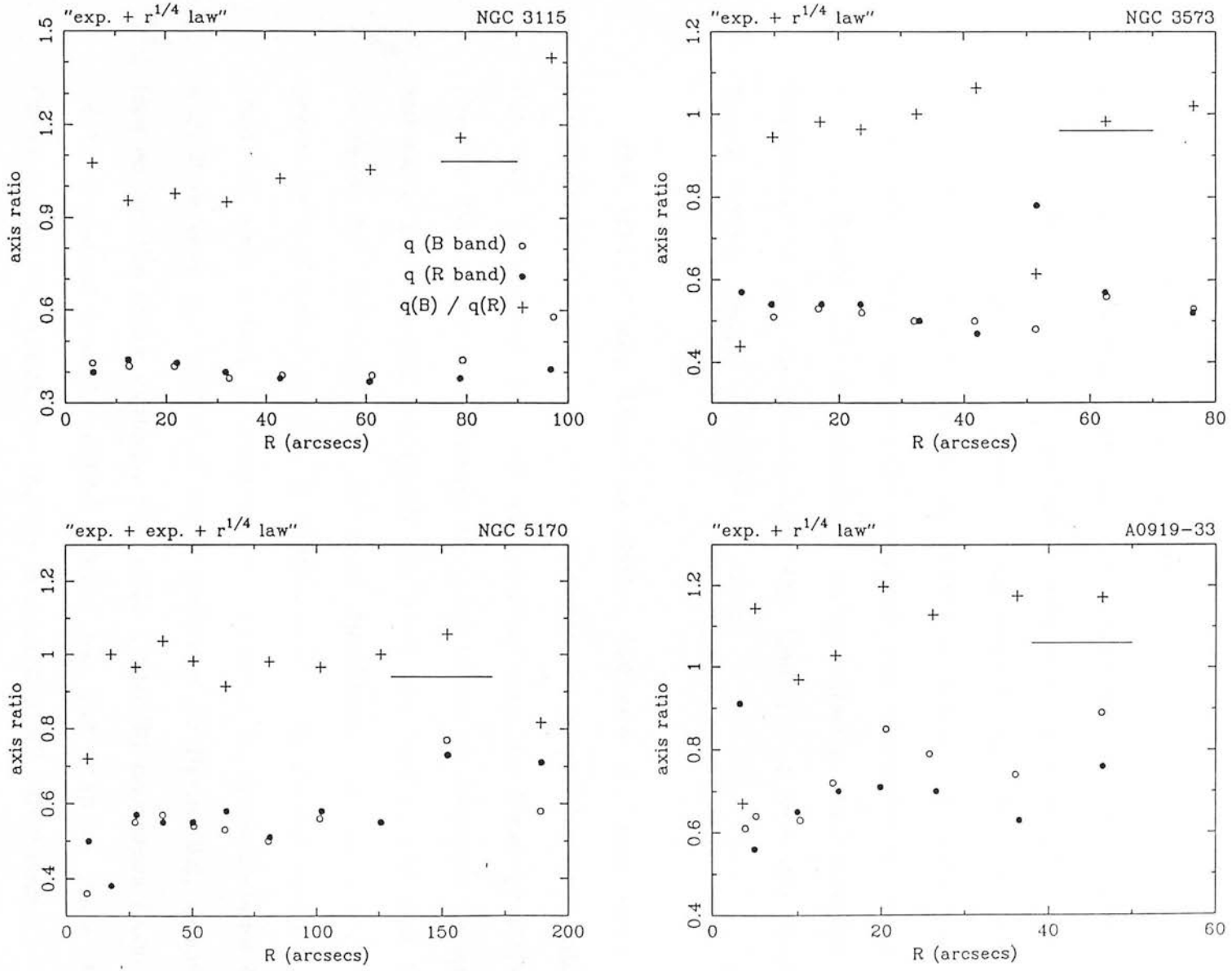
"exp. + r^1/4 law"
NGC 3115
axis ratio
R (arcsecs)
q (B band)
q (R band)
q(B) / q(R)
"exp. + r^1/4 law"
NGC 3573
axis ratio
R (arcsecs)
"exp. + exp. + r^1/4 law"
NGC 5170
axis ratio
R (arcsecs)
"exp. + r^1/4 law"
A0919-33
axis ratio
R (arcsecs)

figure 5.2

comparison difficult. In addition, because all such analyses rely upon due account of the presence of the disc component, such results must be viewed as somewhat model dependant in each case (particularly in the present study in which the disc scalelengths remain quite dissimilar between the respective passbands). Thus, it may be unwise to place too much weight on a detailed comparison between the respective analyses, other than to note that, for the one galaxy in the present sample for which a previous investigation has been undertaken, the results obtained are qualitatively similar to those in figure 5.2. An equivalent shape between the isophotes and isochromes is also in accord with the findings of van der Kruit & Searle (1981b, 1982b).

The lack of any clear correlation between the axis ratio and galactocentric distance strongly suggests that a variable axis ratio is not able to account for the systematics seen in these galaxies in chapter IV. This was confirmed by performing an identical series of iterations but on data for which the local sky background had been changed by the amounts required to bring the observed and predicted luminosity profiles into agreement - figure 5.3 showing the result of such a test. A considerable reduction in the variations of q with $\mathbb{R}$ is seen for NGC 3115 when compared to figure 5.2, somewhat less so for the other systems. The ratio q(B)/q(R) decreases from 1.08 (±0.05, standard error) to 1.00 (±0.01) for NGC 3115 in going from figure 5.1 to 5.2, whilst the change is $\lesssim$ 13 % in all other cases.

In conclusion, the systematic trends noted in chapter IV cannot be accounted for by allowing the $r^{1/4}$ law to possess a variable axis ratio with $\mathbb{R}$. They can only be considered to result either from an

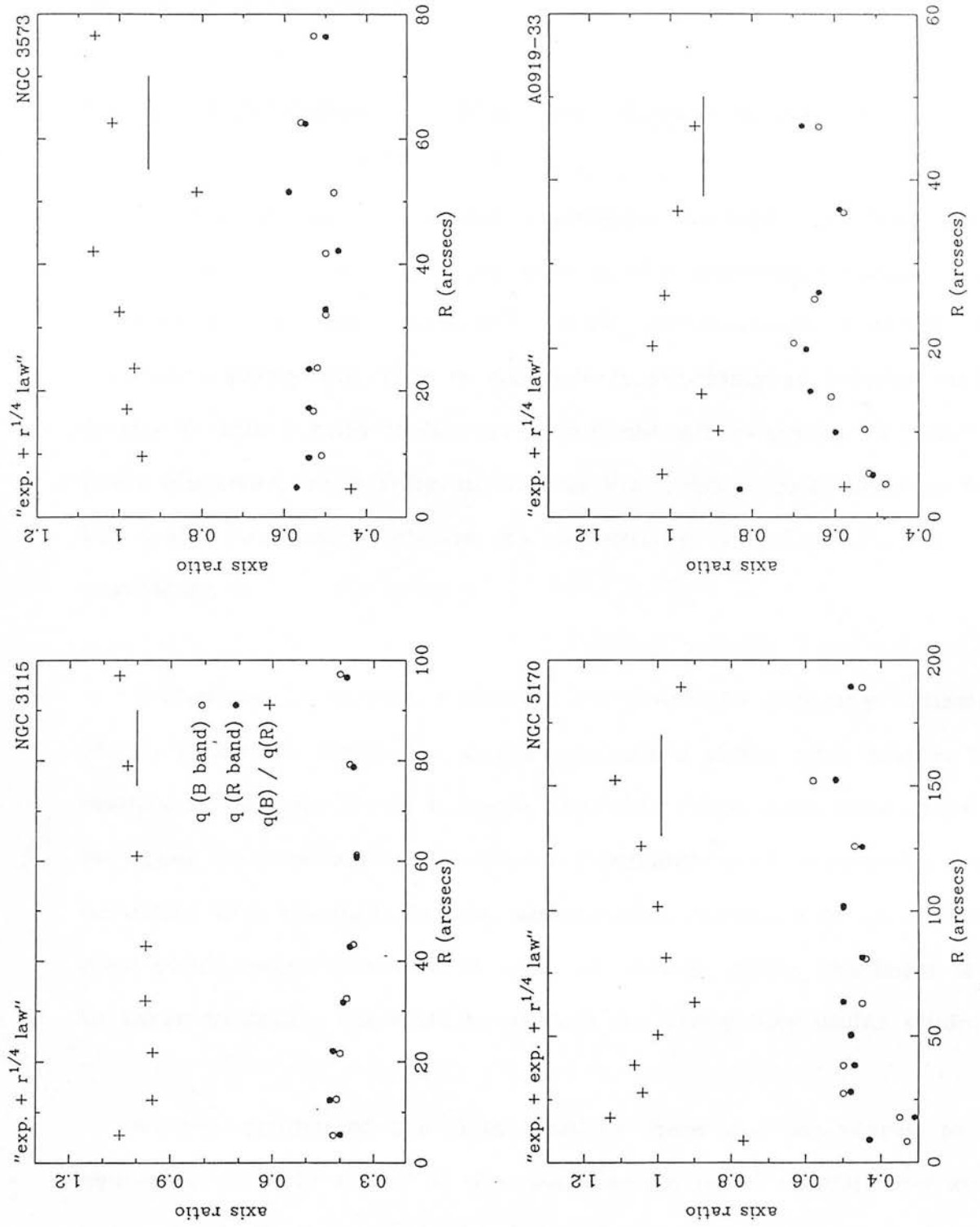
NGC 3573
A0919-33
NGC 3115
NGC 5170
"exp. + r^1/4 law"
"exp. + exp. + r^1/4 law"
axis ratio
R (arcsecs)
q (B band) ○
q (R band) ●
q(B) / q(R) +

figure 5.3

implausibly large error in the assigned local sky background level in each case, or as a result of the fact that the model profiles adopted are inadequate to describe the luminosity distributions observed.

V.3 Parameter differences between the photometric passbands

An equally significant and restrictive condition to that of the systematics at large Z are the consistently discrepant output model parameters for the "best-fit" model combinations between the respective passbands. This is particularly suprising as division of the B and R data frames yields no significant structure in all cases (a point discussed more fully in section V.5 below), thus implying that all scale parameters should be essentially identical in the two passbands.

Unfortunately, previous studies are unable to give any indication of the extent to which the model parameters differ with colour. The studies of van der Kruit & Searle explicitly force such parameters to be equal in all colour bands studied, although such a procedure can be called into question (unless independant modelling of each colour does yield similar parameters) as it is unclear which passband is to be taken to define the scale parameters for the galaxy under study.

As the quality of the data obtained here are considered to be equivalent in both B and R (for the reasons noted above), and since the present disparities are clearly not the result of systematic effects in the respective datasets (removal of which still yield the differences found previously), the other possible source are the differing error distributions adopted in the two cases.

The possible significance of the error distributions adopted in the present work were tested by re-running those "best-fit" model combinations defined in chapter IV, but with minimum errors assigned to each dataset being modelled. The results obtained in each case are outlined in that chapter, but in general the equivalence of those scale parameters which were originally very discordant between B and R can be improved to ~ 20 - 30 % by imposing a suitable lower limit on the error assigned to each data point (typically ~ ± 0.15 - 0.2 μ). The net result of this procedure is to reduce the largest discrepancies between the predicted and observed luminosity distributions - although a visual inspection of the residuals diagrams thus obtained indicates that random scatter ~ ± 0.2 μ still remains within each passband.

The parameters for three galaxies remained discordant after adoption of such a procedure, however. It would appear that the extreme peanut morphology at the brightest isophotes of IC 2531 ensures that such a galaxy cannot be well-described by any set of model combinations tested here (regardless of the corrections applied). Modifying the adopted error distributions in such a way as to bring the $r^{1/4}$ law parameters into better agreement only serves to reduce the similarity between the disc values between B and R. The same general conclusion appears to be true for A0902-68 which, additionally, suffers from the fact that the peanut morphology dominates the total light output in this case. The remaining differences for NGC 3115, whilst smaller in magnitude than those of the previous two cases, are suprising in the light of the seeming simplicity of this galaxy. It seems likely that the limited spatial coverage of the present data, coupled with the correspondingly

limited dynamic range (of only the brightest isophotal levels), has a significant effect on the model parameters derived in the present work.

Considerable improvements are, however, noted in all other cases by the adoption of such a "minimum error" procedure, both for galaxies showing "normal" non-thin disc light distributions and those showing box/peanut morphology. However, the large minimum errors required are not taken as evidence that the data being modelled are only well-defined to these levels of accuracy, but that they are simply the errors one has to adopt in each case to yield repeatable parameters in each colour. This is taken as further evidence of the inapplicability of the fitting functions adopted, at least to the point of requiring consistency between the different passbands to better than ~ 30%.

V.4 Implications of the present results

One particularly important result can be extracted from table 4.1. Ten galaxies in the present sample (seven of them not showing box/peanut morphologies) are found to possess clear non-thin disc populations, although the results of chapter IV explicitly exclude the existence of two model components in these systems. Added to this is the fact that in the case of NGC 891, chapter III shows the non-thin disc light to be best described by any fitting function other than an $r^{1/4}$ law profile - the parameters thus defined being more akin to those of an intermediate component. Thus, there does not appear to be a one-to-one correspondance between the existence of an $r^{1/4}$ law profile in a galaxy and that of an intermediate population.

It is, therefore, possible that the possession of a disc component is a necessary requirement for a galaxy to show evidence of an intermediate population. Of course, I am unable to investigate such a hypothesis further because the present dataset does not specifically include any non-disc galaxies. Nevertheless, such an proposition is important to test as it has a bearing on possible formation schemes for intermediate components, particularly those resulting from events having taken place subsequent to initial galaxy formation. On the basis of recent work by Quinn & Goodman (1986), for example, it appears possible that the accretion of a satellite by a pre-existing two component galaxy could, under certain conditions, give rise to the creation of a "thick disc" component by substantially increasing the random motions of the disc stars in the Z direction. One might, therefore, conclude that table 4.1 merely serves to pinpoint those galaxies in which such an accretion event could have taken place. That the host galaxy concerned is required to have possessed such satellite systems needed to give rise to the disc "thickening" does not appear to be a major constraint (Toomre having argued that almost all galaxies in the NGC catalogue are likely to have undergone mergers at some time in their past). A more restrictive condition is that a disc of some form must exist prior to the creation of the intermediate component itself.

If the work of Schuster & Nissen (1987) is interpreted as evidence for a similar age of all non-thin disc populations seen in our own Galaxy, then to invoke this "disc thickening" mechanism would therefore require the relevant accretion event to have occurred at the same epoch as the formation of each non-disc component. It is unclear at present how substantial the disc is required to be to

account for the intermediate components seen.

In conclusion, from the modelling results in chapter IV it appears that no one model combination, or set of model parameters, appear sufficient to describe the luminosity distributions of all the galaxies analysed in the present dataset.

V.5 Radial disc cutoffs

One of the most suprising, and potentially most significant, conclusions of van der Kruit & Searle (1981a, b, 1982a, b) is the existence of apparent "edges" to the disc components of spiral galaxies, several of which showed a typical e-folding ~ 1 kpc at a position ~ 4.5 scalelengths from the nucleus. If real, such a result implies that star formation is ineffective at, and beyond, these disc positions.

A number of candidates exist within the present dataset for which complete spatial coverage of the disc components is available to allow one to address the existence of such radial cutoffs. However, only NGC 4469 has data to 4.5 disc scalelengths based on the final model parameters in table 4.1.

Surface brightness cuts parallel to, but offset from, the major axis would not suffice to determine the existence of radial cutoffs as one must determine the extent to which the actual disc light falls below that predicted by the model at some specified Z and R. Thus, a search for disc cutoffs should ideally seek systematic overestimations of the model compared to the true disc luminosity distribution at

large R. A study of all "best-fit" diagrams in chapter IV reveal no such systematics at small Z-heights (where the surface brightness is dominated by light from the disc) for NGC 4469 beyond $5h_r$, implying that no radial disc cutoff exists in this case. An inspection of the current data suggests, in fact, that the disc of this galaxy may well extend beyond the edge of the image frames obtained (which correspond to ~ 5.5 scalelengths in the B band).

It might be argued that the nature of the modelling routine itself is such that no evidence for a cutoff would ever be found because the model parameters defining disc and bulge would be modified sufficiently to fit the data regardless (data at small Z being assigned the largest weight). However, were a radial cutoff present, the shape of the luminosity distribution would change substantially when comparing perpendicular surface brightness profiles interior and exterior to the cutoff point. A visual inspection of all profiles taken across NGC 4469 revealed no evidence of such changes. Disc cutoffs were also not seen in any of the other systems outlined above, although in the light of the predictions of van der Kruit & Searle this is to be expected as none of them have data available at sufficiently large R. On the basis of the model parameters in table 4.1, such systems were modelled over data of spatial extents ranging from ~ 0.2 disc scalelengths in the case of A0931-32 to one of ~ 4 scalelengths for A0902-68.

V.6 Colour gradients

An important means by which constraints can be imposed on galaxy formation histories is by placing limits on the existence of

colour gradients within the non-disc components of spiral galaxies.

A first impression of the evidence for such gradients in the present dataset comes from figure 5.4. This illustrates the results obtained by defining the mean colour index within apertures of increasing radius centred on the nuclei of the galaxies concerned. Although 9 of the present sample have photometry in both passbands, only 8 of these have sufficient spatial coverage to allow aperture colour indices to be defined, and only 4 show no evidence of non-linearity/saturation effects at the centre.

From this figure one would deduce that global changes in colour are seen across the spirals/lenticulars studied, with a smooth and more gradual trend towards bluer colours with increasing $\mathbb{R}$ for the two later-type systems (UGC 7170 and IC 2531), and very red central regions in the earlier types, beyond which a roughly constant colour is seen. For the later-type systems, such colour changes amount to -0.016 mag kpc^{-1} in both cases, over radial scales of 1.2 to 10.6 kpc for UGC 7170 and 2.1 to 11.7 kpc in the case of IC 2531. In addition, the range of (B-R) colours implies that the earlier-type systems are inherently redder than are the later-types. Such results are to be expected - late-type galaxies show an increased thin disc contribution (consisting of young, blue stars) and thus have smaller mean (B-R) colours, whilst the more noticeable trend towards bluer colours with increasing $\mathbb{R}$ merely indicates the increasing importance of the disc in such systems. However, diagrams such as figure 5.4 have to be treated with some caution since any circular aperture photometry of the form adopted here must, by definition, include within the aperture regions of the galaxy for which the presence of the dust lane

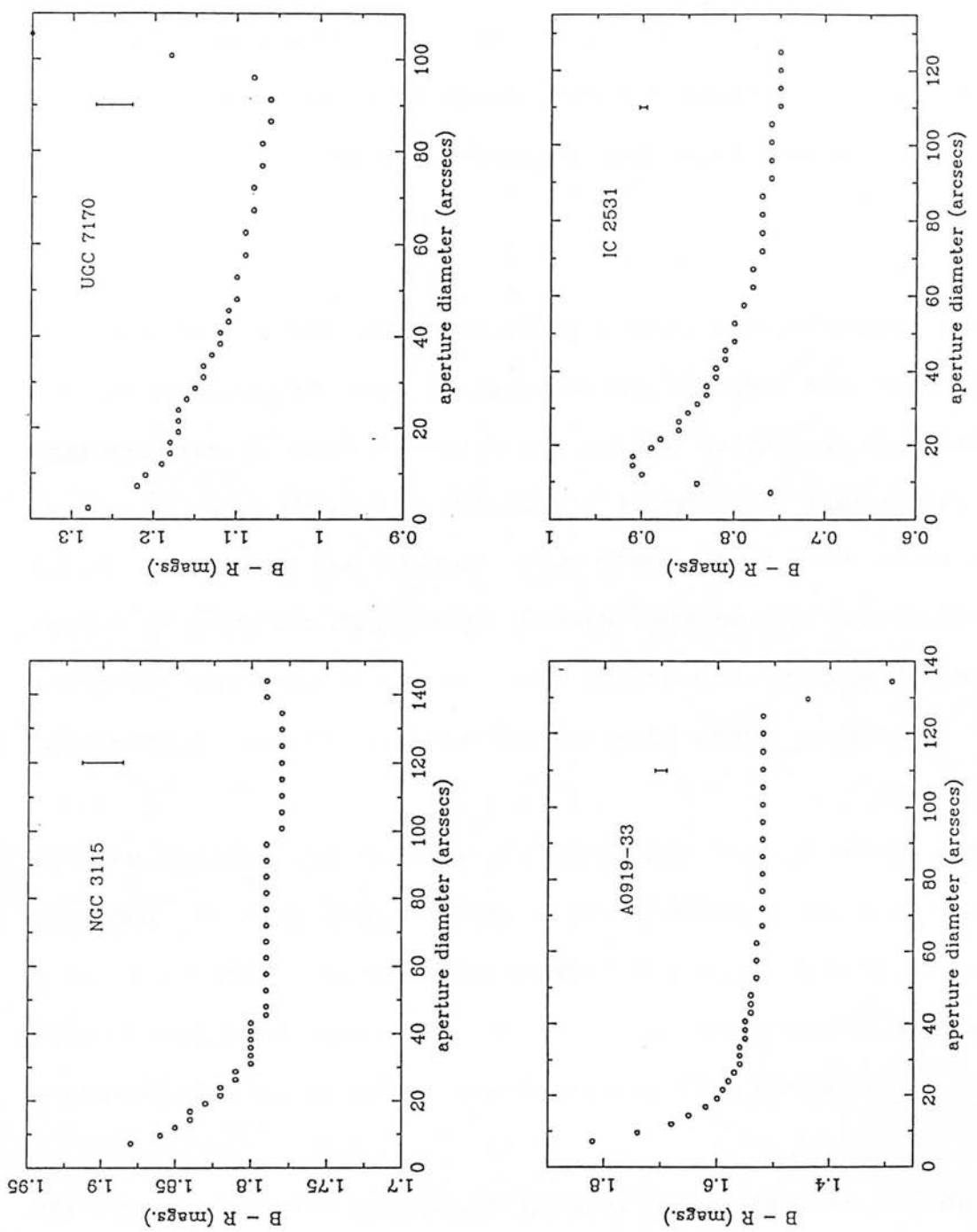
UGC 7170
B − R (mags.)
aperture diameter (arcsecs)
IC 2531
B − R (mags.)
aperture diameter (arcsecs)
NGC 3115
B − R (mags.)
aperture diameter (arcsecs)
A0919−33
B − R (mags.)
aperture diameter (arcsecs)

figure 5.4

precludes the extraction of meaningful results. Furthermore, as the influence of the dust lane varies over differing radial scales, it is impossible to allow for its influence. In particular, the interpretation of colour changes within such apertures is very difficult owing to the inclusion of (likely varying) effects from all constituent components in the galaxies concerned in addition to the effects of the dust lane itself.

Thus, with a view to undertaking a more specific search for the possible existence of colour changes in the non-thin disc regions, the final data arrays used to extract the surface brightness data used in chapter IV were divided to produce a global (B-R) map across each galaxy. Because of the inherent noise which arises when undertaking such a process, the data arrays derived were heavily smoothed using a 9-point smoothing algorithm. Two points are particularly notable from a visual inspection of the contour plots which result :

(1) All nuclear regions show a substantially redder colour than do the rest of each galaxy after division, thus accounting for the pronounced colour changes seen at small $\mathbb{R}$ for both NGC 3115 and NGC 3573 in figure 5.4. Again the presence of the dust lane is likely to be a considerable factor influencing colours at such positions.

(2) Aside from the expectedly complex structure seen in the dust lanes concerned, no large scale colour gradients appear to exist across any galaxy.

The second point was confirmed after deriving variations of (B-R) with both $\mathbb{R}$ and Z for the galaxies in figure 5.4. A binning procedure

was adopted in an attempt to maintain S/N in the mean colours obtained at any position across the galaxy of interest, with the following results :

	colour gradient	parameter range
NGC 3115	0.0004 (± 0.0011) mag kpc^{-1}	$0 < R < 1.4$ kpc
	0.041 (± 0.047) mag kpc^{-1}	$0 < Z < 0.6$ kpc
NGC 3573	-0.0012 (± 0.0032) mag $arcsec^{-1}$	$0 < R < 70$ arcsec
	-0.0011 (± 0.0038) mag $arcsec^{-1}$	$0 < Z < 45$ arcsec
NGC 5170	-0.020 (± 0.009) mag kpc^{-1}	$0 < R < 16$ kpc
	0.0004 (± 0.0467) mag kpc^{-1}	$0 < Z < 3.5$ kpc
A0919-33	0.0010 (± 0.0021) mag $arcsec^{-1}$	$0 < R < 50$ arcsec
	-0.0029 (± 0.0041) mag $arcsec^{-1}$	$0 < Z < 30$ arcsec

The blueward trend in (B-R) with increasing radial distance in the case of NGC 5170 is due to the colour change within the disc component (which dominates the luminosity distribution in this system over almost all R and Z). However, in no other case is there any evidence of a gradient with R or Z (although the limited spatial coverage of NGC 3115 precludes identification of a small gradient over larger dimensions were one to exist). Such a result is somewhat suprising in view of the work of Wirth (1981) and Wirth & Shaw (1983) who found evidence of (B-V) gradients in most of the galaxies in their sample, and in particular a stronger gradient in Z for the latest Hubble types. The above results appear to rule out any such gradients perpendicular to the plane, although the earlier studies would imply that a gradient ~ 3 or 4 times larger in NGC 5170 or A0919-33 than in NGC 3115 and NGC 3573 should be seen. Unfortunately a more detailed comparison is not possible as they do not quote the spatial scales over which the gradients seen by them were measured. Even so, it would be difficult to reconcile the present null detections as being due to limited spatial coverage in all except

NGC 3115 itself.

Additionally, I undertook a search for colour gradients within the box/peanut bulges. In no cases were significant differences noted between these morphologies and the rest of the constituent galaxies. More specifically, differences in colour indices of 0.01 mag. were found for both NGC 2310 and IC 2531 (corresponding to ~ 7 % and 11 % respectively of the standard errors assigned to the colour indices of the box/peanut features themselves), whilst both A0902-68 and NGC 4469 show differences of 0.04 mag. (30 % and 67 % respectively of the standard errors).

The evidence as to whether colour gradients are a common feature of the non-thin disc light in spiral and lenticular galaxies is still uncertain owing to the conflicting conclusions to be found in the literature for additional edge-on candidates. Jensen & Thuan (1982), for example, find no evidence of any such gradients in (B-R) within the non-disc regions of NGC 4565. However, van der Kruit & Searle (1981b, 1982b) find clear evidence of gradients between all the colour indices defined in their studies of both NGC 891 and NGC 7814. The largest gradients seen in the latter systems (i.e. in (U'-F)) are -0.06 (± 0.01) mag. kpc^{-1} for NGC 891 (over $0 \lesssim R \lesssim 15$ kpc) and -0.096 (± 0.041) mag. kpc^{-1} for NGC 7814 (over $1.2 \lesssim Z \lesssim 10.9$ kpc).

The interpretation of colour gradients (or lack thereof) within the context of the stellar population mix of which the non-thin disc regions are comprised is very uncertain as a large number of possible parameters may be involved. However, if one interprets the colour as being due to a metallicity effect, as is now commonly believed to be

the case, then the above results would imply an essentially uniform metallicity distribution over all regions exterior to the thin disc component. A similarity in age is thereby predicted for the constituents of the non-thin disc light if all such populations follow the same age-metallicity relation.

V.7 The intrinsic flattening of spiral bulges

A common misconception in galaxy morphology concerns the shapes of the non-thin disc light in spiral galaxies (which are typically anticipated to have axial ratios ~ 0.8). An inspection of, for example, sky survey plate material immediately confirms galactic bulges to be inherently flat objects. This is particularly well illustrated in figure 5.5 which shows q as a function of the ratio of the non-thin disc light to that of the total luminosity of the galaxy. The latter ratio was derived from the absolute magnitudes of the constituent components (which in turn were those obtained by using the magnitude and scale parameters in table 4.1 and adopting the relations between absolute magnitude, surface brightness and scalelength given in Kodaira et al (1986)). All galaxies in the present sample for which clear non-disc populations are defined in the modelling of chapter IV have axis ratios smaller than 0.69, and ~ 60 % of this subset have $q \lesssim 0.4$. Such ratios are means over the whole dataset in each case, and are thus applicable to all data ranging from that over which the model profile first proved to be the major contributor to the total light distribution (i.e. ~ 20 μ_B along the minor axis and ~ 24.5 μ_B at the largest galactocentric distances) to the limiting surface brightness values of the current photometry (of ~ 26 μ_B).

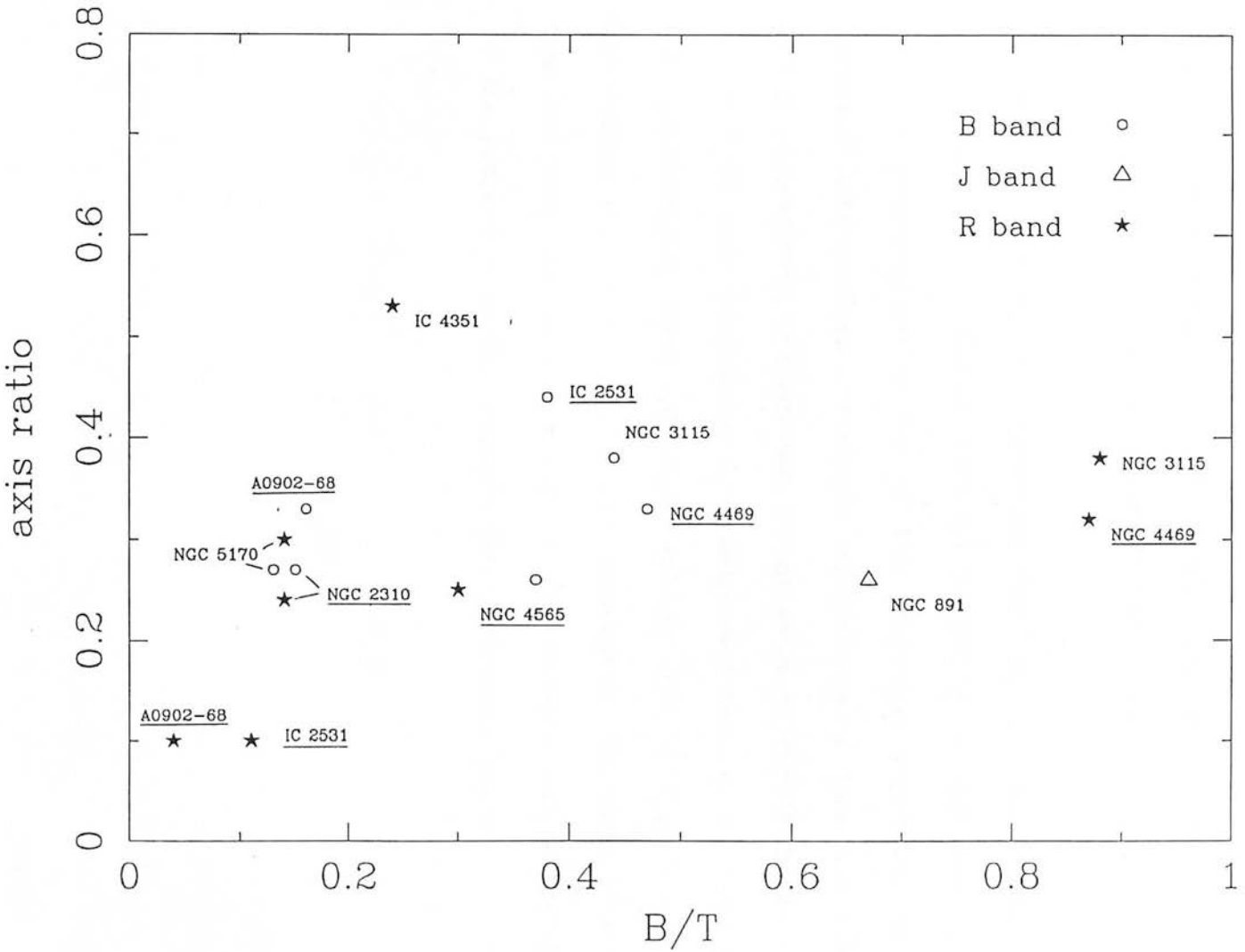
axis ratio
B/T
0
0.2
0.4
0.6
0.8
1
B band
J band
R band
IC 4351
IC 2531
NGC 3115
NGC 4469
A0902-68
NGC 5170
NGC 2310
NGC 4565
NGC 891
A0902-68
IC 2531
NGC 3115
NGC 4469

figure 5.5

Of course, such estimates also include those of a number of box/peanut candidates - these galaxies being underlined in this figure. However, removing the box/peanuts does little to change the above conclusion - mean axis ratios of 0.45 (± 0.08) in B and 0.42 (± 0.06) in R being found when the box/peanuts are not considered and 0.38 (± 0.04) and 0.34 (± 0.05) respectively when they are.

What is particularly interesting from this figure is the lack of any significant correlation between flattening of the non-disc light and the existence or nature of the thin disc population in either passband (the derived correlation coefficients of 0.43 and 0.46 in B and R respectively are not significant even at the 90 % level). This result is of some importance for galaxy evolution, as it indicates that the gravitational field of the disc is not a significant factor influencing the overall morphology exterior to the disc. This implies that the very flat isophotes seen in the present sample are dictated by the properties of the non-thin disc population itself.

- Chapter VI -

The nature of "box" and "peanut" shaped galactic bulges

VI.1 Introduction

Evidence has been available for many years indicating the existence of a number of spiral galaxies which seem to display box- or peanut-shaped central bulges when viewed from an approximately edge-on aspect (see, for example, Burbidge & Burbidge, 1959). By box-shaped are meant bulges whose light distribution shows a pronounced cut-off in both galactocentric distance and Z-height, and hence gives the appearance of being square. Peanut-shaped bulges show similar features but also possess a depression in isophotal shapes along the minor (rotation) axis of the galaxy, thereby giving the semblence of a "figure-of-eight" when viewed in the plane perpendicular to this axis. Such features are illustrated in the montage of intensity contour plots and photographic prints presented in figure 6.1 and also the contour plots of NGC 2310 and NGC 4469 in figure B.2 of appendix B after digital unsharp masking.

To date, however, little work has appeared either concerning the objects already known to display these features or, more generally, of defining precisely how common such structures really are. Their importance stems primarily from the fact that they must be accounted for in any proposed general scheme of formation of spiral galaxies were they shown to be present in a statistically significant fraction of spiral bulges. They would thence provide an additional means of comparing the photometric properties of bulges with ellipticals of similar absolute magnitude. Further, were such features found to be

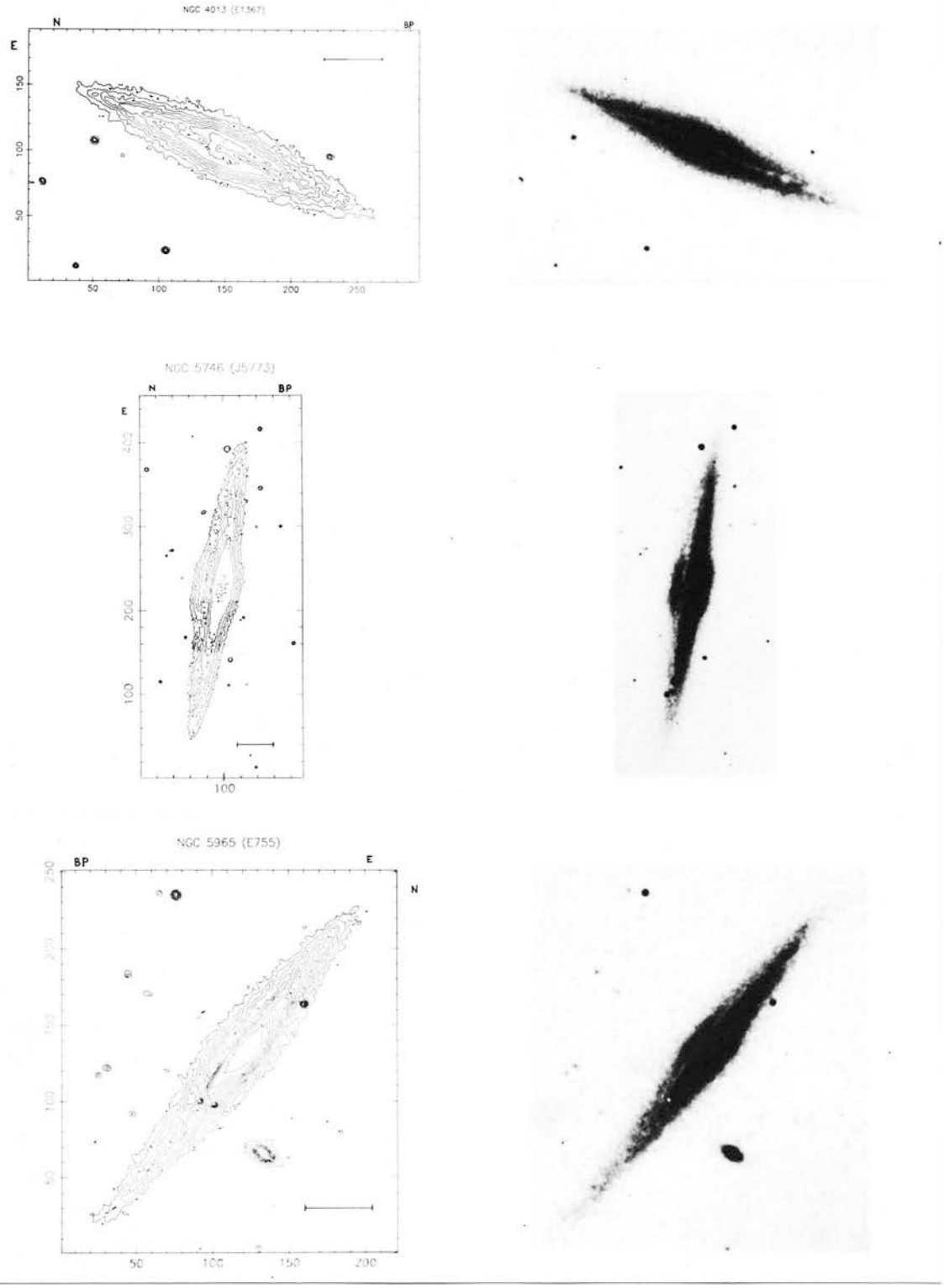

Figure 6.1 : A montage of photographic prints and contour plots for a representative subset of the Sb to Sbc types in the current edge-on galaxies sample. The contour plots are derived from COSMOS mapping mode scans, using a 16μ spot size, of ESO/SERC J or POSS R band survey plates. The relevant plate numbers are given together with the galaxy name, whilst the contours are set at arbitrary logarithmic intensities. The numbered X and Y axes are in pixels and the scalebar represents 50 arcsecs in each case. The photographic material is derived from the same sources as the contour plots, with each print reproduced at normal contrast to the same scale as that of the plot. Prints taken from the POSS are © Palomar Observatory/National Geographical Society.

Additionally, each galaxy carries a descriptor signifying whether it is classified as a clear box/peanut candidate (BP in figure 6.1a); whether it is defined as an uncertain or marginal example (U in figure 6.1b); or where it is considered for the present study that no box/peanut exists (No in figure 6.1c).

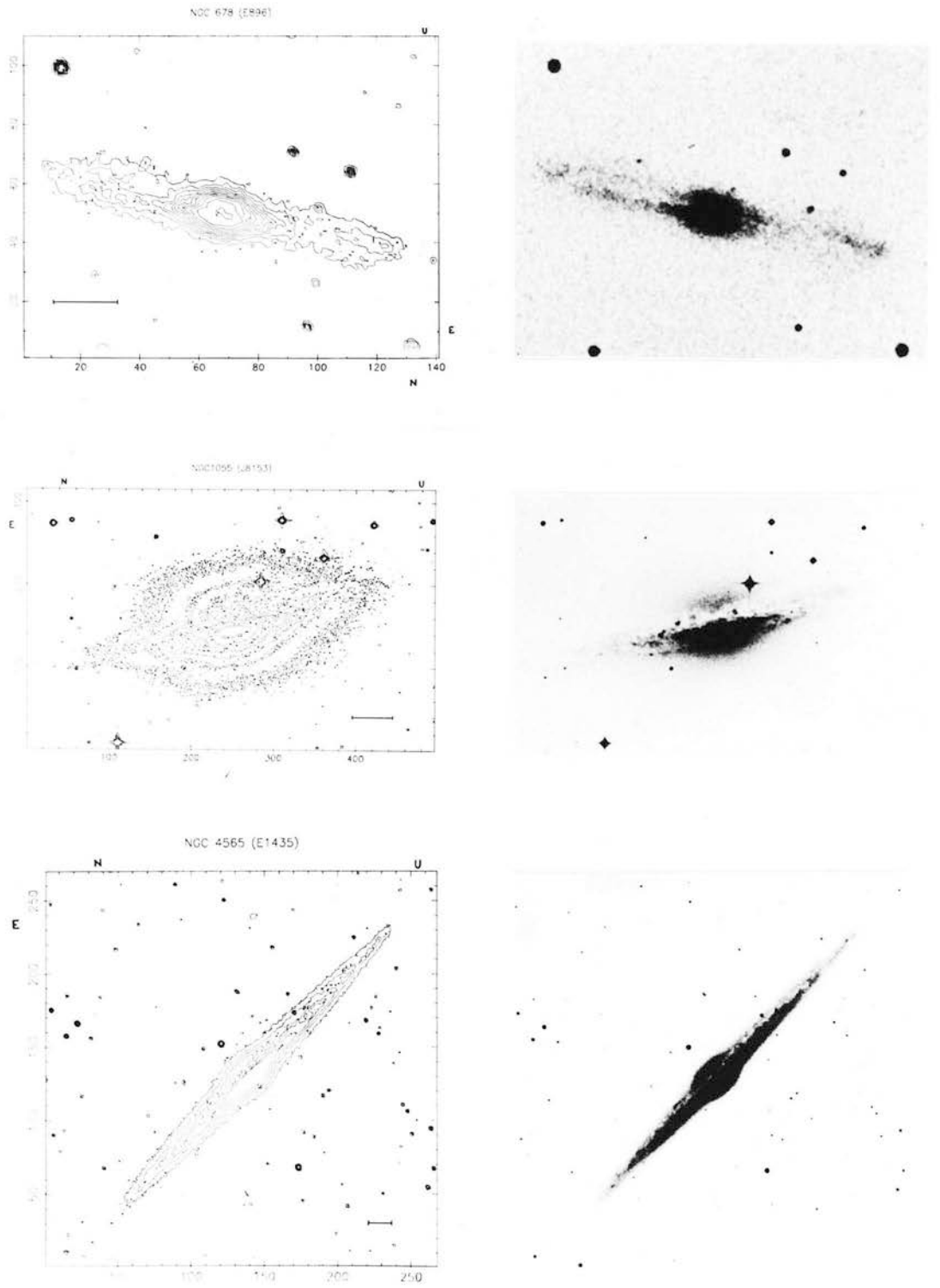
NGC 678 (E896)
U
E
N
20
40
60
80
100
120
140
N
U
E
N
U
E
NGC 4565 (E1435)
N
U
E
100
150
200
250

figure 6.1 (b)

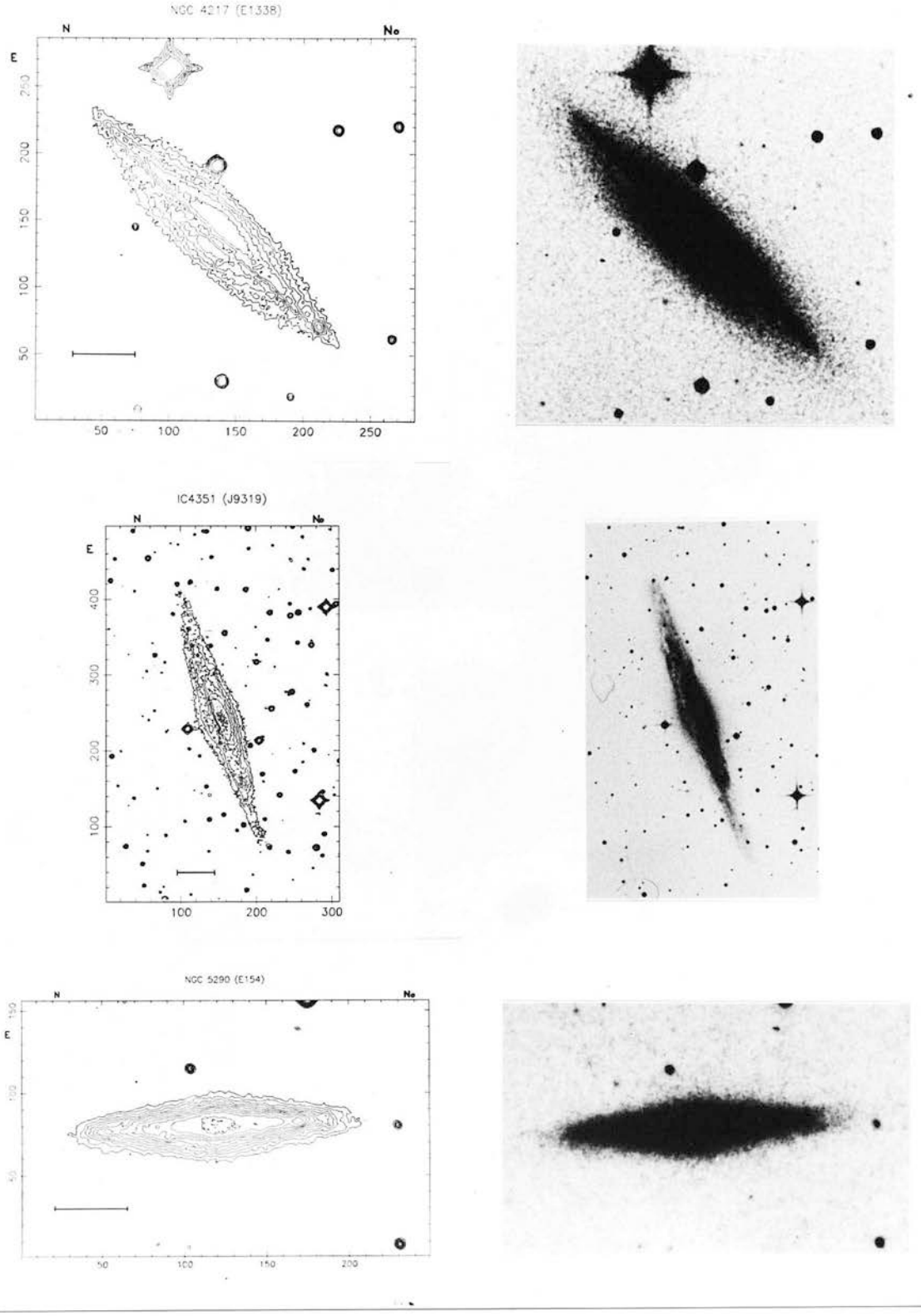
NGC 4217 (E133B)
N
No
E
50
100
150
200
250
IC4351 (J9319)
N
No
E
100
200
300
400
NGC 5290 (E154)
N
No
E
50
100
150
200

figure 6.1 (c)

associated with galaxy mergers, a study of them would provide us with a valuable estimate of the expected frequency of mergers in spiral galaxies since their formation.

It is the potential importance of such distortions in bulge shape, together with the current paucity of available evidence concerning their frequency of occurrence, which has led me to initiate a survey of all 4364 entries of the RC2 supplemented by separate lists of large northern and southern edge-on candidates kindly supplied by Corwin as noted in chapter I.

VI.2 The survey

The present survey is the second to have been carried out with this intention - the first (Jarvis 1986, henceforth J86) centering on all galaxies in the ESO catalogue south of declination -18^{0}. Since the earlier work was carried out using a completely different methodology and a different galaxy source list, it provides a useful means of defining the completeness of my own survey, of identifying the significance of selection effects for both and also to check the results of the earlier study.

VI.2.1 Sample definition

The sample on which this survey is based is that of the 117 large, normal, edge-on spiral and lenticular galaxies defined in chapter I. The choice of sufficiently edge-on candidates is of critical importance for the current work, since the anticipated magnitudes of the bulge distortions of interest are sufficiently small in comparison

to the total light output from the disc that contamination by the latter must be reduced to an absolute minimum.

These objects are collated into groups on the basis of their appearance on the ESO/SERC survey plate material - those not displaying clear box- or peanut-shaped central bulge isophotes being grouped according to their apparent bulge:disc ratio as defined on such plates (henceforth termed disc dominated, bulge dominated and intermediate types). Uncertain cases are further investigated by image enhancement techniques applied to scans from the relevant plate material by COSMOS (such as those discussed in appendix B), or by using previous investigations of the objects concerned to be found in the literature. Successful identifications of 75 % of the "uncertain" cases result from a combination of these procedures. Those which remain undefined are grouped according to their apparent dominance of bulge or disc and not counted with the box/peanuts. Salient parameters of the clear box/peanut systems thus selected are given in table 6.1.

VI.2.2 The identification of box/peanut bulges

Presented in figure 6.1 are a series of isophotal contour plots derived from COSMOS mapping scans of the relevant plates, together with prints also taken from such plates, for a subset of the Sb to Sbc types in my current sample, by way of illustration as to how a box or peanut bulge is defined. Isolation of the peanuts is relatively straightforward, as the edge-on aspect of the sample objects ensures that any depressions along the minor axis are well-defined. The box bulges are less so but the particular features of galaxies possessing

TABLE 6.1 :

object (1)	type (2)	log D_{25} (3)	m_B (4)	$-M_B$ (5)	i (6)	A_H (7)	D (8)	environment (9)
NGC 678	SB(s)b	1.70	13.00	20.74	87	30.9	15.2	cluster
NGC 1055	SBb	1.88	10.79	20.92	79	36.0	10.3	"
NGC 1596	SA0	1.59	11.96	20.10	76	24.5	15.7	"
NGC 2310	S0	1.70	12.16	19.31	79	8.5	9.5	field
NGC 2654	SBab	1.63	11.35	20.99	85	38.6	22.5	"
NGC 2683	SA(rs)b	1.97	9.34	20.17	82	13.3	3.7	"
NGC 3079	SB(s)c	1.88	10.31	21.64	83	38.6	12.0	cluster
NGC 3390	Sb	1.60	12.90	20.65	88	----	----	field
NGC 3957	SA0	1.55	12.91	19.59	87	----	----	cluster
NGC 4013	Sb	1.72	11.17	20.02	90	17.8	8.8	"
NGC 4235	SA(s)a	1.63	12.00	21.39	83	----	----	"
NGC 4388	SA(s)b	1.71	10.65	21.05	80	38.1	18.3	"
NGC 4469	SB(s)0/a	1.59	11.29	20.41	72	16.7	10.7	"
NGC 4565	SA(s)b	2.21	9.06	22.79	86	70.8	8.4	"
NGC 4710	SA(r)0	1.71	11.85	19.85	90	22.3	10.7	"
NGC 4845	SA(s)ab	1.70	11.07	20.22	75	58.5	28.8	"
NGC 4958	SB0(r)	1.61	11.48	20.63	74	8.8	5.4	"
NGC 5389	SAB(r)0/a	1.61	13.20	19.81	73	----	----	"
NGC 5529	Sc	1.77	12.60	21.30	88	71.1	29.6	"
NGC 5746	SAB(rs)b	1.90	10.24	22.34	85	62.5	19.0	"
NGC 5965	Sb	1.73	13.55	20.62	87	57.2	26.2	"
IC 2469	Sa	1.56	12.00	-----	76	----	----	field
IC 2531	Sc	1.74	12.93	20.54	90	62.7	21.9	cluster

Notes to Table 6.1 :

col. (2) : morphological types are derived from those given in the *RC2*.

col. (3) : all major axis dimensions are again taken from the *RC2* with an estimated error ± 0.04 in each case (equivalent to 0.1 arcmins).

col. (4) : where available, values are derived from the *RSA* assuming the prescribed galactic and internal extinction corrections. Otherwise magnitudes reduced to a common (B) system are obtained from the *RC2*, the lists of Longo & de Vaucouleurs (1983, 1985), from Nilson (1975, *UGC*) or from Dixon & Sonnenborn (1980). A typical error ± 0.2 mag is adopted.

col. (5) : the *RSA* is the general source for absolute magnitudes. Other measures are calculated using the values of col. (4) together with recessional velocities given in the *RC2*, *UGC* or *ESO* catalogues or Palumbo, Tanzella-Nitti & Vettolani (1980). If such velocities cannot be found, a mean measure is adopted from the group or cluster to which the galaxy is associated (if it is a cluster member). A typical error is taken as ± 0.4 mag.

col. (6) : for inclination angles (degrees) I generally rely on the large lists of Bottinelli *et al.* (1984, 1985) and Dressler & Sandage (1983) although specific values are also quoted if available. Such measures are compared with values calculated using the quoted (*RC2*) axis ratios, yielding uncertainties ± 5°.

cols (7), (8) : absolute galaxy sizes (A_H in kpc) are derived from Fisher & Tully (1981). The same is true of the distances (D in Mpc) if HI masses are given, otherwise they are calculated using the Bottinelli *et al.* distance moduli. Note that the distance to both NGC 4469 and NGC 4710 is taken to be that of the Virgo cluster. The measure for NGC 2310 comes from a visual estimate of the major axis dimension on the relevant SERC J survey plate and the distance estimate in col. 8 (see chapter IV).

col. (9) : identifications of companions or group/cluster membership are based primarily on information contained in the *UGC* and *ESO* catalogues, although notes given in the *RC2* are also checked. In addition, individual references to studies of specified clusters are used (Virgo by Kraan-Kortweg (1982); Coma by Rood & Baum (1967); Ursa Major by Weekes (1981)) or to clusters in general (Turner & Gott (1976), Geller & Huchra (1983)).

such shapes (namely a general flattening of the isophotes and/or abrupt cut-offs to the light distribution both parallel and perpendicular to the major axis) generally become evident to the educated eye on closer inspection of the plates and without the use of photographic enhancement techniques.

Each object defined in this way was systematically checked in all other available passbands going to roughly the required surface brightness level. I am thus confident of the classifications for the objects isolated in the present work. However, any remaining subjectivity in future studies of this type could be removed completely by the use of techniques, such as those outlined by Lauer (1985), to determine the extent to which the bulge departs from a perfect ellipse. These methods would be most useful for galaxies in which the bulge shapes are considerably less well-defined than those in the present sample.

VI.2.3 Selection effects

Aside from the imposed size limitation, a more obvious concern here is the bias introduced in deciding whether objects are sufficiently edge-on to warrant inclusion in the survey. This effect depends strongly on the prominence of the bulge in each of the galaxies concerned since it is inherently difficult to assign an inclination angle to a galaxy whose disc is weak or heavily masked by bulge light (approximately 25 % of the bulge dominated, 17 % of the intermediate and fewer than 2 % of the disc dominated objects have $i \lesssim 75^0$). Because of the rapid decline in numbers of the latter systems around 75^0, this figure has been adopted as a reasonable estimate of

the expected sample limit.

The actual galaxian luminosity function (i.e. in a volume-limited sample) rises monotonically from an absolute (B) magnitude of -23 to -16 (Sandage & Tammann, 1981). The distributions in M_B for both the box/peanut and non-box/peanut groups (figure 6.2) show a peak at around -20, indicating that this is the point at which selection effects in this parameter first become evident. Although the actual value of this turn-round is not relevant, the equivalence of the distributions in this figure brightward of -20 indicates that both the box/peanut and non-box/peanut subsamples are affected by such a selection bias to the same degree (application of a KS test reveals a similarity between these respective distributions to better than the 97.5 % confidence level). Evidently, any such bias is unimportant in the present survey, as I merely seek to compare the relative properties of these galaxy forms. The same conclusion is found to apply to the respective apparent magnitude distributions brightward of the limiting magnitude of the RC2 (m_B ~ 13.5).

VI.3 Results

VI.3.1 Statistical results from the survey

Of the 117 objects in the final sample, I find 23, or ~ 20 (±4, $\sqrt{N}$ error) %, to show evidence of box/peanut shapes. Of the rest, 12 (~ 10±3 %) are bulge dominated, 59 (~ 50±7 %) disc dominated and 23 are of intermediate form. Moreover, discarding the disc dominated systems in the present sample results in an increase to 17 (~ 29±7 %) in the proportion of box/peanut forms. Assuming the latter exist in galaxies

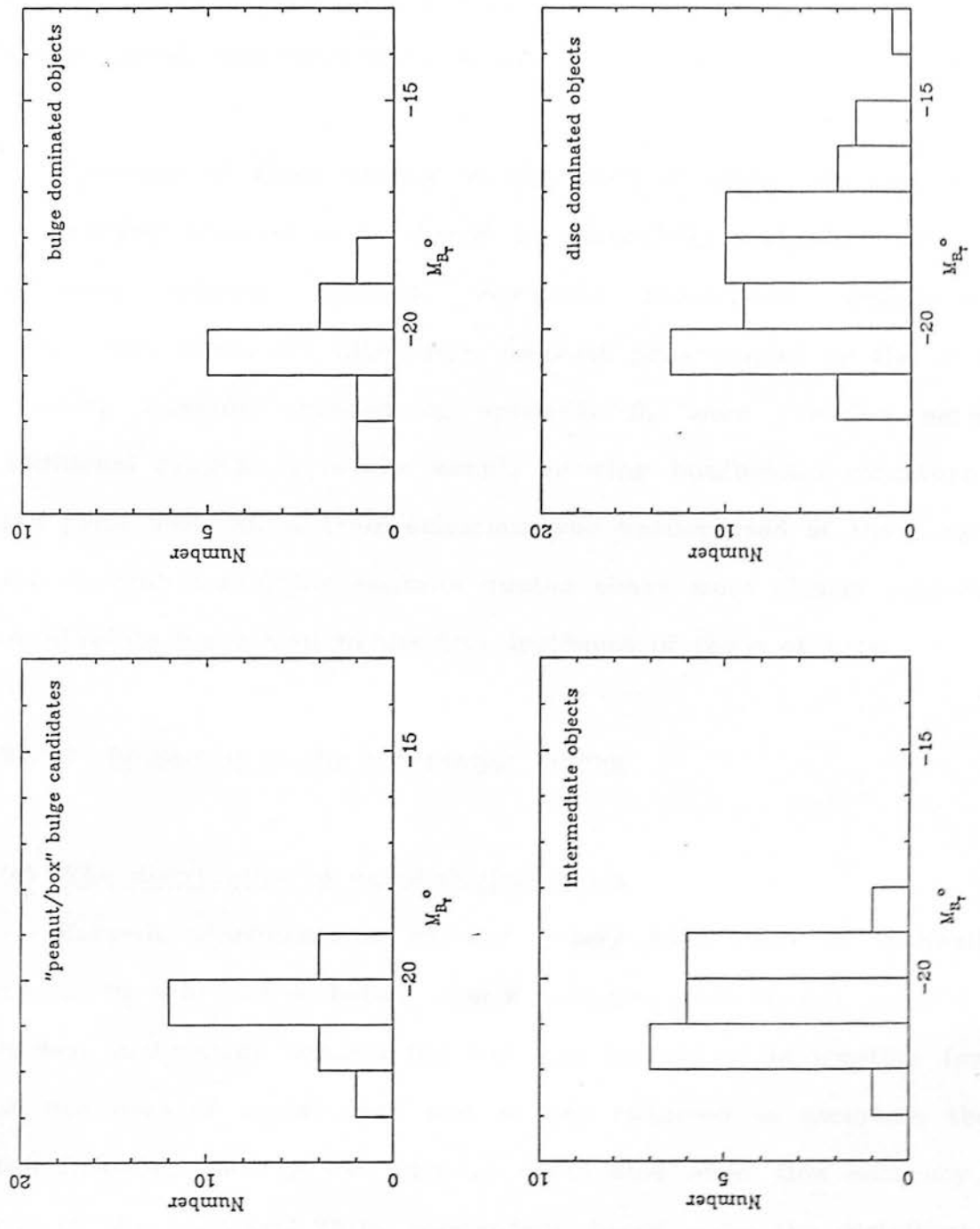

Figure 6.2 : Absolute (total B) magnitude distributions for the respective galaxy bins outlined in the text as derived from the sources outlined in the notes to table 6.1. All distributions appear to be equivalent brightward of -20, and selection effects are considered to be unimportant brighter than this limit.

of all inclinations (there is no reason to suspect that the box/peanuts preferentially reside in galaxies which happen to be seen edge-on) and also systems of all sizes, implies that ~ 610 (±120) of the (2527) normal spirals and (532) lenticulars in the RC2 should be of this form.

Coverage of these bulges on the basis of object appearance on the survey plate material should be essentially complete within the selection criteria imposed. However, subsequent enhancement techniques, either by ultra-high contrast photography or the digital unsharp masking outlined in appendix B, have revealed several additional candidates in the sample showing box/peanut structure at the plate limit. Since their existence was unsuspected at the level of the current study, the estimate quoted above must clearly represent an absolute lower limit to the true incidence of these objects.

VI.3.2 Properties of the box/peanut bulges

(a) The distribution of morphological types

Current classifications of any galaxy regardless of inclination cannot be achieved to better than a subtype, even though galaxies of modest inclinations contain the maximum amount of information (such as openness of spiral arms and so on) required to ascertain their morphologies. Clearly for edge-on candidates even this accuracy is out of the question. Thus, conclusions based upon the distributions presented by J86, and in particular the quoted lack of Sa types, are highly uncertain.

Hence, in table 6.2 (a) are shown the respective distributions in these two surveys over type bins. In this, as in all tables, assigned

Table 6.2 :

sample	S0 - S0/a	Sa - Sab	Sb - Sbc	Sc - Scd	Sd - Sm	totals
(a) The respective box/peanut samples :						
present work	7 (31±12%)	3 (13±8%)	10 (43±14%)	3 (13±8%)	0	23
Jarvis (1986)	19 (46±11%)	6 (15±6%)	15 (37±9%)	1 (2±2%)	0	41
(b) The "comparison" samples:						
present survey non-box/peanuts	21 (22±5%)	6 (6±3%)	18 (19±5%)	35 (38±6%)	14 (15±4%)	94
all normal RC2 spirals & lenticulars	1276 (42±1%)	297 (10±1%)	658 (21±1%)	542 (18±1%)	286 (9±1%)	3059

Table 6.3 :

	GALAXY TYPES			
	box/peanuts	disc dominated	bulge dominated	intermediate
# of objects in clusters	18	38	8	17
% of objects in clusters	78(±18) %	64(±10) %	67(±24) %	74(±18) %

uncertainties are $\sqrt{N}$ values. The present sample shows a strong concentration towards intermediate (Sb - Sbc) and very early (S0 - S0/a) morphologies, with the Sa - Sab's and those later than Sbc being relatively poorly represented. A KS test indicates no statistically significant equivalence between the distributions in this table (they are similar at only the 50 % confidence level). Potential reasons for the differences between them are addressed in section VI.4 below. If, however, one adopts the morphological classifications contained in the ESO catalogue for the galaxies in the J86 sample, the relative dominance of the earliest types is reduced and the later types increased, thereby bringing the resulting distribution into considerably better agreement with the present work (they are now equivalent at the 75 % level). Whilst the ESO measures (based on object appearance within the "quick blue survey") are to be preferred in the sense of being a more internally consistent data set, the personal estimates of Jarvis are based on material reaching a lower limiting magnitude (private communication, 1986).

As those (94) galaxies in the present sample not defined as possessing box/peanut bulges are subject to the same selection process as are the box/peanut candidates, they form a useful subsample to compare with the latter. The result of dividing the morphological type distribution in the box/peanuts by that of this "comparison" sample is shown in figure 6.3 - a strong concentration is evident towards intermediate types, with ~ 70 % found to lie in the range Sa to Sbc. The properties of the comparison sample made use of here are indicated in table 6.2 (b) and illustrated in figure 6.4. Table 6.2 (b) also highlights the distribution of revised Hubble types of all normal spirals and lenticulars in the RC2 regardless of size.

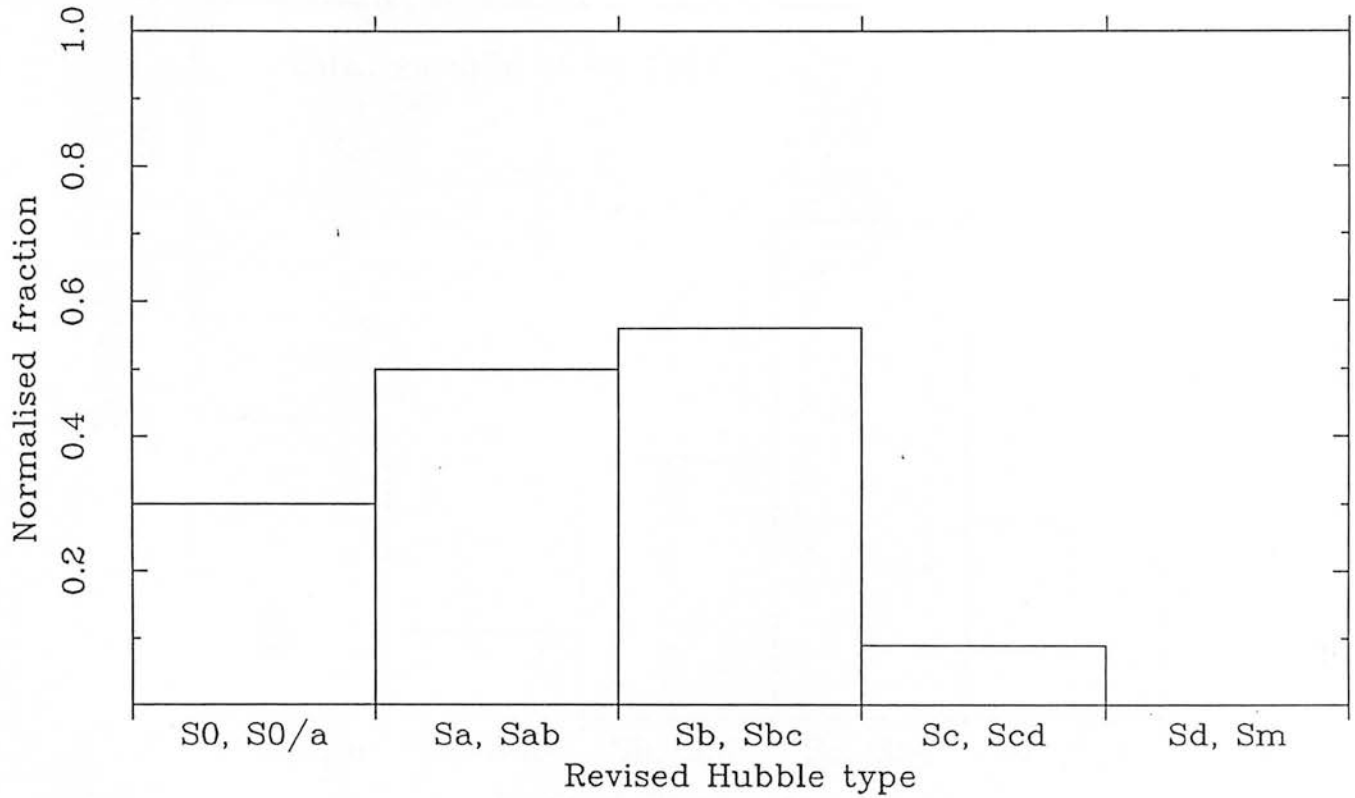

Figure 6.3 : Morphological type distributions for the box/peanuts in the present sample after division by that of the "comparison" sample described in the text.

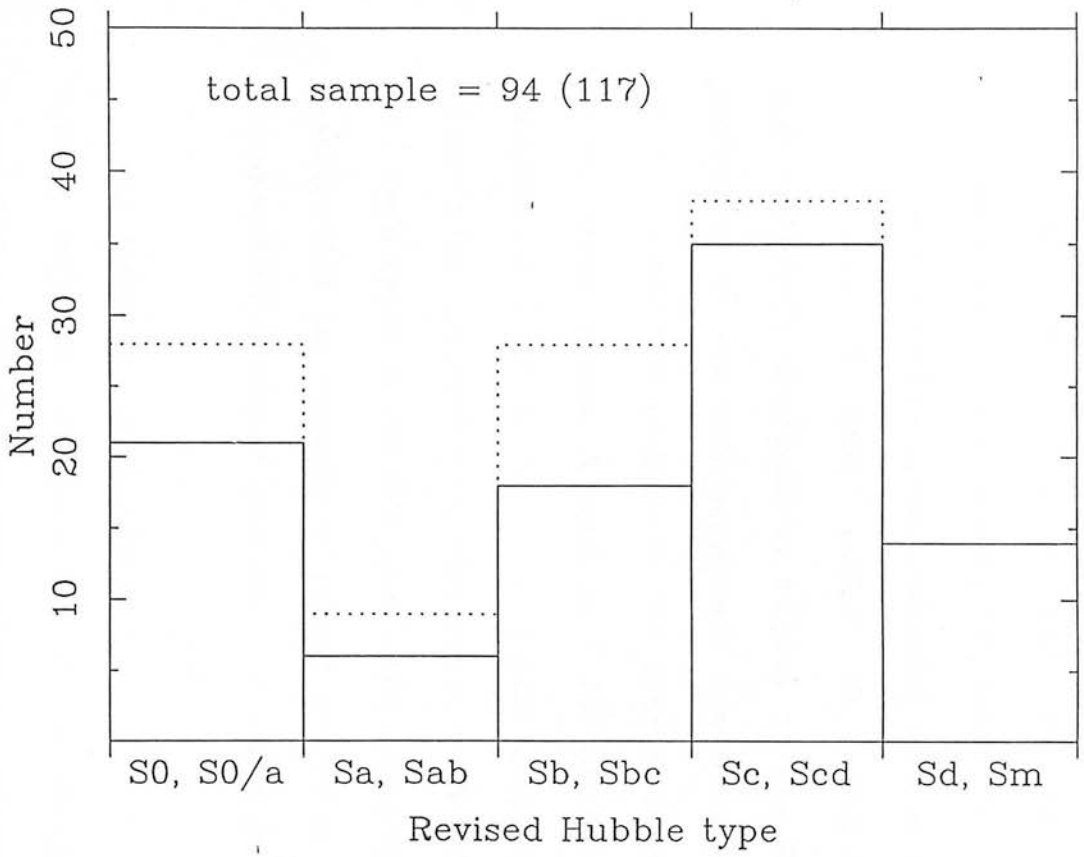

Figure 6.4 : Distributions of revised Hubble types as defined in the RC2 for the current sample. The totals represent the number of objects in each distribution. The solid line marks the distribution of the non-box/peanuts, whilst the dotted line (together with the modified total in brackets) refers to that after addition of the box/peanut candidates.

Statistically, the latter and the combined box/peanut and non-box/peanut distributions are not similar even at the 1 % level, with the principal differences evident at the earliest and latest classifications. Hence, a direct scaling of the box/peanut distribution to the 3059 normal spirals and lenticulars in the RC2 will inevitably lead to an incorrect assessment of the total proportion of box/peanuts within this catalogue over the early and late types (underestimating the former, and overestimating the latter, by a factor ~ 2). To allow for these differences in morphological type distribution with apparent galaxy size, I have scaled the combined box/peanut and non-box/peanut distributions to that of the 3059 normal spirals and lenticulars in the RC2 over each bin of table 6.2, and have thus derived a modified estimate of the proportion of box/peanuts expected in the latter sample. A total of ~ 750 candidates are predicted, the increase of ~ 20 % over the figure derived by a direct scaling between the respective samples arises from the fact that most of the S0 - S0/a types in the RC2 have small apparent sizes. This, of course, assumes that the majority of (small) lenticulars in this source are not mis-classified spirals of moderate inclination (see section VI.4 below).

The majority of box/peanut candidates contained within the earliest type bin of figure 6.3 are of the latest morphologies (i.e. types $S0^+$ to S0/a) and thus show an enhancement of dust and/or evidence of more pronounced disc structure than do the earlier ($S0^-$ to S0) forms. In contrast to the distribution presented by J86, this result serves to strengthen the pronounced peak towards intermediate morphologies already evident in figure 6.3.

(b) Photometric and radio properties of the box/peanut bulges

Section VI.2.3 above has already alluded to the similarity of the absolute magnitudes of all galaxies contained within the present survey (whether thay show evidence of a box/peanut bulge or not). Equally, comparative distributions of both apparent and absolute galaxy dimensions between the box/peanut and comparison samples reveal similarities at better than the 95 % confidence level. The latter are calculated using the formulation given by Fisher & Tully (1981), and using the distance estimates either quoted in the same source or from the lists of Bottinelli et al (1984, 1985). Figure 6.5 (a) shows the relevant distributions in apparent major axis dimensions (log D_{25}) - clearly box/peanuts are likely to occur in host systems having an equally wide range of sizes as those of the non-box/peanuts.

Furthermore, based on the total and HI masses, and the total blue luminosities for those sample objects contained in the study of Fisher & Tully, I find that the galaxies in the present survey which possess well-defined bulges tend to reside in marginally more massive (and brighter) host systems than do the essentially pure disc galaxies, but that the form of the bulge (be it a box/peanut or not) again seems to be irrelevant. Such conclusions are, however, restricted by the small number statistics which result from few of the sample objects being contained in the above HI survey.

The radio properties of the present candidates are based on those galaxies common to the current work and those of Hummel (1980), Dressel & Condon (1978) and Bottenelli et al (1982). The respective distributions shown in figure 6.6 show no statistically significant dependance of radio luminosity (log P_{tot}) or radio flux on the form of

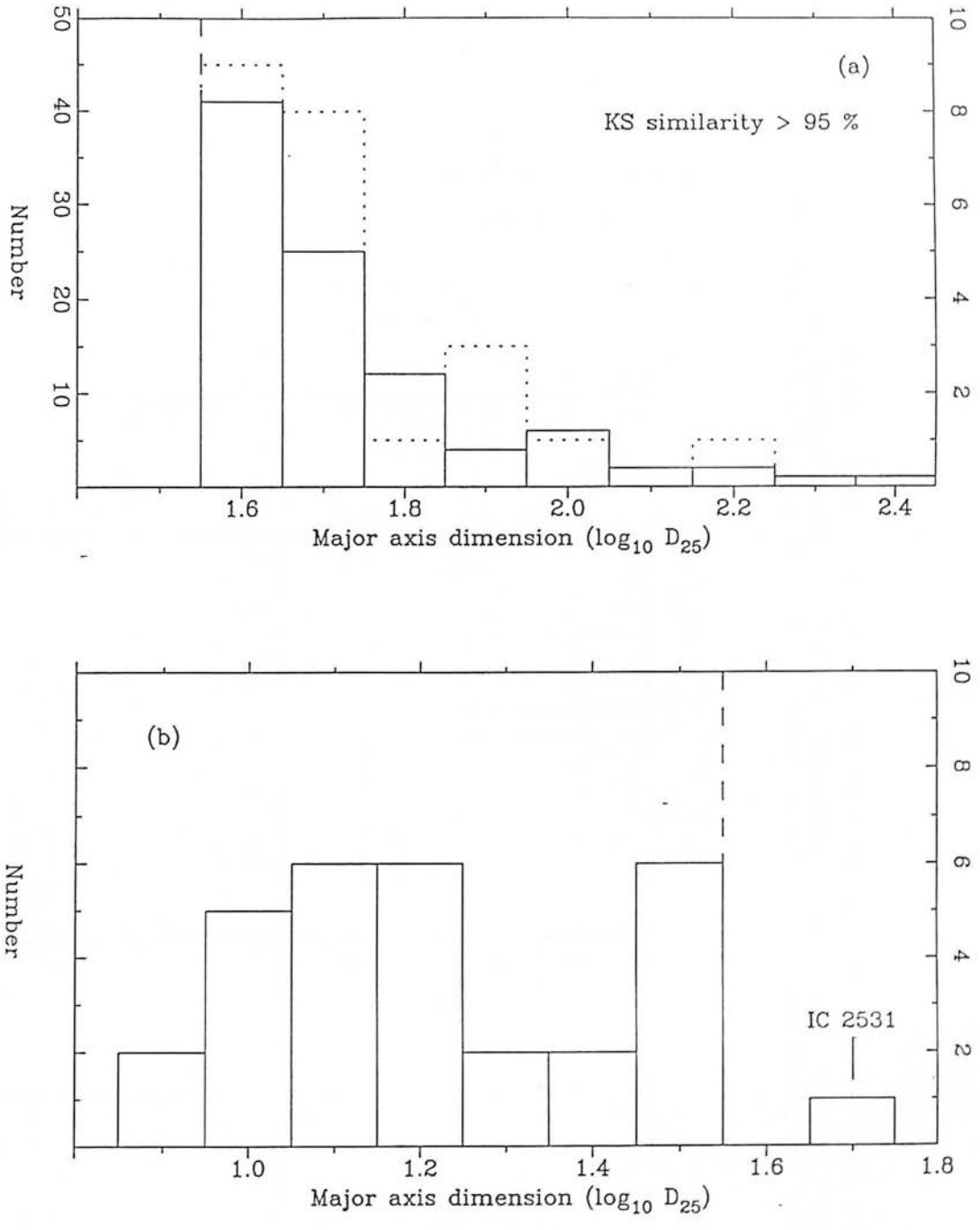

Figure 6.5 : Distribution of major axis dimensions at the 25 mag. arcsec^{-2} isophotal level (log D_{25}) for both the non-box/peanuts (full line, left-hand frequency axis) and the box/peanut candidates (dotted line, right-hand frequency axis) in the current sample (a). The equivalent distribution for those objects contained in the sample of Jarvis (1986) for which such dimensions can be derived is shown in (b). The dashed line at log D_{25} = 1.55 represents the limit of the present survey.

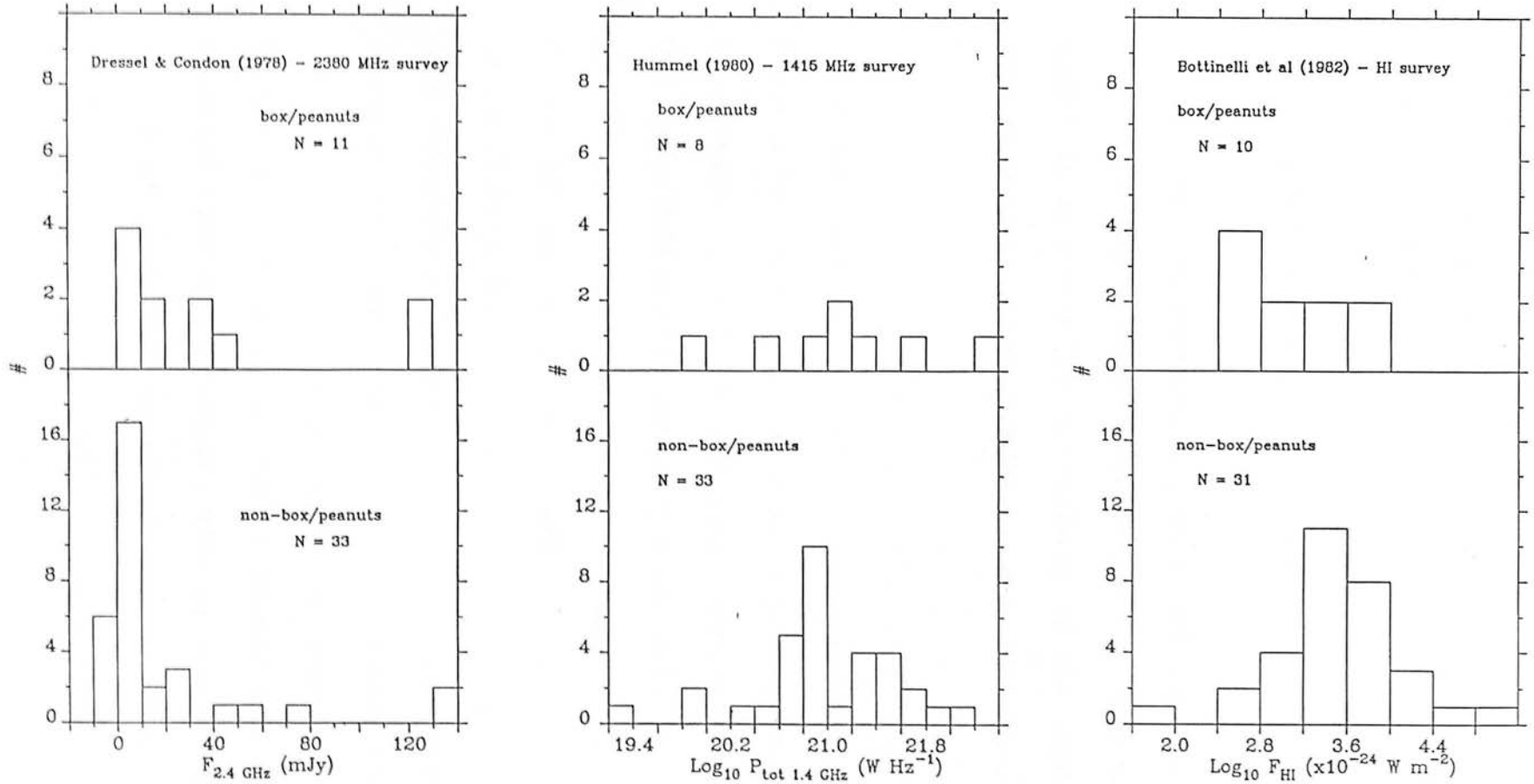

Figure 6.6 : Distributions of radio power (log P_{tot}) and flux (F_{HI}, $F_{2.4\ GHz}$) for the sample objects also contained within the quoted literature surveys at 1.4 GHz, 2.4 GHz and 21 cm. N is the sample size in each case.

the bulge concerned (although the samples are clearly limited). As far as can be derived from the small number of radio observations currently available in these literature sources, the existence of a box/peanut bulge does not appear to correspond to enhanced radio emission from the objects concerned.

VI.3.3 Cluster membership

By using the membership criteria for the box/peanut bulges in the present sample detailed in the notes to table 6.1, the aim of this section is to investigate the validity of the (null) hypothesis that such galaxies are preferentially found in clusters rather than in the field.

In table 6.3 are outlined the actual percentages of box/peanuts found to be cluster or group members as compared to those of all the other types. There is no statistically significant difference between the cluster:field ratio in the box/peanuts to any other galaxy types in the present sample. This result is confirmed if one compares the number of objects in the non-box/peanut bins of table 6.3 to calculated frequencies in these bins assuming all such forms show the same cluster:field frequency as do the box/peanuts. The evaluated product-moment correlation coefficient between such observed and calculated frequencies is 0.998. The marginal, but not statistically significant, evidence of a reduced cluster:field ratio for the disc dominated class in the present work is precisely that expected for galaxies of such late morphological type (Gisler (1980), Dressler (1980)).

VI.3.4 Galaxy counts

With a view to testing the validity of formation models for box/peanuts invoking mergers with small satellite systems, the local galaxy environment around a number of those systems in the present sample has also been investigated. A total of 32 galaxies were surveyed for faint neighbours on both ESO/SERC J and POSS R survey plate/film material within a chosen area of study of 8 x 8 arcmin centered on each object (corresponding to typical absolute dimensions of 40 x 40 kpc).

A comparison of these galaxy counts with those for non-box/peanut objects in both clusters and the field was facilitated by choosing an equivalent region of study around each non-boxy bulge, and preferentially excluding galaxies considered so large that their size would affect the counts in the area specified. In addition, a broad range of morphological type of object was chosen to ensure that the results were not affected by any possible correlation between galaxy counts and types. The results for the mean counts in each case are illustrated in table 6.4 (note that checks of internal consistency are achieved by deriving counts from both J and R survey plates in each case).

It is concluded from this analysis that, whilst those counts for objects found on the ESO/SERC J survey are in general slightly higher than from the R plates (the former survey being considerably deeper than the latter), all such counts are internally consistent within the uncertainties quoted. [It is implicitly assumed in the foregoing arguments, of course, that all the faint objects counted are

Table 6.4 :

galaxy types	passband	galaxy counts (± standard error)	number of galaxies used
NON-BOX/PEANUTS :			
southern field non-box/peanuts	J	27 (±3)	8
southern cluster non-box/peanuts	J	28 (±4)	5
northern field non-box/peanuts	R	21 (±4)	5
northern cluster non-box/peanuts	R	26 (±2)	3
BOX/PEANUTS :			
southern field box/peanuts	J	33 (±4)	3
southern cluster box/peanuts	J	----------	---
northern field box/peanuts	R	22 (±2)	2
northern cluster box/peanuts	R	23 (±6)	6

galaxies. Although I make no allowance here for contamination from faint stars, this effect has to be borne in mind, particularly at lower galactic latitudes.] Results from the Durham-AAT galaxy survey (Ellis, 1981) indicate that, at the plate limit of the ESO/SERC J survey, ~ 30 objects would be expected over the present search area. The counts in table 6.4 (for box/peanuts and non-box/peanuts alike) are, in fact, all quite consistent with the numbers expected from the general distribution of galaxies found in this survey to within ~ 1/4 or 1/2 mag. or so of the J survey plate limit. There is no evidence in the current data for an overdense concentration of small satellite systems around box/peanut bulges compared to any other types. Indeed such results indicate that very few, if any, of these small and faint neighbouring objects would be expected to be physically associated with the survey galaxy in that region of sky.

Magnitude estimates for these nearby neighbours :

Using the available calibrations between object magnitude and size given by King et al (1981) for the J survey material, and by King & Raff (1977) for the POSS B and R plates, I find the typical range of magnitudes for the neighbouring systems to be ~ 16.0 to 22.0 in J (with a mean of ~ 18.5), whilst an equivalent range for the sample galaxies with major axis dimensions between 5 and 7 arcmin is 10.7 to 13.4 in J, with a mean ~ 12.4 (±0.8). Galaxies possessing box/peanut bulges (and indeed all the sample objects) have few, if any, nearest neighbours ~ 6 mag. faintward of the object measured - assuming my failure to detect extremely diffuse (very low surface brightness) neighbours at such distances does not have a statistically significant effect on the results derived.

The appearance of "typical" Local Group members when placed at the distance of each galaxy used to derive the counts given in table 6.4 has also been investigated. In all cases, a satellite system of equivalent absolute magnitude to either the LMC, SMC or an intrinsically bright dwarf elliptical (such as A0058) would be easily isolated in the current study within the area searched. A fainter dwarf elliptical, such as Leo II, would typically be detected in ~ 70 % of the cases.

VI.4 Comparison to previous work

In comparing the results of this study with those of J86, it is immediately noticeable that ones ability to detect box/peanut bulges (as a function of inclination) differs somewhat from the estimated lower limit of ~ 80^0 set in the earlier work. Although the prominence of these bulges are likely to be lost through projection (May et al, 1985), the limit of their detection is not well-defined as it depends on the dominance of the box/peanut concerned over the other populations in the galaxy.

Except for galaxies of the smallest dimensions (for which it becomes increasingly difficult to assign type classifications and delineate morphological features), the construction of the sample in the J86 survey is not biased by any specific selection criterion on galaxy size as is my own. I have therefore made a comparison between the two surveys for all objects in the list of J86 for which such dimensions (based on measures in the ESO catalogue) are available - figure 6.5 (b) showing the result. Only one of the galaxies (IC 2531) in the earlier work is large enough to be included in the present

study, although conversely 3 objects (NGC 3957, NGC 1596 and IC 2469) are not found in the J86 survey despite satisfying the relevant selection criteria.

Of primary significance, however, is the order-of-magnitude discrepancies between the expected frequency of box/peanuts quoted by Jarvis (~ 1.2%) and that found in the present work. Aside from biases in the study of J86 which may have resulted from basing extrapolated total frequencies on the use of galaxy counts in only 20 random fields, a possible reason for the disparity between these surveys arises from the limitation of Jarvis to objects of very small angular sizes as figure 6.5 (b) graphically illustrates. Such a restriction, coupled with the relatively weak appearance of bulges in the morphologically latest systems, strongly suggests an erroneously low detection rate of bulge distortions in these types in the J86 analysis. In addition, the earlier work is often unable to distinguish small, faint spirals of moderate inclinations from S0's seen edge-on and so his study may well also incorrectly assign too many box/peanuts to the very earliest types (as table 6.2 (a) would appear to indicate). This suggests that the very small incidence found by J86 is artificially low, due to the inherent detection problems in his sample galaxies. The angular dimensions of the objects in the present survey are large enough that the nature of the bulge is self-evident, sufficiently so as to minimise such misclassifications and to preclude dust lanes along the minor axis (previously noted by, for example, Hawarden et al (1981) for a number of ellipticals) as being the cause of the dip in isophotes seen in the cases of the peanut bulges. However, it is important to stress that any survey of this kind can only determine a lower limit to the true incidence of box/peanut

bulges.

VI.5 Discussion

Binney & Petrou (1985, henceforth BP) have proposed a series of potential formation mechanisms for box/peanut bulges invoking the use of galaxy mergers, possibly involving small satellite galaxies. In the context of the present study, which preferentially discriminates against objects with relatively low luminosity bulge distortions (the greater proportion of objects studied here possess box bulges of almost comparable luminosity to the systems in which they are found), the modelling of BP favours two alternative schemes amenable to testing using the current results. These are accretion of a large number of small, faint satellite systems or the slow merger of two spirals of equivalent mass.

The first seems unlikely on statistical grounds as it would require the infall of a succession of galaxies all with similar angular momenta with respect to the host galaxy. This is necessary to ensure that all the stars are continually fed into the same portions of action space (or equivalently, have the necessary phase space distribution function over orbital energy and angular momentum) required to generate the appearance of a box bulge. It seems plausible (though not necessary) that the initial distribution of orbital parameters of satellites would be more random than this. Therefore, one should still expect to see evidence of remaining faint neighbours which did not possess the required orbits and thus remain to be accreted. Such systems have not been found around the sample objects to at least 6 magnitudes fainter than the parent, whilst satellites fainter than this, if they

exist at all, seem somewhat unlikely to be able to generate box/peanuts of the required magnitude seen in most of my objects. If the accretion of many faint systems is adopted as a likely formation mechanism, one is, therefore, led to conclude that none are presently seen because all the box/peanuts that could have formed have done so already.

The accretion of a neighbour of roughly equivalent mass to M32 might be expected to generate the box bulge seen in M31 (Kent 1983, 1987) under such a mechanism, although BP suggest that any such process would require an orbital decay timescale typically very much larger than the orbital period of the satellite around its host. The inference is thus that such processes occur over a long time, inconsistent with the above hypothesis (although the proposed scheme for M31 would yield a smaller bulge distortion than noted in the present sample objects). More work is clearly required to clarify this point.

The results presented in section VI.3 indicate that dense cluster environments are not a pre-requisite for the formation of box bulges - those we see in clusters today are just as likely to have formed externally and have been subsequently captured by the gravitational potential of the cluster. Indeed, in a cluster environment, gravitational interactions with neighbouring cluster members might be expected to disrupt the angular momentum distribution specifically required in the BP scheme to form box bulges. Furthermore, if the merger of spirals of equivalent mass is taken as a suitable formation mechanism, then "head-on" collisions are specifically precluded owing to the very large angular momentum transfer likely to be imparted

during such an event. These arguments do not preclude formation by means of field collisions between two spirals of equal mass - indeed, this may presently seem to be the most tenable of the (merger) mechanisms presented by BP. Such a process must, however, be very common and efficient in view of the high proportion of box bulges discovered in the current survey. Equally, I cannot entirely rule out a similar scheme invoking the gradual merger of a field spiral and elliptical, although the elliptical would clearly have to be of low mass to ensure that the spiral itself remains largely intact throughout such an encounter (Gilmore & Shaw (1986) present a more graphic representation of a likely outcome to such an event). Any merger mechanism must also reconcile the seeming lack of enhanced radio emission found in the box/peanut bulges over that observed in "normal" bulges (although it is clearly of some importance to confirm this preliminary conclusion using a larger database of radio observations).

Whilst merger hypotheses present a possible mechanism of forming the bulges found in my sample, the effects of bar formation and development on a host system present an alternative formation mechanism and may be relevant. Purely by way of illustration as to what constraints one might expect to place on presently existing models, the following discussion centres on those proposed by Combes & Sanders (1981, hereafter CS) involving the observations of bar evolution under the influence of an exponential disc and a rigid and spherically symmetric bulge.

Their simulations result in the generation of a bar possessing the desired box/peanut shape seemingly regardless of the degree of bulge

or disc dominance imposed. They propose that the box and peanut bulges are merely manifestations of the same feature, i.e. bars seen along differing lines-of-sight with boxes being those seen end-on and peanuts being bars seen more edge-on. Such an explanation would thus imply a greater frequency of peanuts than boxes (assuming that any bar seen slightly away from exactly end-on looks peanut-shaped) precisely as is found to be the case both in the present study (in which 60 % of the objects are peanuts) and in that of J86. However, peanuts are much easier to define than box bulges using the detection methods outlined in section VI.2.2 above, and thus any surveys involving visual searches will inevitably have inbuilt biases tending to detect the former at the expense of the latter.

Since the present results show a concentration of box/peanuts towards moderately early and intermediate types ($S0^+$ - Sbc), for which bulge:disc mass ratios are ~ 2, the results of CS imply that the greatest number of these systems have formed recently, with the earlier types forming most recently of all. They argue that few box/peanuts earlier than $S0^-$ or S0 are seen since the evolutionary timescale of bars in such galaxies is too long for them to have formed since the galaxy itself has existed. It is also claimed that the later types (where bulge:disc mass ratios ~ unity are found) develop bars so soon after formation of the whole system that any such features, if present, have "faded" sufficiently to become undetectable in this study. However, many other N-body simulations have shown that once formed, bars are generally very stable, clearly precluding any significant fading with time. In addition, the model also makes a specific prediction as to the expected ratio of early:late types in boxes and peanuts in that the later morphologies should show almost

exclusive evidence of box bulges, while the peanuts should become more prominent at earlier types. This is not borne out in the current study - indeed, my results suggest quite the reverse situation to be the case. Potentially the most significant argument against the modelling of CS, however, is that few (if any) other N-body simulations have led to the generation of such bulge shapes. Hence, considerable caution must be adopted as to the significance of the above conclusions, at least until additional codes confirm the results of CS.

The effects of torques (possibly resulting from the presence of a disc rather than specifically from a bar) on the evolution of steady state elliptical galaxies have been investigated by May et al (1985). Their simulation, after application of such a torque, is found to yield the bulge shapes of interest, although in this case the line-of-sight viewing angle does not alter our perspective of such bulge distortions - a peanut bulge being seen as such at all positions perpendicular to the rotation axis of the figure. Only projection effects induced from looking at inclinations far from edge-on are likely to affect the resulting appearance of the bulge so formed.

On the basis of his derived type distributions, Jarvis has suggested that the discs in galaxies earlier than Sa have too small a mass to produce a torque of the required extent to generate the box/peanut, whilst in later types the disc is, conversely, too dominant. My own more broadly peaked distribution, and in particular the considerable number of late-type lenticulars to very early-type spirals, indicates that galaxies may possess a box bulge even when their disc masses are likely to be sufficiently small as to have a

limited effect on the evolution of a bulge and the subsequent formation of a box/peanut. Indeed, recent work (Lauer (1985), Jedrzjewski (1985)) reveals that several elliptical galaxies also show evidence of box-shaped outer isophotes (possibly as many as ~ 20%). [See the candidates studied in appendix B.] In the case of the ellipticals one is clearly able to cite examples in which the effect of a disc is insignificant in the evolution of such isophotal distortions. Thus, present results do not appear to favour models in which disc torques or instabilities are the formation mechanism, assuming that such schemes are universally applicable (i.e. that they do not, for example, depend on the prominance of the bulge). The validity of this assumption is as yet unclear.

VI.6 General conclusions

In this chapter use has been made of the previously defined sample of 117 edge-on normal spirals and lenticulars with major axis dimensions in excess of 5 arcmin. To re-iterate from chapter I, this sample is likely to be complete to m_B ~ 13.5, M_B ~ -20 and inclination angles $\gtrsim 75^0$. The following features result from a study of this sample:

(1). Of the sample objects, 20 (±4) % are box/peanuts - implying that as many as ~ 750 normal spirals and lenticulars in the RC2 are of such forms.

(2). The distribution of morphological types in these box/peanuts shows a strong tendency towards late-type lenticulars to intermediate (Sbc) type spirals, with ~ 70 % lying in the range Sa to Sbc. Both the

earliest lenticulars and spirals later than Sbc are under-represented in these results. The present study is, however, likely to be free from the selection effects which strongly bias the distribution derived by Jarvis (1986), and hence the conclusions of that paper.

(3). No differences are evident between boxy and "normal" bulges for any of the derivable optical or radio properties for the current sample objects. This indicates that the properties of the parent galaxy as a whole are largely independent of the form taken by the bulge present, and is in marked contrast to kinematic studies of a (small) number of box/peanut bulges (e.g. Kormendy & Illingworth (1982), Bertola & Capaccioli (1977)) which reveal the existence of cylindrical rotation - a distinction which gives them the appearance of being kinematically isolated from the general class of spiral bulges.

(4). Box/peanuts are not found preferentially in clusters - dense cluster environments are clearly not required for their formation.

(5). There is no preference for the box/peanut bulges to be surrounded by more faint satellite galaxies than are seen around any other types ~ 6 magnitudes faintward of the host galaxy and down to a limiting (J) magnitude ~ 22.

(6). If merger hypotheses are relevant, the galaxy counts argue against the accretion of small satellites but instead favour the slow mergers between field spirals of like mass. Even in this case such mergers must be very frequent to explain the presently observed numbers of box/peanuts isolated. However, it may yet be premature to disregard hypotheses invoking the accretion of a small number of

more moderately sized satellite galaxies.

(7). Based on the morphological distribution of box/peanuts in the current sample, discs seem an unlikely source of torques possibly required to generate these features. This assumes, of course, a unique torque-generation mechanism of formation in all cases, although this may be an invalid assumption. The discovery of box-shaped ellipticals further indicates that, if such distortions are equivalent to those seen in their spiral counterparts, strong discs are not pre-requisites for the appearance of such features.

(8). If such bulges formed by mergers, the likely timescales for accreted satellites to complete a full rotation period around the host, and hence become dynamically "well-mixed", are likely to be sufficiently short in comparison to the age of the primary that the lack of a colour gradient within the box/peanut bulges (outlined in chapter V) is unlikely to be able to place any strong constraints on the formation histories of these systems. Nevertheless, accretion events involving a companion whose colour is substantially different from that of the typical bulge (i.e. if such a companion possessed a disc) as seems most likely, are explicitly excluded over timescales shorter than the evolutionary lifetimes of the young, blue stars contained therein. These results are, of course, quite consistent with a bar formation mechanism, although the "bar-heating" process can equally only be applied to the more evolved stars within the discs of such systems.

- Chapter VII -

General summary and suggestions for future work

The principal goal of this thesis has been to test the validity of the use of standard fitting functions in attempting an unambiguous description of the luminosity distributions of spiral and lenticular galaxies. In particular, I aimed to ascertain whether the residuals which result from the application of one model combination to the non-thin disc light were sufficiently systematic as to require the incorporation of a further component for their removal.

To this end, some 15 galaxies were observed (having been chosen to represent a wide variation of contribution to the total luminosity from that contained in the non-thin disc), and their constituent model components defined by the application of a least-squares modelling routine. It was found possible (using the present algorithm) to differentiate between two and three component combinations to the point of being able to identify a specific model combination as being the best description of each galaxy (on the basis of the respective goodness-of-fit estimators thus obtained and the requirement of the resultant model parameters to be "realistic" in the context of the data being used). In this context, van der Kruit (1984) notes that a three-component model is apparently able to describe the observed luminosity distribution of NGC 891 better than does a two-component set (a point *not* supported in the analyses in chapter III). He infers that any difference in quality-of-fit between such combinations is a result of differences in the corresponding degrees of freedom. In the

light of the above findings, therefore, I consider this expectation to be incorrect.

However, a detailed inspection of the fits thus obtained reveals many cases in which discrepancies are seen between the predicted and observed luminosity distributions. In general they are most evident as a systematic overestimation of the predicted light distribution to that observed by ~ 0.25 - 0.5 μ at large Z-heights, the removal of which require implausibly large changes in the adopted sky brightness levels determined in chapter II. Furthermore, even after corrections are applied to remove these systematics, the model parameters thus derived are often quite dissimilar between the B and R passbands observed here. The latter effect can, in almost all cases, be accounted for by imposing a more equivalent error distribution on each dataset, although the "minimum errors" required for this process to be successful (typically ± 0.15 - 0.2 μ) are again considered implausible. The parameters derived after these corrections are applied are equivalent to ~ 30 % at best, and the model fits show random variations about the observed profiles of typically 0.25 - 0.3 μ.

In the case of those bulges showing "peanut" morphologies, the model fits underestimate the light at the extremities of these features by as much as 0.75 - 1.0 μ. This amounts to an excess ~ 6 (± 1) % in the B band and ~ 10 (± 2) % in R above the luminosity predicted by the model combinations adopted over the regions most affected. Furthermore, by subtracting the "best-fit" model combinations from the original data frames, I find the peanut morphologies to contribute $\gtrsim$ 20 % of the total non-thin disc light in each passband. These

results strongly suggests that peanut bulges are superposed on the underlying luminosity distributions of the galaxies and are not merely the resulting central concentration of any "outlying" non-thin disc population.

In general, therefore, it appears that the traditional technique of adopting standard fitting functions is not an optimal means of deconvolving the luminosity distributions of galaxies (at least to accuracies of better than ± 0.3 μ), even those cases studied here in which the orientations are most favourable for delineating the non-thin disc components. Nevertheless, in spite of such discrepancies, two galaxies in the present sample (NGC 4565 and NGC 5170) still show statistically significant improvements in their quality-of-fits by the inclusion of a third component, whilst the non-thin disc light of IC 2531 (the only galaxy for which sufficient coverage exists to allow removal of the peanut shapes) can only be adequately described by the incorporation of a two-component model. Those model profiles which appear to delineate the old disc component show constant disc scaleheights (over the total radial extent of the data) of between ± 0.2 and 16 % (and typically ~ 4 %) of the mean values in each case.

In the light of those galaxies studied within this thesis which are seen to display such box/peanut shaped isophotes, it was of some interest to define how common these features are in a more complete sample. An all-sky survey, making use of available sky survey plate material, placed a lower limit of 20 (± 4) % on the frequency of such morphologies within the galaxy sample defined. By implication, ~ 750 normal spiral and lenticular galaxies within the Second Reference

Catalogue (de Vaucouleurs, de Vaucouleurs & Corwin, 1976) should show such features.

Of those galaxies for which multi-colour photometry was obtained, three systems showed a progressively bluer colour with increasing radial distance of ~ 0.016 to 0.020 mag. kpc^{-1}, the source of which was attributed to the influence of the disc component. However, in none of the galaxies studied for which clear non-thin disc populations could be isolated were any detectable gradients evident perpendicular to the disc plane - the gradients thus defined being $\lesssim$ 90 % of the assigned errors of $\pm$ 0.05 mag. kpc^{-1} or $\pm$ 0.004 mag. $arcsec^{-1}$. In addition, no evidence was found for a significant difference in the shapes of the isophotes and isochromes in these systems. For the one galaxy for which photometry extended beyond the radial distance which previous studies in the literature would suggest a disc cutoff might be expected (~ 4.5 disc scalelengths) no such cutoff was noted.

Furthermore, in all galaxies for which clearly identifiable non-thin disc light were seen, such a luminosity distribution is flatter than an axial ratio ~ 0.4 in 60 % of the sample over surface brightnesses ranging from those in which such a component appeared to be a major contributor to the summed model luminosity distribution (~ 20 μ_B along the minor axis and ~ 24.5 μ_B at large R - based on a visual inspection of the model fits illustrated in chapter IV) down to the limit of the data (~ 26 μ_B). The lack of a clear correlation between such flattening and the bulge:total ratio implies that the non-thin disc light does not owe its shape to significant gravitational influence from the disc components.

Suggestions for future work

The model parameters derived in chapter IV were very repeatable in all galaxies and for a wide variety of input estimates. The fact that, taken as a whole, they fall in a narrow area of the parameter space tested indicates that a similar local minimum has been isolated in all cases. However, the possibility that an (improved) alternative solution exists just beyond the region sampled during any particular iteration always exists in the present scheme. As such a limitation is a feature common to any such least-squares algorithm, it is considered that no future improvements in this area will be forthcoming in the future - such procedures always being limited by the need for a specific starting point. However, it is to be hoped that future work on the distribution functions and mass distributions of galaxies will lead to the derivation of a model luminosity profile with which to compare to the observational data but for which a well-defined physical basis exists.

The importance of accreting satellite systems to the evolution of a host galaxy is another area worthy of further study. This is particularly so as such schemes may be responsible for the formation of the intermediate components seen in our own Galaxy and in several external systems. In the light of the similar ages of the bulge and intermediate populations in our own Galaxy, it would appear to be of most importance for such studies to define how much disc is required to account for the intermediate components currently seen. The presence of a thin disc component as a necessary requirement for the existence of an intermediate population is an interesting point for galaxy formation models, and is one amenable to testing by

undertaking a search for, and thence studying the photometric properties of, systems with "thick disc" components but no thin discs.

However, in the light of the seemingly complex nature of the light distributions of apparently "simple" systems, it would seem to be very important also to investigate the properties of the non-thin disc light in spirals and lenticulars from a dynamical viewpoint. The paucity of data currently available for edge-on spirals is very suprising, and more work in this area is clearly required. Indeed, the only studies undertaken thus far with this specific intention are those of Kormendy & Illingworth (1982) and Illingworth & Schechter (1982). However, both adopted long-slit spectroscopy techniques and may well suffer from the inherent limitation of not reaching "true" sky at the edges of the slit as is claimed (the requirement of obtaining sufficient non-disc light to make such spectroscopy feasible inevitably leads to analyses in which such light contaminates the whole slit). In addition, for slit positions parallel to, but offset from, the major axis itself, there remains the possibility that at large $\mathbb{R}$ one is still contaminated by disc light. For example, the Z = 34" parallel cut across the non-thin disc region of NGC 4565 by Kormendy & Illingworth is, on the basis of the modelling undertaken in this thesis, anticipated to be dominated by light from the intermediate component certainly beyond $\mathbb{R} \sim 60"$, and almost certainly so interior to this point. In short, dynamical studies undertaken even for the non-disc components of very edge-on candidates sample light from all the components contributing to the photometric profiles, thus complicating the analysis if one is unaware which component is dominating the light distribution at each region of the galaxy.

Perhaps the most promising means of averting this difficulty may be to use groups of fibres positioned on specially selected points across the non-thin disc regions. By undertaking such observations in galaxies for which detailed photometric decomposition has already been undertaken, one would thus be in a position of extracting kinematic information at points where the relative contributions of the various stellar populations are already defined. Sky measures could be obtained by positioning other fibres over regions far removed from the galaxy under study. It is clearly of considerable importance to search for kinematic distinctions between the different photometric components in a galaxy. As a complement to these kinematic studies, additional photometry would be useful, particularly multi-colour data to allow a more detailed study of the colour distributions of the non-thin disc light in spirals than was possible in the present, rather restricted, observations.

Furthermore, as is evident from the results in chapter IV and V, there is much work to be done concerning the nature of the box/peanut morphologies. No allowance was made within the present modelling routine for such shapes since insufficient data existed beyond these features in almost all galaxies studied here. Thus, the largely unsuccessful fits obtained here suggests that future photometric analyses will have to incorporate luminosity distributions specifically tailored to describe such galaxies. Although these systems are considered to show cylindrical rotation, no studies have yet been optimised to match the dynamical observations with complementary photometry of equivalent quality. Furthermore, such (kinematic) results rely on observations of only two galaxies. Constraints on merger formation mechanisms within these systems could be imposed

by undertaking a systematic search for relatively low luminosity "indicators" such as shells, disc warps, tidal tails and so on. However, such constraints could only be of relevance for recent mergers since the dynamical timescales involved in the subsequent evolution of these morphologies are sufficiently short as to discount these features as being long-lived phenomena. Any study will, however, have to make use of digital electronic devices (or at least other detectors with equally reliable flat-fielding properties).

The results of the data reduction presented in chapter II indicate the care with which a flat-field strategy has to be defined. In particular, the use of flat-fields taken on the inside of the dome is clearly inappropriate - a point echoed in the papers of Baum et al (1981) and Djorgovski (1984). Although they are a considerable improvement over dome flats, strong arguments can equally be levelled against flats taken on the twilight sky (which seem to be unable to remove pixel-to-pixel non-uniformities to better than ~ 1 %).

The technique of drift scanning introduced by J. F. Wright and C. D. Mackay appears to be the best means of removing such device characteristics (the principals of which are well described in Mackay (1986) and references therein). The fact that each region of sky "sees" all the pixels in a column of the array greatly reduces the pixel non-uniformities down this particular column as the device is read out, although one still has to allow for column-to-column variations. The latter point is one which still requires a considerable degree of care (see, for example, the discussion in Wright (1982)). This is particularly true when imaging extended objects whose light is likely to contaminate sky estimates over much larger fractions of each

column. Even so, preliminary indications are of reduced non-uniformities of only ~ 0.1 % or better (Wright (1982); Wright & Mackay (1981) and Mackay (1982, 1986)).

Aside from the obvious benefits of greatly improved flat-fielding and near-perfect colour matching, drift scanning negates the use of separate calibration frames and also allows one the considerable flexibility of increased areal coverage. For imaging of extended objects this is particularly valuable in allowing one to guarantee detection of the sky at sufficient distances from the object itself.

- Appendix A -

In this appendix are presented the tabulated results of the least-squares modelling for all 15 galaxies in the present sample as described in chapter IV. In each case, central surface brightness values are quoted in mag. arcsec^{-2}, whilst all scale parameters are given in kpc unless no distance estimate for the galaxy concerned was available (see the comments in chapter IV). Also included are the sum-of-squares of residuals (FSUMSQ) and the reduced χ^2 appropriate to that particular model combination. The symbol (**) denotes those cases in which convergence to a final solution was not achieved prior to the number of calls to the working subroutine exceeding the imposed upper limit (i.e. the MAXCAL parameter described in chapter III). In these particular cases, the model parameters are those obtained when MAXCAL was first exceeded.

MODEL COMBINATION	MODEL OUTPUT PARAMETERS			"QUALITY-OF-FIT" ESTIMATORS
exp.	μ_o = 17.50 h_z = 5.05 h_r = 22.9			FSUMSQ = 1.20×10^{-3} red. χ^2 = 41.58
$sech^2$	μ_o = 18.33 Z_o = 7.53 h_r = 39.7			FSUMSQ = 5.88×10^{-3} red. χ^2 = 190.80
$r^{1/4}$ law	μ_e = 16.70 θ_e = 5.00 q = 0.30			FSUMSQ = 2.00×10^{-3} red. χ^2 = 42.93
exp. + exp.	μ_o = 17.17 h_z = 3.85 h_r = 18.1	21.63 14.47 69.9		FSUMSQ = 2.92×10^{-4} red. χ^2 = 7.65
$sech^2$ + exp.	μ_o = 22.84 Z_o = 25.25 h_r = 55.6	17.17 h_z = 3.97 18.5		FSUMSQ = 2.88×10^{-4} red. χ^2 = 7.60
$sech^2$ + $sech^2$	DID NOT FIT DATA			
exp. + $r^{1/4}$ law	μ_o = 17.26 h_z = 3.98 h_r = 19.1	μ_e = 22.47 θ_e = 45.71 q = 0.38		FSUMSQ = 2.79×10^{-4} red. χ^2 = 7.34
$sech^2$ + $r^{1/4}$ law	DID NOT FIT DATA			
exp. + exp. + exp.	μ_o = 17.17 h_z = 3.85 h_r = 18.1	21.63 14.47 69.9	54.82 259.4 15.8	FSUMSQ = 2.92×10^{-4} red. χ^2 = 7.79
exp. + $sech^2$ + exp.	μ_o = 17.18 h_z = 3.97 h_r = 18.5	39.83 324.18 118.1	22.84 Z_1 = 25.25 55.6	FSUMSQ = 2.88×10^{-4} red. χ^2 = 7.74
$sech^2$ + $sech^2$ + exp.	DID NOT FIT DATA			
exp. + exp. + $r^{1/4}$ law	μ_o = 17.27 h_z = 3.82 h_r = 17.6	20.49 5.93 40.7	μ_e = 22.96 θ_e = 57.00 q = 0.44	FSUMSQ = 2.77×10^{-4} red. χ^2 = 7.16
exp. + $sech^2$ + $r^{1/4}$ law	μ_o = 17.23 h_z = 3.90 h_r = 18.2	22.68 Z_1 = 10.41 55.4	μ_e = 22.78 θ_e = 54.36 q = 0.47	FSUMSQ = 2.76×10^{-4} red. χ^2 = 7.15
$sech^2$ + $sech^2$ + $r^{1/4}$ law	DID NOT FIT DATA			

Table A.1 : Modelling results for NGC 2295

Table A.2 : Modelling results for NGC 2310

MODEL COMBINATION	B BAND MODEL OUTPUT PARAMETERS	B BAND "QUALITY-OF-FIT" ESTIMATORS	R BAND MODEL OUTPUT PARAMETERS	R BAND "QUALITY-OF-FIT" ESTIMATORS
exp.	μ_o = 20.08 h_z = 0.31 h_r = 2.9	FSUMSQ = 2.14×10^{-4} red. χ^2 = 23.43	μ_o = 19.37 h_z = 0.39 h_r = 5.0	FSUMSQ = 6.13×10^{-4} red. χ^2 = 51.06
$sech^2$	DID NOT FIT DATA		μ_o = 20.43 Z_o = 0.70 h_r = 2.6	FSUMSQ = 9.22×10^{-4} red. χ^2 = 82.57
$r^{1/4}$ law	DID NOT FIT DATA		DID NOT FIT DATA	
exp. + exp.	μ_o = 19.26 22.69 h_z = 0.23 0.51 h_r = 1.4 242.8	FSUMSQ = 8.81×10^{-5} (**) red. χ^2 = 9.13	μ_o = 17.73 21.32 h_z = 0.23 0.56 h_r = 1.4 21.1	FSUMSQ = 9.92×10^{-5} red. χ^2 = 7.16
$sech^2$ + exp.	μ_o = 22.62 18.81 Z_o = 0.75 h_z = 0.18 h_r = 3.6 1.2	FSUMSQ = 4.81×10^{-5} red. χ^2 = 5.38	μ_o = 22.31 17.61 Z_o = 1.00 h_z = 0.22 h_r = 7.2 1.5	FSUMSQ = 8.82×10^{-5} red. χ^2 = 6.18
$sech^2$ + $sech^2$	μ_o = 21.38 22.54 Z_o = 0.40 Z_1 = 0.74 h_r = 2.8 2.7	FSUMSQ = 4.42×10^{-4} red. χ^2 = 53.55	μ_o = 19.40 21.73 Z_o = 0.37 Z_1 = 0.92 h_r = 2.8 2.7	FSUMSQ = 4.68×10^{-4} red. χ^2 = 41.86
exp. + $r^{1/4}$ law	μ_o = 20.81 μ_e = 16.63 h_z = 0.29 e_e = 0.14 h_r = 3.2 q = 0.26	FSUMSQ = 3.81×10^{-5} red. χ^2 = 4.27	μ_o = 18.94 μ_e = 15.81 h_z = 0.25 e_e = 0.18 h_r = 1.8 q = 0.22	FSUMSQ = 6.66×10^{-5} red. χ^2 = 4.33
$sech^2$ + $r^{1/4}$ law	μ_o = 22.20 μ_e = 16.38 Z_o = 0.52 e_e = 0.14 h_r = 3.4 q = 0.31	FSUMSQ = 4.58×10^{-5} red. χ^2 = 5.31	μ_o = 21.13 μ_e = 14.76 Z_o = 0.45 e_e = 0.14 h_r = 3.1 q = 0.27	FSUMSQ = 7.99×10^{-5} red. χ^2 = 5.30
exp. + exp. + exp.	μ_o = 18.89 21.39 119.20 h_z = 0.18 0.40 4.39 h_r = 1.0 6.2 3.0	FSUMSQ = 7.57×10^{-5} red. χ^2 = 7.76	DID NOT FIT DATA	
$sech^2$ + exp. + exp.	μ_o = 22.57 18.81 28.87 Z_o = 0.74 h_z = 0.18 47.30 h_r = 3.6 1.1 2.3	FSUMSQ = 4.75×10^{-5} red. χ^2 = 5.39	DID NOT FIT DATA	
$sech^2$ + $sech^2$ + exp.	DID NOT FIT DATA		DID NOT FIT DATA	
exp. + exp. + $r^{1/4}$ law	DID NOT FIT DATA		DID NOT FIT DATA	
$sech^2$ + exp. + $r^{1/4}$ law	μ_o = 70.49 20.81 μ_e = 16.63 Z_o = 6.03 h_z = 0.29 e_e = 0.14 h_r = 5.2 3.2 q = 0.26	FSUMSQ = 3.81×10^{-5} red. χ^2 = 4.31	DID NOT FIT DATA	
$sech^2$ + $sech^2$ + $r^{1/4}$ law	μ_o = 22.88 22.33 μ_e = 16.24 Z_o = 0.18 Z_1 = 0.54 e_e = 0.13 h_r = 4.0 3.4 q = 0.30	FSUMSQ = 4.39×10^{-5} red. χ^2 = 5.23	DID NOT FIT DATA	

Table A.3 : Modelling results for NGC 3115

MODEL COMBINATION	B BAND MODEL OUTPUT PARAMETERS	B BAND "QUALITY-OF-FIT" ESTIMATORS	R BAND MODEL OUTPUT PARAMETERS	R BAND "QUALITY-OF-FIT" ESTIMATORS
exp.	μ_o = 19.81 h_z = 0.48 h_r = 1.8	FSUMSQ = 1.70×10^{-4} red. χ^2 = 46.31	μ_o = 18.57 h_z = 0.53 h_r = 1.6	FSUMSQ = 3.26×10^{-4} red. χ^2 = 2.27×10^{7}
$sech^2$	μ_o = 20.84 Z_o = 0.75 h_r = 1.9	FSUMSQ = 4.04×10^{-4} red. χ^2 = 108.62	μ_o = 19.68 Z_o = 0.85 h_r = 1.5	FSUMSQ = 3.34×10^{-4} red. χ^2 = 2.27×10^{7}
$r^{1/4}$ law	μ_e = 18.19 e_e = 0.47 q = 0.36	FSUMSQ = 3.06×10^{-5} red. χ^2 = 6.79	μ_e = 15.80 e_e = 0.33 q = 0.42	FSUMSQ = 3.63×10^{-5} red. χ^2 = 2.19×10^{7}
exp. + exp.	μ_o = 17.10 20.14 h_z = 0.11 0.55 h_r = 0.4 2.1	FSUMSQ = 1.11×10^{-4} red. χ^2 = 16.79	μ_o = 18.72 20.57 h_z = 0.52 0.55 h_r = 1.5 1.6	FSUMSQ = 3.26×10^{-4} (**) red. χ^2 = 2.49×10^{7}
$sech^2$ + exp.	μ_o = 21.68 18.68 Z_o = 0.99 h_z = 0.22 h_r = 2.3 0.8	FSUMSQ = 9.81×10^{-5} red. χ^2 = 18.57	μ_o = 20.29 16.55 Z_o = 1.04 h_z = 0.20 h_r = 1.8 0.6	FSUMSQ = 9.69×10^{-5} (**) red. χ^2 = 8.47×10^{6}
$sech^2$ + $sech^2$	DID NOT FIT DATA		DID NOT FIT DATA	
exp. + $r^{1/4}$ law	μ_o = 21.35 μ_e = 18.04 h_z = 0.51 e_e = 0.38 h_r = 2.1 q = 0.38	FSUMSQ = 1.43×10^{-5} red. χ^2 = 3.84	μ_o = 20.77 μ_e = 15.95 h_z = 0.49 e_e = 0.33 h_r = 1.0 q = 0.41	FSUMSQ = 3.11×10^{-5} (**) red. χ^2 = 5.18×10^{6}
$sech^2$ + $r^{1/4}$ law	μ_o = 22.39 μ_e = 18.31 Z_o = 0.18 e_e = 0.49 h_r = 2.7 q = 0.39	FSUMSQ = 1.68×10^{-5} red. χ^2 = 5.06	μ_o = 21.23 μ_e = 16.10 Z_o = 0.49 e_e = 0.37 h_r = 1.3 q = 0.46	FSUMSQ = 2.83×10^{-5} (**) red. χ^2 = 5.39×10^{6}

Table A.4 : Modelling results for NGC 3573

MODEL COMBINATION	B BAND MODEL OUTPUT PARAMETERS	B BAND "QUALITY-OF-FIT" ESTIMATORS	R BAND MODEL OUTPUT PARAMETERS	R BAND "QUALITY-OF-FIT" ESTIMATORS
exp.	μ_o = 21.55 h_z = 11.75 h_r = 44.1	FSUMSQ = 6.60×10^{-4} red. χ^2 = 45.89	μ_o = 20.45 h_z = 13.13 h_r = 42.3	FSUMSQ = 5.48×10^{-4} red. χ^2 = 47.66
$sech^2$	μ_o = 23.09 Z_o = 23.97 h_r = 56.3	FSUMSQ = 2.01×10^{-3} red. χ^2 = 136.71	μ_o = 22.48 Z_o = 28.54 h_r = 65.2	FSUMSQ = 3.08×10^{-3} red. χ^2 = 235.10
$r^{1/4}$ law	μ_e = 19.00 e_e = 8.86 q = 0.44	FSUMSQ = 2.52×10^{-4} red. χ^2 = 9.21	μ_e = 17.94 e_e = 9.43 q = 0.46	FSUMSQ = 3.87×10^{-4} red. χ^2 = 17.05
exp. + exp.	μ_o = 19.68 22.97 h_z = 4.77 20.96 h_r = 19.9 62.9	FSUMSQ = 3.39×10^{-4} red. χ^2 = 12.72	μ_o = 18.36 21.90 h_z = 5.34 21.63 h_r = 16.5 67.0	FSUMSQ = 2.10×10^{-4} red. χ^2 = 13.92
$sech^2$ + exp.	DID NOT FIT DATA		μ_o = 23.70 19.11 Z_o = 43.30 h_z = 7.49 h_r = 67.6 22.8	FSUMSQ = 2.17×10^{-4} red. χ^2 = 17.35
$sech^2$ + $sech^2$	DID NOT FIT DATA		DID NOT FIT DATA	
exp. + $r^{1/4}$ law	μ_o = 21.15 μ_e = 20.61 h_z = 5.72 e_e = 15.76 h_r = 33.6 q = 0.54	FSUMSQ = 1.78×10^{-4} red. χ^2 = 6.55	μ_o = 22.21 μ_e = 15.28 h_z = 18.61 e_e = 3.40 h_r = 86.2 q = 0.61	FSUMSQ = 1.35×10^{-4} red. χ^2 = 8.57
$sech^2$ + $r^{1/4}$ law	μ_o = 23.82 μ_e = 19.26 Z_o = 8.14 e_e = 9.76 h_r = 81.9 q = 0.49	FSUMSQ = 2.17×10^{-4} red. χ^2 = 7.86	μ_o = 23.90 μ_e = 17.32 Z_o = 20.53 e_e = 7.61 h_r = 41.5 q = 0.59	FSUMSQ = 9.53×10^{-5} red. χ^2 = 6.53
exp. + exp. + exp.	DID NOT FIT DATA		μ_o = 16.52 18.81 22.20 h_z = 1.75 6.19 23.91 h_r = 4.6 18.8 76.5	FSUMSQ = 2.02×10^{-4} red. χ^2 = 12.92
$sech^2$ + exp. + exp.	DID NOT FIT DATA		μ_o = 23.77 18.17 21.51 Z_o = 31.85 h_z = 4.74 15.88 h_r = 63.3 15.7 37.6	FSUMSQ = 1.78×10^{-4} red. χ^2 = 12.11
$sech^2$ + $sech^2$ + exp.	DID NOT FIT DATA		DID NOT FIT DATA	
exp. + exp. + $r^{1/4}$ law	DID NOT FIT DATA		μ_o = 23.32 24.47 μ_e = 15.78 h_z = 16.75 103.90 e_e = 4.14 h_r = 3749.7 18.1 q = 0.54	FSUMSQ = 9.13×10^{-5} (**) red. χ^2 = 6.05
$sech^2$ + exp. + $r^{1/4}$ law	DID NOT FIT DATA		μ_o = 24.02 24.51 μ_e = 16.29 Z_o = 21.97 h_z = 119.31 e_e = 4.93 h_r = 41.2 21.3 q = 0.50	FSUMSQ = 5.46×10^{-5} red. χ^2 = 3.87
$sech^2$ + $sech^2$ + $r^{1/4}$ law	DID NOT FIT DATA		μ_o = 24.28 24.71 μ_e = 17.35 Z_o = 13.55 Z_1 = 24.18 e_e = 7.72 h_r = 80.5 36.5 q = 0.60	FSUMSQ = 9.33×10^{-5} red. χ^2 = 6.48

MODEL COMBINATION	MODEL OUTPUT PARAMETERS			"QUALITY-OF-FIT" ESTIMATORS	
exp.	μ_o = 19.43 h_z = 4.50 h_r = 23.6			FSUMSQ = 1.21×10^{-3} red. χ^2 = 16.40	
$sech^2$	DID NOT FIT DATA				
$r^{1/4}$ law	DID NOT FIT DATA				
exp. + exp.	μ_o = 18.03 h_z = 2.26 h_r = 8.9	20.50 5.83 32.7		FSUMSQ = 4.34×10^{-4} red. χ^2 = 5.54	
$sech^2$ + exp.	DID NOT FIT DATA				
$sech^2$ + $sech^2$	DID NOT FIT DATA				
exp. + $r^{1/4}$ law	μ_o = 20.31 h_z = 3.06 h_r = 38.5	μ_e = 17.50 e_e = 3.76 q = 0.42		FSUMSQ = 1.73×10^{-4} red. χ^2 = 2.40	
$sech^2$ + $r^{1/4}$ law	μ_o = 21.68 Z_o = 3.76 h_r = 61.2	μ_e = 17.14 e_e = 3.46 q = 0.39		FSUMSQ = 2.14×10^{-4} red. χ^2 = 3.05	
exp. + exp. + exp.	μ_o = 18.05 h_z = 2.29 h_r = 8.9	20.58 6.00 32.5	20.71 0.61 1828.8	FSUMSQ = 4.11×10^{-4} red. χ^2 = 5.19	(**)
$sech^2$ + exp. + exp.	μ_o = 92.40 Z_o = 22.20 h_r = 805.8	18.03 h_z = 2.26 8.9	20.50 5.83 32.7	FSUMSQ = 4.34×10^{-4} red. χ^2 = 5.67	
$sech^2$ + $sech^2$ + exp.	μ_o = 22.09 Z_o = 1.33 h_r = 1479.3	23.73 Z_1 = 14.87 63.9	18.67 h_z = 3.46 15.1	FSUMSQ = 6.46×10^{-4} red. χ^2 = 8.15	(**)
exp. + exp. + $r^{1/4}$ law	μ_o = 19.93 h_z = 3.29 h_r = 19.0	22.43 2.16 111.7	μ_e = 17.76 e_e = 3.95 q = 0.39	FSUMSQ = 1.47×10^{-4} red. χ^2 = 2.05	
$sech^2$ + exp. + $r^{1/4}$ law	μ_o = 22.41 Z_o = 2.60 h_r = 1462.9	20.19 h_z = 3.51 21.9	μ_e = 17.63 e_e = 3.76 q = 0.39	FSUMSQ = 1.49×10^{-4} red. χ^2 = 2.26	
$sech^2$ + $sech^2$ + $r^{1/4}$ law	μ_o = 21.98 Z_o = 2.36 h_r = 69.2	22.45 5.20 54.6	μ_e = 17.11 e_e = 3.40 q = 0.40	FSUMSQ = 2.01×10^{-4} red. χ^2 = 2.95	

Table A.5 : Modelling results for NGC 4289

Table A.6 : Modelling results for NGC 4469

MODEL COMBINATION	B BAND MODEL OUTPUT PARAMETERS	B BAND "QUALITY-OF-FIT" ESTIMATORS	R BAND MODEL OUTPUT PARAMETERS	R BAND "QUALITY-OF-FIT" ESTIMATORS
exp.	μ_o = 20.70 h_z = 0.53 h_r = 2.1	FSUMSQ = 8.91×10^{-4} red. χ^2 = 22.75	μ_o = 20.41 h_z = 0.97 h_r = 3.1	FSUMSQ = 7.85×10^{-4} red. χ^2 = 85.21
$sech^2$	μ_o = 22.78 Z_o = 1.16 h_r = 3.3	FSUMSQ = 2.09×10^{-3} red. χ^2 = 59.05	μ_o = 21.77 Z_o = 1.48 h_r = 3.5	FSUMSQ = 1.07×10^{-3} red. χ^2 = 141.97
$r^{1/4}$ law	μ_e = 17.22 θ_e = 0.27 q = 0.31	FSUMSQ = 2.76×10^{-4} red. χ^2 = 9.11	μ_e = 14.49 θ_e = 0.21 q = 0.31	FSUMSQ = 5.96×10^{-5} red. χ^2 = 10.25
exp. + exp.	μ_o = 19.92 24.49 h_z = 0.40 1.52 h_r = 1.5 12.0	FSUMSQ = 7.04×10^{-4} red. χ^2 = 12.88	μ_o = 16.58 21.17 h_z = 0.26 1.20 h_r = 0.9 4.0	FSUMSQ = 4.37×10^{-4} red. χ^2 = 39.95
$sech^2$ + exp.	μ_o = 23.85 19.42 Z_o = 1.47 h_z = 0.32 h_r = 4.1 1.2	FSUMSQ = 3.77×10^{-4} red. χ^2 = 8.78	μ_o = 22.32 17.17 Z_o = 1.73 h_z = 0.31 h_r = 4.1 1.1	FSUMSQ = 1.80×10^{-4} red. χ^2 = 17.63
$sech^2$ + $sech^2$	μ_o = 22.78 47.17 Z_o = 1.16 Z_1 = 9.37 h_r = 3.3 1.7	FSUMSQ = 2.09×10^{-3} red. χ^2 = 60.00	μ_o = 21.92 23.31 Z_o = 1.57 Z_1 = 0.68 h_r = 3.5 2.9	FSUMSQ = 1.06×10^{-3} red. χ^2 = 141.43
exp. + $r^{1/4}$ law	μ_o = 20.78 μ_e = 18.45 h_z = 0.38 θ_e = 0.34 h_r = 1.5 q = 0.32	FSUMSQ = 1.34×10^{-4} red. χ^2 = 4.66	μ_o = 19.38 μ_e = 15.23 h_z = 0.36 θ_e = 0.25 h_r = 1.3 q = 0.31	FSUMSQ = 4.57×10^{-5} red. χ^2 = 8.03
$sech^2$ + $r^{1/4}$ law	μ_o = 24.40 μ_e = 16.89 Z_o = 0.65 θ_e = 0.24 h_r = 3.6 q = 0.35	FSUMSQ = 2.20×10^{-4} red. χ^2 = 8.39	μ_o = 23.47 μ_e = 14.83 Z_o = 0.81 θ_e = 0.23 h_r = 3.0 q = 0.33	FSUMSQ = 4.75×10^{-5} red. χ^2 = 9.00
exp. + exp. + exp.	μ_o = 19.93 24.49 26.30 h_z = 0.40 1.52 0.40 h_r = 1.5 12.0 1.5	FSUMSQ = 7.04×10^{-4} red. χ^2 = 13.09	DID NOT FIT DATA	
$sech^2$ + exp. + exp.	μ_o = 23.85 19.42 83.88 Z_o = 1.47 h_z = 0.32 0.90 h_r = 4.1 1.2 3.2	FSUMSQ = 3.77×10^{-4} red. χ^2 = 8.92	DID NOT FIT DATA	
$sech^2$ + $sech^2$ + exp.	DID NOT FIT DATA		DID NOT FIT DATA	
exp. + exp. + $r^{1/4}$ law	μ_o = 20.78 59.94 μ_e = 18.45 h_z = 0.38 5.40 θ_e = 0.36 h_r = 1.5 1.5 q = 0.32	FSUMSQ = 1.34×10^{-4} red. χ^2 = 4.74	DID NOT FIT DATA	
$sech^2$ + exp. + $r^{1/4}$ law	DID NOT FIT DATA		DID NOT FIT DATA	
$sech^2$ + $sech^2$ + $r^{1/4}$ law	DID NOT FIT DATA		DID NOT FIT DATA	

MODEL COMBINATION	MODEL OUTPUT PARAMETERS		"QUALITY-OF-FIT" ESTIMATORS
exp.	μ_o = 19.96 h_z = 30.88 h_r = 68.7		FSUMSQ = 4.97×10^{-4} red. χ^2 = 98.71
$sech^2$	μ_o = 20.66 Z_o = 41.17 h_r = 55.0		FSUMSQ = 2.79×10^{-4} red. χ^2 = 78.86
$r^{1/4}$ law	μ_e = 17.38 e_e = 19.55 q = 0.51		FSUMSQ = 2.10×10^{-5} red. χ^2 = 5.93
exp. + exp.	μ_o = 17.76 h_z = 8.82 h_r = 21.0	20.65 41.78 85.3	FSUMSQ = 4.08×10^{-4} red. χ^2 = 66.69
$sech^2$ + exp.	μ_o = 20.97 Z_o = 46.19 h_r = 59.9	17.20 h_z = 7.36 17.2	FSUMSQ = 1.53×10^{-4} red. χ^2 = 25.00
$sech^2$ + $sech^2$	μ_o = 20.65 Z_o = 40.07 h_r = 54.3	25.32 Z_1 = 136.56 87.0	FSUMSQ = 2.79×10^{-4} red. χ^2 = 78.18
exp. + $r^{1/4}$ law	μ_o = 14.56 h_z = 1.46 h_r = 7.9	μ_e = 17.40 e_e = 19.70 q = 0.51	FSUMSQ = 2.09×10^{-5} red. χ^2 = 5.94
$sech^2$ + $r^{1/4}$ law	μ_o = 23.68 Z_o = 53.52 h_r = 43.3	μ_e = 17.24 e_e = 17.75 q = 0.50	FSUMSQ = 1.62×10^{-5} red. χ^2 = 4.59
exp. + exp. + exp.	DID NOT FIT DATA		
exp. + $sech^2$ + exp.	DID NOT FIT DATA		
$sech^2$ + $sech^2$ + exp.	DID NOT FIT DATA		
exp. + exp. + $r^{1/4}$ law	DID NOT FIT DATA		
exp. + $sech^2$ + $r^{1/4}$ law	DID NOT FIT DATA		
$sech^2$ + $sech^2$ + $r^{1/4}$ law	DID NOT FIT DATA		

Table A.7 : Modelling results for NGC 5078

Table A.8 : Modelling results for NGC 5170

MODEL COMBINATION	B BAND MODEL OUTPUT PARAMETERS	B BAND "QUALITY-OF-FIT" ESTIMATORS	R BAND MODEL OUTPUT PARAMETERS	R BAND "QUALITY-OF-FIT" ESTIMATORS
exp.	μ_o = 20.99 h_z = 0.78 h_r = 6.6	FSUMSQ = 1.55×10^{-4} red. χ^2 = 1.26×10^{7}	μ_o = 19.54 h_z = 0.82 h_r = 6.2	FSUMSQ = 1.46×10^{-4} red. χ^2 = 2.05×10^{6}
$sech^2$	μ_o = 22.02 Z_o = 1.31 h_r = 6.1	FSUMSQ = 4.30×10^{-4} red. χ^2 = 1.26×10^{7}	μ_o = 20.64 Z_o = 1.43 h_r = 5.1	FSUMSQ = 3.79×10^{-4} red. χ^2 = 1.96×10^{6}
$r^{1/4}$ law	μ_e = 18.99 e_e = 0.63 q = 0.14	FSUMSQ = 5.38×10^{-4} red. χ^2 = 1.35×10^{7}	μ_e = 17.13 e_e = 0.60 q = 0.21	FSUMSQ = 3.33×10^{-4} red. χ^2 = 7.78×10^{6}
exp. + exp.	μ_o = 20.35 23.44 h_z = 0.51 1.75 h_r = 5.4 6.8	FSUMSQ = 4.77×10^{-5} red. χ^2 = 3.03×10^{7}	μ_o = 18.53 21.63 h_z = 0.46 1.72 h_r = 4.9 7.0	FSUMSQ = 3.77×10^{-5} red. χ^2 = 5.45×10^{7}
$sech^2$ + exp.	μ_o = 24.65 20.34 Z_o = 3.13 h_z = 0.53 h_r = 5.2 5.5	FSUMSQ = 4.41×10^{-5} red. χ^2 = 2.87×10^{7}	μ_o = 22.88 18.53 Z_o = 3.23 h_z = 0.49 h_r = 5.2 5.0	FSUMSQ = 2.85×10^{-5} (**) red. χ^2 = 5.13×10^{7}
$sech^2$ + $sech^2$	μ_o = 21.19 23.40 Z_o = 0.71 Z_1 = 2.07 h_r = 4.6 4.7	FSUMSQ = 1.06×10^{-4} (**) red. χ^2 = 2.61×10^{7}	μ_o = 19.44 21.95 Z_o = 0.69 Z_1 = 2.24 h_r = 4.4 4.7	FSUMSQ = 6.87×10^{-5} (**) red. χ^2 = 3.60×10^{7}
exp. + $r^{1/4}$ law	μ_o = 20.74 μ_e = 22.44 h_z = 0.56 e_e = 2.24 h_r = 6.9 q = 0.47	FSUMSQ = 4.52×10^{-5} (**) red. χ^2 = 2.26×10^{7}	μ_o = 19.24 μ_e = 19.61 h_z = 0.48 e_e = 1.53 h_r = 9.3 q = 0.46	FSUMSQ = 1.98×10^{-5} red. χ^2 = 1.58×10^{8}
$sech^2$ + $r^{1/4}$ law	μ_o = 21.62 μ_e = 21.36 Z_o = 0.79 e_e = 1.60 h_r = 6.2 q = 0.42	FSUMSQ = 6.21×10^{-5} (**) red. χ^2 = 2.35×10^{7}	μ_o = 20.09 μ_e = 19.25 Z_o = 0.74 e_e = 1.37 h_r = 8.7 q = 0.43	FSUMSQ = 2.09×10^{-5} red. χ^2 = 1.58×10^{8}
exp. + exp. + exp.	DID NOT FIT DATA		DID NOT FIT DATA	
$sech^2$ + exp. + exp.	DID NOT FIT DATA		DID NOT FIT DATA	
$sech^2$ + $sech^2$ + exp.	DID NOT FIT DATA		DID NOT FIT DATA	
exp. + exp. + $r^{1/4}$ law	DID NOT FIT DATA		DID NOT FIT DATA	
$sech^2$ + exp. + $r^{1/4}$ law	DID NOT FIT DATA		DID NOT FIT DATA	
$sech^2$ + $sech^2$ + $r^{1/4}$ law	DID NOT FIT DATA		DID NOT FIT DATA	

Table A.9 : Modelling results for IC 2531

MODEL COMBINATION	B BAND MODEL OUTPUT PARAMETERS	B BAND "QUALITY-OF-FIT" ESTIMATORS	R BAND MODEL OUTPUT PARAMETERS	R BAND "QUALITY-OF-FIT" ESTIMATORS
exp.	μ_o = 19.78 h_z = 0.75 h_r = 6.1	FSUMSQ = 9.86×10^{-4} red. χ^2 = 22.94	μ_o = 19.51 h_z = 0.77 h_r = 10.0	FSUMSQ = 9.16×10^{-4} red. χ^2 = 33.63
$sech^2$	μ_o = 20.95 Z_o = 1.27 h_r = 6.5	FSUMSQ = 2.07×10^{-3} red. χ^2 = 45.82	μ_o = 20.41 Z_o = 1.23 h_r = 8.8	FSUMSQ = 1.51×10^{-3} red. χ^2 = 55.56
$r^{1/4}$ law	μ_e = 15.09 e_e = 0.25 q = 0.18	FSUMSQ = 1.91×10^{-3} red. χ^2 = 24.01	μ_e = 16.70 e_e = 0.46 q = 0.11	FSUMSQ = 1.19×10^{-3} red. χ^2 = 42.96
exp. + exp.	μ_o = 19.09 25.17 h_z = 0.59 5.49 h_r = 4.1 34.8	FSUMSQ = 4.28×10^{-4} red. χ^2 = 6.26	μ_o = 18.08 22.09 h_z = 0.51 1.25 h_r = 3.5 641.0	FSUMSQ = 1.31×10^{-4} (**) red. χ^2 = 6.29
$sech^2$ + exp.	μ_o = 25.60 19.09 Z_o = 6.40 h_z = 0.59 h_r = 15.4 4.2	FSUMSQ = 4.26×10^{-4} red. χ^2 = 6.16	μ_o = 22.18 18.00 Z_o = 1.80 h_z = 0.46 h_r = 21.8 3.8	FSUMSQ = 4.68×10^{-4} red. χ^2 = 16.29
$sech^2$ + $sech^2$	μ_o = 20.78 25.97 Z_o = 1.12 Z_1 = 148.50 h_r = 6.4 7.1	FSUMSQ = 1.62×10^{-3} red. χ^2 = 23.76	μ_o = 19.83 23.09 Z_o = 0.82 Z_1 = 3.17 h_r = 6.7 15.2	FSUMSQ = 1.01×10^{-3} red. χ^2 = 37.70
exp. + $r^{1/4}$ law	μ_o = 20.68 μ_e = 15.45 h_z = 0.56 e_e = 0.28 h_r = 17.4 q = 0.36	FSUMSQ = 3.38×10^{-4} red. χ^2 = 5.65	μ_o = 18.16 μ_e = 21.54 h_z = 0.52 e_e = 2.36 h_r = 2.9 q = 0.05	FSUMSQ = 1.05×10^{-4} red. χ^2 = 4.59
$sech^2$ + $r^{1/4}$ law	μ_o = 21.13 μ_e = 16.04 Z_o = 0.84 e_e = 0.34 h_r = 5.6 q = 0.36	FSUMSQ = 2.11×10^{-4} red. χ^2 = 3.62	μ_o = 20.97 μ_e = 13.29 Z_o = 1.20 e_e = 0.18 h_r = 18.7 q = 0.48	FSUMSQ = 5.93×10^{-4} red. χ^2 = 21.22
exp. + exp. + exp.	μ_o = 18.78 20.25 25.82 h_z = 0.46 0.68 133.91 h_r = 1.8 7.9 14.3	FSUMSQ = 3.53×10^{-4} (**) red. χ^2 = 6.07	μ_o = 18.71 18.89 22.26 h_z = 0.48 0.55 1.38 h_r = 4.5 2.5 600.0	FSUMSQ = 1.21×10^{-4} (**) red. χ^2 = 5.71
$sech^2$ + exp. + exp.	μ_o = 21.42 18.89 24.39 Z_o = 1.02 h_z = 0.51 4.02 h_r = 5.8 2.2 10.8	FSUMSQ = 2.63×10^{-4} red. χ^2 = 4.63	μ_o = 20.63 18.29 22.56 Z_o = 0.75 h_z = 0.53 1.65 h_r = 7.0 2.6 651.7	FSUMSQ = 9.87×10^{-5} (**) red. χ^2 = 4.38
$sech^2$ + $sech^2$ + exp.	μ_o = 21.51 25.30 19.10 Z_o = 1.00 Z_1 = 6.04 h_z = 0.55 h_r = 5.7 8.8 2.5	FSUMSQ = 2.72×10^{-4} red. χ^2 = 4.69	μ_o = 20.84 23.19 17.84 Z_o = 0.87 Z_1 = 2.81 h_z = 0.47 h_r = 13.7 22.1 2.0	FSUMSQ = 2.94×10^{-4} red. χ^2 = 9.21
exp. + exp. + $r^{1/4}$ law	μ_o = 20.10 26.56 μ_e = 13.93 h_z = 0.60 140.21 e_e = 0.17 h_r = 8.3 218.5 q = 0.44	FSUMSQ = 2.45×10^{-4} (**) red. χ^2 = 4.54	μ_o = 18.16 44.21 μ_e = 21.54 h_z = 0.52 55.49 e_e = 2.36 h_r = 2.9 6.8 q = 0.04	FSUMSQ = 1.05×10^{-4} red. χ^2 = 4.65
exp. + $sech^2$ + $r^{1/4}$ law	μ_o = 19.20 21.27 μ_e = 18.29 h_z = 0.44 Z_1 = 0.89 e_e = 0.64 h_r = 1.9 5.4 q = 0.36	FSUMSQ = 1.74×10^{-4} red. χ^2 = 2.90	μ_o = 18.23 21.15 μ_e = 22.94 h_z = 0.53 Z_1 = 0.77 e_e = 4.83 h_r = 2.5 6.7 q = 0.04	FSUMSQ = 9.64×10^{-5} red. χ^2 = 4.16
$sech^2$ + $sech^2$ + $r^{1/4}$ law	μ_o = 21.05 26.44 μ_e = 14.68 Z_o = 0.91 Z_1 = 8.80 e_e = 0.22 h_r = 6.9 207.3 q = 0.45	FSUMSQ = 1.38×10^{-4} (**) red. χ^2 = 2.99	μ_o = 20.10 22.10 μ_e = 12.49 Z_o = 0.63 Z_1 = 1.74 e_e = 0.14 h_r = 6.4 21.6 q = 0.55	FSUMSQ = 3.25×10^{-4} red. χ^2 = 11.30

MODEL COMBINATION	MODEL OUTPUT PARAMETERS			"QUALITY-OF-FIT" ESTIMATORS
exp.	μ_o = 18.54 h_z = 1.13 h_r = 5.3			FSUMSQ = 3.14×10^{-4} red. χ^2 = 17.76
$sech^2$	μ_o = 20.14 Z_o = 2.18 h_r = 8.0			FSUMSQ = 2.00×10^{-3} red. χ^2 = 88.38
$r^{1/4}$ law	μ_e = 15.44 e_e = 0.67 q = 0.31			FSUMSQ = 8.31×10^{-4} red. χ^2 = 31.12
exp. + exp.	μ_o = 16.96 h_z = 0.51 h_r = 1.4	19.15 1.30 6.5		FSUMSQ = 1.76×10^{-4} red. χ^2 = 6.75
$sech^2$ + exp.	μ_o = 22.10 Z_o = 3.05 h_r = 8.1	18.06 h_z = 0.90 3.6		FSUMSQ = 2.25×10^{-4} red. χ^2 = 10.57
$sech^2$ + $sech^2$	μ_o = 20.14 Z_o = 2.18 h_r = 8.0	42.27 Z_1 = -1.63 34.8		FSUMSQ = 1.96×10^{-4} red. χ^2 = 8.97
exp. + $r^{1/4}$ law	μ_o = 19.59 h_z = 1.04 h_r = 9.6	μ_e = 15.09 e_e = 0.55 q = 0.56		FSUMSQ = 6.12×10^{-5} red. χ^2 = 3.55
$sech^2$ + $r^{1/4}$ law	μ_o = 20.70 Z_o = 1.39 h_r = 9.3	μ_e = 15.37 e_e = 0.65 q = 0.54		FSUMSQ = 6.49×10^{-5} red. χ^2 = 4.12
exp. + exp. + exp.	μ_o = 16.97 h_z = 0.51 h_r = 1.4	19.17 1.31 6.5	22.69 0.003 91.4	FSUMSQ = 1.73×10^{-4} red. χ^2 = 6.80
exp. + exp. + $sech^2$	μ_o = 17.05 h_z = 0.53 h_r = 1.6	19.31 1.37 6.5	24.69 Z_1 = 0.86 2.8	FSUMSQ = 1.63×10^{-4} red. χ^2 = 6.58
$sech^2$ + $sech^2$ + exp.	DID NOT FIT DATA			
exp. + exp. + $r^{1/4}$ law	μ_o = 19.56 h_z = 1.04 h_r = 4.8	21.22 1.02 306.2	μ_e = 15.28 e_e = 0.56 q = 0.51	FSUMSQ = 5.59×10^{-5} (**) red. χ^2 = 3.23
exp. + $sech^2$ + $r^{1/4}$ law	μ_o = 19.64 h_z = 1.04 h_r = 5.2	21.42 Z_1 = 1.45 6.8	μ_e = 15.65 e_e = 0.64 q = 0.51	FSUMSQ = 4.56×10^{-5} red. χ^2 = 2.76
$sech^2$ + $sech^2$ + $r^{1/4}$ law	DID NOT FIT DATA			

Table A.10 : Modelling results for IC 4351

Table A.11 : Modelling results for A0902-68

MODEL COMBINATION	B BAND MODEL OUTPUT PARAMETERS	B BAND "QUALITY-OF-FIT" ESTIMATORS	R BAND MODEL OUTPUT PARAMETERS	R BAND "QUALITY-OF-FIT" ESTIMATORS
exp.	μ_o = 20.16 h_z = 1.05 h_r = 6.0	FSUMSQ = 1.41×10^{-3} red. χ^2 = 19.80	μ_o = 18.49 h_z = 0.86 h_r = 7.2	FSUMSQ = 1.53×10^{-3} red. χ^2 = 19.75
$sech^2$	μ_o = 22.38 Z_o = 2.10 h_r = 11.6	FSUMSQ = 8.01×10^{-3} red. χ^2 = 127.72	DID NOT FIT DATA	
$r^{1/4}$ law	μ_e = 16.05 θ_e = 0.42 q = 0.25	FSUMSQ = 1.85×10^{-3} red. χ^2 = 55.73	μ_e = 13.54 θ_e = 0.27 q = 0.19	FSUMSQ = 2.31×10^{-3} red. χ^2 = 49.71
exp. + exp.	μ_o = 19.13 25.57 h_z = 0.75 25.7 h_r = 4.0 618.2	FSUMSQ = 6.16×10^{-4} (**) red. χ^2 = 9.88	μ_o = 17.57 21.95 h_z = 0.69 1.45 h_r = 3.8 939.3	FSUMSQ = 7.30×10^{-4} (**) red. χ^2 = 9.71
$sech^2$ + exp.	μ_o = 25.62 19.13 Z_o = 11.4 h_z = 0.75 h_r = 109.5 4.0	FSUMSQ = 6.13×10^{-4} red. χ^2 = 9.82	μ_o = 22.04 17.57 Z_o = 2.14 h_z = 0.67 h_r = 9.0 3.8	FSUMSQ = 6.30×10^{-4} red. χ^2 = 8.99
$sech^2$ + $sech^2$	μ_o = 22.38 58.70 Z_o = 2.10 Z_1 = 1.72 h_r = 11.6 6.2	FSUMSQ = 8.01×10^{-3} red. χ^2 = 131.14	DID NOT FIT DATA	
exp. + $r^{1/4}$ law	μ_o = 19.12 μ_e = 25.69 h_z = 0.72 θ_e = 19.5 h_r = 3.9 q = 0.27	FSUMSQ = 6.00×10^{-4} red. χ^2 = 9.66	μ_o = 17.62 μ_e = 20.96 h_z = 0.69 θ_e = 2.20 h_r = 3.8 q = 0.09	FSUMSQ = 8.38×10^{-4} red. χ^2 = 12.37
$sech^2$ + $r^{1/4}$ law	μ_o = 22.87 μ_e = 16.29 Z_o = 1.12 θ_e = 0.46 h_r = 12.5 q = 0.33	FSUMSQ = 9.28×10^{-4} red. χ^2 = 40.15	μ_o = 20.80 μ_e = 12.16 Z_o = 1.47 θ_e = 0.19 h_r = 11.6 q = 0.37	FSUMSQ = 1.50×10^{-3} red. χ^2 = 46.97
exp. + exp. + exp.	μ_o = 19.13 25.56 128.95 h_z = 0.75 24.45 43.31 h_r = 4.0 476.8 14.5	FSUMSQ = 6.17×10^{-4} (**) red. χ^2 = 10.16	μ_o = 17.58 21.92 23.22 h_z = 0.69 1.45 0.68 h_r = 3.8 477.9 3.8	FSUMSQ = 7.30×10^{-4} (**) red. χ^2 = 9.97
$sech^2$ + exp. + exp.	μ_o = 25.62 19.26 21.50 Z_o = 11.41 h_z = 0.75 0.75 h_r = 109.3 4.0 4.0	FSUMSQ = 6.13×10^{-4} (**) red. χ^2 = 10.10	μ_o = 22.01 17.57 28.01 Z_o = 2.09 h_z = 0.67 209.3 h_r = 9.0 3.8 430.5	FSUMSQ = 6.28×10^{-4} (**) red. χ^2 = 8.78
$sech^2$ + $sech^2$ + exp.	μ_o = 25.62 157.16 19.13 Z_o = 11.42 Z_1 = 1.89 h_z = 0.75 h_r = 110.42 118.7 4.0	FSUMSQ = 6.13×10^{-4} (**) red. χ^2 = 10.10	μ_o = 22.01 28.00 17.57 Z_o = 2.09 Z_1 = 120.06 h_z = 0.67 h_r = 9.0 298.6 3.7	FSUMSQ = 6.28×10^{-4} (**) red. χ^2 = 8.77
exp. + exp. + $r^{1/4}$ law	μ_o = 19.26 21.35 μ_e = 25.69 h_z = 0.72 0.72 θ_e = 19.50 h_r = 3.9 3.9 q = 0.27	FSUMSQ = 6.00×10^{-4} red. χ^2 = 9.92	μ_o = 17.57 21.94 μ_e = 61.77 h_z = 0.69 1.45 θ_e = 53.42 h_r = 3.8 757.5 q = -115.39	FSUMSQ = 7.31×10^{-4} (**) red. χ^2 = 9.96
exp. + $sech^2$ + $r^{1/4}$ law	DID NOT FIT DATA		μ_o = 17.57 22.04 μ_e = 41.25 h_z = 0.67 Z_1 = 2.14 θ_e = 18.24 h_r = 3.8 9.0 q = -0.61	FSUMSQ = 6.30×10^{-4} red. χ^2 = 9.22
$sech^2$ + $sech^2$ + $r^{1/4}$ law	DID NOT FIT DATA		DID NOT FIT DATA	

Table A.12 : Modelling results for A0919-33

MODEL COMBINATION	B BAND MODEL OUTPUT PARAMETERS	B BAND "QUALITY-OF-FIT" ESTIMATORS	R BAND MODEL OUTPUT PARAMETERS	R BAND "QUALITY-OF-FIT" ESTIMATORS
exp.	μ_o = 21.44 h_z = 6.80 h_r = -7579.8	FSUMSQ = 2.73×10^{-3} (**) red. χ^2 = 77.68	μ_o = 19.92 h_z = 7.76 h_r = 27.5	FSUMSQ = 5.60×10^{-4} red. χ^2 = 11.57
$sech^2$	μ_o = 22.02 Z_o = 11.04 h_r = 34.5	FSUMSQ = 1.92×10^{-3} red. χ^2 = 61.30	μ_o = 21.64 Z_o = 15.00 h_r = 51.6	FSUMSQ = 4.27×10^{-3} red. χ^2 = 81.95
$r^{1/4}$ law	DID NOT FIT DATA		μ_e = 16.76 θ_e = 4.50 q = 0.47	FSUMSQ = 7.77×10^{-4} red. χ^2 = 15.52
exp. + exp.	μ_o = 19.30 21.41 h_z = 1.74 9.18 h_r = 23.5 22.9	FSUMSQ = 1.50×10^{-4} red. χ^2 = 4.86	μ_o = 19.29 20.97 h_z = 4.08 10.54 h_r = 20.2 30.2	FSUMSQ = 4.49×10^{-4} red. χ^2 = 7.71
$sech^2$ + exp.	μ_o = 23.87 20.02 Z_o = 25.14 h_z = 3.94 h_r = 27.7 16.3	FSUMSQ = 2.14×10^{-4} red. χ^2 = 12.46	μ_o = 19.99 20.08 Z_o = 2.55 h_z = 8.16 h_r = 26.9 27.5	FSUMSQ = 4.93×10^{-4} red. χ^2 = 9.65
$sech^2$ + $sech^2$	DID NOT FIT DATA		DID NOT FIT DATA	
exp. + $r^{1/4}$ law	μ_o = 21.05 μ_e = 20.68 h_z = 2.90 θ_e = 12.34 h_r = 51.4 q = 0.63	FSUMSQ = 6.09×10^{-5} red. χ^2 = 2.52	μ_o = 19.92 μ_e = 17.87 h_z = 3.29 θ_e = 6.70 h_r = 78.8 q = 0.69	FSUMSQ = 1.88×10^{-4} red. χ^2 = 4.63
$sech^2$ + $r^{1/4}$ law	μ_o = 22.44 μ_e = 20.19 Z_o = 4.52 θ_e = 10.06 h_r = 59.7 q = 0.58	FSUMSQ = 7.02×10^{-5} red. χ^2 = 3.04	μ_o = 20.96 μ_e = 17.65 Z_o = 5.25 θ_e = 6.24 h_r = 75.7 q = 0.67	FSUMSQ = 1.86×10^{-4} red. χ^2 = 4.75
exp. + exp. + exp.	μ_o = 19.30 21.41 68.80 h_z = 1.74 9.18 0.12 h_r = 23.5 22.9 55.5	FSUMSQ = 1.50×10^{-4} red. χ^2 = 4.93	μ_o = 17.28 19.60 21.75 h_z = 0.74 5.33 12.98 h_r = 23.9 23.2 31.9	FSUMSQ = 4.48×10^{-4} (**) red. χ^2 = 7.79
$sech^2$ + exp. + exp.	μ_o = 22.68 19.50 21.60 Z_o = 2.47 h_z = 2.24 9.65 h_r = 1808.2 11.9 25.4	FSUMSQ = 1.13×10^{-4} red. χ^2 = 3.93	μ_o = 21.65 19.41 21.15 Z_o = 2.60 h_z = 4.46 11.07 h_r = 15.1 20.1 30.6	FSUMSQ = 4.44×10^{-4} red. χ^2 = 7.71
$sech^2$ + $sech^2$ + exp.	DID NOT FIT DATA		DID NOT FIT DATA	
exp. + exp. + $r^{1/4}$ law	μ_o = 20.42 22.39 μ_e = 20.72 h_z = 1.85 7.23 θ_e = 11.05 h_r = 44.3 23.9 q = 0.60	FSUMSQ = 5.06×10^{-5} red. χ^2 = 2.05	μ_o = 20.29 21.05 μ_e = 18.09 h_z = 2.62 5.55 θ_e = 6.97 h_r = 1863.3 29.9 q = 0.69	FSUMSQ = 1.83×10^{-4} (**) red. χ^2 = 4.21
$sech^2$ + exp. + $r^{1/4}$ law	DID NOT FIT DATA		μ_o = 21.19 21.23 μ_e = 18.03 Z_o = 4.70 h_z = 5.80 θ_e = 6.83 h_r = 217.2 30.0 q = 0.68	FSUMSQ = 1.80×10^{-4} red. χ^2 = 4.18
$sech^2$ + $sech^2$ + $r^{1/4}$ law	DID NOT FIT DATA		μ_o = 22.02 21.26 μ_e = 17.65 Z_o = 3.34 Z_1 = 5.62 θ_e = 6.24 h_r = 827.9 70.4 q = 0.67	FSUMSQ = 1.86×10^{-4} red. χ^2 = 4.79

Table A.13 : Modelling results for A0931-32

MODEL COMBINATION	MODEL OUTPUT PARAMETERS		"QUALITY-OF-FIT" ESTIMATORS
exp.	μ_o = 19.54 h_z = 0.17 h_r = 2.2		FSUMSQ = 1.41×10^{-4} red. χ^2 = 3.55
$sech^2$	μ_o = 20.24 Z_o = 0.26 h_r = 5.8		FSUMSQ = 5.14×10^{-4} red. χ^2 = 11.60
$r^{1/4}$ law	μ_e = 20.05 θ_e = 0.5 q = 0.12		FSUMSQ = 7.56×10^{-4} red. χ^2 = 14.04
$sech^2$ + $sech^2$	μ_o = 20.21 Z_o = 0.16 h_r = 0.5	21.33 0.35 56.8	FSUMSQ = 2.68×10^{-4} (**) red. χ^2 = 8.93
$sech^2$ + exp.	μ_o = 20.61 Z_o = 0.19 h_r = 0.5	20.54 h_z = 0.21 88.0	FSUMSQ = 2.67×10^{-4} (**) red. χ^2 = 8.96
exp. + exp.	DID NOT FIT DATA		
exp. + $r^{1/4}$ law	μ_o = 19.77 h_z = 0.17 h_r = 111.9	μ_e = 20.16 θ_e = 0.2 q = 235.9	FSUMSQ = 2.77×10^{-4} (**) red. χ^2 = 6.72
$sech^2$ + $r^{1/4}$ law	μ_o = 20.37 Z_o = 0.22 h_r = 32.2	μ_e = 23.88 θ_e = 2.6 q = 0.18	FSUMSQ = 3.46×10^{-4} (**) red. χ^2 = 8.93

MODEL COMBINATION	MODEL OUTPUT PARAMETERS			"QUALITY-OF-FIT" ESTIMATORS
exp.	μ_o = 20.15 h_z = 6.67 h_r = 78.4			FSUMSQ = 1.18×10^{-3} red. χ^2 = 17.40
$sech^2$	μ_o = 21.21 Z_o = 10.98 h_r = 72.8			FSUMSQ = 2.18×10^{-3} red. χ^2 = 31.31
$r^{1/4}$ law	μ_e = 18.42 θ_e = 6.31 q = 0.14			FSUMSQ = 5.95×10^{-4} red. χ^2 = 7.60
exp. + exp.	μ_o = 19.04 h_z = 3.86 h_r = 38.7	23.06 23.06 3531.6		FSUMSQ = 4.80×10^{-4} (**) red. χ^2 = 6.22
$sech^2$ + exp.	μ_o = 23.01 Z_o = 3.75 h_r = 71.0	20.22 h_z = 6.86 78.2		FSUMSQ = 1.17×10^{-3} red. χ^2 = 17.62
$sech^2$ + $sech^2$	DID NOT FIT DATA			
exp. + $r^{1/4}$ law	μ_o = 19.91 h_z = 3.19 h_r = 59.8	μ_e = 19.84 θ_e = 11.09 q = 0.18		FSUMSQ = 2.62×10^{-4} red. χ^2 = 4.10
$sech^2$ + $r^{1/4}$ law	μ_o = 21.52 Z_o = 4.67 h_r = 91.1	μ_e = 19.00 θ_e = 8.12 q = 0.19		FSUMSQ = 2.56×10^{-4} red. χ^2 = 4.22
exp. + exp. + exp.	DID NOT FIT DATA			
exp. + $sech^2$ + exp.	DID NOT FIT DATA			
$sech^2$ + $sech^2$ + exp.	DID NOT FIT DATA			
exp. + exp. + $r^{1/4}$ law	μ_o = 19.91 h_z = 3.19 h_r = 59.8	118.57 -3.00 74.5	μ_e = 19.84 θ_e = 11.09 q = 0.18	FSUMSQ = 2.62×10^{-4} red. χ^2 = 4.24
exp. + $sech^2$ + $r^{1/4}$ law	μ_o = 20.81 h_z = 3.14 h_r = 42.5	21.85 Z_1 = 4.75 92.5	μ_e = 19.41 θ_e = 9.46 q = 0.19	FSUMSQ = 2.54×10^{-4} red. χ^2 = 4.23
$sech^2$ + $sech^2$ + $r^{1/4}$ law	DID NOT FIT DATA			

Table A.14 : Modelling results for A1611-00

Table A.15 : Modelling results for UGC 7170

MODEL COMBINATION	B BAND MODEL OUTPUT PARAMETERS	B BAND "QUALITY-OF-FIT" ESTIMATORS	R BAND MODEL OUTPUT PARAMETERS	R BAND "QUALITY-OF-FIT" ESTIMATORS
exp.	μ_o = 21.34 h_z = 0.37 h_r = 3.8	FSUMSQ = 5.13×10^{-4} red. χ^2 = 2.06	μ_o = 20.36 h_z = 0.38 h_r = 3.7	FSUMSQ = 7.97×10^{-4} red. χ^2 = 3.35
$sech^2$	μ_o = 22.69 Z_o = 0.55 h_r = 6.1	FSUMSQ = 6.05×10^{-3} red. χ^2 = 24.58	DID NOT FIT DATA	
$r^{1/4}$ law	μ_e = 23.93 e_e = 1.47 q = 0.03	FSUMSQ = 7.94×10^{-3} red. χ^2 = 35.53	μ_e = 22.08 e_e = 1.31 q = 0.06	FSUMSQ = 7.41×10^{-3} red. χ^2 = 32.91
exp. + exp.	μ_o = 21.26 69.94 h_z = 0.36 153.17 h_r = 3.5 -0.2	FSUMSQ = 3.82×10^{-4} (**) red. χ^2 = 1.97	μ_o = 20.07 23.62 h_z = 0.31 0.71 h_r = 2.7 23.1	FSUMSQ = 4.61×10^{-4} red. χ^2 = 1.68
$sech^2$ + exp.	μ_o = 25.99 21.16 Z_o = 1.02 h_z = 0.33 h_r = 5.1 3.3	FSUMSQ = 4.12×10^{-4} red. χ^2 = 1.74	DID NOT FIT DATA	
$sech^2$ + $sech^2$	DID NOT FIT DATA		DID NOT FIT DATA	
exp. + $r^{1/4}$ law	μ_o = 21.22 μ_e = 29.81 h_z = 0.34 e_e = 21.17 h_r = 3.5 q = 0.06	FSUMSQ = 4.42×10^{-4} red. χ^2 = 1.74	μ_o = 20.17 μ_e = 27.20 h_z = 0.34 e_e = 10.92 h_r = 3.2 q = 0.10	FSUMSQ = 4.71×10^{-4} red. χ^2 = 1.71
$sech^2$ + $r^{1/4}$ law	μ_o = 22.54 μ_e = 26.72 Z_o = 0.43 e_e = 11.19 h_r = 6.5 q = 0.58	FSUMSQ = 2.43×10^{-3} red. χ^2 = 11.09	DID NOT FIT DATA	
exp. + exp. + exp.	μ_o = 21.19 26.42 94.54 h_z = 0.34 0.88 11.07 h_r = 3.3 166.0 8.0	FSUMSQ = 4.40×10^{-4} red. χ^2 = 1.84	μ_o = 20.18 21.85 55.57 h_z = 0.28 0.48 -0.08 h_r = 2.3 6.7 100.53	FSUMSQ = 4.49×10^{-4} (**) red. χ^2 = 1.71
$sech^2$ + exp. + exp.	μ_o = 25.99 21.16 55.88 Z_o = 1.02 h_z = 0.33 22.06 h_r = 5.1 3.3 23.6	FSUMSQ = 4.12×10^{-4} red. χ^2 = 1.82	μ_o = 23.43 20.05 27.05 Z_o = 0.75 h_z = 0.30 114.98 h_r = 6.7 2.6 45.4	FSUMSQ = 3.63×10^{-4} (**) red. χ^2 = 1.44
$sech^2$ + $sech^2$ + exp.	DID NOT FIT DATA		DID NOT FIT DATA	
exp. + exp. + $r^{1/4}$ law	μ_o = 21.22 78.88 μ_e = 29.81 h_z = 0.34 -0.98 e_e = 21.17 h_r = 3.5 8.3 q = 0.06	FSUMSQ = 4.42×10^{-4} red. χ^2 = 1.81	μ_o = 20.39 21.34 μ_e = 28.09 h_z = 0.28 0.41 e_e = 15.29 h_r = 2.2 4.9 q = 0.13	FSUMSQ = 4.46×10^{-4} red. χ^2 = 1.70
exp. + $sech^2$ + $r^{1/4}$ law	μ_o = 21.18 25.06 μ_e = 30.36 h_z = 0.32 Z_1 = 0.66 e_e = 58.34 h_r = 3.1 5.9 q = 0.41	FSUMSQ = 4.02×10^{-4} red. χ^2 = 1.68	μ_o = 20.09 23.27 μ_e = 28.11 h_z = 0.30 Z_1 = 0.67 e_e = 23.08 h_r = 2.6 6.6 q = 0.25	FSUMSQ = 3.43×10^{-4} red. χ^2 = 1.38
$sech^2$ + $sech^2$ + $r^{1/4}$ law	DID NOT FIT DATA		DID NOT FIT DATA	

- Appendix B -

Digital Unsharp Masking

This appendix describes a technique which proved useful in the recovery of more structural information within the observational material presented in this thesis than was possible from a simple visual inspection - particularly for those galaxies showing the box/peanut morphology discussed in chapter VI.

An "unsharp mask" is the name given to the version of an original image which has undergone spatial frequency filtering. Such a mask is said to be "unsharp" if it acts only to filter-out the low frequency signal in an image, thus leaving the finer details untouched. Malin (1977) was the first to detail astronomical applications of such a method, and more recently Schweizer & Ford (1984) have outlined the general procedures involved in digitising this technique. They have also pointed out the added value of the digital form over the photographic version in allowing one to create an unsharp mask of a specific luminosity profile (such as an $r^{1/4}$ law) rather than being limited to a simple Gaussian profile - a procedure generating more qualitative information concerning the photometric properties of the galaxies under study.

In essence the process is a combination of smoothing and filtering a given image followed by subsequent manipulation to enhance low surface brightness features (such as shells) or features heavily masked by light from the galactic bulge (such as inner dust lanes).

The steps involved in such a process are as follows :

(1) First one is required to remove as many contaminating stars or faint galaxies as possible - the interpolation routines outlined in chapter II are applied in such situations.

(2) The effects of additional faint stars or general noise (such as that resulting from non-uniformities in the photographic plate) are then suppressed over the region of interest by applying a median filter to the image. The use of such a filter can be particularly advantageous in acting to reduce the effects of faint stars which are superposed on the galaxy of interest and where interpolation routines, such as that adopted in chapter III, prove unreliable and would introduce spurious effects of their own.

(3) The unsharp mask is then created. Such a mask should, by definition, possess all the underlying features of the object concerned (i.e. its overall shape) but should be a sufficiently smoothed version of the original. The creation of such a mask is facilitated by convolving the median-filtered frame with a Gaussian profile of specified σ, the value of which is optimised to ensure considerable enhancement of the input frame over the scale required (but balanced with the correspondingly increased computing time required to achieve the end result).

(4) A suitably created unsharp mask is then subtracted from the median-filtered image so that the smooth "background" is removed, hence allowing one to enhance considerably the contrast of the resultant frame or use further median-filtering to highlight the

features of interest. Such a background will, of course, include not only sky around the object concerned but also all structure on the object itself over scales larger than the box size chosen for the filtering process. Typically only ~ 80 to 85 % of the unsharp mask is actually subtracted as this allows one to preserve the intensity levels between initial and final images (i.e. essentially to improve the visibility of the residual structure after application of such a process).

By way of illustration, below are presented the results of such a procedure in the study of the peanut-shaped elliptical galaxy IC 2977, an object which complements those investigated in chapter VI.

B.1 The application of digital unsharp masking to IC 2977

This object was initially kindly brought to my attention by Dr. B. Jarvis (private communication, 1986). Since I isolated it in the list of shell ellipticals presented by Malin & Carter (1983), it was anticipated that this galaxy would provide a good test of the quality of the procedures outlined above.

The optimised box size over which the median filtering was carried out was found to be 7x7 or 9x9 pixels with the most appropriate choice of σ for the convolving Gaussian profile being of equal size to that of the median filter. Values in excess of 9x9 were not found to improve the quality of the final image. Best results were achieved when only 80 % of the unsharp mask was subsequently removed from the median-filtered image.

The results of such a process are illustrated in figure B.1 which gives a step-by-step guide to the image appearance during processing. The shells are clearly visible after application of the masking process, with several identifiable at both the S.E. and N.W. extremities of the galaxy. Two larger scale, but very much fainter, shell-like features were also identified out to distances of several galaxian radii (not evident on figure B.1). In common with most shell ellipticals studied to date, none of the shells seen here is complete (in the sense of encircling the host system). No further improvement in their final appearance resulted from the application of alternative median filters. The final frame (4) in figure B.1 shows the effect of subtracting the unsharp-masked image from the original - the peanut shape of the underlying elliptical galaxy is particularly evident.

B.2 Unsharp masking of a number of the present sample galaxies

In this section, using the precepts outlined in this appendix, I seek to investigate the existence of possible low surface brightness structure around the bulges of a number of the spirals and lenticulars in the previously defined sample of large, edge-on galaxies discussed in chapter I, supplemented by a number of box-shaped elliptical candidates.

The objects chosen for investigation in this way comprised all those for which CCD observations were available, i.e. those in table 1.1 plus 2x400 secs R band frames of the box-elliptical NGC 7029 taken at the AAT under service observations during August 1986, together with several candidates scanned by COSMOS using the SERC J survey plates. Only one galaxy mapped using POSS material, the box-elliptical

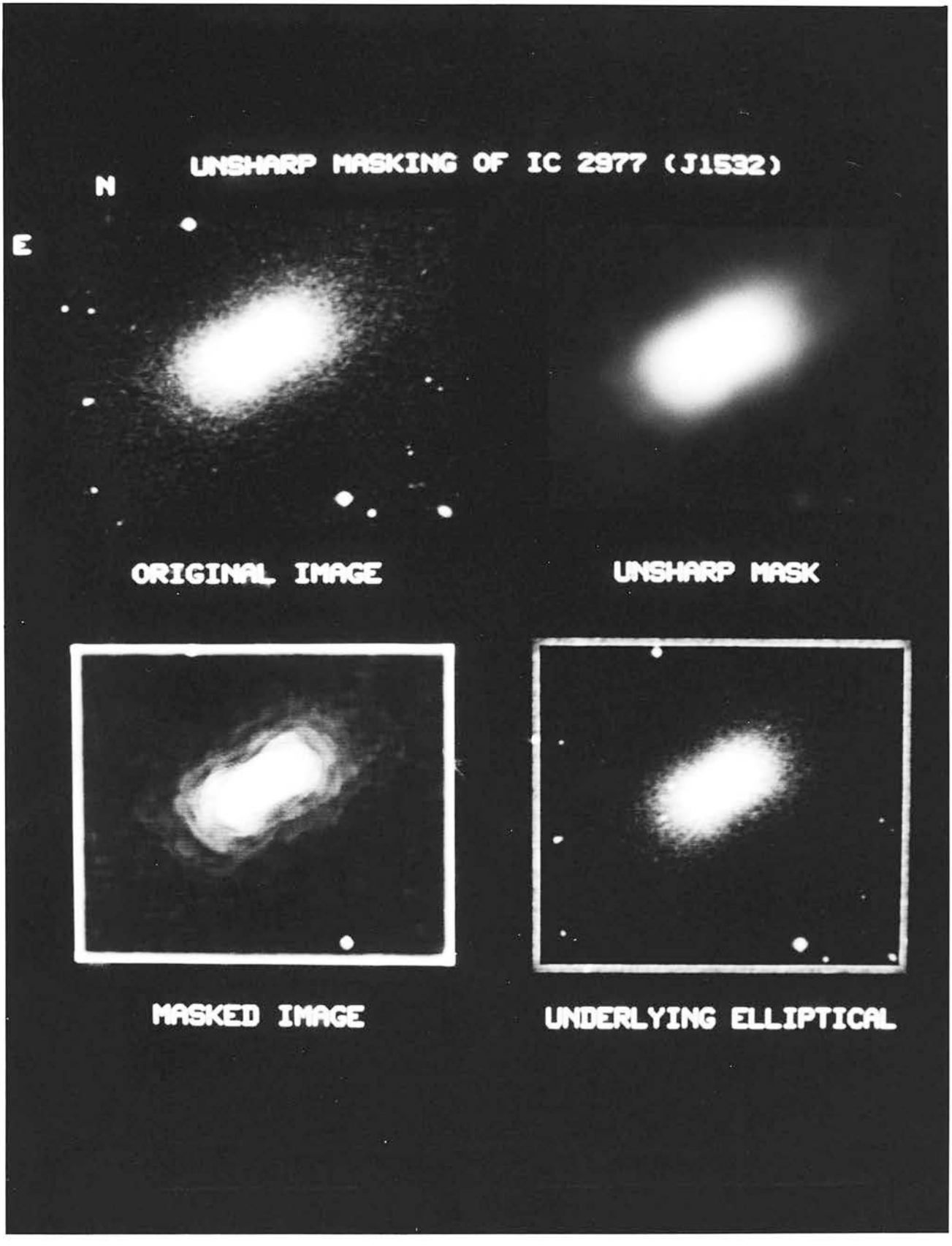
UNSHARP MASKING OF IC 2977 (J1532)
N
E
ORIGINAL IMAGE
UNSHARP MASK
MASKED IMAGE
UNDERLYING ELLIPTICAL

figure B.1

NGC 5322, was used as it was realised that such plates are generally of too poor dynamic range and contrast for such analyses. In the case of galaxies scanned by COSMOS, I focussed on efforts to delineate external features to the bulges concerned since the plate material from which the scans are derived was often found to be saturated in the very central regions of most of the galaxies chosen.

Specific results of such an investigation for those systems analysed from the COSMOS mapping data, or for which CCD data was available, and which responded to such processing are outlined below.

Results for the COSMOS scanned galaxies

NGC 3390 :

Considerable flaring/distortion of the faintest isophotes was evident at both ends of the disc. Such structure was not seen on the original plate used and has such an irregular form that its resulting from warping of the disc seems unlikely.

NGC 3717 :

The isophotes of the inner bulge were seen to display a weak peanut-shaped appearance, although this system is not exactly edge-on.

Results for the CCD galaxies

NGC 2310 :

This galaxy was initially classified as possessing a box bulge at the centre. However, unsharp masking highlighted pronounced depressions along the minor axis at all isophotal levels (the fainter ones gave the general appearance of a peanut shape). Additional

evidence exists for a major axis dust lane (which was seen to extend to the very central regions of the galaxy) - figure B.2 (left) showing the B band isophotes of this galaxy before and after application of such a technique.

NGC 4289 :

Evidence was found of a sharp deviation of the disc light away from the major axis at the N end of the disc and of the possible existence of a peanut shaped central bulge (the latter not being evident on inspection of the original frame), with minor axis isophote "dips" seen either side of the dust lane.

NGC 4469 :

Previous inspection of the image showed, aside from the clear evidence of the peanut bulge, the existence of a major axis dust lane. Unsharp masking revealed that this lane extends to the very centre of the galaxy. The peanut shape was also considerably enhanced by the masking process as is clearly evident in figure B.2 (right). No other (fainter) features were noted in either B or R images, however.

NGC 5170 :

Again images in both B and R of the very central region of the bulge showed a peanut-shaped appearance (even allowing for the very small size of the bulge in this galaxy coupled with it being some way from edge-on). There was, however, no evidence of any low surface brightness features in this galaxy.

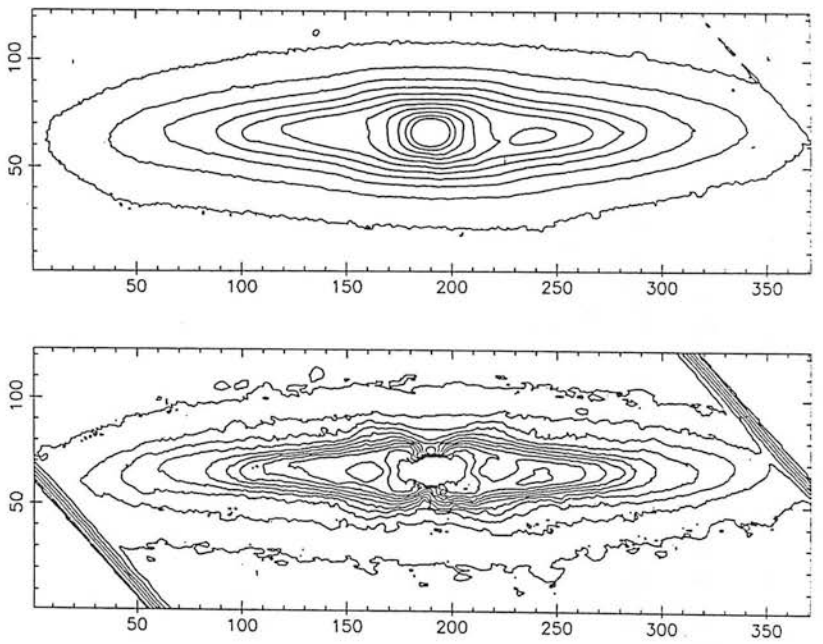

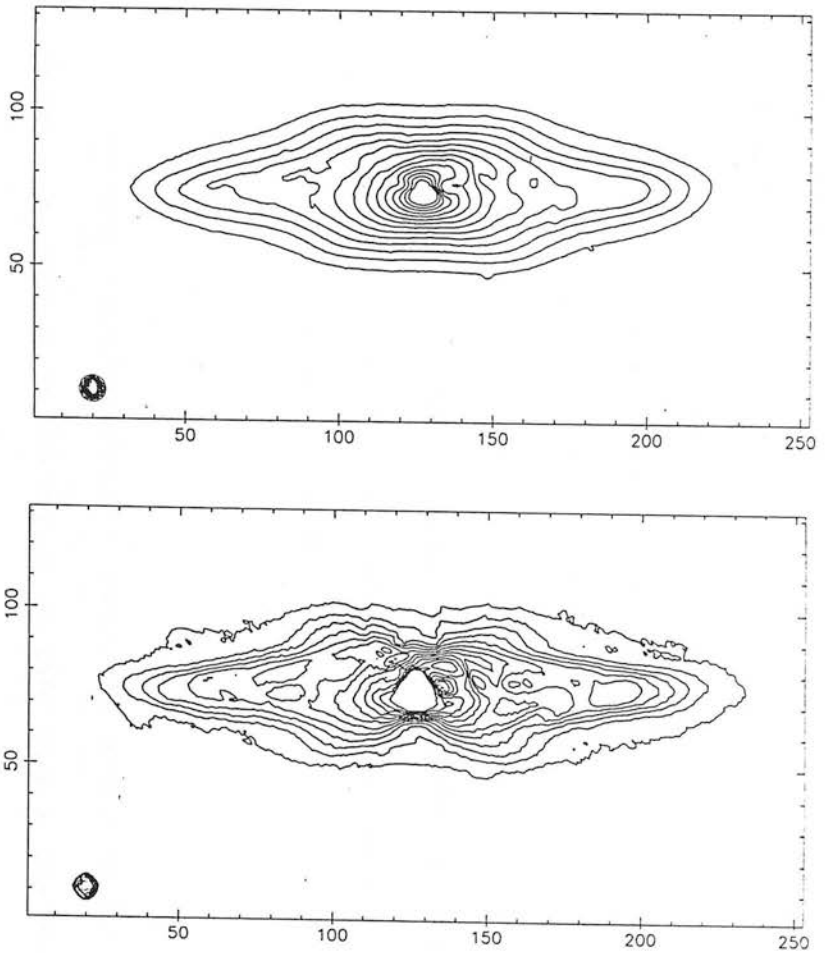

Figure B.2 : Contour plots taken from subregions of the 2000 secs CCD frames of the S0 galaxy NGC 2310 (B) and the S0/a NGC 4469 (R) at the prime focus of the AAT. The upper figures in each case correspond to the original image and the lower ones to that same after digital unsharp masking using a median filtering box size of 9x9 pixels (4x4 arcsecs) and a convolving Gaussian with a σ also of 9 pixels. The contour levels are at equal spacings in logarithmic intensity, and the (X,Y) axes are labelled in pixels (1 pixel ~ 0.48 arcsecs). The diagonal banding at the ends of the plot in the case of NGC 2310 mark the edges of the CCD frame used,

NGC 7029 :

Digital unsharp masking of the (solely R band) frames of this box-shaped galaxy failed to detect any evidence of faint shell structure in the outer regions when adopting median filters of either 7x7 or 9x9 pixels. However, clear evidence was seen for inner disc structure (although this feature was also evident to a lesser degree on the original frames). NGC 7029 is classified as an uncertain E6 by the RC2 but as an S0 by the RSA.

IC 4351 :

Unsharp masking greatly enhances one's ability to trace the spiral arm pattern to the centre in this galaxy. Contrast enhancement of the resulting unsharp masked image obtained from a COSMOS scan of the relevant plate reveals a flattening of the inner bulge - although this is a tentative result as IC 4351 is some 5^{o} from edge-on. The spatial extent of the CCD observations is too limited to allow further conclusions to be drawn.

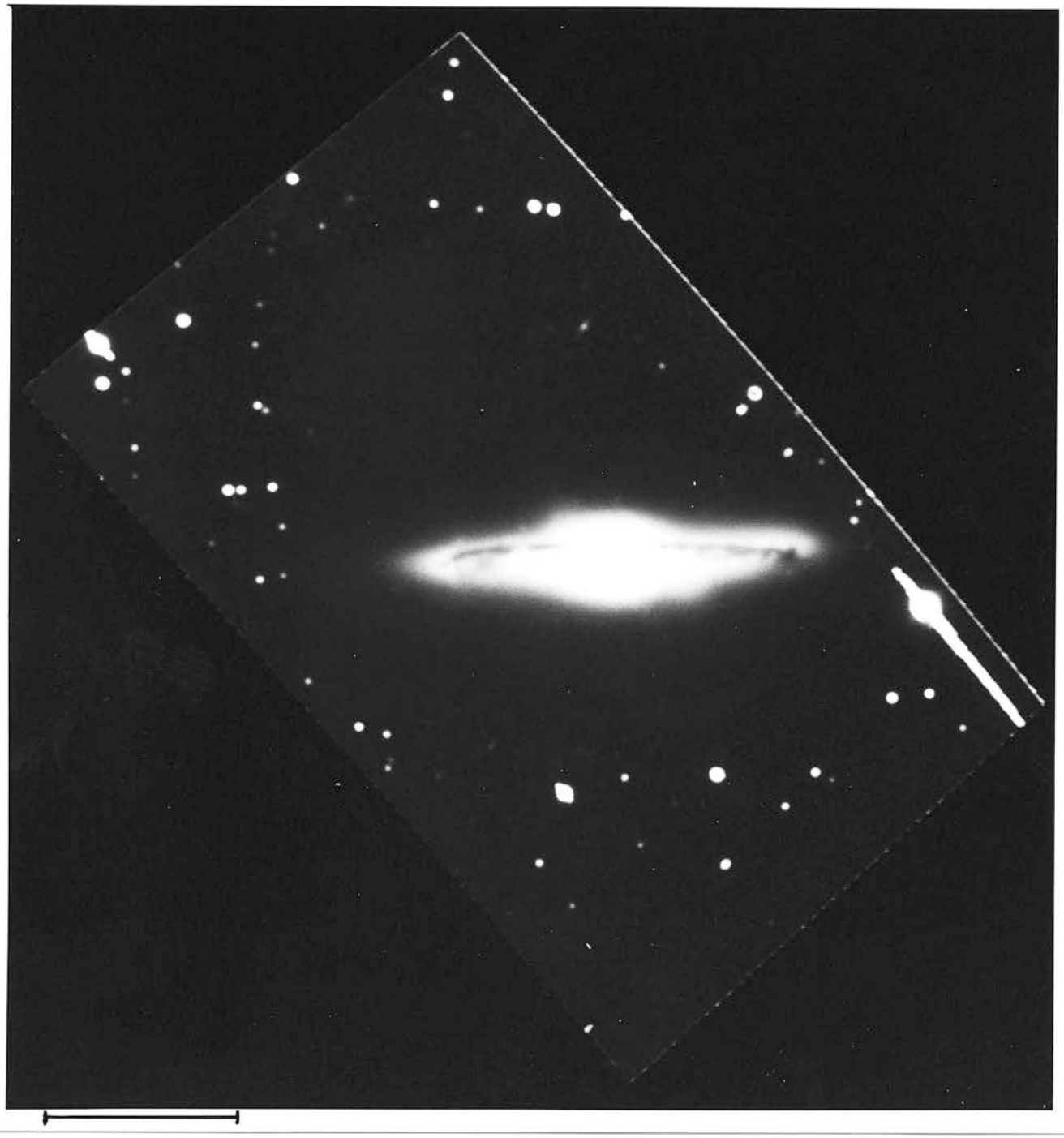

NGC 2295 (R band)

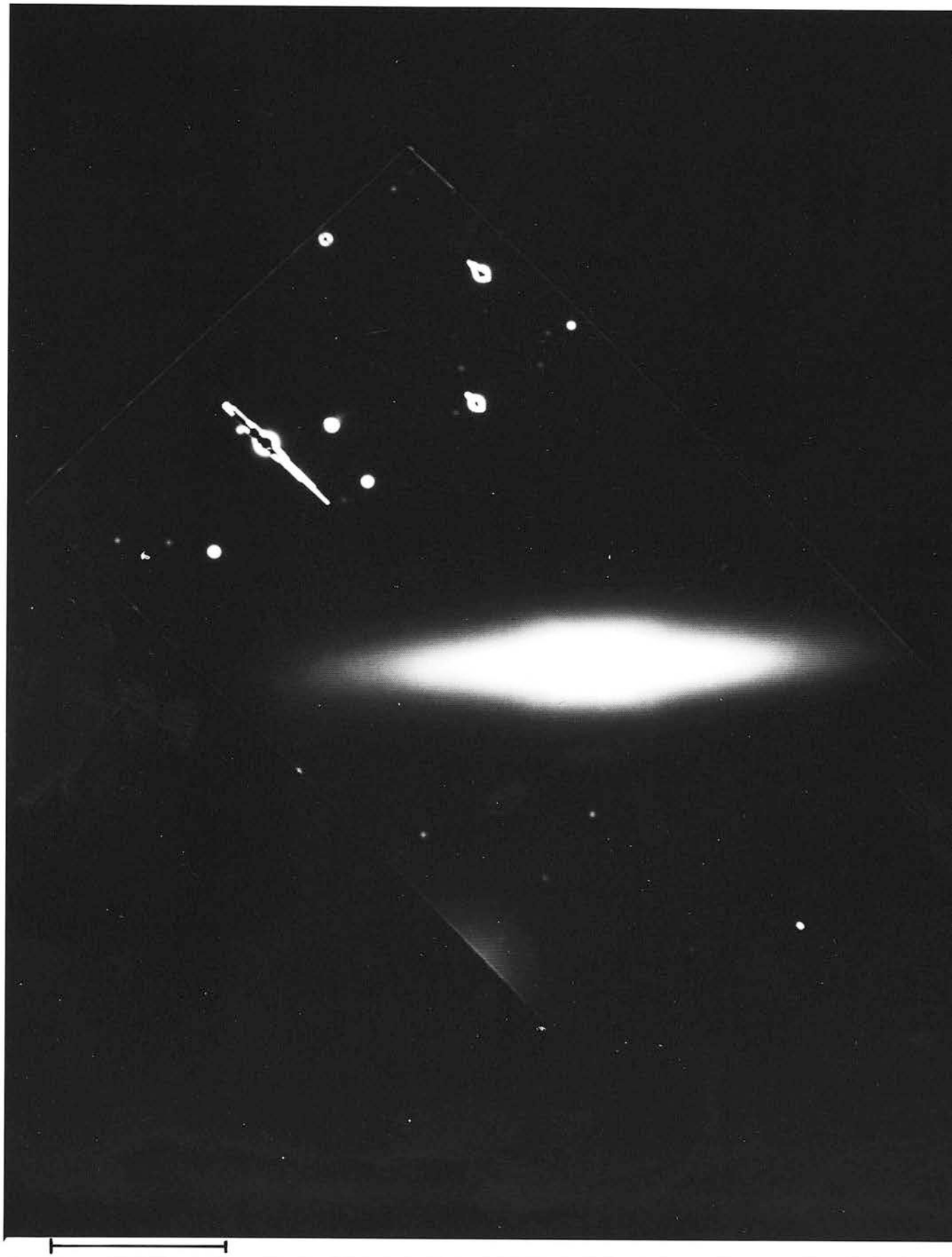

NGC 2310 (R band)

NGC 3573 (R band)

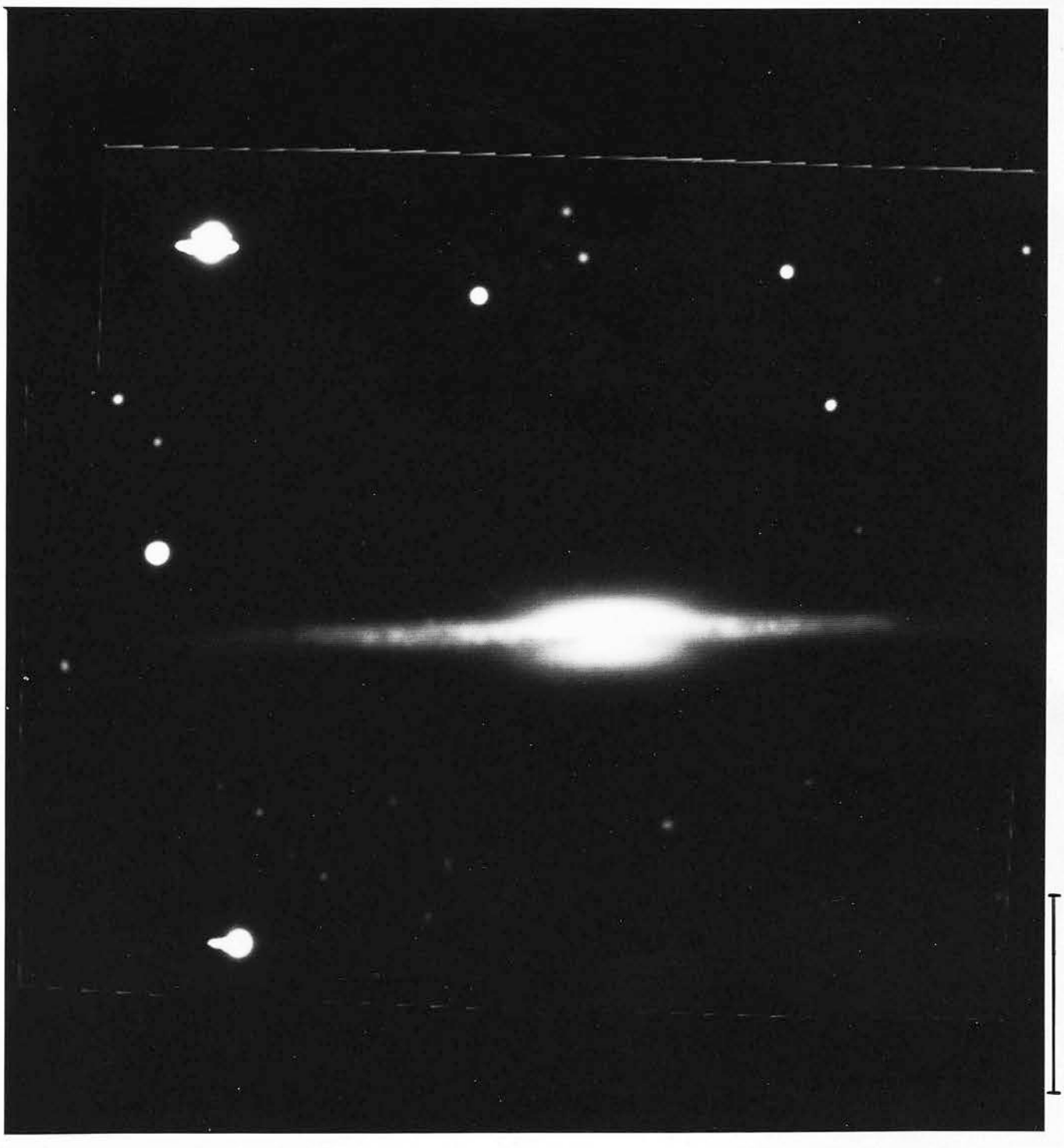

NGC 4289 (R band)

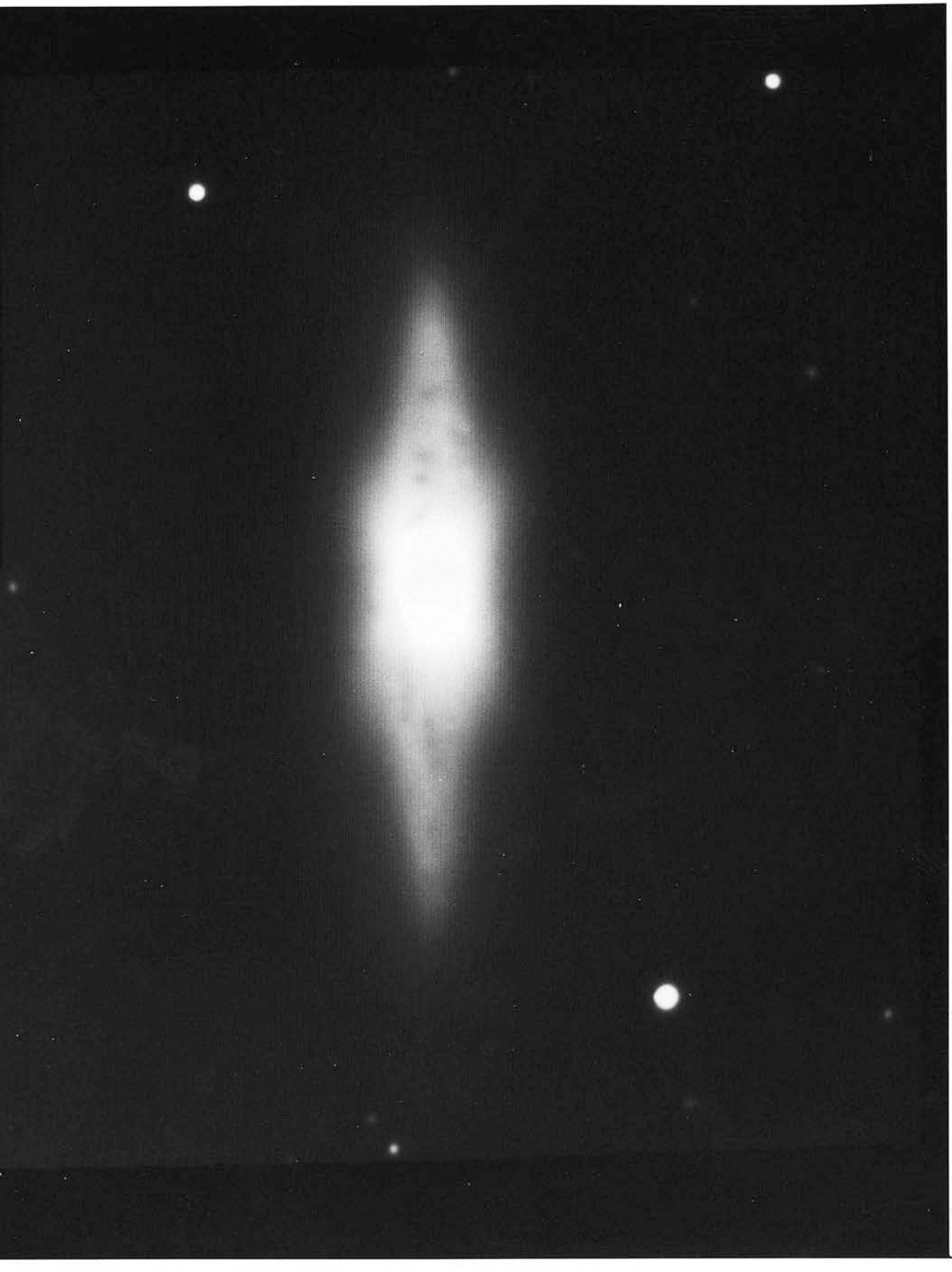

NGC 4469 (R band)

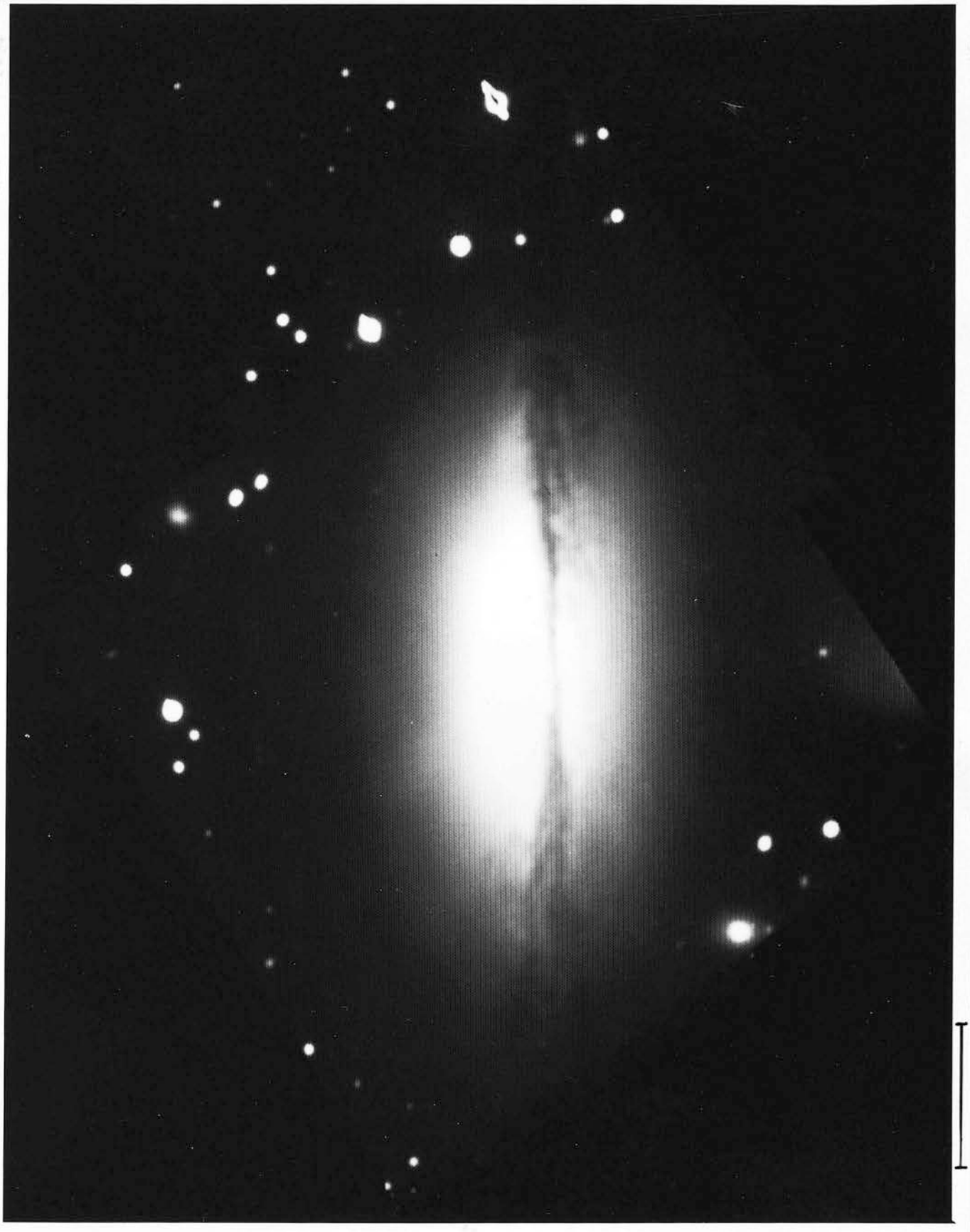

NGC 5078 (R band)

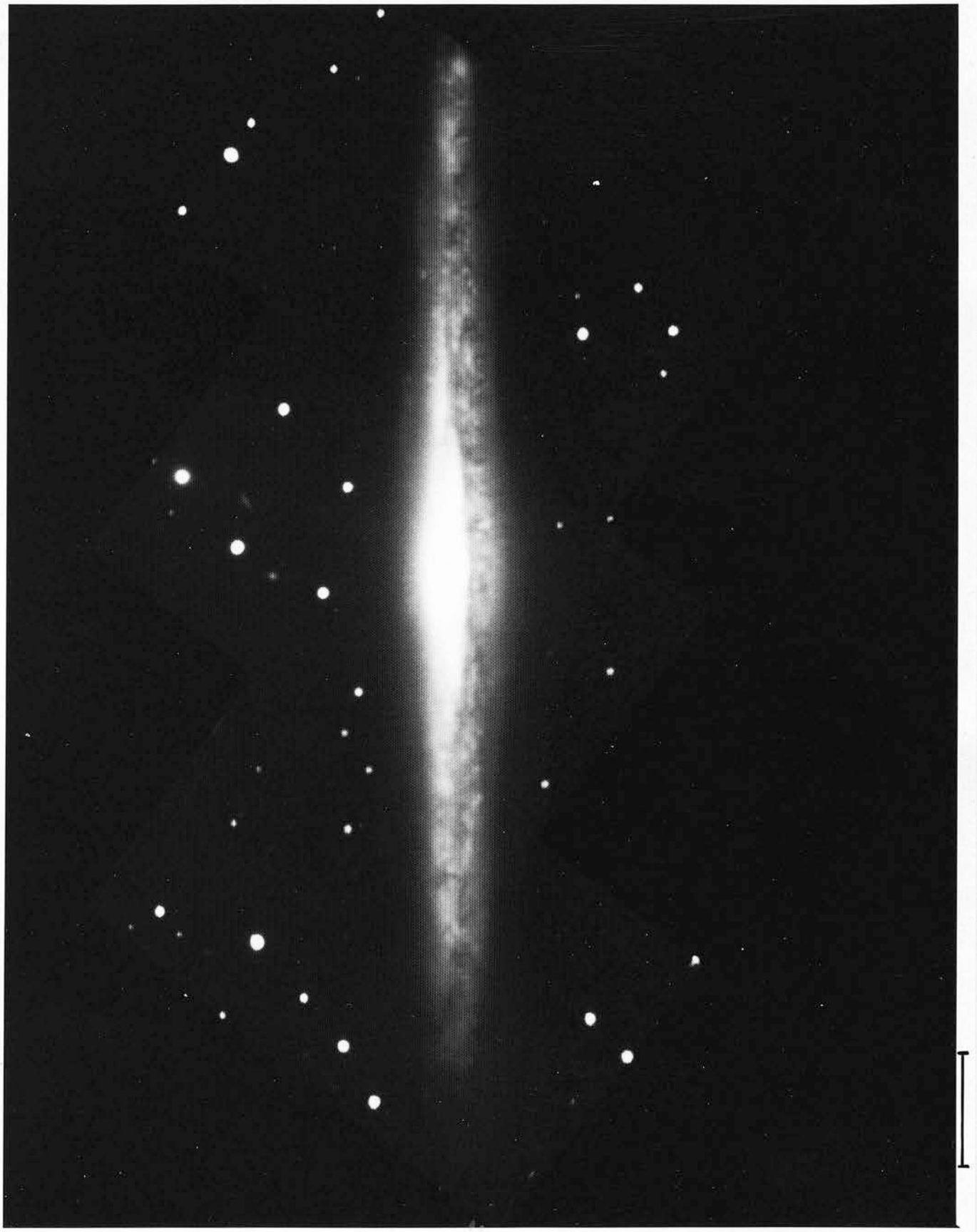

NGC 5170 (B band)

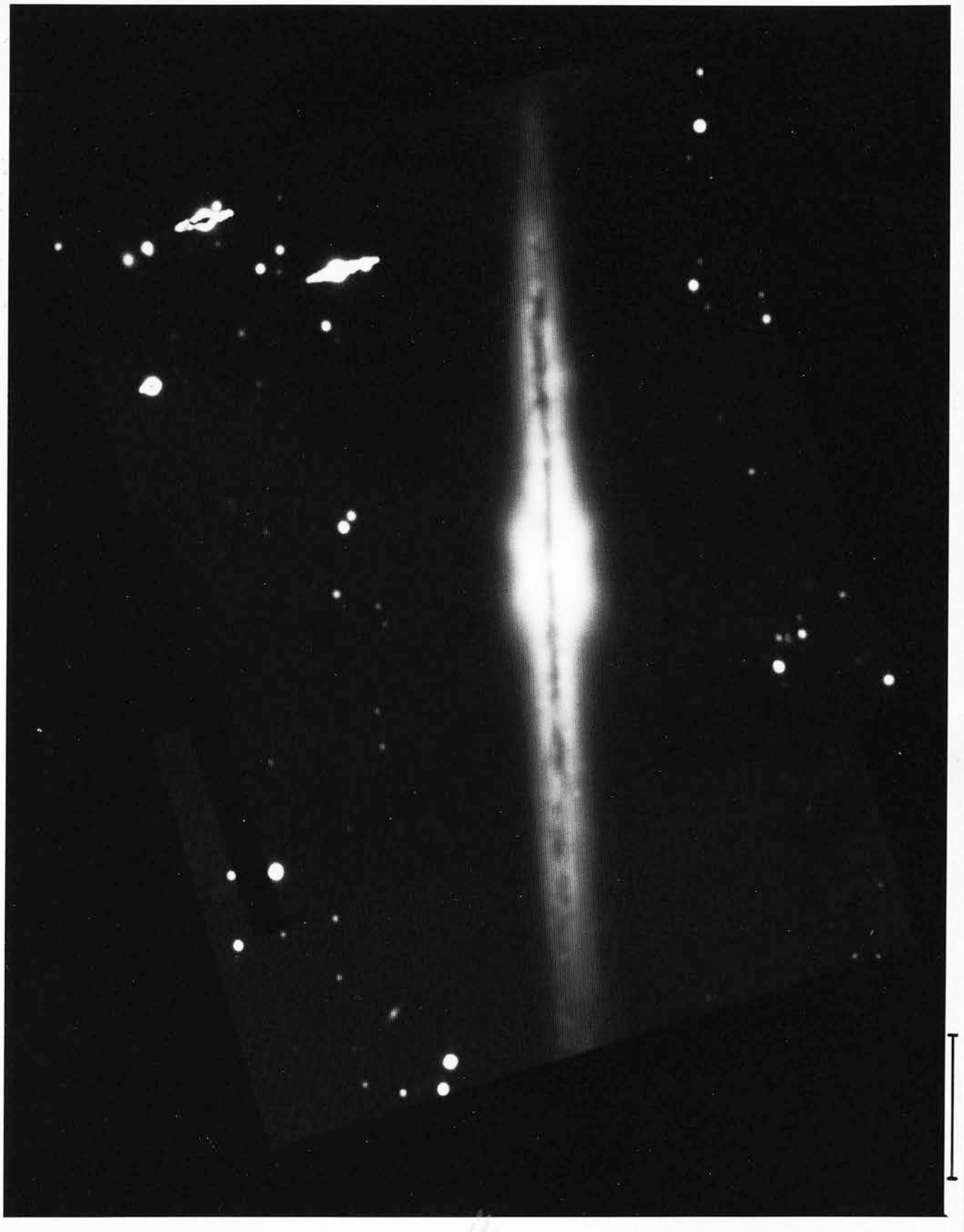

IC 2531 (R band)

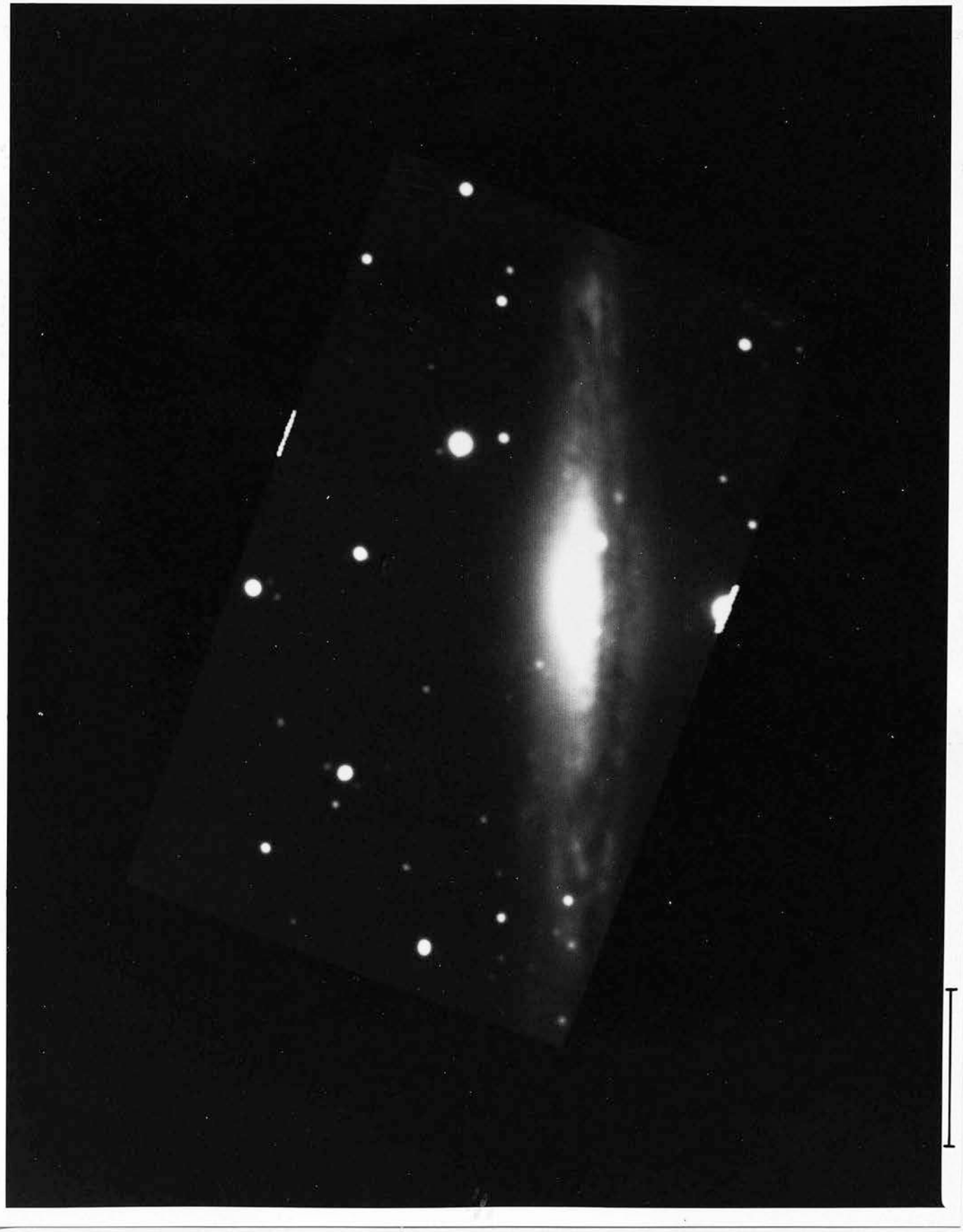

IC 4351 (R band)

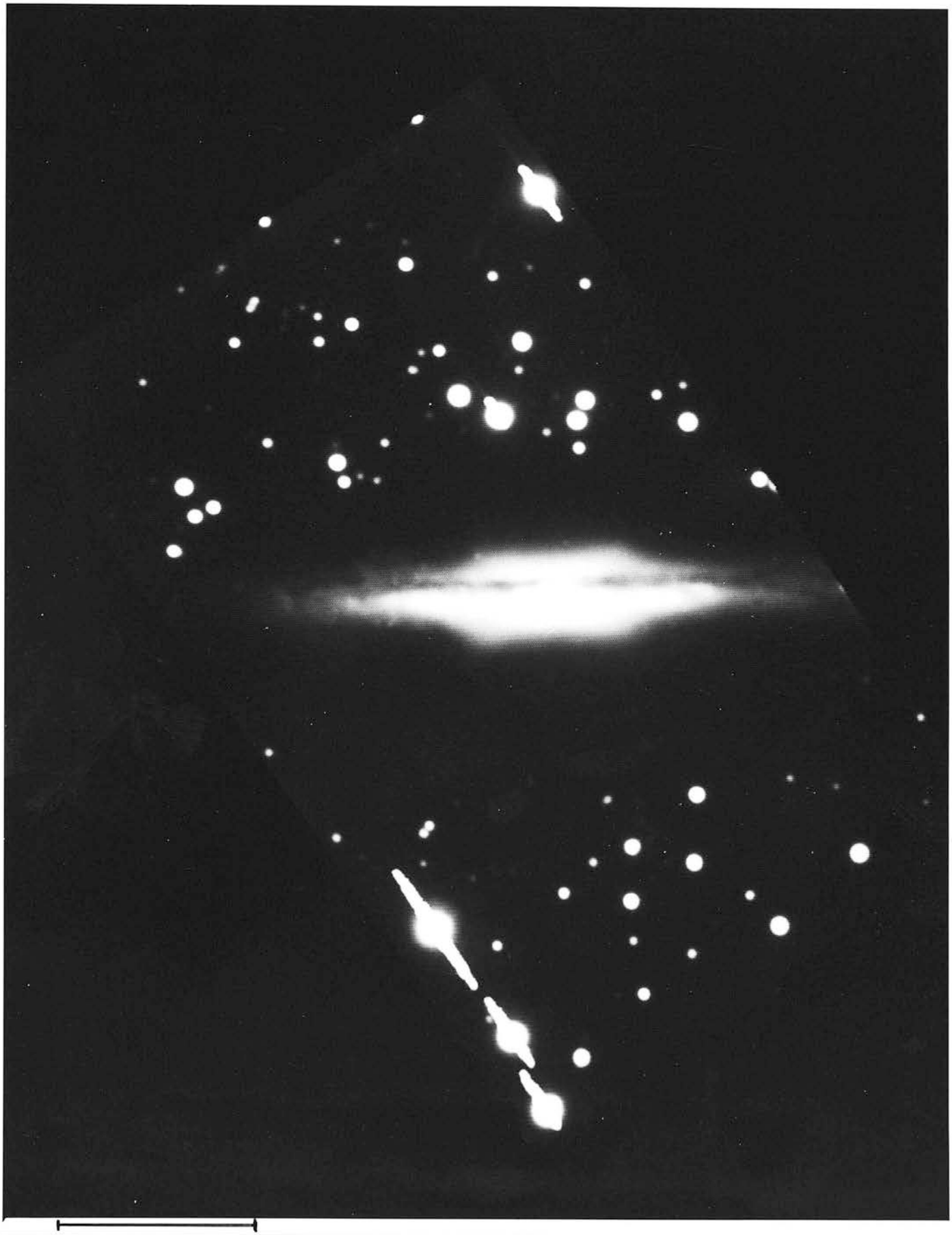

A0902-68 (R band)

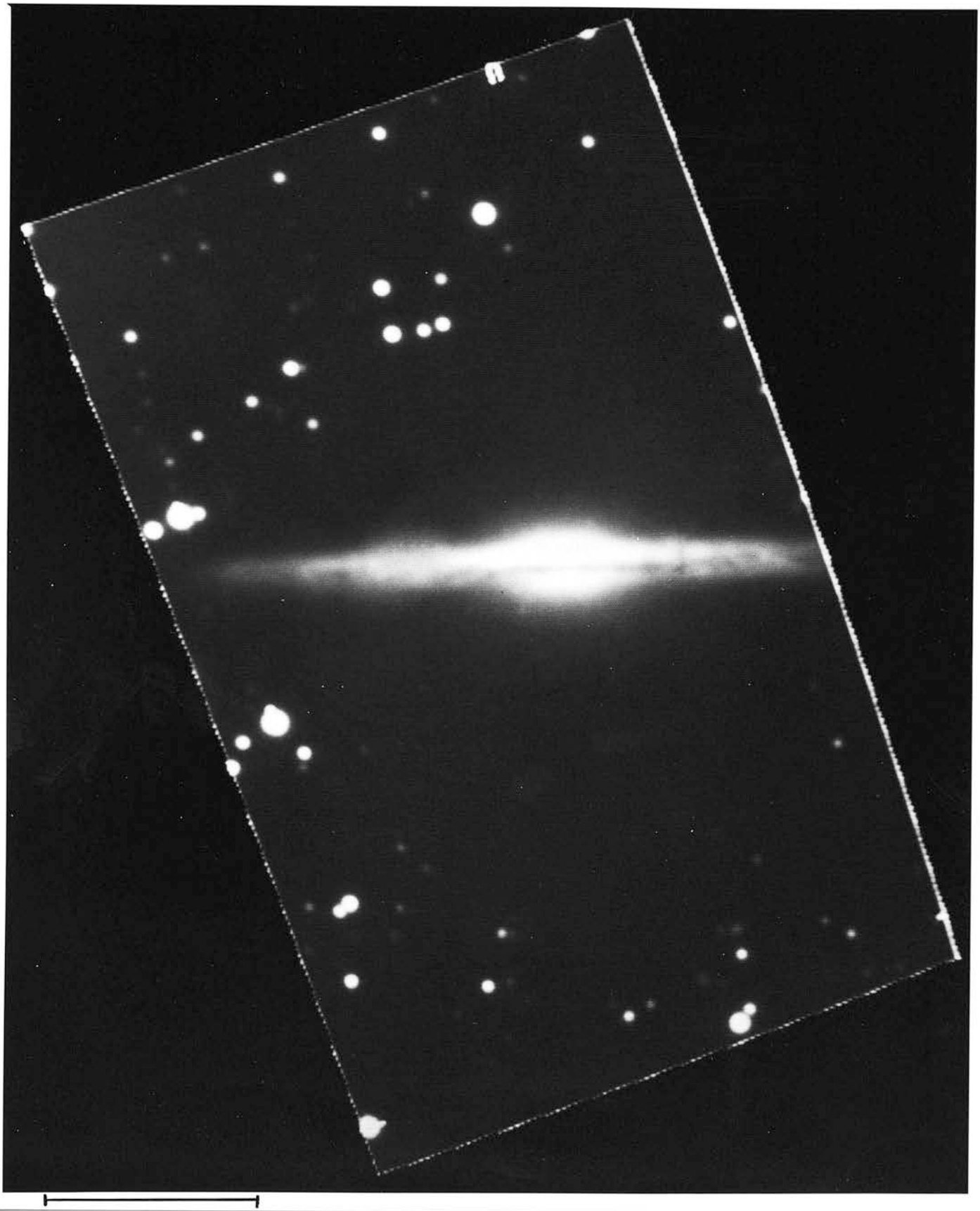

A0919-33 (R band)

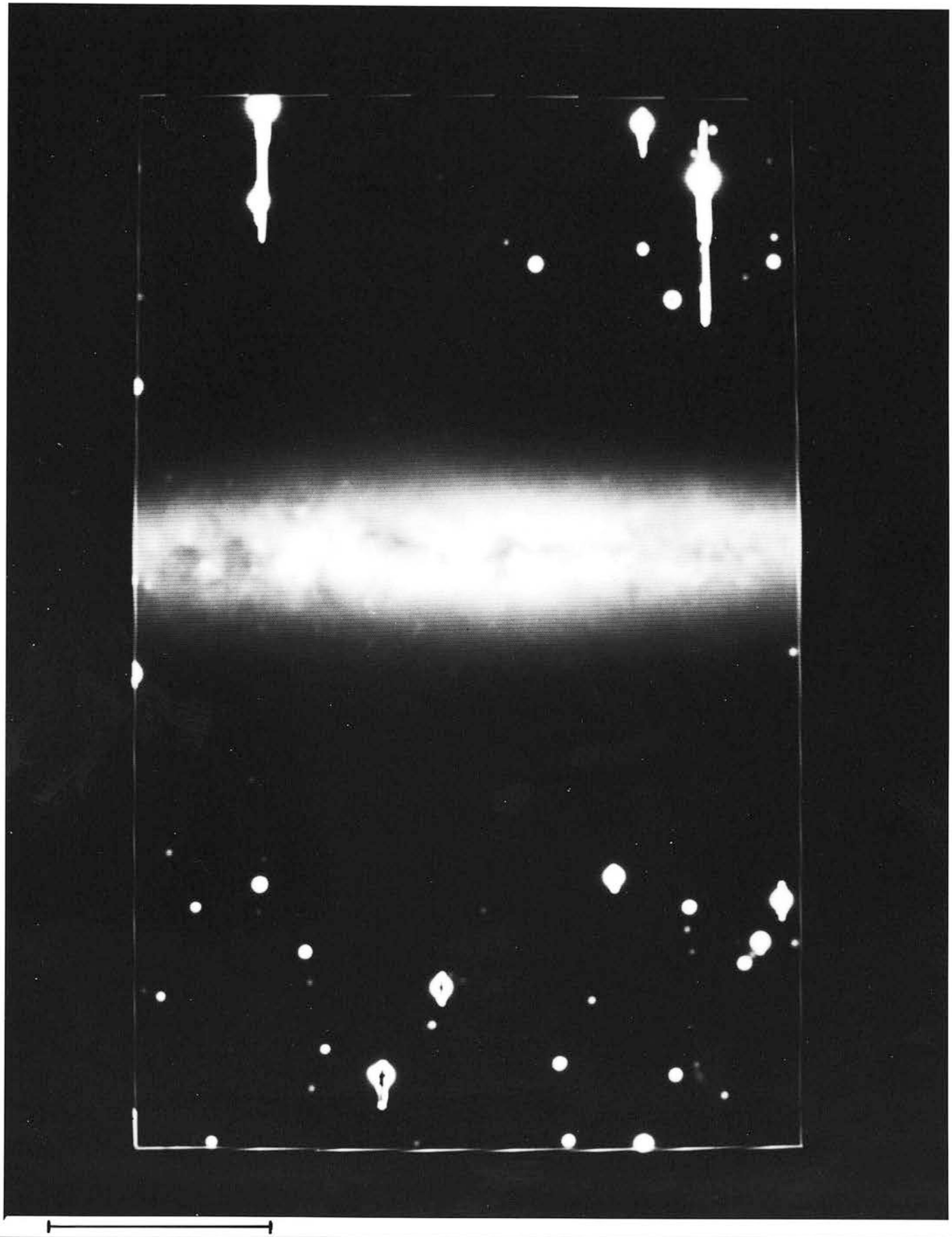

A0931-32 (R band)

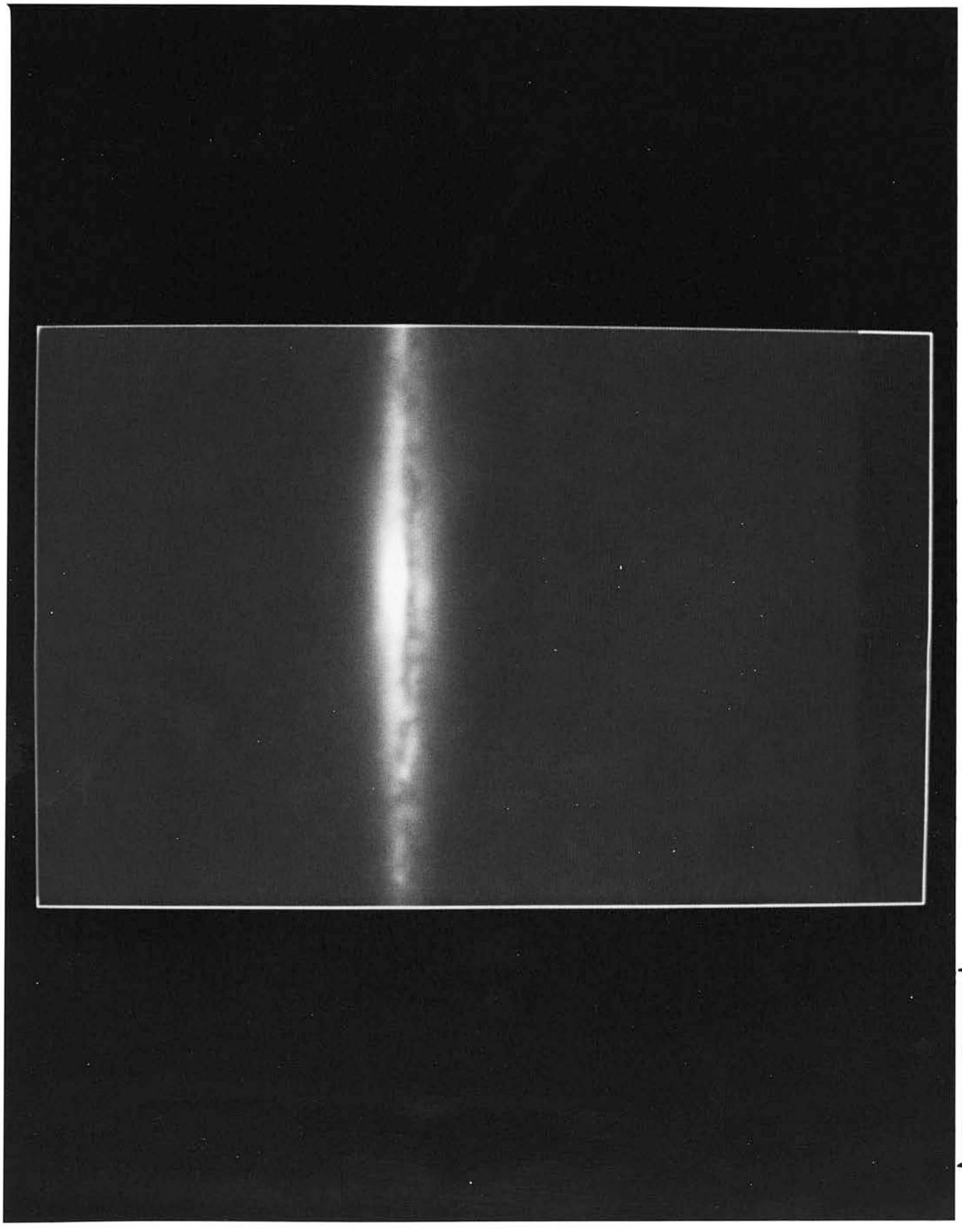

A1611-00 (R band)

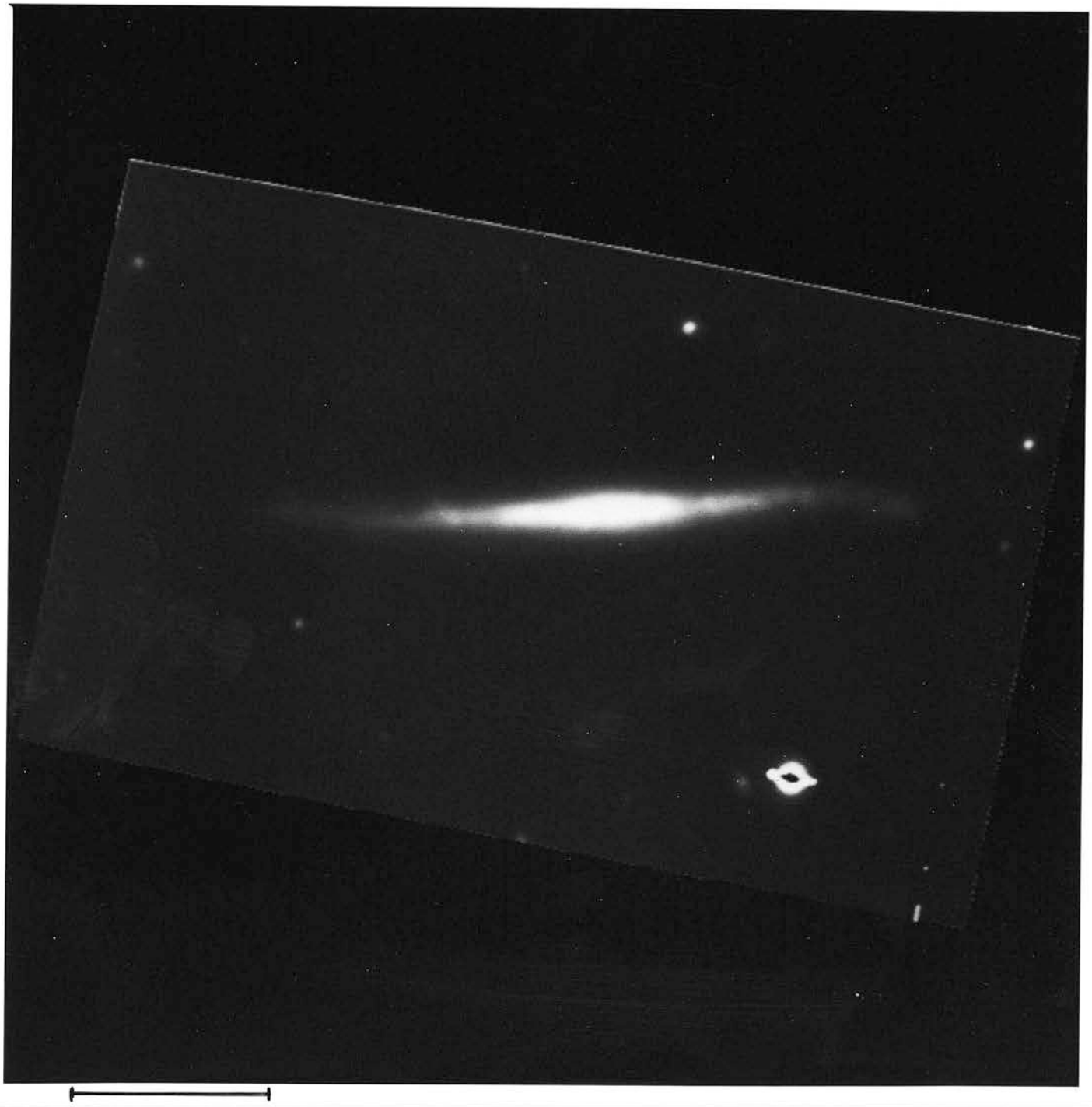

UGC 7170 (R band)

REFERENCES

AAO observers manual, 1981. Edited by J. W. V. Storey, version III.

Bahcall, J. N. & Kylafis, N. D., 1985. Astrophys. J., 288, 252.

Baum, W. A., Thomsen, B. & Kreidl, T. J., 1981.
Proc. S.P.I.E., vol. 290, 24.

Bertola, F. & Capaccioli, M., 1977. Astrophys J., 211, 697. [*BP*]

Binney, J., 1982. Mon. Not. R. astr. Soc., 200, 951.

Binney, J. & Petrou, M., 1985. Mon. Not. R. astr. Soc., 214, 449.

Blouke, M. M., Janesick, J. R., Hall, J. E. & Cowens, M. W., 1981.
Proc. S.P.I.E., vol. 290, 6.

Boroson, T., 1981. Astrophys. J. supp. ser., 46, 177.

Bottema, R., van der Kruit, P. C. & Freeman, K. C., 1987.
Astron. Astrophys., 178, 77.

Bottinelli, L., Gougueheim, L. & Paturel, G., 1982.
Astron. Astrophys. supp. ser., 47, 171.

Bottinelli, L., Gougueheim, L., Paturel, G. & de Vaucouleurs, G.,
1984. Astron. Astrophys. supp. ser., 56, 381.

Bottinelli, L., Gougueheim, L., Paturel, G. & de Vaucouleurs, G.,
1985. Astron. Astrophys. supp. ser., 59, 43.

Burbidge, E. M. & Burbidge, G. R., 1959. Astrophys. J., 130, 20.

Burkhead, M. S. & Kalinowski, J. K., 1974. Astron. J., 79, 835.

Burstein, D., 1979a. Astrophys. J., 234, 435.

Burstein, D., 1979b. Astrophys. J., 234, 829.

Burstein, D., 1979c. Astrophys. J. supp. ser., 41, 435.

Burstein, D. & Heiles, C., 1982. Astron. J., 87, 1165.

Burstein, D. & Heiles, C., 1984. Astrophys. J. supp. ser., 54, 33.

Burstein, D., Dressler, A., Faber, S. M., Stone, R. P. S.,
Lynden-Bell, D., Terlevich, R. & Wegner, G., 1987.
KPNO preprint no. 63.

Camm, G. L., 1950. Mon. Not. R. astr. Soc., 110, 305.

Carter, D., 1977. Mon. Not. R. astr. Soc., 178, 137.

Combes, F. & Sanders, R. H., 1981. Astron. Astrophys., 96, 164. [*CS*]

Corwin, H. E, de Vaucouleurs, A. & de Vaucouleurs, G., 1985.
Texas Monographs in Astronomy no. 4.

Davies, R. L., Efstathiou, G., Fall, S. M., Illingworth, G. & Schechter, P., 1983. Astrophys. J., 266, 41.

Davis, L. E., Cawson, M., Davies, R. L. & Illingworth, G., 1985. Astron. J., 90, 169.

de Vaucouleurs, G., 1953. Mon. Not. R. astr. Soc., 113, 134.

de Vaucouleurs, G. & Buta, R., 1983. Astron. J., 88, 939.

de Vaucouleurs, G. & Capaccioli, M., 1979. Astrophys. J. supp. ser., 40, 699.

de Vaucouleurs, G. & de Vaucouleurs, A., 1972. Mem. R. astr. Soc., 77, 1.

de Vaucouleurs, G., de Vaucouleurs, A. & Corwin, H., 1976. Second Reference Catalogue of Bright Galaxies, University of Texas press [*RC2*].

de Vaucouleurs, G., de Vaucouleurs, A. & Corwin, H. G., 1978. Astron. J., 83, 1331.

Dixon, R. S. & Sonnenborn, G., 1980. A Master List of Non-Stellar Astronomical Objects, Ohio State University Press.

Djorgovski, S., 1984. In "*Proceedings of the workshop on improvements to photometry*", NASA conference publications, CP 2350, p 152.

Dressel, L. L. & Condon, J. J., 1978. Astrophys. J. supp. ser., 36, 53.

Dressler, A., 1980. Astrophys. J. supp. ser., 42, 565.

Dressler, A., 1987. Astrophys. J., 317, 1.

Dressler, A. & Sandage, A., 1983. Astrophys. J., 265, 664.

Eggen. O. J., Lynden-Bell, D. & Sandage, A. R., 1962. Astrophys. J., 136, 748.

Ellis, R., 1981. In "*Origin and Evolution of Galaxies*", NATO ASI, edited by B. J. T. Jones, & J. E. Jones, D. Reidel, Holland, p 277.

ESO observers manual, 1981. Edited by C. Danks, section 1-K.

Fisher, J. R. & Tully, R. B., 1981. Astrophys. J. supp. ser., 47, 139.

Freeman, K. C., 1970. Astrophys. J., 160, 811.

Freeman, K. C., 1979. In "*Photometry, kinematics and dynamics of Galaxies*", edited by D. S. Evans, University of Texas press, p 85.

Geller, M. J. & Huchra, J. P., 1983. Astrophys. J. supp. ser., 52, 61.

Gilmore, G. F., 1984. Mon. Not. R. astr. Soc., 207, 223.

Gilmore, G. F. & Reid, I. N., 1983. Mon. Not. R. astr. Soc., 202, 1025.

Gilmore, G. F. & Shaw, M. A., 1986. Nature, 321, 750.

Gisler, G., 1980. Astron. J., 85, 623.

Goad, J. W. & Roberts, M. S., 1981. Astrophys. J., 250, 79.

Golay, M., 1974. Introduction to Astronomical Photometry,
D. Reidel, Holland, p 47.

Graham, J. A., 1982. Publ. Astr. Soc. Pac., 94, 244.

Griersmith, D., 1980. Astron. J., 85, 789.

Hamabe, M., 1982. Publ. Astr. Soc. Japan, 34, 423.

Hamabe, M., Kodaira, K., Okamura, S. & Takase, B., 1980.
Publ. Astr. Soc. Japan, 32, 197.

Hawarden, T. G., Elson, R. A. W., Longmore, A. J., Tritton, S. B.
& Corwin, H. G., 1981. Mon. Not. R. astr. Soc., 196, 747.

Heiles, C., 1976. Astrophys. J., 204, 379.

Hubble, E., 1930. Astrophys. J., 71, 231.

Hummel, E., 1980. Astron. Astrophys. supp. ser., 41, 151.

Illingworth, G. & Schechter, P. L., 1982. Astrophys. J., 256, 481.

Janesick, J. R., Elliott, T., Collins, S., Marsh, H., Blouke, M. M.
& Freeman, J., 1984. Proc. S.P.I.E., vol. 501, 2.

Jarvis, B. J., 1986. Astron. J., 91, 65. [*J86*]

Jedrzjewski, R. I., 1985. PhD thesis, University of Cambridge.

Jensen, E. B. & Thuan, T. X., 1982. Astrophys. J. supp. ser., 50, 421.

Jorden, P. R., Thorne, D. J. & van Breda, I. G., 1982.
Proc. S.P.I.E., vol. 331, 87.

Kent, S. M., 1983. Astrophys. J., 266, 562.

Kent, S. M., 1984. Astrophys. J. supp. ser., 56, 105.

Kent, S. M., 1985. Astrophys. J. supp. ser., 59, 115.

Kent, S. M., 1987. Astron. J., 94, 306.

King, I. R., 1962. Astron. J., 67, 471.

King, I. R., 1966. Astron. J., 71, 64.

King, I. R., 1978. Astrophys. J., 222, 1.

King, I. R. & Raff, M., 1977. Publ. Astr. Soc. Pac., 89, 120.

King, D.J., Birch, C. J., Johnson, C., & Taylor, K. N. R., 1981. Publ. Astr. Soc. Pac., 93, 385.

Kodaira, K., Watanabe, M. & Okamura, S., 1986. Astrophys. J. supp. ser., 62, 703.

Kormendy, J., 1977a. Astrophys. J., 217, 406.

Kormendy, J., 1977b. Astrophys. J., 218, 333.

Kormendy, J., 1980. In Proc. ESO workshop on 2D photometry, edited by P. Crane & K. Kjar, p 191.

Kormendy, J., 1985. Astrophys. J., 295, 73.

Kormendy, J. & Illingworth, G., 1982. Astrophys. J., 256, 460.

Kormendy, J. & Illingworth, G., 1983. Astrophys. J., 265, 632.

Kraan-Korteweg, R. C., 1982. Astron. Astrophys. supp. ser., 47, 505.

Lauberts, A., 1982. ESO/Uppsala Catalogue of Galaxies, European Southern Observatory [*ESO*].

Lauberts, A. & Sadler, E., 1984. "*A compilation of UBVRI photometry for Galaxies in the ESO/Uppsala Catalogue*", ESO scientific report no. 3.

Lauer, T. R., 1985. Mon. Not. R. astr. Soc., 216, 429.

Longo, G. & de Vaucouleurs, A., 1983. Texas Monographs in Astronomy no. 3.

Longo, G. & de Vaucouleurs, A., 1985. Texas Monographs in Astronomy no. 3a.

Mackay, C. D., 1982. Proc. S.P.I.E., vol. 331, 146.

Mackay, C. D., 1986. Ann. Rev. Astron. Astrophys., 24, 255.

Malin, D. F., 1977. A.A.S. Photo Bulletin, 16, 10.

Malin, D. F. & Carter, D., 1983. Astrophys. J., 274, 534.

May, A., Van Albada, T. S. & Norman, C. A., 1985. Mon. Not. R. astr. Soc., 214, 131.

Michard, R., 1985. Astron. Astrophys. supp. ser., 59, 205.

Mihalas, D. & Binney, J. J., 1981. Galactic Astronomy : structure and kinematics, W. H. Freeman.

Morton, D. C. & Chevalier, R. A., 1973. Astrophys. J., 179, 55.

Neito, J.-L., 1983. Astron. Astrophys. supp. ser., 53, 383.

Nilson, P., 1973. Uppsala General Catalogue of Galaxies, Uppsala Astronomiska Observatoriums Annaler, 6 [*UGC*].

Okamura, S., 1977. Annals Tokyo Astr. Obs., 16, no. 3, 111.

Palumbo, G. G. C., Tanzella-Nitti, G. & Vettolani, G., 1980. Catalogue of Radial Velocities of Galaxies, Gordon & Breach.

Persson, S. E., Frogel, J. A. & Aaronson, M., 1979. Astrophys. J. supp. ser., 39, 61.

Quinn, P. J. & Goodman, J., 1986. Astrophys. J., 309, 472.

Rood, H. J. & Baum, W. A., 1967. Astron. J., 72, 398.

Rubin, V. C., Peterson, C. J. & Ford, W. K., 1980. Astrophys. J., 239, 50.

Sandage, A., 1961. Hubble Atlas of Galaxies, Carnegie Institution of Washington.

Sandage, A., 1973. Astrophys. J., 183, 711.

Sandage, A., 1978. Astron. J., 83, 904.

Sandage, A., 1986. Ann. Rev. Astron. Astrophys., 24, 421.

Sandage, A. R., Freeman, K. C. & Stokes, N. R., 1970. Astrophys. J., 160, 831.

Sandage, A. & Tammann, G. A., 1981. Revised Shapley-Ames Catalogue of Bright Galaxies, Carnegie Institution of Washington [*RSA*].

Sandage, A. & Visvanathan, N., 1978. Astrophys. J., 223, 707.

Schombert, J. M. & Bothun G. D., 1987. Astron. J., 92, 60.

Schuster, W. J. & Nissen, P. E., 1987. In Proc. ESO workshop on "*Stellar evolution & dynamics in the outer of the Galaxy*", ed. by M. Azzopardi, in press.

Schweizer, F., 1976. Astrophys. J. supp. ser., 31, 313.

Schweizer, F. & Ford, W. K., 1984. In "*New Aspects of Galaxy Photometry*", Lecture Notes in Physics, edited by J. L. Nieto, Springer-Verlag, p 145.

Shaw, M. A. & Gilmore, G. F., 1986. In "*Spectral Evolution of Galaxies*", edited by C. Chiosi & A. Renzini, D. Reidel, p 477.

Simien, F. & de Vaucouleurs, G., 1986. Astrophys. J., 302, 564.

Simkin, S., 1975. Dudley Obs. Rep., 9, 401.

Spitzer, L., 1942. Astrophys. J., 95, 329.

Strom, K. M. & Strom, S. E., 1978. Astron. J., 83, 73.

Strom, S. E., Strom K. M., Goad, J. W, Vrba, F. J. & Rice, W., 1976. Astrophys. J., 204, 684.

Strom, K. M., Strom, S. E., Jensen, E. B., Moller, J., Thompson, L. A. & Thuan, T. X., 1977. Astrophys. J., 212, 335.

Thompson, I. B., Boroson, T. A. & Shectman, S. A., 1982. In Carnegie Inst. yearbook, p 630.

Tsikoudi, V., 1977. PhD thesis, University of Texas.

Tsikoudi, V., 1979. Astrophys. J., 234, 842.

Turner, E. L. & Gott, J. R., 1976. Astrophys. J. supp. ser., 32, 409.

UKSTU Handbook, 1983. Edited by Tritton, S. B., Science & Engineering Research Council.

van der Kruit, P. C., 1979. Astron. Astrophys. supp. ser., 38, 15.

van der Kruit, P. C., 1984. Astron. Astrophys., 140, 470.

van der Kruit, P. C., 1987a. In "*The Galaxy*", NATO ASI, edited by G. F. Gilmore & R. F. Carswell, D. Reidel, Holland p 27.

van der Kruit, P. C. & Searle, L., 1981a. Astron. Astrophys., 95, 105.

van der Kruit, P. C. & Searle, L., 1981b. Astron. Astrophys., 95, 116. [*KS81*].

van der Kruit, P. C. & Searle, L., 1982a. Astron. Astrophys., 110, 61.

van der Kruit, P. C. & Searle, L., 1982b. Astron. Astrophys., 110, 79.

Watanabe, M., Kodaira, K. & Okamura, S., 1982. Astrophys. J. supp. ser., 50, 1.

Weekes, T. C., 1981. Astron. J., 86, 1415.

West, R. M., Surdej, J., Schuster, H.-E., Muller, A. B., Laustsen, S. & Borchkhadze, T. M., 1981. Astron. Astrophys. supp. ser., 46, 57.

Whitmore, B. C. & Kirshner, R. P., 1981. Astrophys. J., 250, 43.

Whitmore, B. C. & Kirshner, R. P., 1982. Astron. J., 87, 500.

Whitmore, B. C., Kirshner, R. P. & Schechter, P. L., 1979. Astrophys. J., 234, 68.

Williams, T. B., 1975. Astrophys. J., 199, 586.

Wirth, A., 1981. Astron. J., 86, 981.

Wirth, A. & Shaw, R., 1983. Astron. J., 88, 171.

Wright, J. F., 1982. PhD thesis, University of Cambridge.

Wright, J. F. & Mackay, C. D., 1981. Proc. S.P.I.E., vol. 290, 160.

Young, A. T., 1974. Methods of Experimental Physics, vol. 12A, edited by N. P. Carleton, Academic Press, p. 123.

SURFACE BRIGHTNESS DISTRIBUTIONS IN TWO EDGE-ON SPIRAL GALAXIES

M.A.Shaw
Dept. of Astronomy, Univ. of Edinburgh, Edinburgh, U.K.

G.F.Gilmore
Institute of Astronomy, Madingley Road, Cambridge, U.K.

1. INTRODUCTION

Of considerable importance to modelling the formation and early evolution of galaxies is the relationship between the spheroids of spirals and SO's, and those of ellipticals. In this context, the isolation of a thick disc in our own Galaxy (Gilmore et al. (1985)) and in other spirals (van der Kruit (1984); herafter vdK) - aside from their initial discovery in SO's by Burstein (1979) - has added significance because the luminosity profiles of several spirals seem to be dominated by this component over considerable ranges of galactocentric distance (R) and height (Z). On the other hand, "elliptical-like" spheroids, generally characterised by the de Vaucouleurs $r^{1/4}$ law, seem to be barely detectable in many galaxies in complete contradiction to our preconception that this model adequately describes all forms of galaxian spheroids.

Here we present analyses of the surface brightness distributions in the two well known nearby edge-on spirals NGC 4565 and NGC 891 (adopted distances of 10 and 9.5 Mpc respectivly). This is the first such an investigation of the NGC 4565 profiles presented by Jensen & Thuan (1982; herafter JT), while other recent data on this galaxy (van der Kruit & Searle 1981; herafter KS1) are used to supplement those of JT. The analysis of NGC 891 (from van der Kruit & Searle 1981; herafter KS2) is included both to extend the results of vdK and to complement those on NGC 4565.

2. THE ADOPTED MODELS

In attempting to describe the thin disc in the following analysis, we have made the, now usual, assumption of a locally isothermal and self-gravitating sheet. In its present form the model used is that first proposed (and more fully described) by KS1, reducing to the following expressions in terms of surface brightness

C. Chiosi and A. Renzini (eds.), Spectral Evolution of Galaxies, 477–484.
© 1986 by D. Reidel Publishing Company.

$$\mu(R,Z) = \begin{cases} \mu(0,0)\ [1+(R^2/2h_R^2)\ln(R/2h_R)]\ \mathrm{sech}^2(Z/Z_0) & \text{for } R \ll h_R \\ \mu(0,0)\ [(\pi R/2h_R)^{1/2}\exp-(R/h_R)]\ \mathrm{sech}^2(Z/Z_0) & \text{for } R \gg h_R \end{cases}$$

$\mu(0,0)$ mag arcsec^{-2} (herafter "μ") being the central surface brightness.

Implicit in the derivation of this model is the approximation of a constant scaleheight with R. Although it is not an immediately obvious result, KS1 have given some evidence to support its validity.

Modified forms of the above equations are also used to represent a possible thick disc (with a suitable choice for h_R and scaleheight $(Z_1/2)$. Alternatively, the familiar exponential model is also applied

$$L(R,Z) = L_0\ \exp-[(R/h_r) + (Z/h_Z)]$$

h_Z being the thick disc scaleheight.

A spheroid component is represented either by an exponential similar to that of the thick disc, or by the more usual de Vaucouleurs $r^{1/4}$ law

$$\log(L/L_0) = -3.33[(\theta/\theta_E)^{1/4} - 1]$$

where $\theta = (q^2R^2 + Z^2)^{1/2}$, q being the axis ratio, and θ_E is the effective radius.

3. RESULTS

3.1 NGC 4565

In this section we present the results of a full analysis of the existing B band data of JT for NGC 4565 - the running of single, two or three component fitting iterations being used in an attempt to describe the form of these observed profiles.

Major discrepencies, when compared to the actual data, are generated by the adoption of either single or two component model fits. For example, a two component thin disc and spheroid combination consistently underestimates the amount of light present in the galaxy at intermediate Z (typically $\sim$2.4 to 5.1 kpc) by as much as 1.2 μ (amounting to $\sim$30 times the quoted errors of JT). Similar underestimations are revealed, but in this case in the outer regions of each profile (Z in excess of 3.4 kpc), by the superposition of a thin disc and thick disc - the dicrepencies here running from 0.5 to 3.0 μ or $\sim$3 to 20 times quoted errors. In neither of these cases do the discrepencies appear to be model dependant nor systematic in origin.

Observations are, on the other hand, very well described by a combination of all three of the components noted above - as figure 1 shows. For such a combination, the thin disc has a (Z_0) scaleheight of 0.82 kpc comparing quite favourably with that found by KS1 and with the currently accepted value for our own Galaxy as deduced from star counts. The resultant thick disc scaleheights also prove to be independant of R, having values of 0.84 kpc for the exponential and 0.80 kpc

($Z_1/2$) for the sech^2 model forms - such values again in accord with the existing data. The spheroid, it turns out, is equally well described by exponential or $r^{1/4}$ laws. Use of the former gives rise to an unambiguous increase in scaleheight with R although this trend, rather than describing any fundamental property of the spheroid, merely seems to indicate the increasing dominance of this component over the other two as R increases. This is supported by the fact that at large Z ($\gtrsim$8.7 kpc or $\sim 3\theta_\varepsilon$), the (h_Z) scaleheight of the spheroid approaches a limiting value of 3.1 kpc.

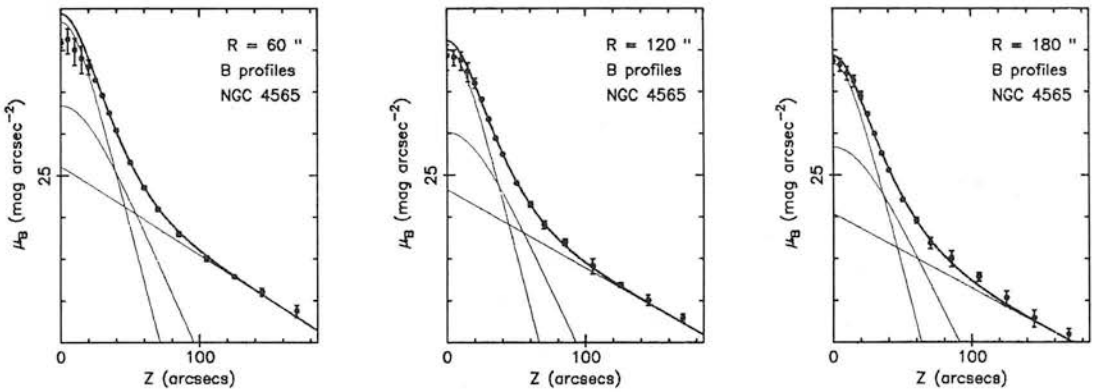

Figure 1. Selected surface brightness profiles of NGC 4565 with superimposed three component (thin disc, thick disc plus spheroid) fits and associated errors. R is the galactocentric distance.

Isophote shapes provide a more graphic representation of the above. We find clear evidence of global isophotal flattening with R for all models used, further deconvolution of these isophotes into their respective components indicating the presence of a very highly flattened thick disc at all R underlying a much rounder spheroid (albeit still a little flatter than one might expect from a preconception that it is of the same form as an elliptical galaxy) - see fig 3.

3.2 NGC 891

We now apply the same modelling procedure used above to the existing J(λ4700Å) and F(λ6400Å) band data on NGC 891 from KS2. The three examples shown in figure 2 clearly indicate how well described these profiles are by the combination of a thin disc and an exponential thick disc (the sech^2 form is unable to model the thick disc in this case). The best-fit thin disc scaleheights (Z_0) are 0.94 kpc in F and 0.99 kpc in J, while for the thick disc the scaleheight (h_Z) is 1.92 kpc in both bands (it is again constant for all R). The appropriate central surface brightnesses of the two components are given in table 1.

The isophote shapes of this thick disc noticeably flatten beyond ~ 8.3 kpc as figure 3 shows. Interior to this the isophotes are moderately rounded and are consistent with ellipses having axis ratios of between 0.6 and 0.66 (compared to the 0.6 adopted by vdK and the range 0.6 to 0.7 quoted by Bahcall & Kylafis (1985)), so in this respect the thick disc seems a little different to that of NGC 4565. Inspection of the relative scaleheights in table 1 supports this result.

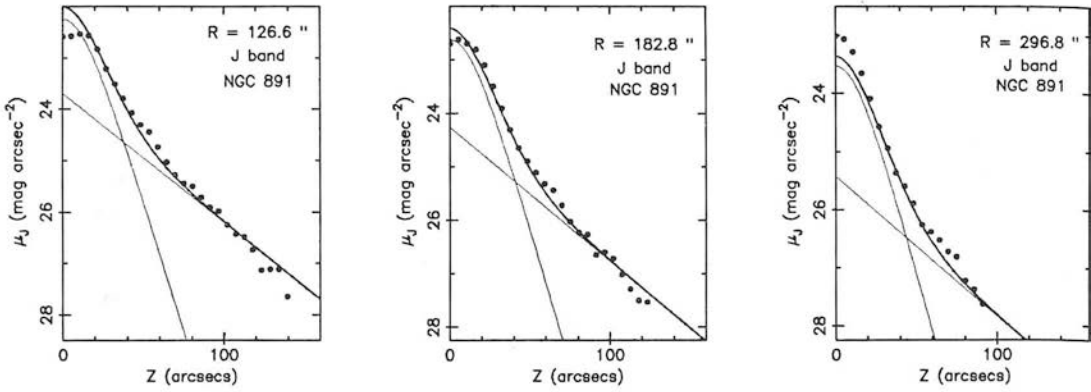

Figure 2. Selected J surface brightness profiles of NGC 891 with superimposed two component fits using a thin disc and exponential thick disc.

Hence, taking the above photometric data in isolation, we see no evidence for a spheroid in this galaxy down to a limiting surface brightness ~26.5 or 27μ in F and ~27.5 to 28μ in J. It is quite possible, of course, that a spheroid component does exist but that it is only apparent at levels fainter than this. Indeed, if this is the case, and if we can use the results of NGC 4565 (for which the spheroid only becomes prominent around μ_B ~27μ) as a guide, then we might expect such a component in NGC 891 also to appear only around 27 - 27.5 μ in J assuming the galaxies to be fairly similar. This is very close to the limit of the current photometry and so the failure to detect a spheroid is not really suprising.

Problems in analysing NGC 891 first become apparent only when one wishes to try and model all the profiles with one component alone or when one insists on adding to the models a spheroid brighter than ~27μ . Use of just such a bright spheroid together with a thin disc, for example, generates disagreements very similar to those noted in the case of NGC 4565 between the predicted and observed surface brightness distributions. Here, as found previously, such discrepencies can only be eliminated by the addition of a third component - the thick disc - to the models.

4. POSSIBLE PROBLEMS

Some of the general problems associated with profile deconvolution of edge-on spirals have been addressed by, for example, Kormendy (1982) - two of these are of particular concern here.

The first is the effect that even a small amount of internal absorption due to gas and dust might have on the resultant parameters - in particular those of the thin disc. In the case of NGC 891, for which we have good multicolour data analysed with the above techniques, such absorption is the likely cause of differences in both thin disc and thick disc central surface brightnesses - and to a lesser degree the thin disc scaleheights - between the J and F bands. As far as the scaleheights are concerned, the greater problem of obscuration in J gives rise to artificially flattened profiles at small Z (artificially compared to F that is). To continue to fit the data in such a situation, the thin disc scaleheight in the J band must be correspondingly increased. The preferential light loss in J also results in the central surface brightnesses of both thin and thick discs appearing fainter there than in F.

The second major concern lies with the effect on the parameter values of galaxy inclination, although with an inclination $\approx 89^{\circ}$ such

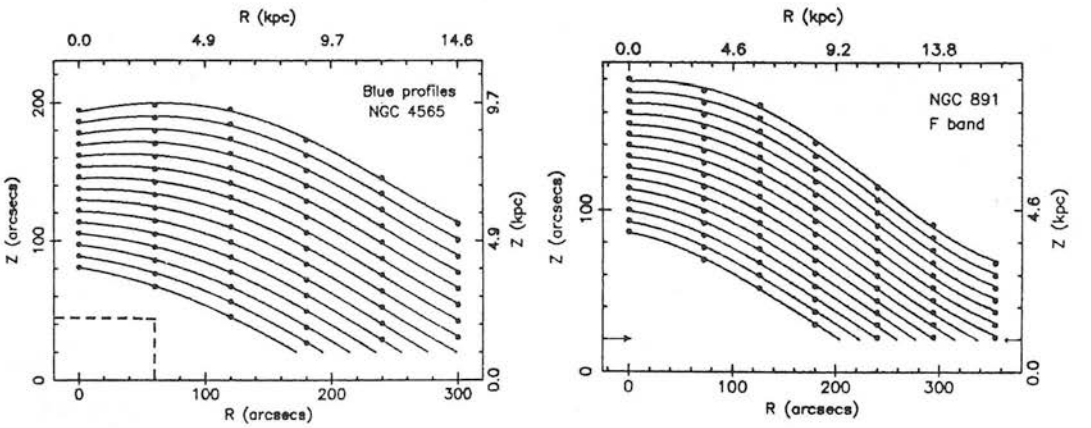

Figure 3. Isophote shapes of the spheroid of NGC 4565 (left) and the thick disc of NGC 891 (right) both derived using exponential models. Each curve corresponds to a specific surface brightness - in the case of NGC 4565 running from 26.2μ (bottom curve) to 29.0μ (top) and for NGC 891 from 24.2μ (bottom) to 27.0μ (top). The dashed box for NGC 4565 represents the area of significant contamination by the "peanut" bulge, while arrows on the NGC 891 plot marks the Z-height below which dust obscuration and thin disc contamination are likely to be a problem.

a difficulty is not as severe for NGC 891 as it is likely to be for NGC 4565 (for which i is only 85° - 86°). The effects on NGC 4565 will only become apparent in our analysis when we have completed a study of the red profiles of JT.

5. DISCUSSION

We see no evidence in the photometry of NGC 891 by KS2 (currently the best available on this galaxy) for the existence of a spheroid, the profiles being very well described by a locally isothermal thin disc in combination with an exponential thick disc, both possessing uniform scaleheights at all R. The constancy of the thick disc scaleheight in both J and F, together with only marginal evidence for a (J-F) colour gradient with R or Z in the KS2 data (despite strong evidence of (U′-F) gradients), argues in favour of a uniform age to this component. In agreement with the contour plots presented by KS2, the thick disc becomes progressivly flatter at large R.

Analysis of NGC 4565 suggests the presence of a thin disc resembling that of NGC 891 even to a similar scaleheight, and a thick disc again having a constant scaleheight with R. In addition, a spheroid (becoming progressively more dominant for $Z \gtrsim 8.7$ kpc) has had to be invoked because of the failure of single or two component modelling to reproduce adequately the observed profiles. The isophote maps indicate a moderate flattening of the spheroid, but a high degree to the thick disc.

Aside from the obvious advantage of being relatively nearby, another of the major motivations for studying these two galaxies in particular has been to investigate how they might resemble our own Galaxy were it viewed from a similar aspect, and a strong case has been recently been made for NGC 891 in this regard (vdK). The existence of a warp in the disc of NGC 4565 - a feature in common with our own Galaxy - together with the similarities of its parameters derived above to those of the Galaxy and NGC 891, argue that NGC 4565 is also a good candidate for such a comparison.

However, it has been stressed that additional problems of interpretation arise when modelling NGC 4565 because of the presence both of the warp and also the so-called "peanut" bulge. In particular, vdK has argued that residual light from the warp contaminates the outer spheroid sufficiently to lead to the observed flattening of the isophotes. Thus we have attempted to estimate the degree of importance of either to our conclusions. It seems that despite the obvious dominance by the bulge of the minor axis profile, it is not of fundamental significance to our results mainly because it becomes unimportant beyond $R \sim 3$ kpc (i.e. $\sim 1\,\theta_e$) and $Z \sim 2$ kpc. In our analysis, however, further investigation of the bulge is hampered partly by dust obscuration but in particular by the inherent uncertainties resulting from subtraction of all the other components.

An investigation into the likely effect of the warp is best addressed using the KS1 data for NGC 4565 because it has not been smoothed over all the galaxy quadrants. A comparison of surface brightnesses at

corresponding points in the (R,Z) plane over the whole galaxy (together with even a brief inspection of the contour plots presented by KS1 themselves) clearly shows this warp only to be present over regions fainter than $\mu_B \sim 27$ μ and R in excess of ~23 kpc. However, flattening in the thick disc - and to a lesser extent in the spheroid - first becomes noticeable at much brighter magnitudes and much smaller R. It is also important to note that the same degree of global isophotal flattening is seen in all quadrants and is not appreciably different in that containing the strongest evidence for the warp. Even if it is both more extensive and more complex than is assumed - admittedly rather naively in this discussion - we suspect the warp may be too faint to have a significant effect on the above conclusions.

As for the importance of these isophote shapes, even modest deviations of such shapes from true ellipses in any spheroid are highly significant because, as pointed out by Binney & Petrou (1985), they arise from correspondingly much larger deviations in the underlying three dimensional structure of the galaxy. In analysing these shapes, therefore, it is interesting to note the recent study of variations in ellipticity for a large sample of E's and SO's presented by Michard

TABLE I - Derived and adopted parameters for NGC 4565 and NGC 891

component	models	NGC 4565	NGC 891
thin disc	sech^2	$\mu(0,0)$ = 21.12 (±0.30) mag arcsec^{-2}	$\mu(0,0)$ = 20.16 (±0.05) mag arcsec^{-2} in F 21.30 (±0.30) mag arcsec^{-2} in J
		Z_0 = 0.82 (±0.02) kpc	Z_0 = 0.94 (±0.01) kpc in F 0.99 (±0.03) kpc in J
		h_r = 5.5 kpc	h_r = 4.9 kpc
thick disc	exp.	$\mu(0,0)$ = 21.44 (±0.20) mag arcsec^{-2}	$\mu(0,0)$ = 21.60 (±0.12) mag arcsec^{-2} in F 22.40 (±0.19) mag arcsec^{-2} in J
		h_r = 5.5 kpc	h_r = 4.9 kpc
		h_z = 0.84 (±0.09) kpc	h_z = 1.92 (±0.14) kpc
	sech^2	$\mu(0,0)$ = 23.10 (±0.40) mag arcsec^{-2}	
		h_r = 5.5 kpc	--------
		Z_1 = 1.60 (±0.19) kpc	
spheroid	$r^{1/4}$ law	μ_0 = 24.20 (±0.30) mag arcsec^{-2}	
		q = 0.7	--------
		Θ_e = 2.9 kpc	
	exp.	$\mu(0,0)$ = 24.20 (±0.30) mag arcsec^{-2}	
		h_r = 5.5 kpc	--------
		h_z = 3.1 (±0.2) kpc for $Z \gtrsim 180$ "	

(1984). These results show that the shape of a galaxy flatter than E3 varies in a fashion which is qualitatively similar to the observed behaviour of the global (i.e. thick disc plus spheroid) isophotes of NGC 4565. Extending the conclusions of Michard, a natural explanation of this result is that E galaxies also have a two component (thick disc plus spheroid) structure as seen in NGC 4565 after thin disc subtraction. There exists, therefore, the interesting possibility that flattened (thick disc) structure is an integral part of a spheroidal galaxy, leading in turn to the possibility that thin and thick disc structure are unrelated in spirals.

6. ACKNOWLEDGEMENTS

We would like to thank in particular Piet van der Kruit for supplying his data on NGC 4565 and NGC 891 in such a usable form, and also Trinh Thuan for allowing the analysis of the NGC 4565 data. Tim Hawarden provided several very helpful comments on the manuscript. MAS acknowledges the support of an Science & Engineering Research Council studentship.

REFERENCES

Bahcall, J.N. and Kylafis, N.D.: 1985, *Ap. J.*, 288, 252
Binney, J. and Petrou, M.: 1985, *M.N.R.A.S.*, 214, 449
Burstein, D.: 1979, *Ap. J.*, 234, 435
Gilmore, G.F., Reid, I.N. and Hewett, P.: 1985, *M.N.R.A.S.*, 213, 257
Jensen, E.B. and Thuan, T.X.: 1982, *Ap. J. Supp.*, 50, 421 (JT)
Kormendy, J.: 1982 in *Morphology and Dynamics of Galaxies, 12th Adv. course Swiss Soc. of Astron. & Astrophys., Geneva Obs. Publ.*
Kruit, P.C. van der: 1984, *A. & A.*, 140, 470 (vdK)
Kruit, P.C. van der and Searle, L.: 1981, *A. & A.*, 95, 105 (KS1)
Kruit, P.C. van der and Searle, L.: 1981, *A. & A.*, 95, 116 (KS2)
Michard, R.: 1984, *A. & A.*, 140, L39